

Copyright

by

Jacob G. Kapitan

2006

**Structural Assessment of Bridge Piers with Damage similar to Alkali  
Silica Reaction and/or Delayed Ettringite Formation**

**by**

**Jacob G. Kapitan, B.S.C.E.**

**Thesis**

Presented to the Faculty of the Graduate School of

The University of Texas at Austin

in Partial Fulfillment

of the Requirements

for the Degree of

**Master of Science in Engineering**

**The University of Texas at Austin**

**May 2006**

**Structural Assessment of Bridge Piers with Damage similar to Alkali  
Silica Reaction and/or Delayed Ettringite Formation**

**Approved by  
Supervising Committee:**

---

**John E. Breen**

---

**Oguzhan Bayrak**

## **Dedication**

I would like to dedicate this thesis to my parents who put the happiness and well being of their four children in front of their own interests for the greater part of their lives. It is to them that I owe my good fortune in life.

## **Acknowledgements**

I would like to acknowledge the work of Dr. John E. Breen. His guidance and assistance provided me with the best possible experience as a graduate student. The style and manner with which I was treated as a student made me the envy of my peers. He has positively influenced my knowledge of structural engineering and life.

In addition, I would like to thank Daniel Fuchs for his assistance in the laboratory. Daniel played an integral role in the completion of my experimental program. Daniel earned my respect and friendship by going out of his way to perform quality work.

Finally, I would like to thank Dr. Oguzhan Bayrak and Tyler Ley for offering their assistance to the project whenever called upon. They have gone out of their way many times for me. For this, I express my gratitude.

# **Structural Assessment of Bridge Piers with Damage similar to Alkali Silica Reaction and/or Delayed Ettringite Formation**

Jacob G. Kapitan, M.S.E.

The University of Texas at Austin, 2006

SUPERVISOR: John E. Breen

In recent years, it has been discovered that some structural elements of the I-10 and I-35 corridor passing through San Antonio, Texas (San Antonio Y) are suffering from premature concrete deterioration related to alkali-silica reaction (ASR) and/or delayed ettringite formation (DEF). While there is considerable evidence of materials related distress, the degree of damage to structural capacity has not been quantified. In a comprehensive search of literature, very little research has been identified that quantifies the amount of structural damage caused by ASR and/or DEF on the load carrying capacity of structural piers. Due to the fact that this integral stretch of interstate highway sees a large volume of traffic, it is desirable to determine a method of assessing the degree of structural

damage, and the necessity of taking remedial actions. The purpose of this thesis is to develop an assessment methodology which can be used by The Texas Department of Transportation (TxDOT) to evaluate the current and future integrity of structural elements in the San Antonio Y. The key steps included in the methodology are conducting a literature review on the effects of ASR and/or DEF on the structural properties of reinforced concrete, evaluating in-situ engineering properties of existing concrete, investigating the basis for the original design, and performing an experimental investigation to determine the effect of cracking on the load carrying capacity of typical SAY piers. This thesis presents the findings from this research.

## Table of Contents

<b>CHAPTER 1 INTRODUCTION.....</b>	<b>1</b>
1.1 Problem Statement .....	1
1.2 Background .....	2
1.2.1 The San Antonio Y.....	2
1.2.2 Concrete Materials Issues.....	3
1.2.3 Structural Issues .....	6
1.3 Objective and Scope.....	9
1.4 Organization.....	10
<b>CHAPTER 2 LITERATURE REVIEW AND PROJECT PLAN.....</b>	<b>12</b>
2.1 Diagnosis of ASR and DEF .....	12
2.1.1 External Diagnosis of ASR .....	12
2.1.2 Internal Diagnosis of ASR .....	15
2.1.3 External Diagnosis of DEF .....	16
2.1.4 Internal Diagnosis of DEF.....	16
2.2 Effects of ASR and DEF on Engineering Properties of Concrete.....	17
2.2.1 The Effect of ASR on the Compressive Strength of Concrete.....	17
2.2.2 The Effect of ASR on the Tensile Strength of Concrete.....	19
2.2.3 The Effect of ASR on the Elastic Modulus and Creep Properties of Concrete .....	20
2.3 Effects of ASR and DEF on Structural Properties of Reinforced Concrete .....	21
2.3.1 The Effect of ASR on the Axial Strength of Reinforced Concrete.....	22
2.3.2 The Effect of ASR on the Flexural Strength of Reinforced Concrete .....	23
2.3.3 The Effect of ASR on the Shear Strength of Reinforced Concrete.....	24



2.3.4	The Effect of ASR on Bond Strength.....	24
2.3.5	The Effect of ASR on Bearing Strength.....	28
2.3.6	The Effect of ASR on Deflections .....	32
2.4	Applicable Full-Scale Load Testing.....	33
2.4.1	Hanshin Expressway Piers .....	33
2.4.2	Johannesburg Portal Frame .....	35
2.4.3	A26 Highway Bridge Deck.....	37
2.5	Conclusions from the Literature.....	37
2.6	Structural Assessment Plan .....	39
2.6.1	Overview .....	39
2.6.2	Design Factors affecting Experiments and Assessment.....	39
2.6.3	Evaluation of the Structural Capacity of Sound and Damaged Piers..	40
2.6.4	Evaluation of the Current Structure .....	41
<b>CHAPTER 3 DESIGN FACTORS AFFECTING EXPERIMENTS AND ASSESSMENT .....</b>		<b>42</b>
3.1	In-situ Engineering Properties.....	42
3.1.1	Concrete Testing .....	42
3.1.2	Reinforcing Steel Testing.....	43
3.2	Applicable Loads.....	44
3.2.1	Design Loads.....	44
3.2.2	Loads on Columns in the DD Spine.....	47
3.3	Special Design Considerations.....	48

<b>CHAPTER 4 EXPERIMENTAL PROGRAM .....</b>	<b>50</b>
4.1 Modeling of DD Spine Columns.....	50
4.2 Load Used For Experimental Research.....	52
4.3 Method of Cracking .....	54
4.3.1 Splitting Wedges .....	54
4.3.2 Hydraulic Packers .....	56
4.4 Design of Model Columns .....	57
4.4.1 Column Dimensions and Reinforcement .....	58
4.4.2 Footing Dimensions and Reinforcement.....	60
4.4.3 Placement of Instrumentation.....	62
4.4.3.1 Stain Gauges.....	62
4.4.3.2 Strain Meters .....	63
4.4.3.3 Load Monitoring .....	65
4.4.3.4 External Gauges .....	65
4.4.4 Bearing Pads and Spreader Beam .....	67
4.4.5 Concrete Mix Design .....	69
4.5 Testing.....	70
<b>CHAPTER 5 RESULTS FROM EXPERIMENTAL PROGRAM.....</b>	<b>74</b>
5.1 Specimen S1 .....	74
5.1.1 Load Capacity .....	74
5.1.2 Deflection Measurements.....	75
5.1.3 Strain Measurements .....	75
5.1.4 Failure . .....	78
5.1.5 Damage .....	78
5.2 Specimen S2.....	81
5.2.1 Load Capacity .....	81
5.2.2 Deflection Measurements.....	82

5.2.3 Strain Measurements .....	83
5.2.4 Failure . .....	84
5.2.5 Damage .....	86
5.3 Specimen C1 .....	87
5.3.1 Load Capacity .....	87
5.3.2 Deflection Measurements and Cracking .....	88
5.3.3 Strain Measurements .....	88
5.3.4 Failure . .....	89
5.3.5 Damage .....	89
5.4 Specimen C2 .....	90
5.4.1 Load Capacity .....	90
5.4.2 Deflection Measurements and Cracking .....	91
5.4.3 Strain Measurements .....	92
5.4.4 Failure . .....	93
5.4.5 Damage .....	94
5.5 Specimen C1-R .....	94
5.5.1 Load Capacity .....	95
5.5.2 Deflection Measurements and Cracking .....	95
5.5.3 Strain Measurements .....	96
5.5.4 Failure . .....	96
5.5.5 Damage .....	96
<b>CHAPTER 6 INTERPRETATION OF TEST RESULTS .....</b>	<b>98</b>
6.1 Introduction .....	98
6.2 Suggested Structural Assessment Methodology .....	98
6.2.1 Review Current Literature.....	98
6.2.2 Perform In-situ Site Investigations.....	99
6.2.3 Determination of Material Strengths.....	99

6.2.4 LRFR Provisions .....	100
6.2.5 Review of Original Design Calculation .....	100
6.2.6 Evaluation of the Structural Integrity of Existing Elements .....	101
6.2.7 Remedial Measures .....	102
6.3 Application of Assessment Methodology to Pier DD7 .....	102
6.3.1 Negative Factors Affecting Existing Pier Capacity .....	102
6.3.1.1 Literature Review .....	102
6.3.1.2 Review of Original Design Calculations.....	102
6.3.1.3 Effect of Cracking on Deflections and Capacity.....	106
6.3.2 Positive Factors Affecting Existing Pier Capacity .....	110
6.3.3 Net Affect of Factors on Pier Capacity .....	111
6.3.4 Remedial Measures .....	114
<b>CHAPTER 7 CONCLUSIONS AND IMPLEMENTATION.....</b>	<b>116</b>
7.1 Brief Summary .....	116
7.2 Conclusions .....	117
7.3 Implementation.....	119
7.4 Recommendations For Future Research .....	119
<b>APPENDIX A ADDITIONAL DESIGN INFORMATION .....</b>	<b>121</b>
A.1 Original Design Calculations .....	121
A.2 Application of Assessment Methodology to Pier DD7 .....	148

<b>APPENDIX B ADDITIONAL EXPERIMENTAL PROGRAM INFORMATION .....</b>	<b>149</b>
B.1 Interaction Failure Slices.....	149
B.2 Biaxial Column v2.3 Output .....	157
B.3 P vs. M Interaction Curves .....	168
B.4 Reinforcement Details.....	170
B.4.1 Prototype Pier Reinforcement .....	170
B.4.2 Model Pier Reinforcement .....	172
B.4.3 Footing Reinforcement for Model Pier .....	176
B.5 Formwork	178
B.5.1 Cracking Experiment.....	178
B.5.2 Model Pier .....	179
B.5.3 Footing for Model Pier .....	181
B.6 Position of External Gauges .....	182
B.6.1 Specimen S2 .....	182
B.6.2 Specimen C1 .....	183
B.6.3 Specimen C2 .....	184
B.6.4 Specimen C1-R .....	185
B.7 Position of Dial Gauges on Precracked Specimens .....	186
B.7.1 Specimen C1 .....	186
B.7.2 Specimen C2 .....	187
B.7.3 Specimen C1-R .....	188
<b>APPENDIX C ADDITIONAL EXPERIMENTAL RESULTS .....</b>	<b>189</b>
C.1 Specimen S2.....	189
C.2 Specimen C1 .....	192
C.2.1 Load vs. Deflection .....	192
C.2.2 Load vs. Strain.....	194

C.3	Specimen C2 .....	197
	C.3.1 Load vs. Deflection .....	197
	C.3.2 Load vs. Strain.....	199
C.4	Specimen C1-R .....	202
	C.4.1 Load vs. Deflection .....	202
	C.4.2 Crack Elongation.....	204
<b>APPENDIX D ADDITIONAL INTERPRETATION OF RESULTS INFORMATION .</b>		<b>205</b>
D.1	Strut and Tie Modeling .....	205
	D.1.1 Model Results.....	205
	D.1.2 Transverse Reinforcement in Model Pier.....	211
	D.1.3 Modified Strut-and-Tie Model .....	215
D.2	Bearing on Critical Pad .....	217
<b>REFERENCES .....</b>		<b>226</b>
<b>VITA .....</b>		<b>230</b>

## List of Figures

Figure 1.1: General Location of Column Spine DD .....	3
Figure 1.2: ASR and/or DEF Damage in Reinforced Concrete (DD-6) .....	4
Figure 1.3: ASR and/or DEF Damage in Reinforced Concrete (DD-7) .....	4
Figure 1.4: DEF Related Damage in DD-6 .....	5
Figure 2.1: Severe Map Cracking (CSA 2000) .....	13
Figure 2.2: Longitudinal Cracking of Spine DD Column .....	14
Figure 2.3: Microcracking in Aggregate Particles (Fournier 2004) .....	15
Figure 2.4: Static Load Bond Strength Test Results (Ahmed 1999, Materials)...	26
Figure 2.5: Bond Fatigue Life of ASR Damaged Specimens (Ahmed 1999, Materials) .....	27
Figure 2.6: Bearing Test Reinforcement (Ahmed 1999, Structural) .....	29
Figure 2.7: Bearing Capacity Test Results for Eccentrically Loaded Specimens (Ahmed 1999, Structural) .....	30
Figure 2.8: Small, Biaxially Loaded Test Specimens (Ahmed 1999, Structural) 30	30
Figure 2.9: Bearing Capacity Size Effect (Ahmed 1999, Structural) .....	31
Figure 2.10: Observed Crack Widths (Ahmed 1999, Structural) .....	32
Figure 2.11: Damaged Pier Cap (Imai 1987) .....	33
Figure 2.12: Hanshin Load Test Schematic (Imai 1987) .....	34
Figure 2.13: Severely Damaged Portal Frame (Blight 2000) .....	35
Figure 2.14: Schematic of Portal Frame (Blight 2000) .....	36
Figure 2.15: A29 Load Test Results (Baillemont 2000) .....	37
Figure 3.1: AASHTO Design Loads (AASHTO 1983) .....	44
Figure 3.2: AASHTO Design Loads Continued (AASHTO 1983) .....	45
Figure 3.3: Reference Axes .....	46
Figure 3.4: Design Load Distribution on Bearing Pads .....	48
Figure 3.5: Biaxial Load Distribution on Bearing Pads .....	49
Figure 4.1: Prototype and Model Columns .....	51
Figure 4.2: Splitting Wedge Test Specimen .....	55
Figure 4.3: Cracked Specimen using Splitting Wedges .....	55
Figure 4.4: Wedge Penetration vs. Crack Width for Splitting Wedge Method ...	56
Figure 4.5: Hydraulic Packer .....	56
Figure 4.6: Hydraulic Packer Test Setup .....	57
Figure 4.7: Design Location of PVC Pipes .....	59
Figure 4.8: Column Reinforcement Cage .....	60
Figure 4.9: Footing Dimensions .....	61
Figure 4.10: Footing Reinforcement Cage .....	61
Figure 4.11: Position of Strain Gauges .....	62

Figure 4.12: Strain Meter .....	63
Figure 4.13: Position of Strain Meters .....	64
Figure 4.14: Installed Strain Meters .....	64
Figure 4.15: Test S2 Linear Potentiometers .....	66
Figure 4.16: Crack Measuring Apparatus .....	67
Figure 4.17: Bearing Pad Dimensions and Layout .....	68
Figure 4.18: Spreader Beam .....	69
Figure 4.19: Test Setup .....	72
Figure 4.20: Specimen S2-Setup .....	73
Figure 5.1: S1-Load vs. Longitudinal Reinforcement Strain .....	76
Figure 5.2: S1-Load vs. Transverse Reinforcement Strain .....	77
Figure 5.3: S1-Load vs. Concrete Strain .....	77
Figure 5.4: S1-Initial Sign of Damage .....	79
Figure 5.5: S1-Concrete Crushing .....	80
Figure 5.6: S1-Fractured Transverse Ties .....	80
Figure 5.7: S2-Load vs. X-Axis Deflection .....	82
Figure 5.8: S2-Load vs. Y-Axis Deflection .....	83
Figure 5.9 (a-h): S2-Failure Sequence .....	85
Figure 5.10: S2-Bearing Failure .....	87
Figure 5.11: C2-Crack Widths .....	92
Figure 5.12: Specimen C2 Transverse Strain Measurements .....	93
Figure 5.13 (a-d): Specimen C1-R Damage .....	97
Figure 6.1: Strut-and-Tie Model for Reduced Scale Model Column .....	104
Figure 6.2: Load vs. X-direction Tip Deflection .....	107
Figure 6.3: Load vs. Y-direction Tip Deflection .....	108
Figure 6.4: Effect of Cracking on Bearing Capacity .....	110
Figure 6.5: Potential Column Reserve Capacities ( $f'_c = 5840$ psi) .....	113
Figure 6.6: Potential Column Reserve Capacities ( $f'_c = 3600$ psi) .....	113
Figure 6.7: Remedial Confining Forces .....	115
Figure A.1: Original Design Calculations (1 of 27) .....	121
Figure A.2: Original Design Calculations (2 of 27) .....	122
Figure A.3: Original Design Calculations (3 of 27) .....	123
Figure A.4: Original Design Calculations (4 of 27) .....	124
Figure A.5: Original Design Calculations (5 of 27) .....	125
Figure A.6: Original Design Calculations (6 of 27) .....	126
Figure A.7: Original Design Calculations (7 of 27) .....	127
Figure A.8: Original Design Calculations (8 of 27) .....	128
Figure A.9: Original Design Calculations (9 of 27) .....	129
Figure A.10: Original Design Calculations (10 of 27) .....	130
Figure A.11: Original Design Calculations (11 of 27) .....	131
Figure A.12: Original Design Calculations (12 of 27) .....	132
Figure A.13: Original Design Calculations (13 of 27) .....	133



Figure A.14: Original Design Calculations (14 of 27).....	134
Figure A.15: Original Design Calculations (15 of 27).....	135
Figure A.16: Original Design Calculations (16 of 27).....	136
Figure A.17: Original Design Calculations (17 of 27).....	137
Figure A.18: Original Design Calculations (18 of 27).....	138
Figure A.19: Original Design Calculations (19 of 27).....	139
Figure A.20: Original Design Calculations (20 of 27).....	140
Figure A.21: Original Design Calculations (21 of 27).....	141
Figure A.22: Original Design Calculations (22 of 27).....	142
Figure A.23: Original Design Calculations (23 of 27).....	143
Figure A.24: Original Design Calculations (24 of 27).....	144
Figure A.25: Original Design Calculations (25 of 27).....	145
Figure A.26: Original Design Calculations (26 of 27).....	146
Figure A.27: Original Design Calculations (27 of 27).....	147
Figure A.28: Biaxial Load Distribution .....	148
Figure B.1: Interaction Slice, Load Case I-2 Lane.....	149
Figure B.2: Interaction Slice, Load Case I-3 Lane.....	150
Figure B.3: Interaction Slice, Load Case II.....	151
Figure B.4: Interaction Slice, Load Case III-2 Lane .....	152
Figure B.5: Interaction Slice, Load Case III-3 Lane .....	153
Figure B.6: Interaction Slice, Load Case V .....	154
Figure B.7: Interaction Slice, Load Case VI-2 Lane.....	155
Figure B.8: Interaction Slice, Load Case VI-3 Lane.....	156
Figure B.9: Program Output (1 of 12).....	157
Figure B.10: Program Output (2 of 12).....	158
Figure B.11: Program Output (3 of 12).....	159
Figure B.12: Program Output (4 of 12).....	160
Figure B.13: Program Output (5 of 12).....	161
Figure B.14: Program Output (6 of 12).....	162
Figure B.15: Program Output (7 of 12).....	163
Figure B.16: Program Output (8 of 12).....	164
Figure B.17: Program Output (9 of 12).....	165
Figure B.18: Program Output (10 of 12).....	166
Figure B.19: Program Output (11 of 12).....	167
Figure B.20: Program Output (12 of 12).....	168
Figure B.21: Interaction Curve, Case III-2 Lane Loading .....	168
Figure B.22: Interaction Curve, Cases I, 2 and 3 Lane Loading.....	169
Figure B.23: Prototype Column Reinforcement (1 of 2) .....	170
Figure B.24: Prototype Pier Reinforcement (2 of 2).....	171
Figure B.25: Model Pier Reinforcement (1 of 4).....	172
Figure B.26: Model Pier Reinforcement (2 of 4).....	173
Figure B.27: Model Pier Reinforcement (3 of 4).....	174

Figure B.28: Model Pier Reinforcement (4 of 4).....	175
Figure B.29: Footing Reinforcement for Model Pier (1 of 2).....	176
Figure B.30: Footing Reinforcement for Model Pier (2 of 2).....	177
Figure B.31: Cracking Experiment Formwork .....	178
Figure B.32: Model Pier Formwork (1 of 2).....	179
Figure B.33: Model Pier Formwork (2 of 2).....	180
Figure B.34: Footing Formwork .....	181
Figure B.35: S2 – Position of External Gauges .....	182
Figure B.36: C1 – Position of External Gauges .....	183
Figure B.37: C2 – Position of External Gauges .....	184
Figure B.38: C1-R – Position of External Gauges .....	185
Figure B.39: C1 – Position of Dial Gauges.....	186
Figure B.40: C2 – Position of Dial Gauges.....	187
Figure B.41: C1-R – Position of Dial Gauges.....	188
Figure C.1: S2 – Load vs. Longitudinal Reinforcement Strain.....	189
Figure C.2: S2 – Load vs. Transverse Reinforcement Strain.....	190
Figure C.3: S2 – Load vs. Concrete Strain.....	191
Figure C.4: C1 – Load vs. X-direction Deflection.....	192
Figure C.5: C1 – Load vs. Y-direction Deflection.....	193
Figure C.6: C1 – Load vs. Longitudinal Reinforcement Strain .....	194
Figure C.7: C1 – Load vs. Transverse Reinforcement Strain .....	195
Figure C.8: C1 – Load vs. Concrete Strain .....	196
Figure C.9: C2 – Load vs. X-direction Deflection.....	197
Figure C.10: C2 – Load vs. Y-direction Deflection.....	198
Figure C.11: C2 – Load vs. Longitudinal Reinforcement Strain .....	199
Figure C.12: C2 - Load vs. Transverse Reinforcement Strain .....	200
Figure C.13: C2 - Load vs. Concrete Strain.....	201
Figure C.14: C1-R – Load vs. X-direction Deflection.....	202
Figure C.15: C1-R – Load vs. Y-direction Deflection.....	203
Figure C.16: C1-R – Crack Elongation.....	204
Figure D.1: S-T-M Model (1 of 6) .....	205
Figure D.2: S-T-M Model (2 of 6) .....	206
Figure D.3: S-T-M Model (3 of 6) .....	207
Figure D.4: S-T-M Model (4 of 6) .....	208
Figure D.5: S-T-M Model (5 of 6) .....	209
Figure D.6: S-T-M Model (6 of 6) .....	210
Figure D.7: Model Pier Reinforcement (1 of 2).....	211
Figure D.8: Model Pier Reinforcement (2 of 2).....	212
Figure D.9: Equivalent Tensile Reinf. Loading (1 of 2).....	213
Figure D.10: Equivalent Tensile Reinf. Loading (2 of 2).....	214
Figure D.11: Modified S-T-M (1 of 2).....	215
Figure D.12: Modified S-T-M (2 of 2).....	216

Figure D.13: Bearing Calculations (1 of 9).....	217
Figure D.14: Bearing Calculations (2 of 9).....	218
Figure D.15: Bearing Calculations (3 of 9).....	219
Figure D.16: Bearing Calculations (4 of 9).....	220
Figure D.17: Bearing Calculations (5 of 9).....	221
Figure D.18: Bearing Calculations (6 of 9).....	222
Figure D.19: Bearing Calculations (7 of 9).....	223
Figure D.20: Bearing Calculations (8 of 9).....	224
Figure D.21: Bearing Calculations (9 of 9).....	225

## LIST OF TABLES

Table 2.1: Concrete Compressive Strength Reduction .....	18
Table 2.2: Concrete Tensile Strength Reduction .....	19
Table 2.3: Elastic Modulus Reduction .....	20
Table 3.1: Concrete Testing Results .....	42
Table 3.2: Rockwell Hardness Testing .....	43
Table 3.3: Factored Column Design Loads (With Centrifugal Force).....	46
Table 3.4: Factored Column Design Loads (Without Centrifugal Forces) .....	47
Table 4.1: Load Eccentricities (Without Centrifugal Forces) .....	53
Table 4.2: Model Column Design Load.....	54
Table 4.3: Concrete Mix Design .....	69
Table 4.4: Compressive Strengths.....	70
Table 5.1: Specimen S1 Load Capacity .....	75
Table 5.2: Specimen S2 Load Capacity .....	81
Table 5.3: Specimen C1 Load Capacity.....	88
Table 5.4: Specimen C2 Load Capacity.....	91
Table 5.5: Specimen C1-R Load Capacity.....	95
Table 6.1: Transverse Reinforcement Capacity .....	104
Table 6.2: Test Specimen Crack Widths.....	106
Table 6.3: Ultimate Load vs. Crack Width .....	109

# **CHAPTER 1**

## **Introduction**

### **1.1 PROBLEM STATEMENT**

In recent years, it has been discovered that some structural elements of the I-10 and I-35 corridor passing through San Antonio, Texas (San Antonio Y) are suffering from concrete durability related forms of distress. It has been determined through TxDOT Project 0-4085 that this distress is a result of two forms of concrete durability related phenomena, alkali-silica reaction (ASR) and delayed ettringite formation (DEF) (Folliard 2005). Due to the fact that this integral stretch of interstate highway sees a large volume of traffic, it is desirable to determine a method of assessing the degree of damage and the necessity of taking remedial actions. If serious damage requires remedial action, it is then desirable to determine methods which can be used to repair the existing structures in order to avoid reconstruction. In order to formulate a solution to this problem, the current load carrying capacity of the structural elements under consideration must be evaluated. While there is considerable evidence of material distress, very little research has been conducted which attempts to quantify the amount of structural damage caused by ASR and DEF on the load carrying capacity of columns. It is therefore necessary to attempt to simulate the existing damage and try to determine its effect through experimental research.

## **1.2 BACKGROUND**

### **1.2.1 The San Antonio Y**

The San Antonio Y is a stretch of interstate highway that passes through San Antonio, Texas in Bexar County. It is a combination of interstate highways 10 and 35. In the late 1980s, portions of this section of highway were elevated above ground. The bulk of the construction on this project took place in 1986 and 1987 under federal aid project number I35-2(190)154.

As noted in the problem statement, it has been discovered that a series of columns in this section of elevated roadway are experiencing materials related distress. This series of columns is labeled spine DD as per the construction documents and is located just north of Market Street in downtown San Antonio as shown in Figure 1.1. When viewing the construction documents, the general plan of this spine of columns begins on page 395 at station 388+80 and ends on page 404 at station 439+28. These piers were chosen for further investigation under TxDOT Project 0-5218.

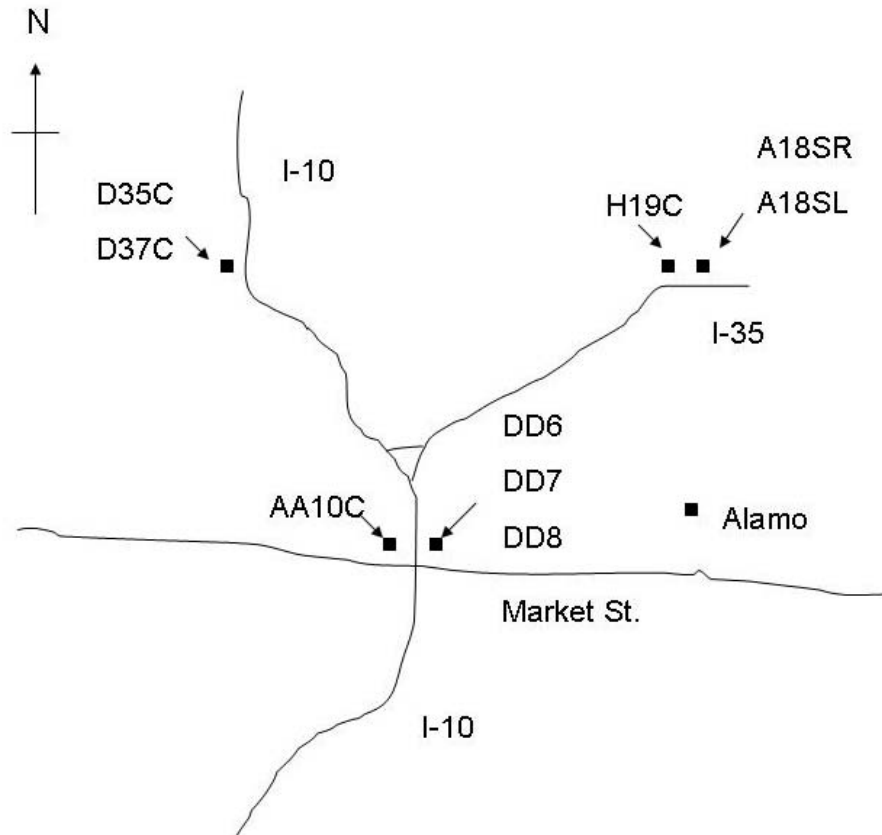


**Figure 1.1: General Location of Column Spine DD**

### **1.2.2 Concrete Materials Issues**

Through testing conducted at the Concrete Durability Center at The University of Texas at Austin, it has been found that many structural elements in the San Antonio Y, including the columns in spine DD, are suffering from materials related distress. The two main causes for distress are Alkali-Silica Reaction (ASR) and/or Delayed Ettringite Formation (DEF) (Folliard 2005). ASR and DEF are both chemically related internal forms of deterioration in concrete. Figures 1.2 and 1.3 are illustrations of the type of damage that can occur in reinforced concrete suffering from ASR and/or DEF.



*Figure 1.2: ASR and/or DEF Damage in Reinforced Concrete (DD-6)*



*Figure 1.3: ASR and/or DEF Damage in Reinforced Concrete (DD-7)*



ASR is a well known form of concrete deterioration. For ASR to take place the following three key components must be present in the concrete: sufficient alkali content, reactive silica in the aggregate, and moisture. When all three elements are present, a chemical reaction takes place between the alkalis and the reactive aggregate. A byproduct of this reaction is an expansive gel. When exposed to moisture, the gel swells and causes internal expansive forces to form in the concrete which can cause cracking (CSA 2000).

DEF is another form of durability related distress in concrete. It is a type of internal sulfate attack where ettringite forms several months or years after the concrete has hardened. DEF can be attributed to a thermal decomposition mechanism. Ettringite which is formed in the early age of the concrete is destroyed by high temperatures ( $>158^{\circ}F$ ). Then, when the concrete element is later exposed to moisture, ettringite develops again as sulphate ions are released into the concrete. This crystal growth of ettringite causes swelling forces to form in the concrete which can cause cracking (Colleparidi 2003). Figure 1.4 is an illustration of DEF related damage in column DD-6 in the San Antonio Y.



*Figure 1.4: DEF Related Damage in DD-6*

Through studies done on cores taken from various elements of the San Antonio Y, researchers at The University of Texas at Austin were able to determine that many structural elements in the San Antonio Y have a large potential for future expansion. This research revealed that the potential for future expansion as a result of both ASR and DEF exists. Advanced petrographic techniques and Scanning Electron Microscope methods were used in order to attempt to evaluate the damage that has occurred in several of the structural elements. Significant internal damage was found to have occurred in elements DD-6, DD-7, and H19-C. The results of these findings indicate that a large portion of the damage in these structural elements is related to DEF. In summary, many structural elements in the San Antonio Y have suffered from or have a high potential of suffering from deterioration related to ASR and/or DEF ( Folliard 2004). It should be noted that research related to materials topics involving the San Antonio Y is still in progress at The University of Texas under TxDOT Project 0-5218. These material topics are not the focus of this thesis which centers on structural concerns that may or may not be materials related.

### **1.2.3 Structural Issues**

In order to properly evaluate the integrity of the existing structure, some key elements must be investigated. In particular, the strength degradation of the existing columns must be quantified. In order to do this, the effect that the ASR/DEF type cracking has on the columns must be determined. It is also important to determine the reserve capacity, if any, that these columns possess. The assessment of the structural integrity of the columns should attempt to consider all major variables. These variables may include strength degradation, quality of design, and accuracy of loads.

The strength degradation as referred to in this text is whatever loss in load carrying capacity that a structural element may exhibit when compared to its initial load carrying capacity prior to any form of deterioration. Strength degradation can be caused by weakening of concrete, corrosion of reinforcing steel, fire, or any other form of attack which has an effect of reducing the ultimate strength of the structural element. In this case, the investigation is being conducted to determine the possibility of strength degradation as a direct result of cracking due to the two forms of chemical attack known as ASR and DEF.

In order to properly evaluate an existing structural element, it is important to consider several aspects. One aspect is the comparison of actual material strengths and dimensions versus the designer's expectations before construction. Considerable reserve or deficiency is possible if actual material strengths differ from design assumptions. The second aspect is the potential mode of failure under expected loading. This includes mode of failure, region of failure, and type of failure. In particular, a concrete column subjected to both axial load and flexure has three primary potential modes of failure. These modes are failure under combined axial load and flexure due to yielding of the longitudinal reinforcing steel and/or crushing of the concrete, failure in shear, and local or bearing failure. Shear failures in this case are unlikely due to the large axial loads and relatively small shearing forces which are exerted on the type of structural element under investigation. Columns designed to carry large moments are often governed by yielding of the reinforcement in tension. These columns are designed at or below the point on the axial load versus moment interaction diagram where the strain in the reinforcing steel causes yielding at the same time the strain in the concrete causes crushing (i.e. the balance point). Columns which are designed above this point on the interaction curve are governed by the concrete crushing prior to yielding in tension of the longitudinal reinforcing steel.

For very small eccentricities, the reinforcement can yield in compression prior to concrete crushing. Columns can also fail in bearing as a result of large local compressive stresses in the local zone under the point of application of the load.

When discussing behavior of structural elements, there are two general types of failures, ductile and brittle. Ductile failures provide two key elements that are beneficial to the structural engineer. First and foremost ductile failures allow for the redistribution of forces throughout a structural element and its surrounding structural system. They also provide early warning to the engineer that the structure may be under distress. Of the modes of failure listed previously, flexural tensile yielding of the longitudinal reinforcement can be characterized as a ductile failure mode. Brittle failures can be characterized by a sudden rapid failure which is usually catastrophic. Brittle failures do not allow for the redistribution of forces. Of the failure modes mentioned in the previous paragraph, shear, bearing, and concrete crushing can all be described as brittle failures. In design provisions under AASHTO, larger factors of safety are used when brittle type failures may occur.

There are two specific types of regions within a structural element in which failures can occur. These regions can be defined as B-regions and D-regions. These regions can be differentiated through the application of Saint Venant's principle. D stands for discontinuity regions and B stands for bending regions. Saint Venant's principle implies that local stresses due to concentrated loads or geometrical discontinuities become uniform at a distance away from the region equal to or greater than the largest dimension of the loaded region or geometrical discontinuity (Gere 1997). Thus B-regions exist where the strains are linear, and D-regions exist in all areas where the strains are not linear. In B-regions Bernoulli's hypothesis of plane sections remaining plain is satisfied (i.e. linear strain profile throughout the cross-section of the element). In contrast, D-

regions are characterized as areas where the strain profile exhibits significant nonlinearities as a direct result of either statical and/or geometrical discontinuities (Bergmeister 1993). Failures which occur in either of these two regions must be treated differently and analyzed accordingly.

In addition to strength degradation, accuracy of design, and accuracy of loads will also be considered in the structural evaluation. In order to properly determine the capacity of a structural element, the assumptions that were used in design must be determined and considered in the evaluation. Also, the loads that are actually on the structure can be much different than those used for design. It is therefore desirable to determine which loads were used in design and how they relate to the actual loads on the structure.

In summary, there are many non-materials related issues which must be considered when attempting to evaluate the integrity of a structural element suffering from materials related deterioration. In this case the key issues which must be investigated are the actual versus as-built material properties, strength degradation, accuracy of design, and accuracy of loads.

### **1.3 OBJECTIVE AND SCOPE**

The objective of this portion of Project 5218 is to attempt to evaluate the structural integrity of the existing columns in spine DD of the San Antonio Y. In order to accomplish this task, it is important to consider the actual versus as-built material properties and dimensions, strength degradation, accuracy of design, and accuracy of loads. To properly evaluate strength degradation the governing failure mode of the structural element under consideration must be determined. Only then can an attempt be made to quantify the effect of the strength degradation in columns that may result from severe concrete deterioration related to ASR and/or DEF. A large amount of materials related research has been

conducted on this segment of highway. However, no attempt has been previously made to translate this materials information into any form of structural assessment. In addition, no attempt has been made to evaluate the existing piers without materials related damage. As a result, an attempt will be made to gain a better understanding of the structural integrity of the columns in the DD spine of the San Antonio Y by reviewing information in the current literature and conducting an experimental program which attempts to evaluate the existing structural element and quantify the strength degradation that may have occurred in the piers.

#### **1.4 ORGANIZATION**

This thesis is organized into seven main chapters which are listed as follows:

- Chapter one provides an introduction to the project, which outlines the problem, provides relevant background information, describes the key objectives and scope, and lists the organization of the thesis.
- Chapter two consists of a review of the current literature related to ASR and DEF, and its effect on concrete structures. In addition, chapter two provides an outline of the structural assessment plan for this project.
- Chapter three is a review of design factors affecting the experiments and structural assessment of the piers under investigation.
- Chapter four provides details of the experimental program including cracking procedure, test specimen design, and testing.
- Chapter five lists the results from the experimental program for all of the test specimens.
- Chapter six attempts to provide some interpretation of the results by comparing the information listed in chapter five. In addition, chapter six

will provide an assessment of the current structural integrity of the piers in the San Antonio Y.

- Chapter seven provides conclusions reached as a direct result of this research study. It outlines ways in which these conclusions may be implemented on future research that may be conducted relating to this project or actions that may be taken regarding the existing structure.

## **CHAPTER 2**

### **Literature Review and Project Plan**

#### **2.1 DIAGNOSIS OF ASR AND DEF**

When studying structural elements suffering from deterioration, the first step is determining the cause of distress. In concrete elements the cause of distress can be a result of materials related and/or structural related issues. If the problem is materials related, it is important to determine which durability related form of distress is taking place. In the case of the San Antonio Y, the distress is believed to be a result of ASR and DEF. It is therefore important to outline how a structure can be diagnosed as having ASR and/or DEF related deterioration.

##### **2.1.1 External Diagnosis of ASR**

Concrete suffering from ASR related deterioration exhibits some distinct external characteristics. Symptoms of ASR which can generally be identified through field inspection are as follows: expansion causing deformation, relative movement and displacement, cracking, surface discoloration, gel exudations, and pop-outs. It is worth noting that these symptoms are not necessarily a definitive indication that ASR is the sole source of the problem. It is therefore important to consider other factors which can help identify whether or not ASR is the primary cause of concrete deterioration.

Environmental conditions can help identify the cause of cracking. Expansion and cracking due to ASR is usually most extensive when the concrete is exposed to moisture. It has also been found that surfaces of concrete exposed to sun, frost action, and wetting and drying cycles also show more severe cracking and deterioration (Fournier 2004).



The type of movements and displacements that a structural element experiences can indicate whether or not ASR is at the source of the problem. It is typical for the amount of ASR to vary throughout the volume of a structural element. Therefore, elements affected by ASR typically exhibit uneven or differential concrete swelling causing relative movement, misalignment, and distortion (Fournier 2004).

The type of cracking can also give an indication as to whether or not ASR is causing the deterioration. There are four key factors which influence the pattern of cracking which results from ASR including: geometry of the concrete element, environmental conditions, the presence and pattern of reinforcement, and the loads applied to the structural element. Map cracking is often associated with, but not exclusive to, concrete elements suffering from ASR which do not experience major stresses or are unrestrained (Fournier 2004). An example of map cracking as a result of ASR is shown in Figure 2.1.

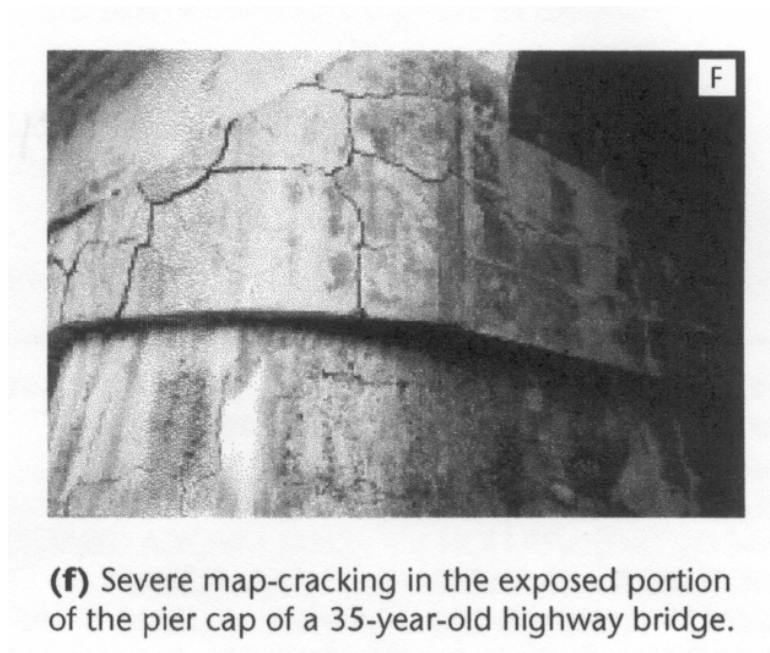


**Figure 2.1: Severe Map Cracking (CSA 2000)**

Cracking associated with ASR will generally reflect the reinforcement pattern or the direction of major stresses in restrained or significantly stressed elements. Longitudinal cracking along the path of the primary reinforcement is typical in reinforced concrete columns and beams. This type of cracking is typical of the columns in the DD spine of the San Antonio Y as shown in Figure 2.2.



***Figure 2.2: Longitudinal Cracking of Spine DD Column***

Multiple cracking patterns can exist simultaneously in concrete elements suffering from ASR (Fournier 2004). It should also be noted that the various types of cracking mentioned in this section are not exclusive to ASR and can be associated with other forms of concrete distress.

Other symptoms which may exist but are not limited to ASR are discoloration, surface deposits, and pop-outs. Surface exudations in the form of ASR gel often exist in structural elements suffering from ASR. However, it is good practice to sample the deposits to ensure that they are composed of ASR gel (Fournier 2004). All the symptoms listed in this section are a good preliminary indication that ASR may be the primary cause of deterioration. However, in order

to conclusively define the source of the problem some physical testing is necessary.

### **2.1.2 Internal Diagnosis of ASR**

The best method of determining whether or not ASR is at the source of materials related deterioration is to perform a petrographic examination of cores taken from the damaged structural elements. One trait which can occur as a result of ASR and can be observed by a petrographic examination is microcracking. Microcracking due to ASR usually exists in the aggregate particles and the cement paste-aggregate interface. In severe cases microcracks can extend from the aggregate particles to the cement paste. Figure 2.3 illustrates microcracking through aggregate particles on a polished concrete section.

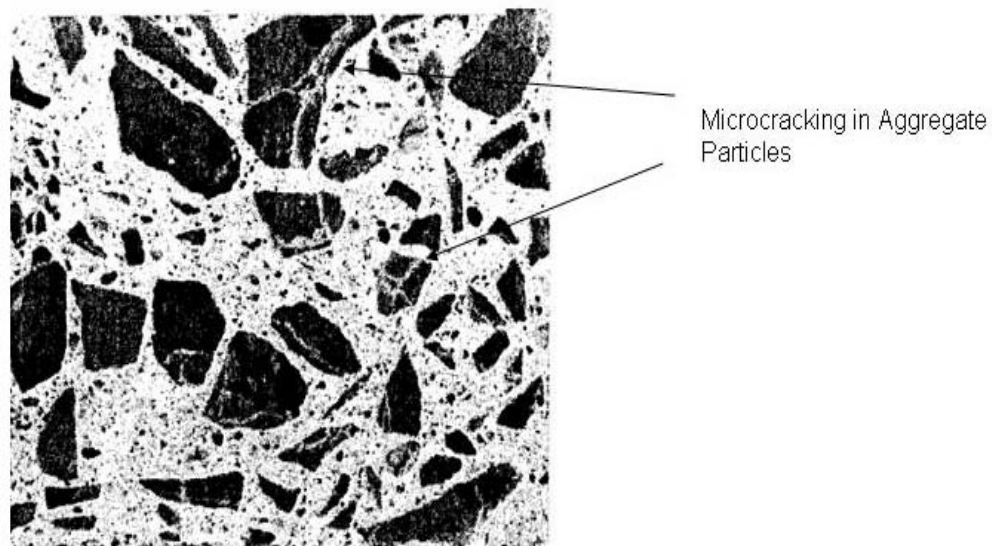


***Figure 2.3: Microcracking in Aggregate Particles (Fournier 2004)***

A second trait which can be observed is the presence of secondary reaction products or ASR gel. This gel can be found in the gaps produced by microcracking in the aggregate particles and the cement paste. Dark reaction rims

may also be observed around the internal periphery of the reactive aggregate particles (Fournier 2004).

Expansion testing on concrete cores can also be used to diagnose ASR. This testing involves placing concrete cores in a highly alkaline environment at moderately high temperatures ( $176^{\circ}F$ ) in order to trigger expansion due to ASR while preventing DEF. This test results in an upper bound giving the maximum possible value for future expansion (Folliard 2005).

### **2.1.3 External Diagnosis of DEF**

Structures under material related distress as a result of DEF exhibit many of the same external symptoms as those suffering from ASR. DEF can be linked to deterioration resulting in expansion causing deformation, relative movement and displacement, cracking, and pop-outs. The primary difference between the two mechanisms of deterioration is the presence of gel which is a secondary reaction product of ASR and does not form as a result of DEF. It is therefore necessary to perform experimental work to confirm the presence of DEF (Folliard 2005).

### **2.1.4 Internal Diagnosis of DEF**

The presence of deterioration related to DEF can be diagnosed through petrographic examination of cores and expansion testing. Concrete cores suffering from DEF will display large amounts of ettringite, gapping of aggregates, and cracking through both the aggregate and the cement paste upon petrographic examination. Expansion tests which involve soaking cores in water at  $73^{\circ}F$  can also help determine the future potential of DEF related expansion. Soaking the cores in water helps to lower their pH which promotes DEF while preventing ASR. This test gives a good indication of the potential for future expansion which may result from DEF (Folliard 2005). In conclusion, when

determining the primary source of distress, it is important to note that sufficient evidence of ASR and/or DEF from multiple cores must be gathered from the experimental study to confirm that the distress is dominated by ASR and/or DEF.

## **2.2 EFFECTS OF ASR AND DEF ON ENGINEERING PROPERTIES OF CONCRETE**

When performing structural evaluations of concrete elements suffering from materials related deterioration, it is important to consider what effect the deterioration has on the engineering properties of concrete. Engineering properties that need to be evaluated are compressive strength, tensile strength, modulus of elasticity, and bond strength. Considerable research has been performed in relation to these properties regarding deterioration resulting from ASR. However, very little information exists which relates the effect of DEF induced expansion to the engineering properties of concrete. It has therefore been decided to focus herein on the structural effects of ASR and omit any DEF related discussion regarding these properties.

### **2.2.1 The Effect of ASR on the Compressive Strength of Concrete**

The effect of ASR on the compressive strength of concrete is dependent upon the amount of restraint present in the specimen. It is therefore advantageous to review material testing for both unrestrained and restrained concrete.

#### **2.2.1.1 *Unrestrained Concrete***

ASR has a distinct effect on the unconfined compressive strength of concrete. In tests done by Clayton, specimens were made with a reactive ASR mix and tested in both cube compression and tall prism compression. The results indicated up to a thirty percent loss in compressive strength when compared to twenty eight day values. Specimens were tested at various levels of expansion, and it was found that the compressive strength reduced as the expansion

increased. However, this trend continued only to a level of expansion of 500 microstrain, after which the values remained relatively constant (Clayton 1989).

Testing done in Japan on cores taken from an actual structure suffering from ASR also indicated a reduction in compressive strength. Preliminary testing conducted shortly after the structure was diagnosed as having ASR indicated the compressive strength could have been lowered by ASR (Okado 1989). Additional tests conducted on the same structure over an eleven year period indicated an additional reduction in the compressive strength of the concrete on the order of thirteen percent (Ono 2000).

A report issued by The Institution of Structural Engineers (IStructE) confirms the above arguments that the concrete strength is reduced by ASR. However, this report contradicts the findings of Clayton that the compressive strength remains constant above a level of expansion of 500 microstrain. The results found in the report issued by IStructE can be viewed in Table 2.1 (IStructE 1992).

**Table 2.1: Concrete Compressive Strength Reduction**

	Percentage strength as compared with unaffected concrete for various levels of expansion				
	500 (microstrain)	1000 (microstrain)	2500 (microstrain)	5000 (microstrain)	10000 (microstrain)
Cube Compression	100	85	80	75	70
Uniaxial Compression	95	80	60	60	*

A guide issued by The Canadian Standards Association (CSA) International in 2000 indicated that a reduction in the unrestrained compressive strength of concrete on the level of sixty percent is possible as a result of ASR related deterioration (CSA 2000). From these readings it can be concluded that ASR has a significant strength reducing effect on unrestrained concrete.

### 2.2.1.2 *Restrained Concrete*

Concrete suffering from ASR which is restrained behaves differently when compared to unrestrained concrete. ASR induces swelling pressures, which when the concrete is restrained, have a prestressing effect. This allows the concrete to retain most of its compressive strength (Blight 1996). The report issued by IStructE supports this evidence by stating that concrete in actual structures is generally restrained and in a biaxial or triaxial state of stress. This restraint reduces the damage to the concrete and increases the residual mechanical properties (IStructE 1992). It can therefore be concluded that at reasonable levels of expansion the majority of the compressive strength of concrete is retained in situations where the concrete is adequately restrained from swelling.

### 2.2.2 **The Effect of ASR on the Tensile Strength of Concrete**

Evidence in the literature has shown that ASR has a conclusive, negative effect on the tensile strength of concrete. In addition to compression testing, Clayton also performed cylinder splitting, flexure, and gas pressure tension testing on ASR affected concrete. His results indicated up to a sixty percent reduction in the tensile strength of the concrete (Clayton 1989). These results are substantiated by the report issued by IStructE. Table 2.2 indicates the reduction in tensile capacity of specimens suffering from ASR when tested using the splitting tension or torsional tension strength testing methods (IStructE 1992).

**Table 2.2: Concrete Tensile Strength Reduction**

	Percentage elastic modulus as compared with unaffected concrete for various levels of expansion				
	500 (microstrain)	1000 (microstrain)	2500 (microstrain)	5000 (microstrain)	10000 (microstrain)
Tension	100	85	80	75	70

The report issued by CSA International provides further indication that the tensile strength of concrete can be lowered as a result of ASR. Values of reduction ranging from forty to eighty percent were reported. These values are somewhat dependent on the method of testing, with values closer to forty percent resulting from splitting or torsional testing, and values closer to eighty percent resulting from gas pressure testing (CSA 2000). In conclusion, large reductions in the tensile strength of concrete can be expected when evaluating concrete suffering from ASR related deterioration.

### **2.2.3 The Effect of ASR on the Elastic Modulus and Creep Properties of Concrete**

Much of the research done on ASR indicates that it has a reducing effect on the elastic modulus of concrete. Values reported by IStructE on concrete core samples indicate a reduction in the elastic modulus. The results from this report can be viewed in Table 2.3 (IStructE 1992).

**Table 2.3: Elastic Modulus Reduction**

	Percentage strength as compared with unaffected concrete for various levels of expansion				
	500 (microstrain)	1000 (microstrain)	2500 (microstrain)	5000 (microstrain)	10000 (microstrain)
Elastic Modulus	100	70	50	35	30

Tests done by Blight on cores taken from a reinforced concrete portal frame also indicated a significant reduction in the elastic modulus. Elastic deformations recorded for ASR damaged concrete were on the order of three and one half times that of non-deteriorated concrete. Long term testing on these specimens also indicated an increase in creep strain at a level of two and a half to



four times the magnitude when compared to unaffected concrete (Blight 1996). CSA International reports that the elastic modulus can be reduced by thirty percent. It is also worth noting that the reduction in the modulus and the increase in creep strain can reduce the prestressing effect mentioned in the section on concrete compressive strength in this text (CSA 2000).

Although there is definitive evidence that ASR reduces the elastic modulus of core samples, there are conflicting opinions as to whether or not this reduction takes place in actual structures. Tests conducted in Japan on cores taken from an existing structure indicated a reduction in the elastic modulus of the concrete. However, when analyzing the results from a load test conducted on the same structure, it was back calculated that the reduction in the modulus was not significant. It was therefore suggested that this difference may be a result of the release of restraint that the cores experience when compared to the existing structure (Okado 1989). Contrary to these results, Blight found good agreement between values predicted using a reduced modulus and the results of a full scale load test (Blight 1989). In summary, it can be seen that deterioration in the form of ASR significantly reduces the modulus and increases the creep strain of concrete cores. However, the degree to which ASR reduces the elastic modulus of the actual structure cannot be certain at this time.

### **2.3 EFFECTS OF ASR AND DEF ON STRUCTURAL PROPERTIES OF REINFORCED CONCRETE**

When evaluating reinforced concrete elements suffering from ASR and/or DEF, it is imperative to determine what effect these reactions have on the structural properties of such elements. Structural properties which may need to be evaluated are axial strength, flexural strength, shear strength, bond strength, bearing strength, and deflections. Substantial research has been performed in

relation to many of these properties regarding deterioration resulting from ASR. On the contrary, very little documentation exists which relates the effect of DEF related expansion to the structural properties of concrete. It has therefore been decided to focus on the effect of ASR and omit any DEF related discussion regarding the structural properties of reinforced concrete at this time.

### **2.3.1 The Effect of ASR on the Axial Strength of Reinforced Concrete**

It is important to consider the effect that damage resulting from ASR has on structural elements which are stressed with large axial loads. While performing structural evaluations of actual structures suffering from ASR, Wood found that if the reinforcing steel forms an adequate three dimensional cage the ultimate strength loss is minimal until secondary deterioration from spalling concrete or corrosion of the reinforcing steel becomes serious. However, where adequate confinement is not present the loss in ultimate strength can be substantial (Wood 1983).

In tests conducted by Takemura on nearly full-scale specimens, it was found that if adequate confinement is present, ASR can actually increase the ultimate load bearing capacity of columns. This was believed to be a result of the effective prestressing forces that are induced in the axial steel as a result of ASR. These forces resulted in the axial reinforcement yielding in compression at a higher ultimate load. However, in column specimens where adequate confinement was not present, the transverse reinforcement yielded prior to compression yielding of the axial reinforcement. This resulted in a thirty percent reduction in ultimate load bearing capacity (Takemura 1999).

The report issued by IStructE in 1992 questioned the validity of Takemura's findings, stating that the results may not be accurate due to the fact that the test method used to accelerate ASR may have distorted the concrete

properties. This document argues that the concrete compressive strength is reduced by ASR and delamination can occur along the plain of the primary reinforcement. Cracks of 0.012 inches (0.3 mm) or larger in the vicinity of the main edge reinforcement are described to be significant evidence of cover delamination. This delamination can reduce the effective cross-section of the column and result in loss of some buckling restraint of the primary reinforcement (IStructE 1992). In conclusion, if adequate confinement is provided and expansion has not caused delamination of the concrete cover, then the majority of the ultimate load bearing capacity of members damaged by ASR under large axial loads is believed to be retained.

### **2.3.2 The Effect of ASR on the Flexural Strength of Reinforced Concrete**

The report issued by The Institution of Structural Engineers indicated that ASR does not have a significant effect on the flexural strength of reinforced concrete beam elements. This is provided that free expansion does not exceed 6000 microstrain. Expansion levels above this value have indicated losses in flexural strength of up to twenty five percent (IStructE 1992). These findings were confirmed by test done on reinforced concrete beams by Monette. Monette tested singly reinforced concrete beams which were made with a reactive mix and subjected to the following conditioning regimes: non-loaded, statically loaded or dynamically loaded to their service level. After significant expansion had taken place, the beams were tested, and it was concluded that the ultimate flexural capacity of the deteriorated beams was maintained (Monette 2000). It can therefore be concluded that at moderate levels of expansion, ASR has little effect on the ultimate flexural strength of reinforced concrete.

### **2.3.3 The Effect of ASR on the Shear Strength of Reinforced Concrete**

Tests performed in order to quantify the effect of ASR on the shear strength of reinforced concrete have indicated no significant decrease in the shear capacity of such elements. In some tests the shear capacity was even found to increase as a result of ASR related expansion. This increase is believed to be a result of the prestressing effect resulting from the restrained ASR expansion. Tests indicated good behavior with anchorages to the main reinforcement as small as 3.4 times the bar diameter (IStructE 1992). However, the negative effect of ASR on the tensile strength of concrete should be considered when evaluating the shear strength. If the concrete element under consideration relies on the concrete for some or all of the required shear strength, then ASR can have a negative effect on shear capacity by reducing the tensile strength of the concrete (Siemes 2000). In conclusion, if adequate shear reinforcement is provided, very little reduction in shear capacity can be expected from deterioration resulting from ASR.

### **2.3.4 The Effect of ASR on Bond Strength**

Deterioration related to ASR can reduce the bond strength in reinforced concrete. Tests conducted by Chana on anchorage bond and lap bars for both ribbed and smooth bars have found very little effect on bond when adequate cover is provided. Free expansions up to 4000 microstrain showed no significant effect provided the bars were restrained by stirrups and a concrete cover of at least 4 bar diameters was provided. On the contrary, a fifty percent reduction in bond strength was found for bars not restrained by stirrups and with a cover around 1.5 times the bar diameter. In these cases, the reduction in bond strength was found to be proportional to the reduction in splitting tensile strength which occurred as a result of ASR (IStructE 1992).

Additional testing was conducted by Ahmed on tensile bond strength of concrete damaged by ASR under static and fatigue loading. Results from the static tests showed a reduction in bond strength of around twenty percent for specimens damaged by ASR when compared to control specimens. This trend was present until the extreme shortness of the lap length governed the response. The results from the static test are listed in Figure 2.4.

**Table 4—Detail of specimens and static test results**

Beam code no.	Lap length <sup>‡</sup>	Ultimate load, kN	Percent change	Percent change related to Datum B6-A	Percent change related to Datum B6-C	Calculated U.L., kN <sup>§</sup>		Where failure occurred
						BS 8110	BS 5400	
B1-A*	5Ø	6.3	4.55	72.37	—	3.04 (2.69) <sup>  </sup>	5.26	Flexural span
B1-C†	5Ø	6.6		—	71.05	3.25 (2.77)	5.53	Flexural span
B2-A	8Ø	8.2	5.75	64.00	—	4.77 (4.24)	8.18	Flexural span
B2-C	8Ø	8.7		—	61.84	5.12 (4.36)	8.59	Flexural span
B3-A	12Ø	10.6	17.83	53.51	—	6.95 (6.20)	11.79	Flexural span
B3-C	12Ø	12.9		—	43.42	7.52 (6.38)	12.34	Flexural span
B4-A	20Ø	13.2	21.89	42.11	—	10.92 (9.82)	18.05	Flexural span
B4-C	20Ø	16.9		—	25.88	12.01 (10.64)	18.79	Flexural span
B5-A	32Ø	17.0	17.87	25.44	—	15.87 (14.46)	25.03	Flexural span
B5-C	32Ø	20.7		—	9.21	17.96 (14.93)	28.28	Flexural span
B6-A	No lap (datum)	22.8	4.18	—	—	—	—	Flexural span
B6-C	No lap (datum)	23.9		—	—	—	—	Flexural span

\*A = ASR.

†C = control.

‡Bar diameter = Ø = 8 mm.

§Ultimate load = surface area × 1.4β√f<sub>cm</sub> or surface area × 1.4β (f<sub>i</sub>/0.3) for BS 8110 and BS 5400, respectively. Surface area = π × diameter × lap length.

||f<sub>cm</sub> = 28-day compressive strength used.

**Table 5—Comparison of experimental and theoretical bond strength values**

Beam code no.	Lap length <sup>‡</sup>	Ultimate load, kN	Percent change	Surface area of bars, mm <sup>2</sup>	Bond strength, N/mm <sup>2</sup>	1.4β√f <sub>cm</sub> <sup>§</sup>	1.4β (f <sub>i</sub> /0.3) <sup>  </sup>	Where failure occurred
B1-A*	5Ø	6.3	4.55	1005.31	11.00	5.19	9.10	Flexural span
B1-C†	5Ø	6.6			11.48	5.49	9.59	Flexural span
B2-A	8Ø	8.2	5.75	1608.49	9.12	5.19	9.10	Flexural span
B2-C	8Ø	8.7			9.60	5.49	9.59	Flexural span
B3-A	12Ø	10.6	17.83	2412.74	8.07	5.19	9.10	Flexural span
B3-C	12Ø	12.9			9.92	5.49	9.59	Flexural span
B4-A	20Ø	13.2	21.89	4021.24	6.22	5.19	9.10	Flexural span
B4-C	20Ø	16.9			8.16	5.49	9.59	Flexural span
B5-A	30Ø	17.0	17.87	6031.86	5.62	5.19	9.10	Flexural span
B5-C	30Ø	20.7			7.01	5.49	9.59	Flexural span
B6-A	No lap (datum)	22.8	4.18	—	—	5.19	9.10	Flexural span
B6-C	No lap (datum)	23.9			—	5.49	9.59	Flexural span

\*A = ASR.

†C = control.

‡Bar diameter = Ø = 8 mm.

§β = 0.5. Theoretical values according to BS 8110.

||β = 0.5. Theoretical values according to BS 5400. Surface area of bar = (πdL); and bond strength = (force/surface area of bar).

*Figure 2.4: Static Load Bond Strength Test Results (Ahmed 1999, Materials)*

Upon completion of the fatigue portion of the testing, it was found that ASR causes a dramatic reduction in the fatigue life of reinforced concrete beams when the lap splice is in the bending zone. As the lap length increases, the effect of ASR on fatigue life decreases. This phenomenon is illustrated in Figure 2.5. When no lap splice is present, the fatigue life is only slightly reduced by ASR (Ahmed 1999, Materials).

*Fig. 15—Deflection of ASR and sound concrete Beam B4, with lap length 20 $\phi$  versus number of cycles.*

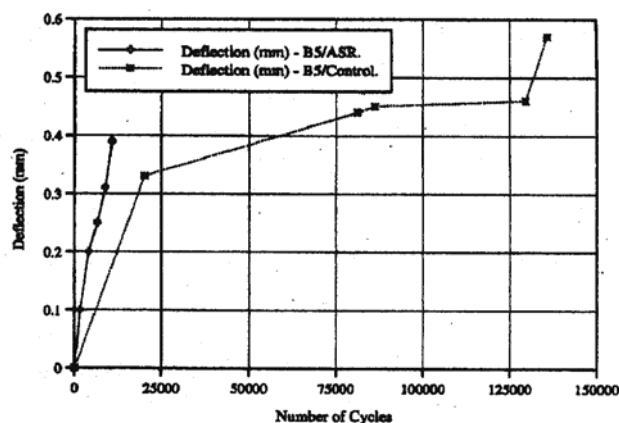


*Fig. 16—Deflection of ASR and sound concrete Beam B5, with lap length 32 $\phi$  versus number of cycles.*

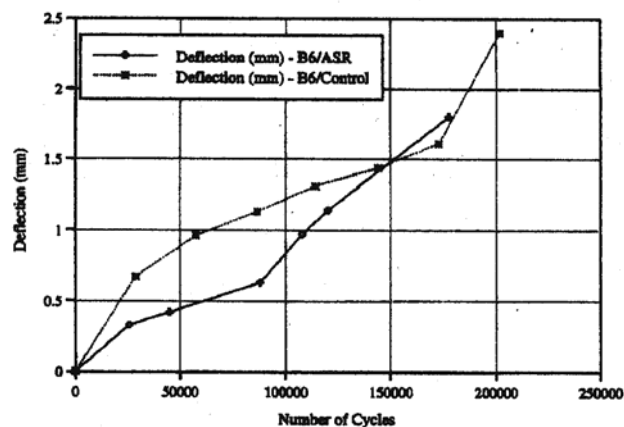


**Figure 2.5: Bond Fatigue Life of ASR Damaged Specimens (Ahmed 1999, Materials)**

It should be noted that the concrete cover, which was slightly less than four bar diameters, was not taken into account in this study. In general, it can be concluded that ASR has an ultimate strength reducing effect on bond strength. The amount of reduction is affected by the following factors: type of loading, position of splices, length of splices, and the presence of adequate stirrups and concrete cover.

### **2.3.5 The Effect of ASR on Bearing Strength**

Little information exists to date on how damage resulting from ASR affects the bearing strength of reinforced concrete. The pioneering study was done by Ahmed at The University of London. Tests were done on small and large sized plain and reinforced concrete specimens. These tests also took into account varying amounts of reinforcement and concentric, eccentric, and biaxial loading conditions. Figure 2.6 illustrates the three different reinforcement patterns that were used in this study.



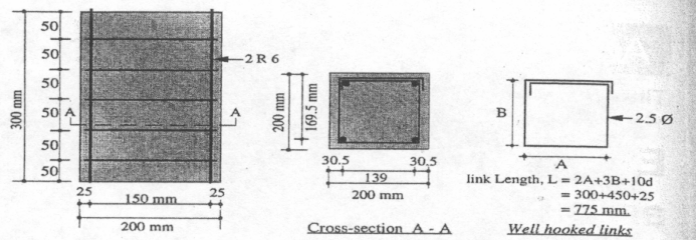


Fig. 3—Reinforcement class 1: three-dimensional cage of very well anchored reinforcement.

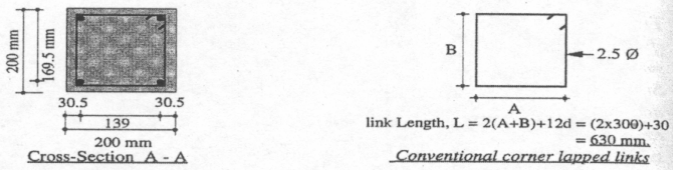


Fig. 4—Reinforcement class 2: three-dimensional cage of conventionally anchored reinforcement (conventional corner-lapped links).

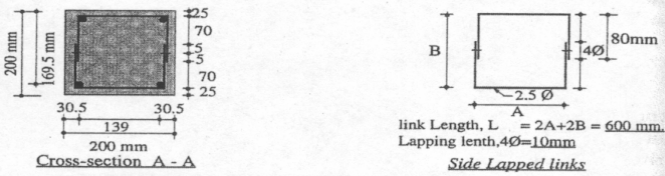


Fig. 5—Reinforcement class 3a: two-dimensional cage of reinforcement in two faces with side-lapped links.

**Figure 2.6: Bearing Test Reinforcement (Ahmed 1999, Structural)**

The results from the smaller test specimens damaged by ASR indicated a significant reduction in the ultimate bearing strength. This reduction decreased as the amount of confining reinforcement increased. A reduction in capacity due to ASR was also observed in the eccentric and biaxial loading conditions. The reduction in tensile strength which results from ASR causes a significant reduction in the bearing capacity of concrete when it is subjected to eccentric loading. The small ASR damaged specimens loaded eccentrically experienced losses of ultimate bearing capacity in the neighborhood of thirty-five to forty percent. The results from these tests as well as pictures of test specimens are shown in Figures 2.7 and 2.8.

**Table 4—Square loaded plate (50 x 50 x 15 mm), biaxial on specimen (200 x 200 x 300 mm)**

Specimen code (1)	Eccentricity, mm (2)		$R = A/A'$ (3)	Cracking bearing stress, $N/mm^2$ (4)	Ultimate bearing stress, $N/mm^2$ (5)	Percent loss of UBS (6)	UBS/cube strength (7)	Percent loss of $\eta$ (8)	UBS/cylinder tensile strength (9)	Percent loss of $\eta'$ (10)
	$e_x$	$e_y$								
R1-A	25	25	16	57.2	99.2	34.4	2.25	23.21	22.40	26.80
R1-C	25	25	16	139.6	142.0	—	2.93	—	30.60	—
R2-A	25	25	16	41.6	77.2	44.4	1.88	34.97	18.56	37.95
R2-C	25	25	16	136.0	138.8	—	2.86	—	29.91	—
R3a-A	25	25	16	44.4	76.8	32.6	1.85	21.28	18.46	24.87
R3a-C	25	25	16	108.4	114.0	—	2.35	—	24.57	—
R3b-A	25	25	16	55.6	67.60	36.9	1.63	26.24	16.25	29.65
R3b-C	25	25	16	102.8	107.2	—	2.21	—	25.10	—
Plain-A	25	25	16	50.0	61.2	41.2	1.47	31.31	14.71	34.36
Plain-C	25	25	16	100.0	104.0	—	2.14	—	22.41	—

$\eta$  = nondimensional ratio of ultimate bearing stress to concrete cube compressive strength.  
 $\eta'$  = nondimensional ratio of ultimate bearing stress to tensile splitting strength.

**Figure 2.7: Bearing Capacity Test Results for Eccentrically Loaded Specimens (Ahmed 1999, Structural)**



(c)

Fig. 9—200 x 200 x 300-mm concrete blocks tested under 50 x 50-mm square bearing plate positioned: (a) concentrically; (b) eccentrically; and (c) biaxially.

**Figure 2.8: Small, Biaxially Loaded Test Specimens (Ahmed 1999, Structural)**

It is important to observe that amount of strength reduction observed in the small specimens did not hold true for the larger sized specimens. The reduction in ultimate bearing strength due to ASR was around twenty percent for these specimens. This size effect can be viewed in Figure 2.9. It is possible that this increase in capacity is due to the fact that the larger specimens did not experience as much ASR related damage as their smaller counterparts. The crack widths that were measured for the various test specimens are listed in Figure 2.10 (Ahmed 1999, Structural).

**Table 10—Size effect on bearing capacity of sound and ASR concrete**

Specimen code (1)	Eccentricity, mm (2)		$R = A/A'$ (3)	Cracking bearing stress, N/mm <sup>2</sup> (4)	Ultimate bearing stress, N/mm <sup>2</sup> (5)	Percent loss of UBS (6)	UBS/cube strength (7)	Percent loss of $n$ (8)	UBS/cyl- inder ten- sile strength (9)	Percent loss of $n'$ (10)
	$e_x$	$e_y$		$q_c$	$q'_c$		$n$		$n'$	
Small reinforced ASR specimen	0	0	16	72.00	79.60	44.6	1.92	35.14	19.13	38.19
Small reinforced control specimen	0	0	16	127.6	143.60	—	2.96	—	30.95	—
Large reinforced ASR specimen	0	0	16	66.75	105.02	17.2	2.63	3.44	25.25	7.64
Large reinforced control specimen	0	0	16	89.00	126.83	—	2.62	—	27.34	—
Small unreinforced (plain) ASR specimen	0	0	16	40.80	62.80	52.4	1.51	44.49	151.0	46.92
Small unreinforced (plain) control specimen	0	0	16	111.2	132.0	—	2.72	—	28.45	—
Large unreinforced (plain) ASR specimen	0	0	16	44.50	91.67	24.0	2.21	11.24	22.04	15.23
Large unreinforced (plain) control specimen	0	0	16	102.35	120.60	—	2.49	—	26.00	—
Small reinforced ASR specimen	0	25	16	60.00	78.0	44.3	1.88	34.95	18.75	37.85
Small reinforced control specimen	0	25	16	111.6	140.0	—	2.89	—	30.17	—
Large reinforced ASR specimen	0	50	16	66.75	84.11	13.3	2.03	13.25	20.22	3.30
Large reinforced control specimen	0	50	16	89.00	97.01	—	2.34	—	20.91	—
Small unreinforced (plain) ASR specimen	0	25	16	34.00	61.40	44.8	1.48	35.37	14.76	38.42
Small unreinforced (plain) control specimen	0	25	16	108.0	111.20	—	2.29	—	23.97	—
Large unreinforced (plain) ASR specimen	0	50	16	79.21	79.21	16.4	1.91	2.05	19.04	6.80
Large unreinforced (plain) control specimen	0	50	16	94.79	94.79	—	1.95	—	20.43	—

$n$  = nondimensional ratio of ultimate bearing stress to concrete cube compressive strength.  
 $n'$  = nondimensional ratio of ultimate bearing stress to tensile splitting strength.

**Figure 2.9: Bearing Capacity Size Effect (Ahmed 1999, Structural)**

**Table 11—Crack width, mm, observed on surface and side of ASR specimens**

Reinforcement class	R1	R2	R3a	R3b	Plain
Surface (200 x 200 x 300 mm)	6.4	6.1	6.8	4.8	4.4
Side (200 x 200 x 300 mm)	3.0	3.8	4.4	3.0	3.8
Surface (400 x 400 x 600 mm)	—	4.8	—	—	4.4
Side (400 x 400 x 600 mm)	—	2.8	—	—	7.0

R1/2/3a, 3b = specimen reinforced with lateral reinforcement Class 1/2/3a, 3b;  
 C = control or sound concrete mix;  
 A = ASR concrete mix; and  
 Plain-A/C = plain, unreinforced, concrete specimen cast from Mix A (ASR) or Mix C (control).

*Figure 2.10: Observed Crack Widths (Ahmed 1999, Structural)*

In summary, ASR can significantly reduce the ultimate bearing capacity of reinforced concrete. The amount of reduction in capacity resulting from ASR is a function of the position of the load, the amount of confinement, and the extent of the ASR induced damage.

### 2.3.6 The Effect of ASR on Deflections

Although ASR has been found to significantly reduce the elastic modulus in concrete cores, it does not necessarily cause a large increase in the deflections of actual structures. A study conducted by Blight using core testing, finite element analysis, and full-scale load testing to assess the structural integrity of a reinforced concrete portal frame supports this argument. While testing cores taken from the actual structure, a difference of 3,000 ksi (21GPa) was found when comparing the elastic modulus of sound concrete to that of deteriorated concrete. However, when comparing the results from the load test to the predicted values attained from the finite element analysis a reduction in the elastic modulus of only 1,000 ksi (7 GPa) gave good correlation between predicted and actual deflections (Blight 1989). In a similar study conducted in Japan on reinforced concrete

bridge piers, a full-scale load test revealed only a small increase in deflections when comparing severe ASR damaged piers to sound piers. This increase ranged from ten to twenty percent (Imai 1987). In conclusion, ASR often reduces the elastic modulus of concrete core samples by a significant amount. However, due to the variability of ASR throughout a structural element, using values of elastic modulus obtained from severely damaged cores can result in overestimating the actual increase in deflections that may occur in the actual structure as a result of ASR. It should be noted, however, that damage due to ASR does result in an overall increase in deflections.

## 2.4 APPLICABLE FULL-SCALE LOAD TESTING

Several full-scale load tests have been conducted on various structural elements which were severely damaged by ASR. These tests were performed in order to determine the effect of ASR related deterioration on an actual structure. The results indicate that although the damage related to ASR may appear to be very severe, its overall effect on the load carrying capacity of the structure may not be a major reason for concern.

### 2.4.1 Hanshin Expressway Piers

In 1982 a full-scale load test was conducted on concrete bridge piers severely damaged by ASR. Figure 2.11 illustrates some of the damaged observed on the pier.

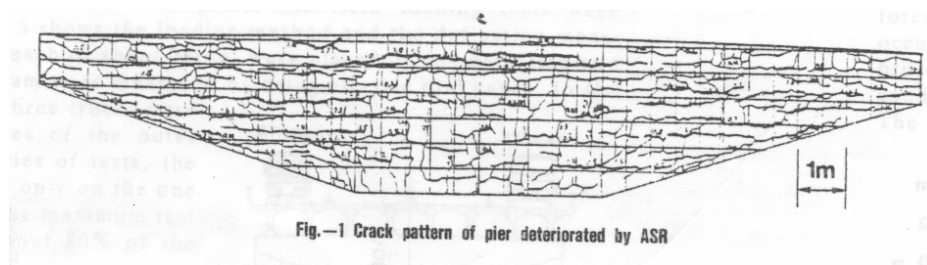


*Figure 2.11: Damaged Pier Cap (Imai 1987)*

In addition to the full-scale load test, a finite element analysis was conducted in order to attempt to predict the behavior of the damaged piers. Concrete properties were determined from cores taken from the actual structure. When conducting the load test, the piers were loaded to eighty percent of the design live load and deflections were recorded. Figure 2.12 shows a basic schematic of the load test conducted on the bridge.

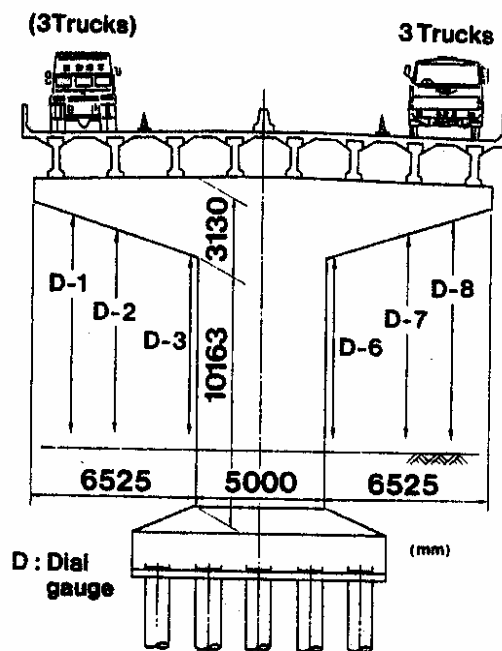


**Fig. — 3 Schematic view of loading test**

*Figure 2.12: Hanshin Load Test Schematic (Imai 1987)*

The finite element analysis was used to predict the behavior of the sound piers. Upon completion of the load test, good correlation was found between the finite element analysis and the load test on the sound piers. The results also indicated only a minimal increase in deflections due to ASR related deterioration. From these results, it was concluded that the stiffness and load carrying capacity of the piers was not significantly reduced by the ASR related damage (Imai 1987).

#### 2.4.2 Johannesburg Portal Frame

A reinforced concrete portal frame severely damaged by ASR was load tested twice, once in 1982 and a second time in 1988. By 1988 the ASR induced damage had produced cracks as large as 0.59 inches (15 mm) in width. Figure 2.13 is an illustration of the severely damaged portal frame.

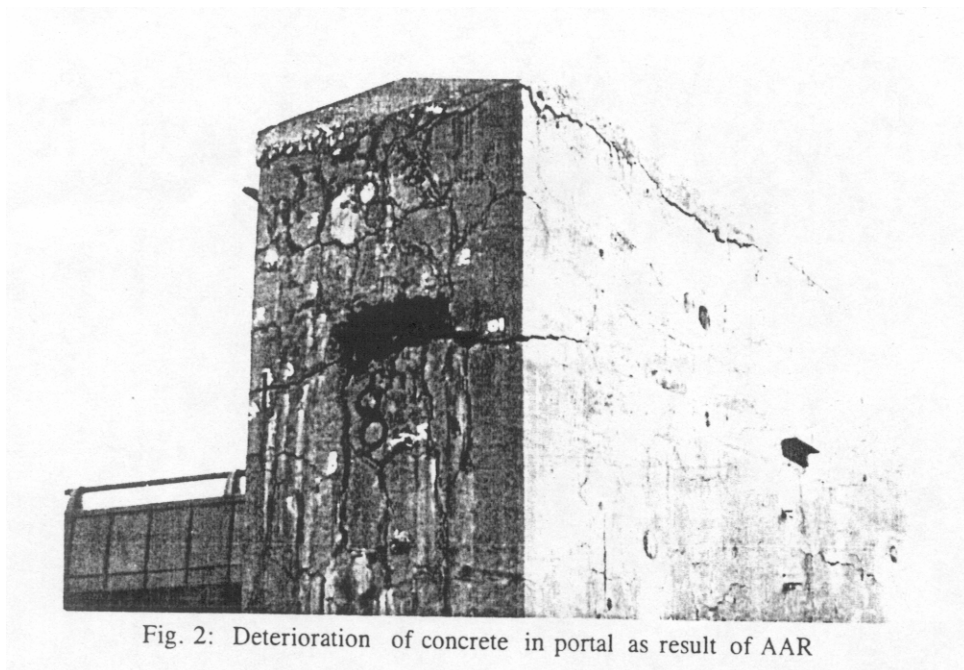


***Figure 2.13: Severely Damaged Portal Frame (Blight 2000)***

Before the first load test, an elastic finite element analysis was conducted using concrete properties determined from cores taken from the structure. The original load test was conducted in order to compare the actual behavior of the structure to the behavior determined analytically. The second test was performed in order to confirm the results from the first test and to determine whether or not additional deterioration had affected the load carrying capacity of the structure. The tests conducted in 1982 loaded the frame to eighty four percent of the

respective design live load. The test conducted in 1986 used a load which was three percent less than the load used in 1982.

The results from the tests indicated good correlation between predicted and actual values for deflections and rotations, although the predicted values for deflections were slightly overestimated. This can be attributed to a slightly low assumed value of elastic modulus which was used in the finite element analysis. The overall deflections were minimal, which indicated that even though ASR related damage was severe, adequate structural integrity of the frame was preserved. It was concluded that in practice where design loads often exceed actual loads applied to the structure, adequate safety of ASR damaged structures does not seem to be of major concern (Blight 1989). In 2000 a report was issued summarizing the properties of the concrete over the twenty year period which this study was conducted. In this report a schematic of the portal frame and the changes made over this period were listed and can be viewed in Figure 2.14 (Blight 2000).

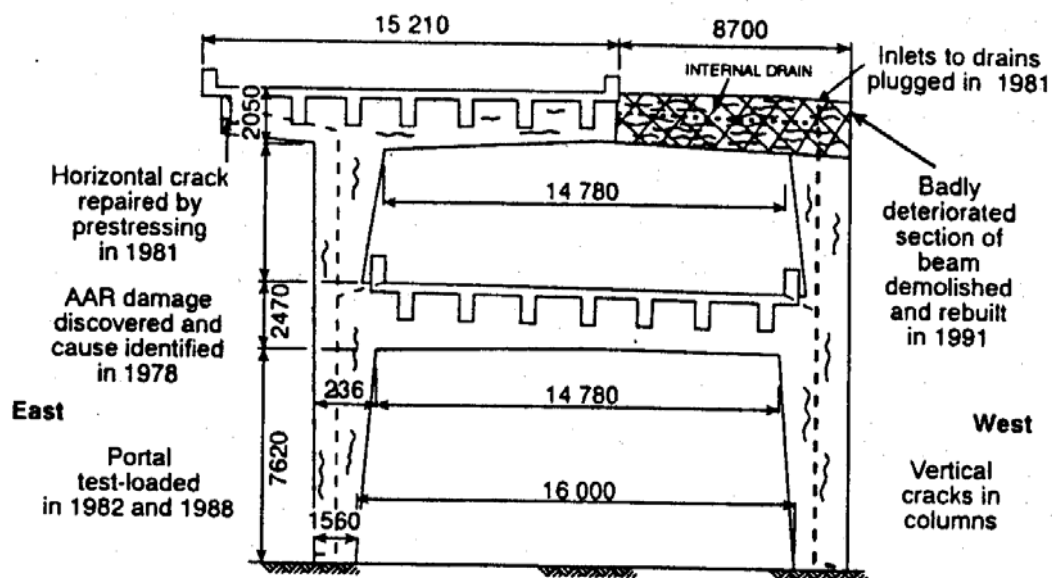


Figure 2.14: Schematic of Portal Frame (Blight 2000)



### 2.4.3 A26 Highway Bridge Deck

Sections of the A26 highway in the north-eastern part of France are suffering from ASR and sulfate attack. Portions of the bridge deck were selected for full-scale load testing. Cracking due to ASR at the time of testing ranged from 0.008 inches (0.2 mm) to 0.039 inches (1.0 mm) in width. The test was conducted in order to compare deflections of an undamaged portion of the deck to those of a damaged portion. The results of the test are listed in Figure 2.15.

TABLE 2 : Loading Test Maximal Displacements in mm.

Loading case	Deck	Sensor 0	Sensor 1	Sensor 2	Sensor 3	Sensor 4
1	not deteriorated	0.255	0.22	0.215	0.19	0.13
	deteriorated	0.31	0.32	0.275	0.265	0.20
2	not deteriorated	0.47	0.40	0.385	0.30	0.30
	deteriorated	0.515	0.53	0.41	0.32	0.37
3	not deteriorated	0.70	0.595	0.59	0.50	0.40
	deteriorated	0.765	0.76	0.605	0.52	0.47
3 1982	not deteriorated	0.6				
	deteriorated	0.6				
4	not deteriorated	0.68	0.56	0.54	0.42	0.44
	deteriorated	0.735	0.68	0.58	0.44	0.52

Figure 2.15: A29 Load Test Results (Baillemont 2000)

The test was done in order to determine the loss in stiffness that may occur as a result of ASR. The results of the load test indicated a local loss in stiffness of approximately ten percent in the most deteriorated portion of the deck. However, the overall stiffness of the entire deck was found to adequately compensate for the local loss. It was therefore concluded that no additional reinforcement of the bridge deck was necessary (Baillemont 2000).

## 2.5 CONCLUSIONS FROM THE LITERATURE

The conclusions that can be drawn from the current literature pertaining to the effects of ASR and DEF on the structural behavior of reinforced concrete are:

- In studying reinforced concrete structures suffering from durability related deterioration, it is important to conduct both visual and experimental inspections of the damaged concrete in order to determine if ASR and/or DEF are at the source of the problem.
- ASR has a distinct effect on the mechanical properties of concrete. ASR related damage can result in loss of compressive strength in unconfined concrete and significant reduction in tensile strength. Some reduction in the modulus of elasticity is also likely to occur.
- The type of structural element and its primary mode of failure will determine if ASR has a major effect on the ultimate capacity of the element. Structural elements with adequate confinement subjected to large axial loads are likely to retain most of their capacity. At moderate levels of expansion ASR has little effect on the ultimate capacity of structures which fail in flexure. If adequate transverse reinforcement is provided, reduction in shear capacity is also not a major concern. However, ASR can significantly reduce the bond and bearing strength of reinforced concrete sections in addition to increasing deflections in the overall structure.
- Although ASR can cause very unsightly damage, full-scale load tests on beams, columns, and pier type structures have generally indicated that structures damaged by ASR retain most of their stiffness and provide adequate reserve capacity at service load levels.

## **2.6 STRUCTURAL ASSESSMENT PLAN**

### **2.6.1 Overview**

After reviewing the literature regarding ASR and DEF and conducting a site visit, it has been determined that a structural assessment methodology for evaluating the distressed piers in the San Antonio Y must be developed. Application of this methodology will help determine the in-place integrity of the damaged elements. The key factors included in the structural assessment methodology are as follows: investigation of design factors affecting experiments and assessment, evaluation of the structural capacity of sound and damaged piers, and an evaluation of the in-place structure. An experimental study is to be conducted in order to answer the key questions which come with generating the assessment methodology.

### **2.6.2 Design Factors affecting Experiments and Assessment**

The design factors affecting the experiments and structural assessment consist of three key components. These components are the in-situ engineering properties of the structure, the applicable loads on the structure, and any special design considerations that have become apparent during the investigation.

#### ***2.6.2.1 In-situ Engineering Properties***

It has been determined necessary to conduct experimental testing to help determine the in-place properties of the materials used in construction of the key structural elements under consideration. Testing on cores taken from the structure will be done in order to obtain important properties such as compressive strength and modulus of elasticity. Due to the lack of documentation in the construction documents, it is also necessary to identify the yield strength of the steel used in

construction. This will be accomplished through Rockwell Hardness testing on pieces of steel found in cores taken from the structure.

#### ***2.6.2.2 Applicable Loads***

The next step is to evaluate the loads used to design the original structure. This involves reviewing the original design loads and determining which loads apply to the elements under consideration.

#### ***2.6.2.3 Special Design Considerations***

While conducting an in-depth investigation on an existing structure, it is often necessary to consider and evaluate assumptions made during the original design process. Therefore, the original design will be reviewed, and any special considerations will be discussed.

### **2.6.3 Evaluation of the Structural Capacity of Sound and Damaged Piers**

After the loads and material properties have been determined, the next step is to determine the structural capacity of the pier chosen for in-depth study. Experimental testing on model piers will be done in order to ascertain this information. An experimental program is to be developed which involves construction and testing of both sound and damaged piers. A method will be developed to mechanically induce cracking into model piers in an attempt to generate a worst case scenario of the cracking in the actual columns. The results from the experimental study are to be used to determine the critical mode of failure in the existing columns while also attempting to quantify the amount of reserve capacity that may exist in the damaged piers.

#### **2.6.4 Evaluation of the Current Structure**

After the critical mode of failure and the maximum capacity of the model columns have been determined, the in-place strength of the existing columns can be evaluated. This will involve reviewing applicable information obtained from the experimental study in addition to using strut-and-tie modeling to analyze the forces in the model pier. Through reviewing the experimental results in conjunction with the results from analysis, an evaluation of the in-place strength and the current structural integrity of the piers can be made.

# CHAPTER 3

## Design Factors Affecting Experiments and Assessment

### 3.1 IN-SITU ENGINEERING PROPERTIES

#### 3.1.1 Concrete Testing

When evaluating an existing structure, it is important to gain detailed information about the in-place material properties of that structure. For this reason concrete cores were taken from critical elements of the San Antonio Y. Concrete cores were obtained from structural elements DD6 and DD7. The cores were then tested in compression. The results from these tests and the assumed concrete strength used for design are given in Table 3.1.

**Table 3.1: Concrete Testing Results**

Column Designation	DD6	DD7	Design Value
Compressive Strength (psi)	8400	5780	3600

*Concrete in an area represented by core tests shall be considered structurally adequate if the average of three cores is equal to at least 85 percent of  $f'_c$  and no single core is less than 75 percent of  $f'_c$  (ACI 318-05 R 5.6.5.4).* In this case the concrete core testing revealed that there is a significant reserve capacity between the assumed concrete compressive strength that was the basis for the design and the measured in-place compressive strength of the structural elements under investigation.

### 3.1.2 Reinforcing Steel Testing

A copy of the original design notes for the piers under investigation was furnished by the TxDOT Project Director. In these design notes, the specified minimum yield strength of the reinforcing steel was 40 ksi. However, there was some uncertainty as to whether or not 40 ksi steel was used in the actual construction of the piers. Several documents from the construction records indicated that the steel had a minimum yield strength of 60 ksi. However, this evidence was not considered to be conclusive because the documents did not include steel from the DD series of columns.

Due to the lack of complete information in the construction documents, it was necessary to perform testing in order to determine the in-place tensile strength of the steel used in the construction of the columns in the DD spine of the San Antonio Y. Small pieces of steel were obtained from cores taken from structural elements DD7 and DD10. The pieces of steel obtained were number four bars representing the transverse reinforcement in the columns. Rockwell Hardness testing was done on the steel in order to determine the tensile strength of the steel. This was done in an attempt to determine whether or not the steel used in the construction of the piers met the requirements for reinforcement with minimum yield strength of 60 ksi. The testing was done for a Rockwell C Hardness Scale. The results from the testing are given in Table 3.2.

**Table 3.2: Rockwell Hardness Testing**

Pier	Reading	Tensile Strength (ksi)
DD7	18.3	106
DD10	19.5	109

From these results it was determined that the steel used in the construction of the DD spine of the San Antonio Y met the requirements for steel with minimum yield strength of 60 ksi.

### 3.2 APPLICABLE LOADS

In order to evaluate the existing columns, the applicable loads on the structure needed to be determined. This information was also necessary to determine which load case to use in the experimental study.

#### 3.2.1 Design Loads

The governing code at the time the structure was designed was the AASHTO 1983 Standard Specifications for Highway Bridges. The various load cases used in design, as reflected by the design notes, were determined from this specification. Figure 3.1 illustrates the load table used in the design.

Table 3.22.1A Table of Coefficients  $\gamma$  and  $\beta$

Col. No.	1	2	3	3A	4	5	6	7	8	9	10	11	12	13	14
GROUP	$\gamma$	$\beta$ FACTORS													
		D	(L+I) <sub>n</sub>	(L+I) <sub>p</sub>	CF	E	B	SF	W	WL	LF	R+S+T	EQ	ICE	%
SERVICE LOAD	I	1.0	1	1	0	1	$\beta_E$	1	1	0	0	0	0	0	100
	IA	1.0	1	2	0	0	0	0	0	0	0	0	0	0	150
	IB	1.0	1	0	1	1	$\beta_E$	1	1	0	0	0	0	0	**
	II	1.0	1	0	0	0	1	1	1	1	0	0	0	0	125
	III	1.0	1	1	0	1	$\beta_E$	1	1	0.3	1	1	0	0	125
	IV	1.0	1	1	0	1	$\beta_E$	1	1	0	0	0	1	0	125
	V	1.0	1	0	0	0	1	1	1	1	0	0	1	0	140
	VI	1.0	1	1	0	1	$\beta_E$	1	1	0.3	1	1	1	0	140
	VII	1.0	1	0	0	0	1	1	1	0	0	0	0	1	133
	VIII	1.0	1	1	0	1	1	1	1	0	0	0	0	0	140
LOAD FACTOR DESIGN	IX	1.0	1	0	0	0	1	1	1	1	0	0	0	0	150
	X	1.0	1	1	0	0	$\beta_E$	0	0	0	0	0	0	0	100
	I	1.3	$\beta_D$	1.67*	0	1.0	$\beta_E$	1	1	0	0	0	0	0	
	IA	1.3	$\beta_D$	2.20	0	0	0	0	0	0	0	0	0	0	
	IB	1.3	$\beta_D$	0	1	1.0	$\beta_E$	1	1	0	0	0	0	0	
	II	1.3	$\beta_D$	0	0	0	$\beta_E$	1	1	1	0	0	0	0	
	III	1.3	$\beta_D$	1	0	1	$\beta_E$	1	1	0.3	1	1	0	0	
	IV	1.3	$\beta_D$	1	0	1	$\beta_E$	1	1	0	0	0	1	0	
	V	1.25	$\beta_D$	0	0	0	$\beta_E$	1	1	1	0	0	1	0	
	VI	1.25	$\beta_D$	1	0	1	$\beta_E$	1	1	0.3	1	1	1	0	
VII	1.3	$\beta_D$	0	0	0	$\beta_E$	1	1	0	0	0	0	1		
VIII	1.3	$\beta_D$	1	0	1	$\beta_E$	1	1	0	0	0	0	0	1	
IX	1.20	$\beta_D$	0	0	0	$\beta_E$	1	1	1	0	0	0	0	1	
X	1.30	1	1.67	0	0	$\beta_E$	0	0	0	0	0	0	0		

Culvert

Not Applicable

Culvert

(L + I)<sub>n</sub> - Live load plus impact for AASHTO Highway H or HS loading  
 (L + I)<sub>p</sub> - Live load plus impact consistent with the overload criteria of the operation agency.

**Figure 3.1: AASHTO Design Loads (AASHTO 1983)**



\*1.25 may be used for design of outside roadway beam when combination of sidewalk live load as well as traffic live load plus impact governs the design, but the capacity of the section should not be less than required for highway traffic live load only using a beta factor of 1.67. 1.00 may be used for design of deck slab with combination of loads as described in Article 3.24.2.2.

$$^b\text{Percentage} = \frac{\text{Maximum Unit Stress (Operating Rating)}}{\text{Allowable Basic Unit Stress}} \times 100$$

For Service Load Design

% (Column 14) Percentage of Basic Unit Stress

No increase in allowable unit stresses shall be permitted for members or connections carrying wind loads only.

$\beta_E = 0.70$  for vertical loads on Reinforced Concrete Boxes.  
 $\beta_E = 1.00$  for lateral loads on Reinforced Concrete Boxes.  
 $\beta_E = 1.00$  for vertical and lateral loads on all other culverts.

For culvert loading specifications, see Article 6.2.

$\beta_E = 1.0$  and  $0.5$  for lateral loads on rigid frames (check both loadings to see which one governs). See Article 3.20.

For Load Factor Design

$\beta_E = 1.3$  for lateral earth pressure for rigid frames excluding rigid culverts.

$\beta_E = 0.5$  for lateral earth pressure when checking positive moments in either rigid frames or rigid culverts, including reinforced box culverts. This complies with Article 3.20.

$\beta_E = 1.0$  for vertical earth pressure

$\beta_D = 0.75$  when checking member for minimum axial load and maximum moment or maximum eccentricity . . . . . For

$\beta_D = 1.0$  when checking member for maximum axial load and minimum moment . . . . . Design

$\beta_D = 1.0$  for flexural and tension members

$\beta_E = 1.0$  for Rigid Culverts including Reinforced Concrete Boxes

$\beta_E = 1.5$  for Flexible Culverts

For Group X loading (culverts) the  $\beta_E$  factor shall be applied to vertical and horizontal loads.

$$\begin{aligned} \text{Group (N)} = & \gamma[\beta_D \cdot D + \beta_L(L + I) + \beta_C CF + \beta_E E \\ & + \beta_B B + \beta_S SF + \beta_W W + \beta_{WL} WL \\ & + \beta_L \cdot LF + \beta_R(R + S + T) + \beta_{EQ} EQ \\ & + \beta_{ICE} ICE] \end{aligned} \quad (3-10)$$

where

- N = group number;
- $\gamma$  = load factor, see Table 3.22.1A;
- $\beta$  = coefficient, see Table 3.22.1A;
- D = dead load;
- L = live load;
- I = live load impact;
- E = earth pressure;
- B = buoyancy;
- W = wind load on structure;
- WL = wind load on live load—100 pounds per linear foot;
- LF = longitudinal force from live load;
- CF = centrifugal force;
- R = rib shortening;
- S = shrinkage;
- T = temperature;
- EQ = earthquake;
- SF = stream flow pressure;
- ICE = ice pressure.

**Figure 3.2: AASHTO Design Loads Continued (AASHTO 1983)**

The loads used for designing the columns were dominated by dead load. The unfactored dead load on each pier was 1800 kips, while the unfactored live load was only 88 kips per lane. Other forces that were included in the design are listed as follows: superstructure wind, substructure wind, live load wind,

overturning force, longitudinal braking force, and centrifugal force. A very conservative single overall column design that incorporated the absolute worst case of forces acting on any single pier was used for the design of all of the piers. The calculations used for the design of the piers are given in Appendix A. Table 3.3 lists the values that were used for the final design of the columns in the San Antonio Y. Figure 3.2 shows the reference axes for the column.

**Table 3.3: Factored Column Design Loads (With Centrifugal Force)**

AASHTO Load Case	I		II	III		V	VI	
	2 Ln.	3 Ln.	2-3 Ln.	2 Ln.*	3 Ln.	2-3 Ln.	2 Ln.	3 Ln.
Number of Lanes	2 Ln.	3 Ln.	2-3 Ln.	2 Ln.*	3 Ln.	2-3 Ln.	2 Ln.	3 Ln.
Axial Load (kips)	2720	2855	2340	2570*	2650	2250	2470	2550
YY Moment (ft*kips)	6375	5517	3840	6235*	5947	3690	5996	5720
XX Moment (ft*kips)	0	0	1000	1200*	1410	2818	3010	3215

\* taken to be the governing load case for the experimental program

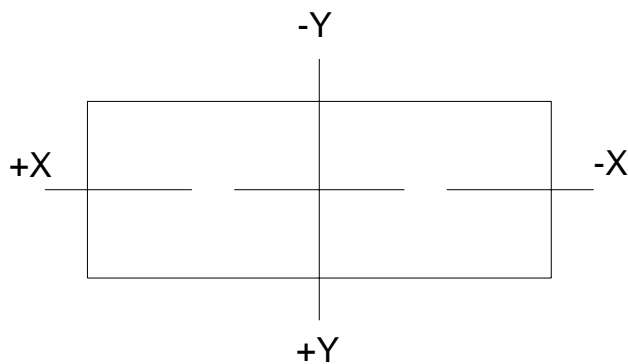


**Figure 3.3: Reference Axes**

### 3.2.2 Loads on Columns in the DD Spine

The actual loads on the columns in the DD spine are different from the values used for designing the columns. After reviewing the plans, it was seen that the stretch of roadway which the DD spine of columns support was built with very little curvature. Therefore, the centrifugal force moments for this portion of roadway approach zero. However, as indicated in section 3.2.1, substantial moments due to centrifugal forces were considered as a portion of the transverse moment in the original design of the columns. In addition, examination of the biaxial load interaction curves indicated that the load case which was taken as the governing load case had a large centrifugal force component. As a result, the loads actually used for the design of these columns are in significant excess of the loads that would have needed to be used in the design of this section of roadway to meet the AASHTO Specifications. This brings substantial reserve capacity in addition to the effects of increased concrete strength and steel strength.

Table 3.4 lists the loads on the columns with the centrifugal portion of the load omitted.

**Table 3.4: Factored Column Design Loads (Without Centrifugal Forces)**

AASHTO Load Case	I		II	III		V	VI	
	2 Ln.	3 Ln.	2-3 Ln.	2 Ln.*	3 Ln.	2-3 Ln.	2 Ln.	3 Ln.
Number of Lanes	2 Ln.	3 Ln.	2-3 Ln.	2 Ln.*	3 Ln.	2-3 Ln.	2 Ln.	3 Ln.
Axial Load (kips)	2720	2855	2340	2570*	2650	2250	2470	2550
YY Moment (ft*kips)	4776	3359	3840	4636*	3789	3690	4459	3645
XX Moment (ft*kips)	0	0	1000	1200*	1410	2818	3010	3215

\* taken to be the governing load case for the experimental program

From the comparison of Tables 3.3 and 3.4 it can be seen that the transverse moment is significantly reduced (approximately 25%) when the centrifugal force

is omitted. Due to the fact that there is very little curvature present in this section of roadway, there are practically no centrifugal force moments. The inclusion of these moments in the design of the existing columns has built a fairly substantial reserve strength into these piers.

### 3.3 SPECIAL DESIGN CONSIDERATIONS

After experimental testing began, it was determined that other aspects of the original design of the structure needed further review. While testing the first two undamaged model specimens, it was observed that the failure for both specimens was in the local zone underneath the most heavily loaded bearing pad. This local failure prompted further investigation into the original design of the bearings in the actual piers.

Review of the original design calculations (included in Appendix A) showed that the bearing pads were not designed for the worst loading case. A typical pier such as DD7 has the heavy girder diaphragm sections bearing on four elastomeric bearing pads. Figure 3.4 is an illustration of the method of load distribution chosen for the design of the original bearing pads.

Distribution of Loads to Bearing Pads in Original Design Calculations

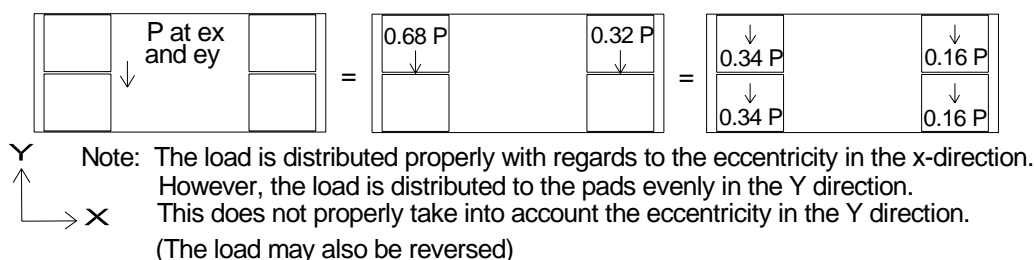


**Figure 3.4: Design Load Distribution on Bearing Pads**

The actual bridge piers are loaded biaxially. In this load case, the force on the pier is not distributed equally onto the four bearing pads. Neither is it distributed equally about one axis as shown in Figure 3.4. In the biaxial case, as a result of

having eccentricity in two directions, one pad is much more heavily loaded than the remaining three. Figure 3.5 illustrates this type of load distribution. This biaxial effect increases the load on the most heavily loaded pad from  $0.34P$  to  $0.56P$ , an almost 65% increase.

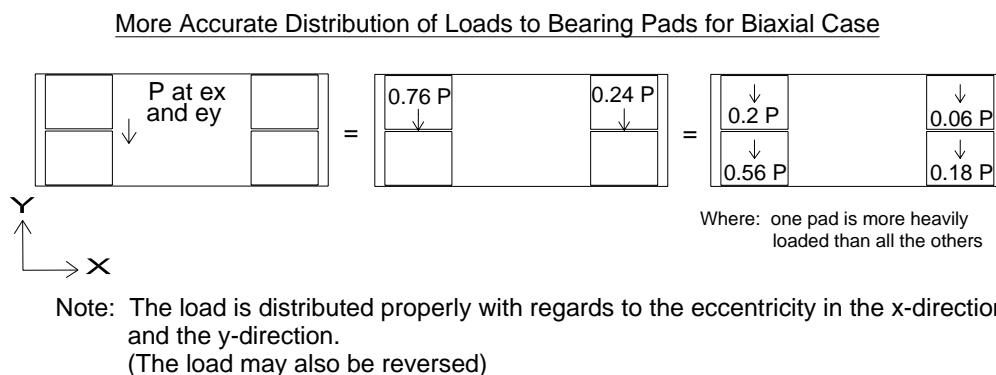


**Figure 3.5: Biaxial Load Distribution on Bearing Pads**

This type of load distribution was not taken into account in the original design of the bearing pads and the local zone beneath the pads. In addition to this inaccurate distribution of loads, a service bearing stress of 1,116 psi was used in the actual design. However, at the time of design, the applicable design specifications (AASHTO 1983) recommended a design service level bearing stress of 800 psi. These two critical assumptions made in the design process have resulted in the local zone underneath the critical pad becoming the weak link in the column. This in turn has resulted in a reduction in the ultimate strength capacity of the columns. Fortunately, as will be shown later, the reduction due to the bearing problem was more than adequately offset by the increased material strengths and the unnecessary inclusion of centrifugal force moments. This provides a net reserve capacity to help counter any degradation from ASR and/or DEF.

## CHAPTER 4

### Experimental Program

#### 4.1 MODELING OF DD SPINE COLUMNS

The pier chosen for experimental investigation was DD7. This pier has a Type I designation and was the standard pier used in the construction of the DD spine of the San Antonio Y. A direct modeling procedure was used to scale down the column for laboratory testing. In direct modeling, all physical dimensions are reduced by a constant scale factor. Material properties such as concrete compressive strength and modulus of elasticity as well as reinforcement yield strength represent closely those of the prototype. If these conditions are met, it has been shown that most behavioral conditions are closely matched (ACI SP 24).

*Test results obtained in an exploratory investigation of modeling techniques for approximately one-eighth scale structural concrete models indicate that the required materials compatibility, fabrication precision, and loading accuracy can be obtained in lightly reinforced flexural members (Aldridge 1970). With proper consideration of the laws of similitude, there have been many successful model studies in which overall prototype responses have been correctly predicted even though certain details of the behavior may not have been reproduced (Zia 1970).*

The scale factor for the model columns was determined by reducing the diameter of the number eleven bars present in the prototype column to the diameter of a number three bar for the model columns. This approach resulted in a scale factor equal to 1/3.67. The basic shape and dimensions of both the

prototype and model columns are depicted in Figure 4.1. The figure illustrates that although there has been a large decrease in size when comparing the prototype and model columns, the cross-section of the model column still has relatively large overall dimensions. The same scale factor used on the dimensions and reinforcing steel was also used to scale the loads on the column. It should be noted that in accordance with direct modeling similitude theory the axial load is reduced by the square of the scale factor, and the moments are reduced by the cube of the scale factor (Zia 1970).

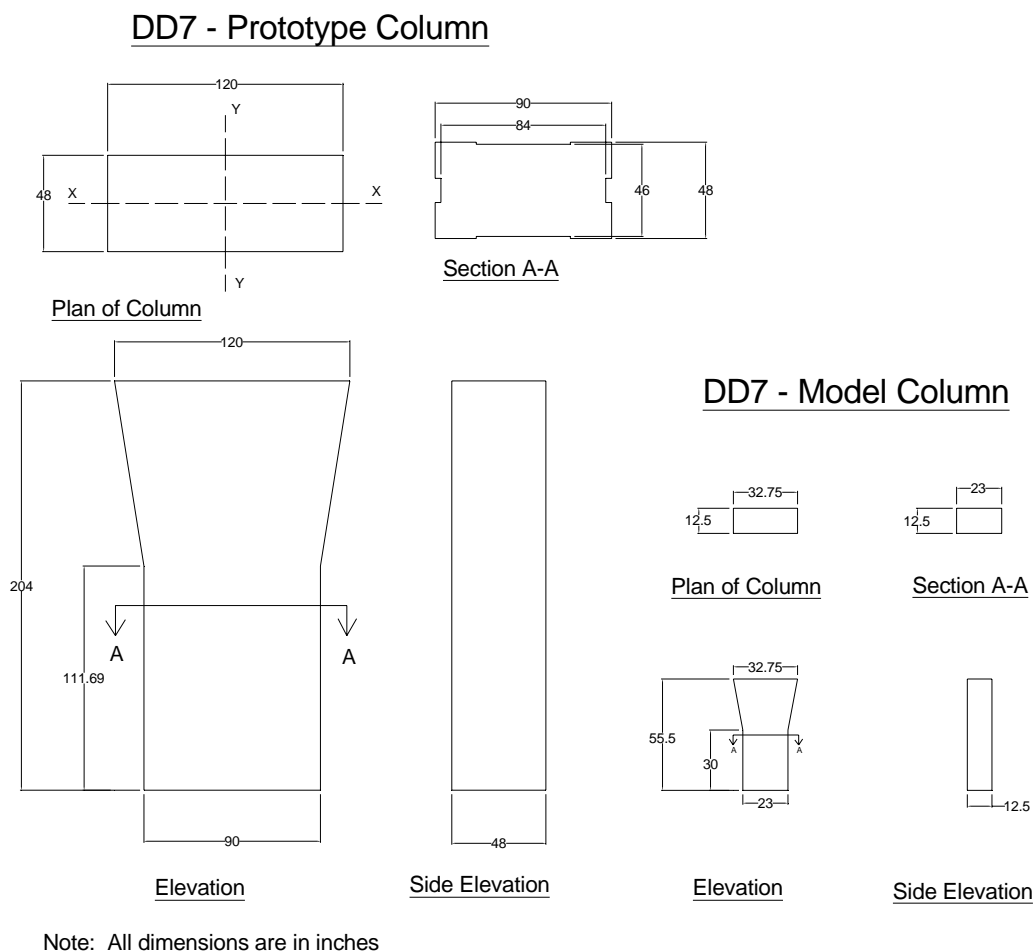


**Figure 4.1: Prototype and Model Columns**

## 4.2 LOAD USED FOR EXPERIMENTAL RESEARCH

In conducting the experimental study, it was desirable to limit the loading to one combination of loads. The load combination used for the experimental study was chosen on a worst case basis, while also taking into account feasibility of testing. According to AASHTO's 2005 Guide Manual for Condition Evaluation and Load Resistance Factor Rating (LRFR) of Highway Bridges, *where deemed necessary by the Engineer, load rating of substructure elements and checking of stability of substructure components, such as abutments, piers, and walls, should be done using the Strength I load combination and load factors of LRFD Article 3.4.1 (AASHTO LRFR).* However, it was still determined beneficial to review all of the design load combinations before deciding on a final load case for testing.

Axial load and moment interaction diagrams were generated for the prototype pier. The computer program Biaxial Column v2.3, developed by the Florida Department of Transportation, was used to generate the biaxial interaction diagrams for the pier. The load cases listed in Table 3.4 were plotted on their respective slices of the interaction diagram using the original design compressive strength in order to determine the worst case loading scenario. From these plots (given in Appendix B), it was determined that the case VI, 2 lane loading was the most critical load case. However, according to AASHTO LRFR, it is not necessary to consider transient loads such as wind or temperature when checking the load capacity of substructure elements (AASHTO LRFR). Wind, temperature, shrinkage, and creep forces account for a large portion of the design moments in load case VI. Therefore, this load case is in excess of the loading required for the evaluation of columns as per AASHTO LRFR 2005 Provisions.

The second aspect of choosing the experimental load combination was to determine the feasibility of loading. Due to laboratory constraints, it was



necessary to generate the axial load plus biaxial bending loading condition using axial load positioned simultaneously at eccentricities about the XX and YY axes. The eccentricities for the various load cases were determined as listed in Table 4.1.

**Table 4.1: Load Eccentricities (Without Centrifugal Forces)**

AASHTO Load Case	I		II	III		V	VI	
	2 Ln.	3 Ln.	2-3 Ln.	2 Ln.*	3 Ln.	2-3 Ln.	2 Ln.	3 Ln.
Number of Lanes								
Axial Load (kips)	2720	2855	2340	2570*	2650	2250	2470	2550
YY Eccentricity (in)	21.1	14.2	19.7	21.6*	17.2	19.7	21.7	17.2
XX Eccentricity (in)	0	0	5.2	5.6*	6.4	15	14.6	14.4

\* taken to be the governing load case for the experimental program

Upon review of the load eccentricities, it was determined that the large XX axis eccentricities present in load cases V and VI posed a significant problem in relation to feasibility of testing. It was determined that tensile loads would need to be introduced to the back side of the column if one of these loading combinations was to be simulated in the laboratory. It was concluded that testing model columns with these load combinations was not feasible. As a result of feasibility of testing and being composed of large transient loads, load cases V and VI were not chosen for testing. For these reasons, it was decided to move to the next most critical load combination. From the interaction slices, load case III, 2 lane loading was determined to be the next most critical load combination. This load case is much more feasible with regards to experimental testing, and comparison of the biaxial interaction diagrams generated using Biaxial Column v2.3 (given in Appendix B) indicated this load case (with biaxial bending) to be more critical than the uniaxial load case I recommended by AASHTO LRFR. Thus, it is more conservative to use this load case for the experimental study than

the AASHTO LRFR required case. The respective design axial load and eccentricities for the model column, after applying the scale factor combination for similitude requirements, are listed in Table 4.2.

**Table 4.2: Model Column Design Load**

	Design Axial Load (kips)	YY Eccentricity (in)	XX Eccentricity (in)
Model Column	191	5.9	1.5

### **4.3 METHOD OF CRACKING**

Three different methods of cracking were studied to simulate the damage in the actual structure. These three methods include forming cracks using splitting wedges, using hydraulic packers, and by actual use of ASR and/or DEF reactive concrete. It was decided, because of time requirements to produce actual materials induced cracking and the urgent need for some assessment of the cracking effect on strength, that using ASR and/or DEF reactive concrete would be explored in later phases of this study. In order to evaluate the best method for mechanical cracking, an experimental study was conducted using the splitting wedges and the hydraulic packers. The results of these experiments are given in the following sections.

#### **4.3.1 Splitting Wedges**

In order to determine the effectiveness of using splitting wedges to crack concrete, a limited experimental study was conducted. A series of 15in. x 15 in. x 40 in. reinforced concrete columns were constructed. PVC pipes were sawed in half and inserted into the formwork before the concrete was cast. The PVC pipes were used to provide sleeves for the wedges to be inserted. Figure 4.2 shows a test specimen.



***Figure 4.2: Splitting Wedge Test Specimen***

Dial gauges were then mounted onto the concrete column and the wedges were driven inward. Figure 4.3 shows a tested specimen.



***Figure 4.3: Cracked Specimen using Splitting Wedges***

The wedge penetration versus crack width was measure and plotted. The graphs in Figure 4.4 show that the wedge penetration to crack width remained relatively

linear and that the width could be controlled by wedge penetration. It was also observed that the cracks tended to travel along the line of the wedges. This confirmed that a longitudinal crack of significant size and controlled width could be formed along the entire length of the column using this method. It was concluded that using wedges to effectively split a column in four pieces was a feasible method.

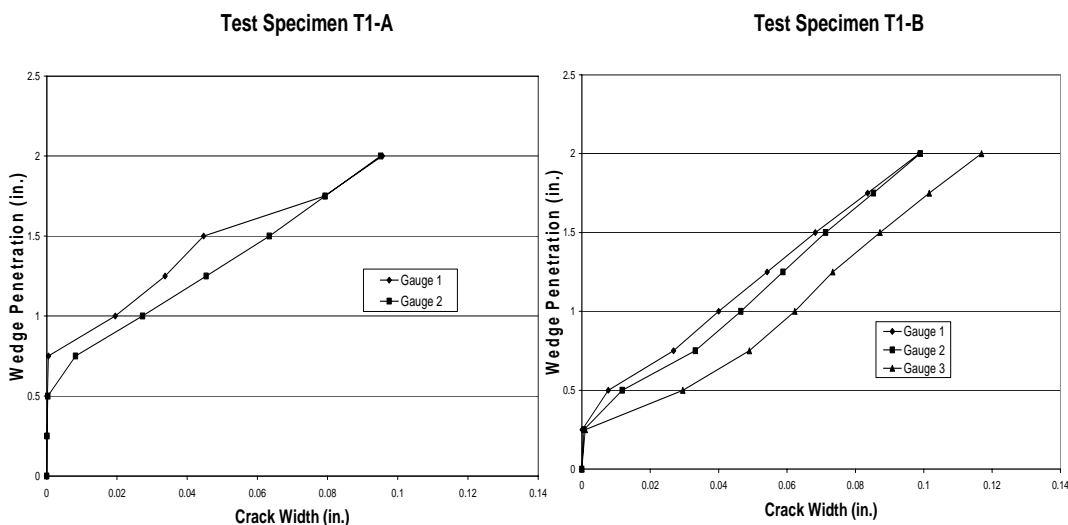


**Figure 4.4: Wedge Penetration vs. Crack Width for Splitting Wedge Method**

### 4.3.2 Hydraulic Packers

The second method that was investigated involved using hydraulic packers to produce cracking. The packers are inserted into a circular opening in the concrete. Then hydraulic fluid is pumped into the packer which causes them to expand uniformly. One of the packers used in this study is shown in Figure 4.5.



**Figure 4.5: Hydraulic Packer**

A test was conducted using four such packers on a similar reinforced concrete column. Figure 4.6 illustrates the setup used to test with the packers.



*Figure 4.6: Hydraulic Packer Test Setup*

Although the packers were able to produce cracking in the model column, it was very hard to control the crack width. In addition, in order to produce relatively large cracks the packers had to be pressurized to a level near their maximum capacity. As a result of these limitations, it was decided that using hydraulic packers to crack the model concrete columns was not the most desirable method.

#### **4.4 DESIGN OF MODEL COLUMNS**

As noted in section 4.1, it was decided to use a scaled down version of column DD7 in the San Antonio Y to conduct the main experimental portion of

the testing. It was decided to focus the testing in this phase solely on the behavior of the column. For this reason the footing details were not modeled in this study. Modeling the footing and the column together would be very complicated and would not allow the column behavior to be studied. Footing type problems are scheduled to be studied at a later time. A total of four pier specimens were tested in the experimental program. However, one specimen was repaired and tested again. Therefore, a total of five tests were conducted. The columns were designated as either S or C columns. S indicates sound concrete, and C indicates cracked concrete. Hence, the specimens included in the experimental study are: S1, S2, C1, C2, and C1-R, where R indicates a repaired column. The details of the design of the model test specimens are given below.

#### **4.4.1 Column Dimensions and Reinforcement**

The dimensions of the column were chosen by reducing the dimensions of column DD7 by the scale factor (1/3.67). Figure 4.1 shows the dimensions of both the prototype and model columns. The reinforcement pattern used to make the model columns was an exact scaled down replica of the reinforcing pattern of a Type I Pier. The reinforcing pattern was obtained from the construction drawings used for the original structure. Detailed drawings of the reinforcement in the prototype and model columns are available in Appendix B. Number 3 reinforcing bars were used in place of number eleven bars for the longitudinal reinforcement in the columns. The longitudinal reinforcement was extended to the bottom of the footing and 90 degree hooks were used to ensure proper anchorage. D1.4 deformed wire was used in place of number 4 bars for the transverse reinforcement. It should be noted that D1.4 wire is a raised rib wire with a diameter of 0.135 inches which is nearly the exact diameter needed for reducing the number 4 bar used in the prototype ties by a scale factor of 1/3.67.

PVC pipes were sawed in half and installed in the reinforcing cage to provide sleeves for the splitting wedges. The design location of the 1.5 inch PVC tubes is shown in Figure 4.7. Figure 4.8 is a picture of a fully constructed column reinforcement cage with the PVC pipes installed.

## Design Location of PVC Pipes

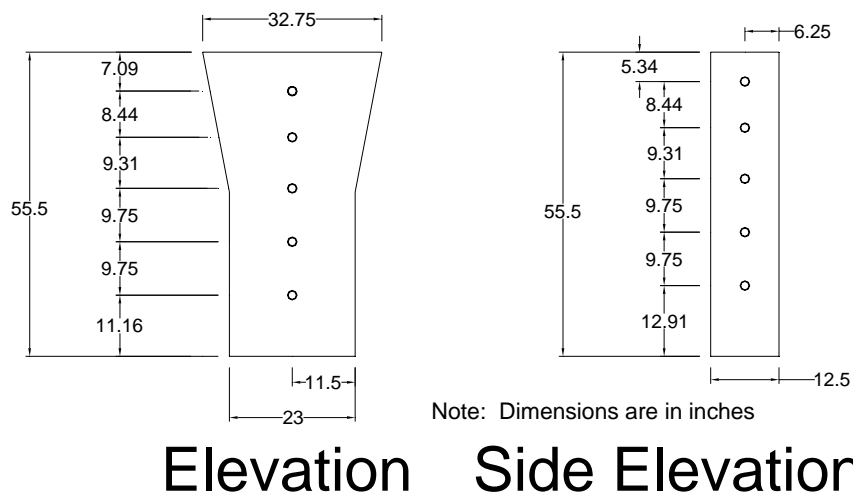


***Figure 4.7: Design Location of PVC Pipes***



*Figure 4.8: Column Reinforcement Cage*

#### **4.4.2 Footing Dimensions and Reinforcement**

The footing was designed to behave elastically when subjected to an axial load equal to the maximum axial capacity of the column. This was done in order to assure that the column behavior was isolated. The final footing dimensions are shown in Figure 4.9. The original footing was designed as a 54 in. x 54in. square. However, one side was later extended to 57.5 inches to provide adequate cover for PVC tubes which were inserted into the footing. The purpose of the PVC tubes was to provide holes through which the footing could be fastened down to the strong floor. These tubes were later proved unnecessary when testing the first column revealed that the footing did not need to be fastened to the strong floor.



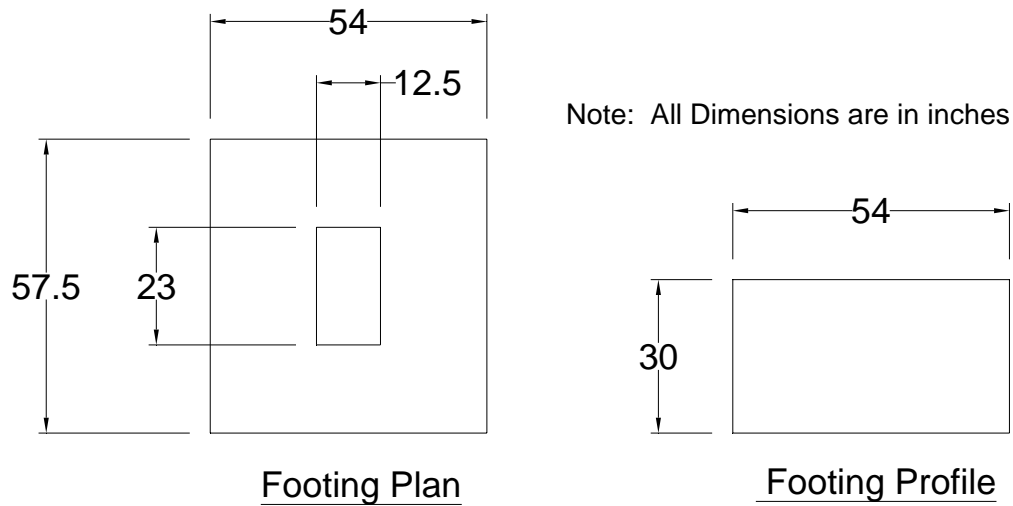


***Figure 4.9: Footing Dimensions***

The reinforcement used in the footing consisted of 2-way mats of number 5 bars in the top and bottom layers of the footing. In addition, stirrups in the form of number 3 bars were provided in both directions. A detail of the reinforcement used in the footing is provided in Appendix B. Figure 4.10 is an illustration of a fully constructed reinforcement cage which was placed in one of the footings.

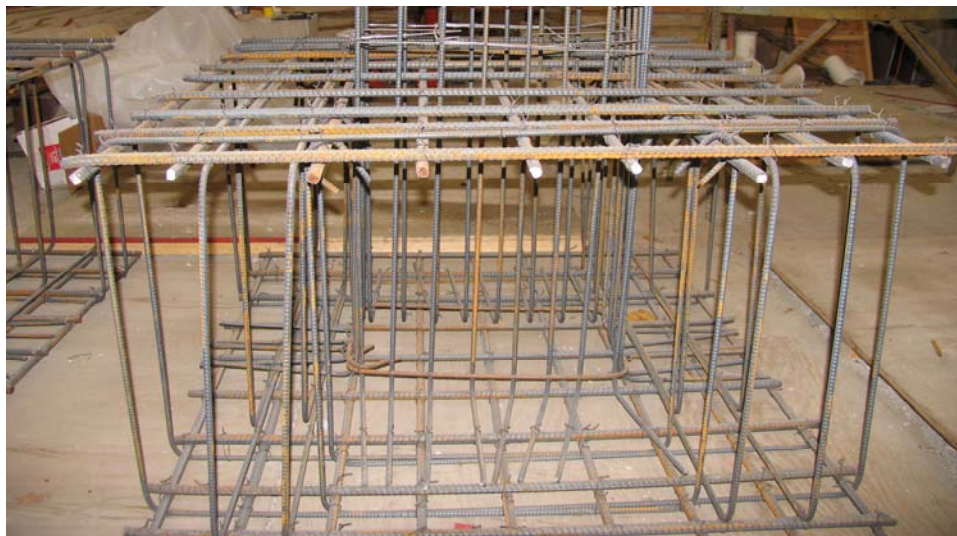


***Figure 4.10: Footing Reinforcement Cage***

### 4.4.3 Placement of Instrumentation

When deciding where to install the internal gauges it was decided to position all of the strain gauges and strain meters in the same horizontal plane of concrete. The idea behind this philosophy was to try and determine whether or not plane sections remained plane during the loading and subsequent failure of the columns. The layer chosen was in the bottom half of the column, twenty three inches up from its base. Based on the geometry of the section and the type of loading, this layer was initially believed to be a critical location for column behavior governed by combined axial load and biaxial bending.

#### 4.4.3.1 Stain Gauges

A total of twelve strain gauges were used to measure the strain in the longitudinal and transverse reinforcing steel in each specimen. The breakdown and general location of these gauges is shown in Figure 4.11.

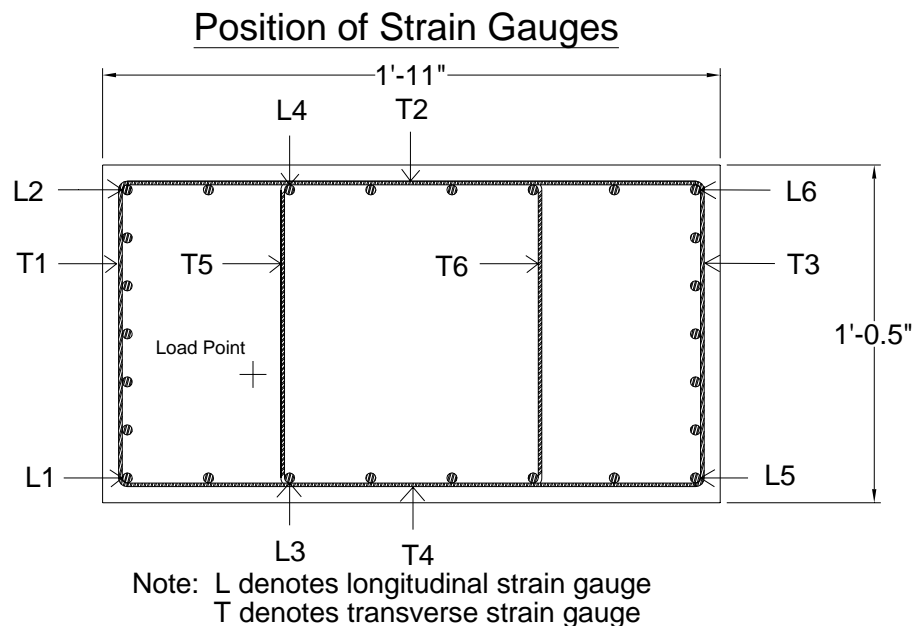


**Figure 4.11: Position of Strain Gauges**

#### 4.4.3.2 Strain Meters

In addition to the twelve strain gauges used to measure strain in the reinforcing steel, eight strain meters were constructed to measure the strain in the concrete. The concrete strain meters were constructed by attaching a strain gauge to a threaded aluminum rod. Aluminum was used because it has a similar modulus of elasticity to that of concrete. The gauge was then painted with gauge coat and wrapped with BLH Barrier E and Teflon tape. Then the device was sealed using heat shrink tubing. Finally, two nuts were fastened to either end of the rod creating a gauge length of four inches. Figure 4.12 is a detail of the strain meters used in the experiment, and Figure 4.13 shows their design location in the cross-section of the column. Figure 4.14 is a picture of the strain meters installed in a model column specimen.

Strain Meter

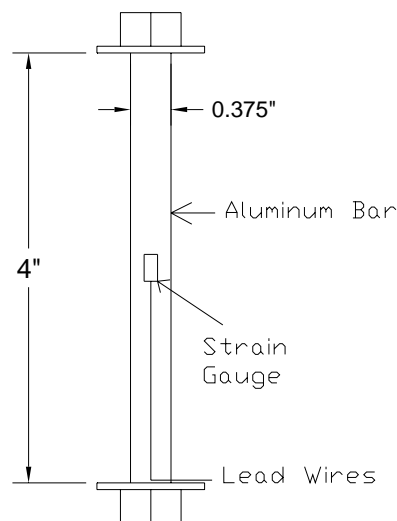


**Figure 4.12: Strain Meter**

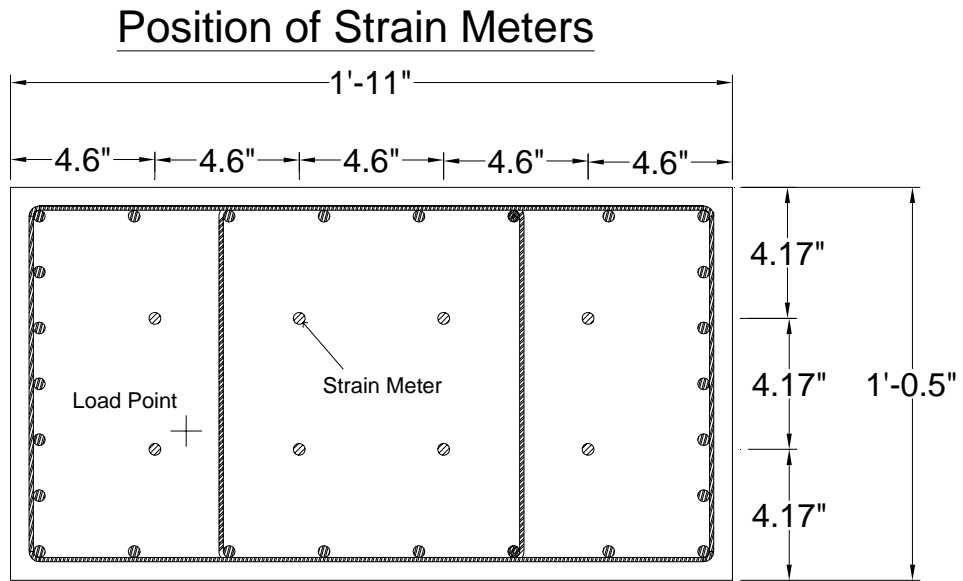


**Figure 4.13: Position of Strain Meters**

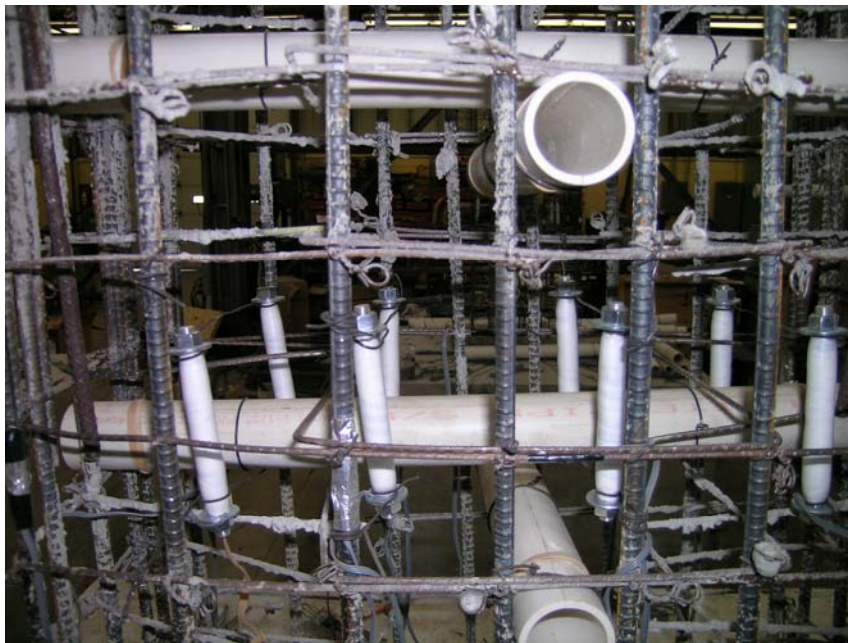


**Figure 4.14: Installed Strain Meters**

#### ***4.4.3.3 Load Monitoring***

A calibrated 10,000 psi pressure transducer was used with a ram of known piston area to measure the load applied on the specimens. The readings from the pressure transducer were cross checked against a calibrated pressure dial gauge to ensure accuracy.

#### ***4.4.3.4 External Gauges***

Linear potentiometers were used to measure the deflection of the test specimens. Potentiometers were placed on two sides of the column at three points along its height corresponding to locations near the base, midpoint, and top. The potentiometers were placed close to the centerline of the column in both directions. Figure 4.15 shows the potentiometers prior to testing specimen S2. The exact positions of the gauges for each of the five tests are listed in Appendix B. A mechanical dial gauge was also used to verify readings taken from the linear potentiometers.



***Figure 4.15: Test S2 Linear Potentiometers***

For the pre-cracked specimens dial gauges were fastened to the columns prior to cracking. These devices were used to measure initial crack width in addition to crack elongation during loading. For the first cracked specimen (C1) the gauges were placed near the mid-height. For the remaining cracked specimens (C2 & C1-R) the dial gauges were placed near the top of the column where the cracking in the actual structure is most severe. Figure 4.16 shows the apparatus used to measure the initial crack width and elongation.

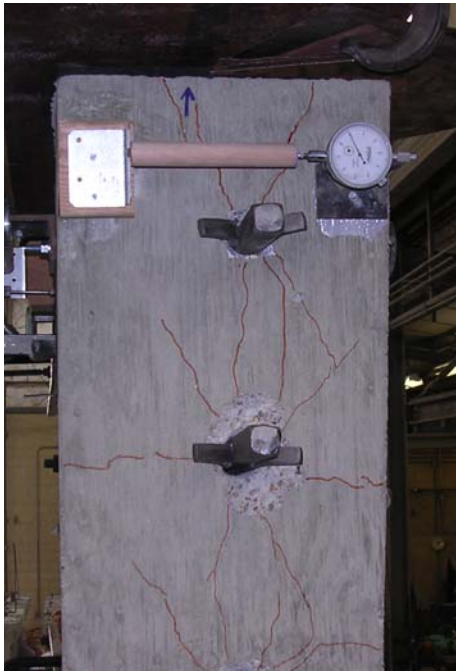
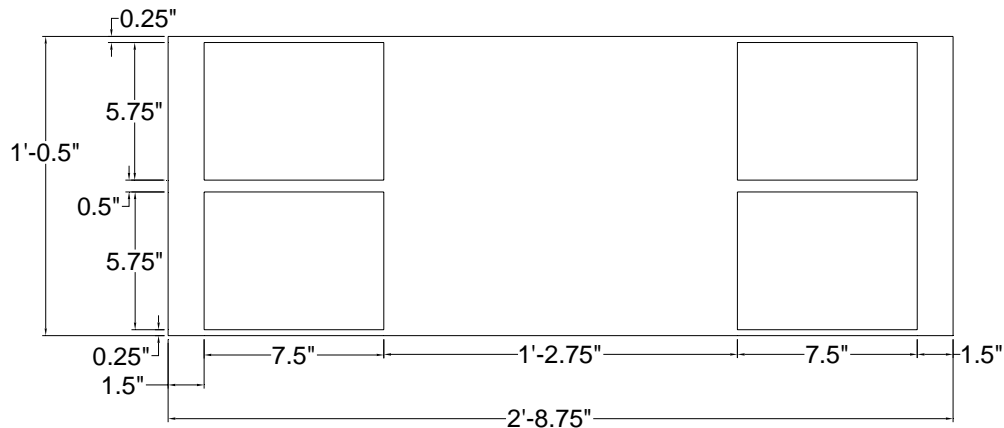


*Figure 4.16: Crack Measuring Apparatus*

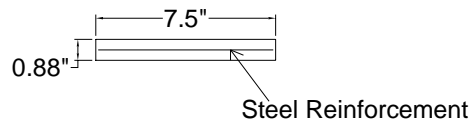
#### **4.4.4 Bearing Pads and Spreader Beam**

In order to properly represent the way the load is applied to the actual structure, scaled down versions of the bearing pads used in the construction of DD7 were used in the experimental program. Bearing pads available at Ferguson Laboratory were cut to the proper length, width, and height. Initially unreinforced pads were used for test specimen S1. However, it was later determined that a layer of reinforcement was necessary to properly model the existing pads. Therefore, new pads with a layer of steel reinforcement were cut for the remaining tests. These pads were placed at the same location (taking into account scaling of dimensions) as the prototype bearing pads. Figure 4.17 shows the location and dimensions of the bearing pads used in the experiment.

## Bearing Pad Dimensions and Layout



Plan View



Profile View

***Figure 4.17: Bearing Pad Dimensions and Layout***

A heavily reinforced spreader beam was used to distribute the load from the ram to all four pads. The beam was designed to be very stiff in order to provide proper load distribution to the bearing pads. A W14x 109 section with stiffeners welded at the critical locations was determined to be an adequate section. The spreader beam is shown in Figure 4.18.





*Figure 4.18: Spreader Beam*

#### **4.4.5 Concrete Mix Design**

The goal of the concrete design used to cast the model specimens was to match as closely as possible the concrete strength of the existing piers while also taking into account scaling of the maximum aggregate size. The maximum aggregate size for the columns in the DD spine, as reported in the construction documents, was 1.5 inches. Therefore, a maximum aggregate size of 3/8 inches was chosen for the model columns. The proportions for the mix design chosen for the model columns are listed in Table 4.3.

**Table 4.3: Concrete Mix Design**

Model Column Concrete Mix Design	
Cement (lbs./yd <sup>3</sup> )	564
Fly Ash (lbs./yd <sup>3</sup> )	0
Coarse Aggregate (lbs./yd <sup>3</sup> )	1625
Fine Aggregate (lbs./yd <sup>3</sup> )	1469
Water (lbs./yd <sup>3</sup> )	280
Admixture (lbs./yd <sup>3</sup> )	16.8

All four specimens were cast on the same day with concrete from one ready mix truck. The concrete was provided by Capital Aggregates. Concrete cylinders (6 in. x 12 in.) were made at the same time the concrete was being placed in the columns. The cylinders were used to measure the 28-day compressive strength in addition to the compressive and tensile strength of the concrete on the day of testing. Table 4.4 illustrates the close correlation between compressive strength of concrete cores taken from DD7 and the compressive strength of the concrete used in the model columns.

**Table 4.4: Compressive Strengths**

DD7 (f'c)	Model Columns (f'c)					
Core Strength (psi)	28-day (psi)	83-day (psi)	94-day (psi)	98-day (psi)	102-day (psi)	106-day (psi)
5780	4900	5800	5800	5800	5900	5900

The close correlation between these values greatly enhances the validity of this study.

#### 4.5 TESTING

The model concrete columns were tested on the elevated strong floor at The Ferguson Research Laboratory. A structural steel frame in conjunction with a hydraulic ram was used to load the specimens monotonically. The steel frame was fastened to the strong floor using 3 inch diameter bolts. The bolts were post-tensioned with a force approximately equal to 90 kips/bolt to ensure the frame was secure during the loading process.

Individual test specimens were moved into place underneath the frame using machinery skates. A pneumatic pump was used in combination with the ram to lift each specimen off of the skates and lower it down onto the strong floor.

The specimen and ram were then moved into position. The hydraulic ram was attached to a plate with rollers allowing displacement in the transverse direction. The ram was rolled into the proper position then clamped into place. In order to provide the second eccentricity, the specimen was then offset from the center of the ram in the longitudinal direction. A plum bob was used to align the center of the ram with the load point. The bearing pads were then positioned on the top of the column and the spreader beam was moved into place using chain hoists. With the exception of the first test, a spherical seat was then attached to the ram. The spherical seat provided a smooth contact surface between the ram and the spreader beam while also allowing the column to rotate freely. The strain gauges and linear potentiometers were then connected to the data acquisition system. The linear potentiometers were moved into the proper position on the column and the gauges were zeroed out.

The column was loaded in 50 kip increments until damage began to appear. After that load level was reached, the load increments were reduced to 25 kips until the specimen failed. Any cracks that formed during the loading process were properly marked and photographed between each load increment. Figures 4.19 and 4.20 show the setup used to test the model columns. After testing was complete, the specimens were removed from the test setup. At which time, a hammer was used to chip away loose concrete near the failure zone. Then, final photographs of the failure zone were taken. This process was repeated for each of the remaining tests.

It should be noted that several problem areas arose during the testing of the first specimen. For test specimen S1, the linear pots used to measure deflections were attached to the frame. While testing, the frame slipped relative to the floor at a load of 285 kips introducing error into the deflection readings. For this reason, it was decided to measure deflections independent of the testing

frame for the remaining specimens. The frame did not slip during the remainder of the tests. In addition to this problem, a spherical seat was not used for the first test. It is likely that this resulted in some improper distribution of load on the column. Also, the PVC tubes cast into the specimens crushed during the first test. It was determined to insert steel into the open sleeves for specimen S2 to match the behavior of columns with wedges. Finally, unreinforced bearing pads were used to test column S1 in contrast to reinforced pads which were used for the remaining specimens. These factors need to be taken into consideration when analyzing the test results. Much greater confidence is given to the results of tests two through five than those of test one.



***Figure 4.19: Test Setup***



*Figure 4.20: Specimen S2-Setup*

## **CHAPTER 5**

### **Results from Experimental Program**

#### **5.1 SPECIMEN S1**

The first experimental test was performed on specimen S1 on February 14, 2006. This test was conducted in order to determine the behavior of an undamaged model column when subjected to combined axial load and biaxial bending. The results from the test are given in the following sub-sections.

##### **5.1.1 Load Capacity**

Before testing began, the load capacity of the column based on combined biaxial load and bending was predicted using the program Biaxial Column v2.3 and the concrete compressive strength determined a few days prior to testing. Subsequent to testing when it had become apparent that the weak link in the column was the local zone under the bearing pad, the ultimate unfactored bearing stress under the critical pad was also calculated using the current 2005 AASHTO LRFD design specifications. This value was used to calculate the ultimate unfactored load of the column for the case in which bearing under the critical pad governs the failure of the column. The specimen was loaded with the ram load applied at the loading point given in Table 4.2 until failure occurred. Table 5.1 compares the predicted biaxial-flexure and bearing capacities of the column to the actual capacity determined from the test. The table shows close correlation between predicted biaxial-flexure capacity and experimental results. However, there is a large test overstrength between the predicted bearing capacity failure load and the experimental results. This overstrength does not correlate with the

type of failure as discussed in section 5.1.4. This difference is probably due to errors introduced as a result of the test setup used for this specimen.

**Table 5.1: Specimen S1 Load Capacity**

	Predicted Biaxial-Flexure Capacity (Sound Column)	Predicted Bearing Capacity (Sound Column)	Test Failure Load (Sound Column)
Maximum Load (kips)	595	463	600
Compressive Strength (psi)	5800	5800	5800

### 5.1.2 Deflection Measurements

As noted in section 4.5 of the previous chapter, error was introduced into the deflection measurements when testing specimen S1. Therefore, no deflection measurements are reported for this test.

### 5.1.3 Strain Measurements

Strains were measured in the reinforcing steel and the concrete during the testing process. The strains were measured in one cross-section of the column approximately 23 inches up from its base. Figures 5.1-5.3 show the load vs. strain graphs for the longitudinal steel, transverse steel, and concrete. The lines in the plots for the longitudinal steel and concrete load vs. strain curves were smoothed using trend lines. These plots show that the strain remained relatively linear in this portion of the column. The strain in the reinforcing steel was below the value at which yielding is expected to begin (0.002 in./in.). In addition, the strain in the concrete was well below the value at which crushing is expected to occur (0.003 in./in.). This shows that this section of the column still had adequate capacity to

carry load even though the failure load of the entire column had been reached. As a result, it can be surmized that the full potential capacity of the column cross-section was not realized, and the strains in the concrete and steel at this section are not critical. This is a direct result of the type of failure which is discussed in the next section.

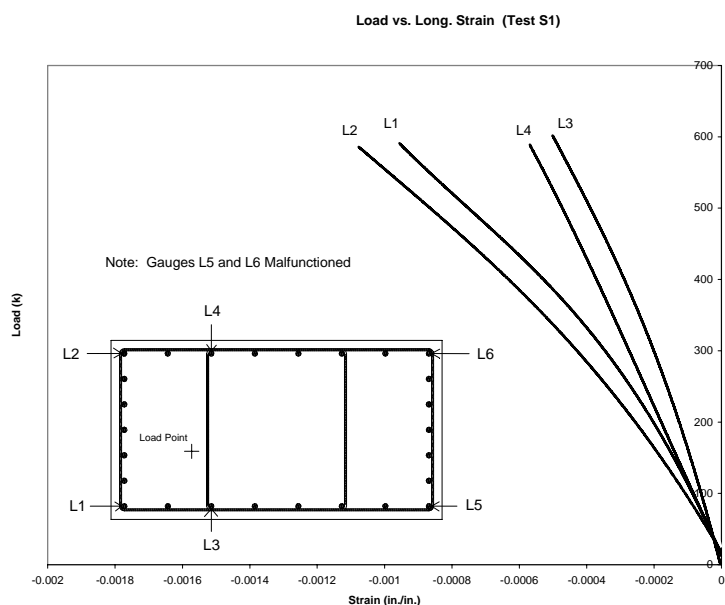


**Figure 5.1: S1-Load vs. Longitudinal Reinforcement Strain**



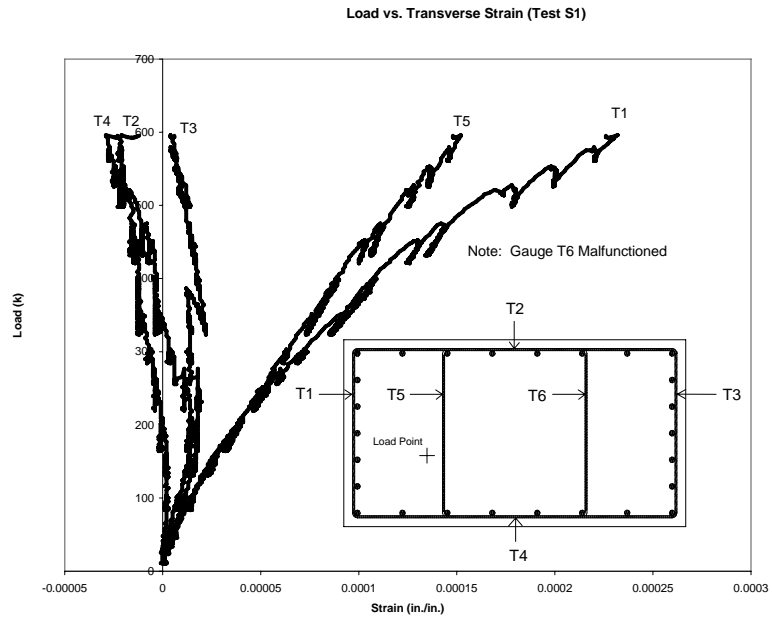


**Figure 5.2: S1-Load vs. Transverse Reinforcement Strain**

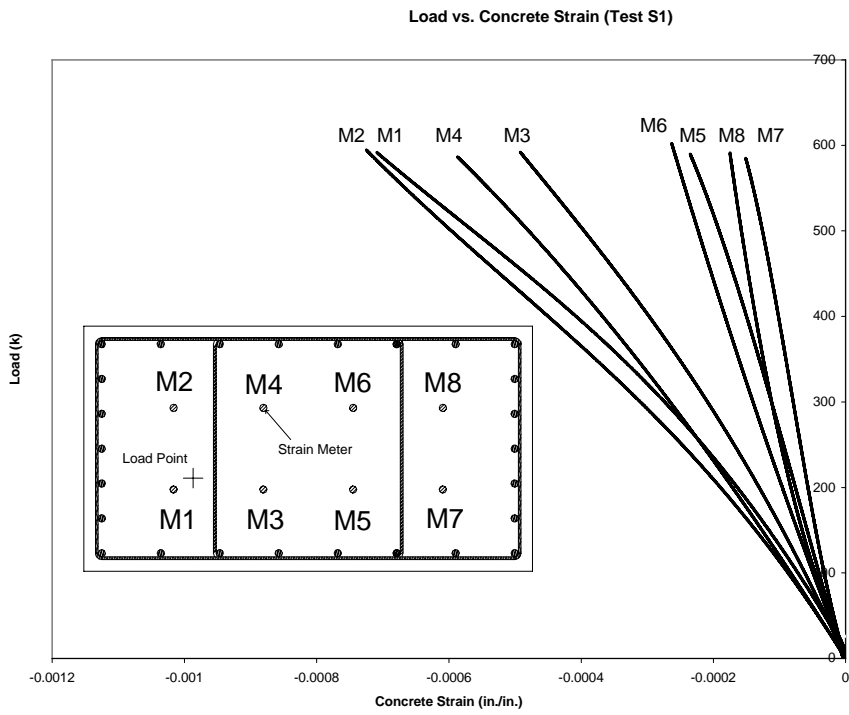


**Figure 5.3: S1-Load vs. Concrete Strain**

#### **5.1.4 Failure**

When discussing the failure of specimen S1, the three aspects of the failure that are addressed are location of the failure, type of failure, and mode of failure. The failure in specimen S1 occurred in the local zone directly underneath the most heavily loaded bearing pad. The failure was a brittle type failure. When the load reached approximately 66 percent of the ultimate load, large cracks began to form as shown in Figure 5.4. The concrete cover near the most heavily loaded pads began to spall at a load of 88 percent of the ultimate capacity. When the ultimate load was reached, the specimen failed suddenly and was no longer able to carry load at or near the maximum value. The mode of failure was diagnosed as concrete crushing due to excessive bearing stresses under the most heavily loaded bearing pad.

#### **5.1.5 Damage**

The substantial portion of damage in specimen S1 was directly underneath the most heavily loaded bearing pad. The first sign of damage observed while testing was a longitudinal crack which formed at 400 kips or 66 percent of ultimate just behind the back side of the bearing pads located on the most heavily loaded side of the column. This initial cracking is shown in Figure 5.4. This crack was observed on both sides of the column.

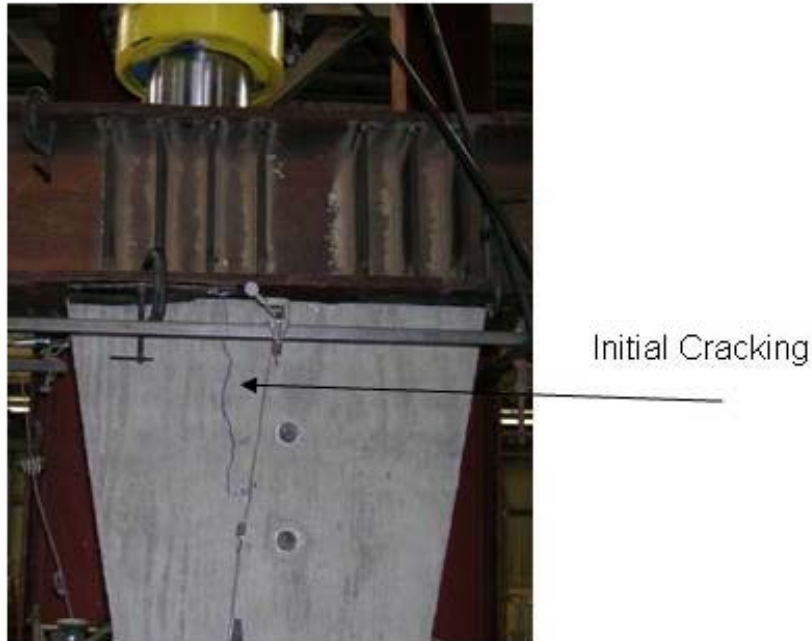


***Figure 5.4: S1-Initial Sign of Damage***

When the specimen was loaded to approximately 88 percent of the failure load, the concrete cover began to spall. As the load was increased to ultimate, the concrete under the two most heavily loaded bearing pads began to crush. The majority of the damage was observed directly under the most heavily loaded pad. The initial crushing of the concrete is clearly illustrated in Figure 5.5. After completing the test and removing the loose concrete fragments, it could be seen that the transverse reinforcement near the top of the column had fractured. Figure 5.6 shows the fractured transverse tie near the top of the column. In conclusion, the column sustained significant damage under the two most heavily loaded pads with the most damage directly underneath the pad with the largest load. The damage sustained in this local area resulted in failure of the specimen.



*Figure 5.5: S1-Concrete Crushing*

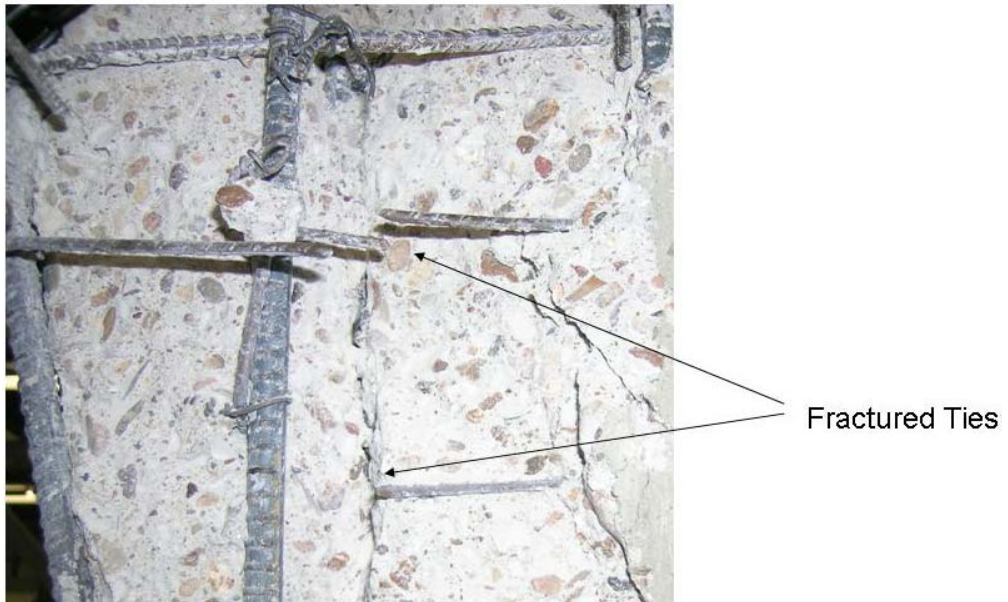


*Figure 5.6: S1-Fractured Transverse Ties*

## 5.2 SPECIMEN S2

The second experimental test was performed on undamaged specimen S2 on February 24, 2006. As discussed in chapter 4, significant changes were made to improve the test setup for this and future specimens. As a result, it was desirable to test another undamaged specimen with the new test setup before testing any intentionally damaged columns. The results from the test are given in the following sub-sections.

### 5.2.1 Load Capacity

Before testing began, the load capacity of the column was predicted using the same procedure used for specimen S1. The specimen was then loaded until failure occurred. Table 5.2 compares the predicted capacities of the column to the actual capacity determined from the test. The table shows a significant reduction (20%) between the predicted load capacity based on biaxial-flexure and the actual load capacity determined from experimental testing. However, the experimental results show close correlation with the capacity predicted using the critical bearing stress (within 5%).

**Table 5.2: Specimen S2 Load Capacity**

	Predicted Biaxial-Flexure Capacity (Sound Column)	Predicted Bearing Capacity (Sound Column)	Test Failure Load (Sound Column)
Maximum Load (kips)	595	463	478
Compressive Strength (psi)	5800	5800	5800

## 5.2.2 Deflection Measurements

For this test, deflection measurements were taken at three locations along both sides of the column. In addition, a mechanical dial gauge was used to take manual readings while testing. Figures 5.7 and 5.8 show the load vs. deflection plots for both the transverse (X) and longitudinal (Y) directions.

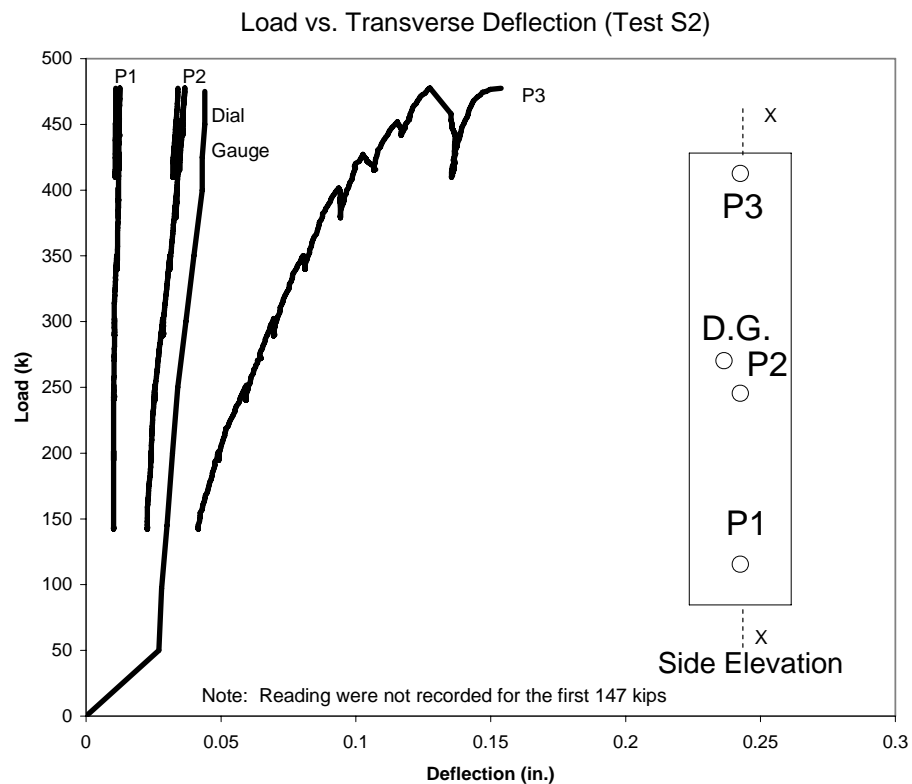


*Figure 5.7: S2-Load vs. X-Axis Deflection*

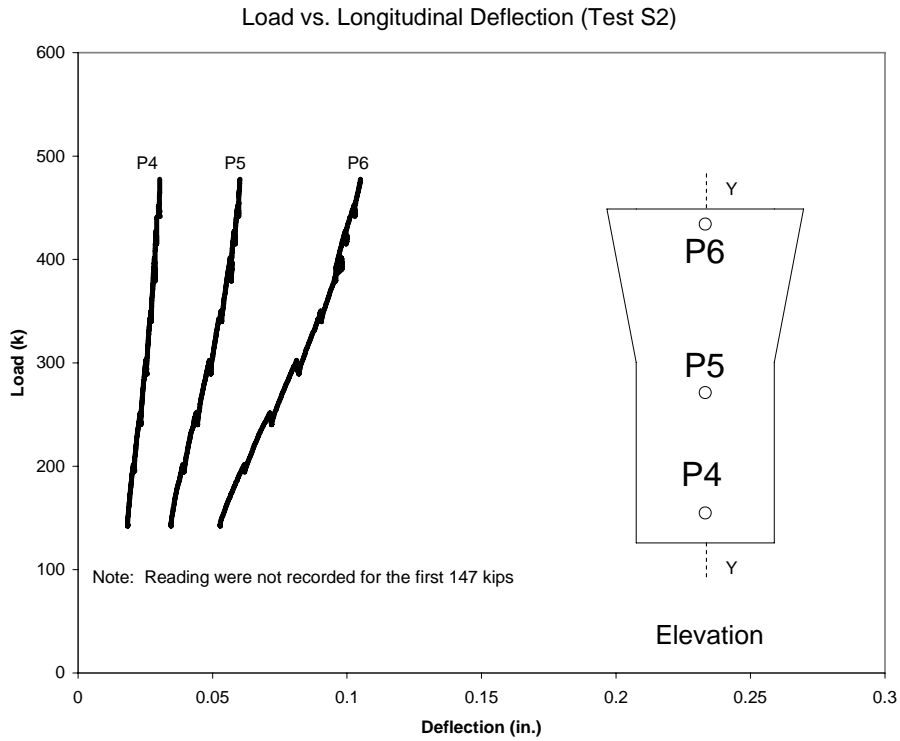


**Figure 5.8: S2-Load vs. Y-Axis Deflection**

As can be seen from the graphs, the columns experience a maximum deflection near the top which decreases to very small values near the base. The overall deflections are relatively small and are consistent with the loads that are being applied to the column.

### 5.2.3 Strain Measurements

Strains were measured in the reinforcing steel and the concrete during the testing process. The strains were measured in one cross-section of the column approximately 23 inches up from its base. The strain measurements obtained are given in Appendix C. The maximum strain observed in the longitudinal steel was -0.0012 in./in. (negative indicates compression), and the maximum concrete strain

was -0.0007 in./in. These values are well below expected values near failure. As stated before, the gauges were not in the critical failure zone for the column. Therefore, they do not show the most critical strain values in the specimens at the time of failure.

#### **5.2.4 Failure**

Like specimen S1, the failure in specimen S2 occurred in the local zone directly underneath the most heavily loaded bearing pad. The failure was a brittle type failure. When the ultimate load was reached, the specimen was not able to sustain this load, resulting in a loss of load carrying capacity and subsequent failure. Like specimen S1, the mode of failure was diagnosed as concrete crushing due to excessive bearing stresses. Figures 5.9a – 5.9h show the progression of failure for specimen S2.



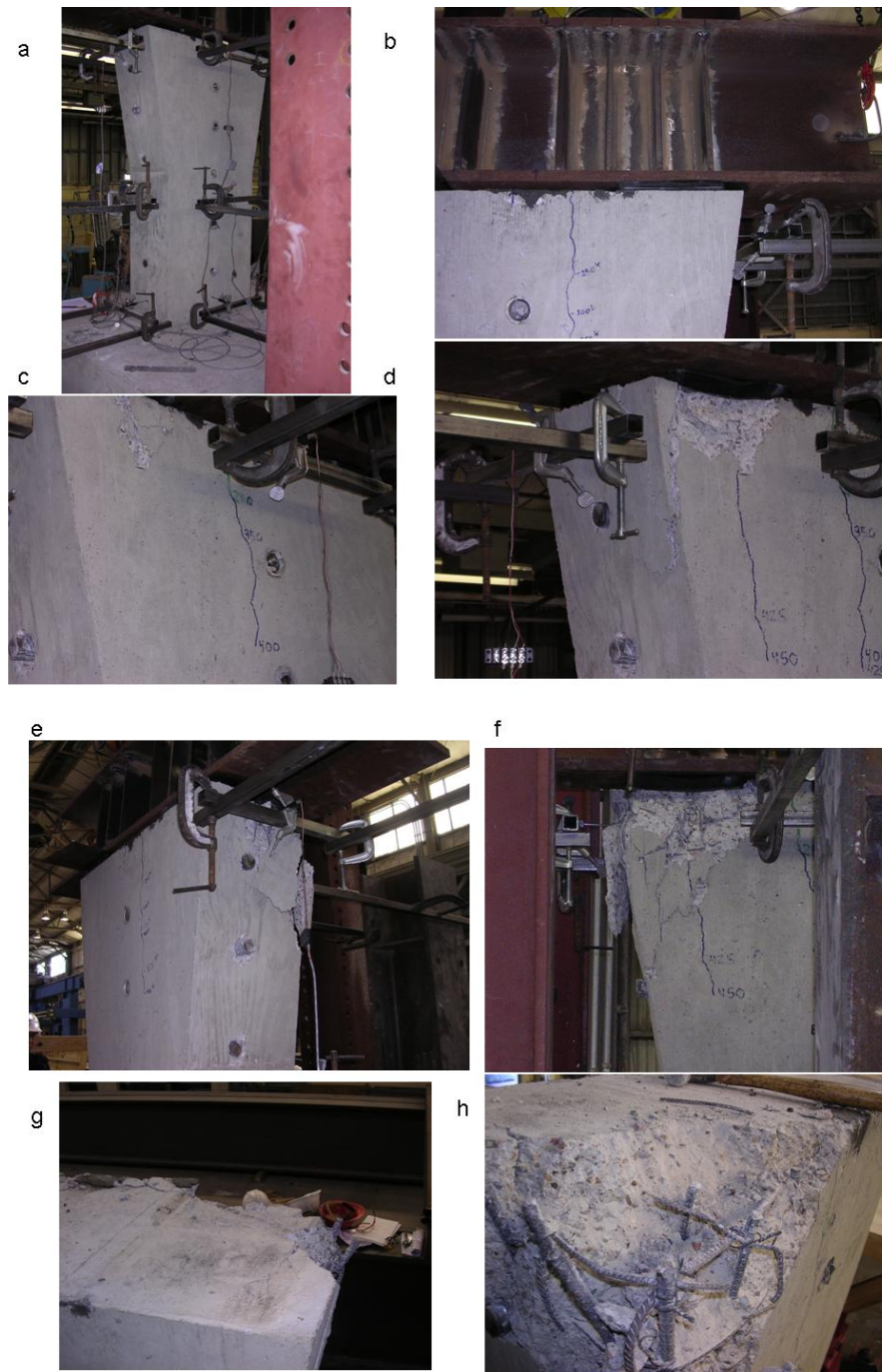


**Figure 5.9 (a-h): S2-Failure Sequence**

The mode of failure for this column can help explain why the predicted biaxial-flexure capacity is nearly 20 percent more than the experimental capacity. The biaxial-flexure capacity of the column was predicted using moment interaction curves where failure due to local stresses is not taken into account. Because the failure was in the local zone, the full capacity of the column cross-section was not developed. This is supported by the strain measurements in the concrete and longitudinal reinforcing steel, which are provided in Appendix C. Therefore, the actual capacity of the column was limited by bearing and was considerably lower than the predicted capacity based on axial load and flexure. Calculations based on bearing and the local zone capacity indicate a capacity within 5 percent of that attained in testing.

#### **5.2.5 Damage**

The substantial portion of the damage in specimen S2 was directly underneath the most heavily loaded bearing pad. As shown in Figure 5.9b, the first sign of damage observed while testing was a longitudinal crack which formed at approximately 52 percent of the ultimate load just behind the back side of the bearing pads located on the most heavily loaded side of the column.

When the specimen was loaded to an amount approximately equal to 400 kips (85% of max), the cover concrete near the most heavily loaded pad began to spall (Figure 5.9c). When the maximum load of 475 kips was reached, the concrete underneath the most heavily loaded pad crushed (Figure 5.9f). After completing the test and removing the loose concrete fragments, it was observed that unlike specimen S1, the transverse reinforcement near the top of column S2 had not fractured. Figure 5.10 shows the most heavily damaged corner of the column after completion of the test. This figure clearly indicates that the column failed as a result of concrete crushing underneath the most heavily loaded pad.



*Figure 5.10: S2-Bearing Failure*

### **5.3 SPECIMEN C1**

The third experimental test was performed on specimen C1 on February 27, 2006. This specimen was cracked using splitting wedges prior to loading. The crack width was determined by scaling down the largest observed crack width (as of March 1, 2006) in the lower portion of column DD7. The crack width observed in the field was 0.078 inches, which scaled down to a width of 0.02 inches. Dial gauges were placed near the mid-height of the model column on all four sides to measure the crack widths that were generated using the splitting wedges. The results from the test are listed in the following sub-sections.

#### **5.3.1 Load Capacity**

The load capacity of the test specimen was predicted using the same procedure as the previous two tests. The specimen was then loaded until failure occurred. Table 5.3 compares the predicted capacity of a sound column to the

actual capacity of the damaged column determined from experimental testing. The table shows a 20 percent reduction between the predicted biaxial-flexure load capacity of a sound column and the actual load capacity of a damaged column. However, there is only a 3 percent difference between predicted and tested values when using bearing capacity to predict the ultimate load.

**Table 5.3: Specimen C1 Load Capacity**

	Predicted Biaxial-Flexure Capacity (Sound Column)	Predicted Bearing Capacity (Sound Column)	Test Failure Load (Damaged Column)
Maximum Load (kips)	595	463	476
Compressive Strength (psi)	5800	5800	5800

### 5.3.2 Deflection Measurements and Cracking

Deflection measurements were taken using the same procedure that was used to test specimen S2. The load vs. deflection plots are given in Appendix C. The deflections measured during testing were very small. The maximum tip deflections were 0.14 inches in the X-direction and 0.05 inches in the Y-direction. Very little deflection was measured near the base of the column. Crack elongations were also measured during testing and are given in Appendix C. Very little elongation was observed for specimen C1.

### 5.3.3 Strain Measurements

Strains were measured in the reinforcing steel and the concrete during the testing process and are given in Appendix C. Similarly to specimen S2, the strains were measured in one cross-section of the column approximately 23 inches

up from its base. Due to the position of the gauges the strain measuring devices gave little information about the critical section of the column.

#### **5.3.4 Failure**

Like specimens S1 and S2, the failure in specimen C1 occurred in the local zone directly underneath the most heavily loaded bearing pad. The failure was a brittle type failure. Like specimens S1 and S2, the mode of failure was diagnosed as concrete crushing due to excessive bearing stresses. As was the case with specimen S2, there was good correlation between predicted values using critical bearing stress and actual test results. When comparing the test results in Tables 5.2 and 5.3, it can be seen that the pre-cracking of specimen C1 had little effect on the overall capacity of the column.

#### **5.3.5 Damage**

The substantial portion of the damage in specimen C1 was directly underneath the most heavily loaded bearing pad. Similar to specimens S1 and S2, the first sign of damage observed was a longitudinal crack which formed just behind the back side of the bearing pads located on the most heavily loaded side of the column. The crack began to form at a load of 300 kips (63% of ultimate).

When the specimen was loaded to an amount approximately equal to 400 kips (85% of max), the cover concrete under the most heavily loaded pad began to spall. This behavior was nearly identical to the behavior of specimen S2. When the maximum load of 476 kips was reached, the concrete underneath the most heavily loaded pad crushed. Like specimen S2, the transverse ties near the bearing area did not fracture in specimen C1. The behavior of specimens S2 and C1 were very similar. Both specimens failed at nearly the same load while experiencing comparable damage.

## **5.4 SPECIMEN C2**

The fourth experimental test was performed on specimen C2 on March 3, 2006. This specimen was cracked using splitting wedges prior to loading. The crack width was determined by scaling down the largest observed crack width (as of January 9, 2006) at the top of column DD6. This crack was the largest crack observed in the DD-spine columns. The crack width observed in the field, which was measured using a wire gauge, was 0.177 inches. This scaled down to a crack width of 0.048 inches for specimen C2. Dial gauges were placed near the top of the model column on all four sides to measure the crack widths that were generated using the splitting wedges. The elongation of the cracks was also measured during loading. The results from the test are given in the following subsections.

### **5.4.1 Load Capacity**

Again the load capacity of a sound column was predicted for both the biaxial flexure and bearing cases. The specimen was then loaded until failure occurred. Table 5.4 compares the predicted capacity of a sound column to the actual capacity of the damaged column determined from experimental testing. The table shows a reduction in capacity of approximately 4 percent when comparing the actual capacity to the undamaged capacity predicted using the critical bearing stress.

**Table 5.4: Specimen C2 Load Capacity**

	Predicted Biaxial-Flexure Capacity (Sound Column)	Predicted Bearing Capacity (Sound Column)	Test Failure Load (Damaged Column)
Maximum Load (kips)	600	471	451
Compressive Strength (psi)	5900	5900	5900

#### **5.4.2 Deflection Measurements and Cracking**

Deflection measurements were taken using the same procedure that was used to test specimen S2. The load vs. deflection plots are given in Appendix C. The deflections measured during testing were very small. The maximum tip deflections were 0.19 inches in the X-direction and 0.04 inches in the Y-direction.

The elongation of the preformed cracks was measured during the testing of specimen S2. The cracks on the north and south face of the column experienced very little elongation during loading. However, the crack on the east face of the column more than doubled in size. Figure 5.11 shows the behavior of the cracks during loading.

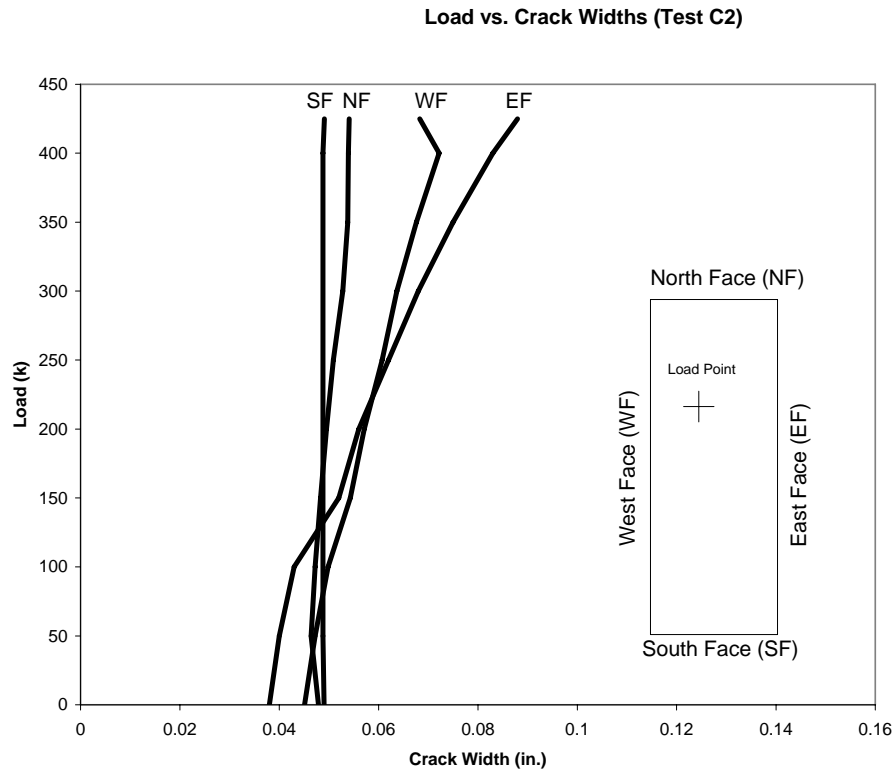


**Figure 5.11: C2-Crack Widths**

### 5.4.3 Strain Measurements

Strains were measured in the reinforcing steel and the concrete during the testing process. The strains were measured at the same location as the previous specimens and are given in Appendix C. It should be noted that significant initial strains were observed in the transverse reinforcement as a result of the precracking. These initial strains in the column ties, which were well removed from the failure zone, did not change very much during the subsequent loading. Figure 5.12 shows the strain measurements in the transverse reinforcement for specimen C2.



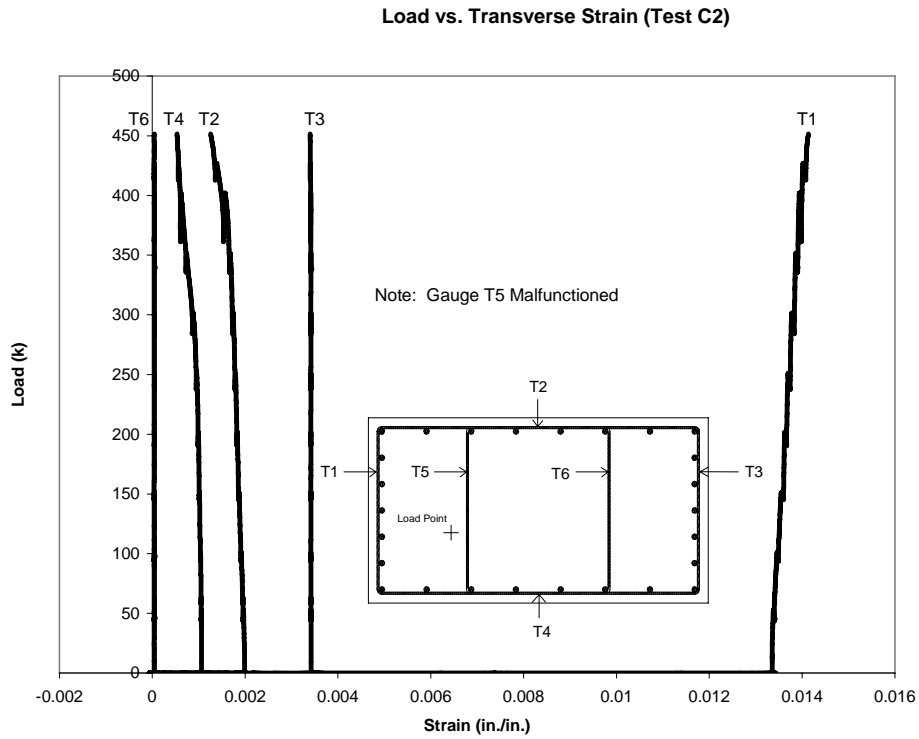


**Figure 5.12: Specimen C2 Transverse Strain Measurements**

#### **5.4.4 Failure**

Like the previous three specimens, the failure in specimen C2 occurred in the local zone directly underneath the most heavily loaded bearing pad. The failure was a brittle type failure. Like the other specimens, the mode of failure was diagnosed as concrete crushing due to excessive bearing stresses. When comparing the test results in Tables 5.4 and 5.3, it can be seen that the increased pre-cracking of specimen C2, when compared to specimen C1, reduced the capacity of the column by about 6 percent.

#### **5.4.5 Damage**

The majority of the damage in specimen C2 was directly underneath the most heavily loaded bearing pad. Even though the crack widths on the east and west face of the column were increasing as load was being applied, the first sign of damage observed was a longitudinal crack which formed at a load of 150 kips (33% of ultimate) just behind the back side of the bearing pads located on the most heavily loaded side of the column. This crack was only observed on the east face of the column until a load of 300 kips (67% of ultimate) was reached. At this point, the crack was apparent on both the east and west faces of the column. The concrete cover began to spall at a load approximately equal to 89 percent of the ultimate load. The concrete under the most heavily loaded bearing pad crushed at a load of 451 kips. Unlike specimens S2 and C1, the transverse ties near the bearing area fractured in specimen C2. The strain measurements taken for the transverse reinforcement in specimen C2 indicate that the precracking induced large initial strains prior to any loading. It is likely that these large initial strains helped contribute to the failure of the transverse ties. In conclusion, the damage in specimen C2 was similar to that of S2 and C1 with the exception of fracturing of the transverse ties and failure at a slightly lower load.

#### **5.5 SPECIMEN C1-R**

The fifth and final experimental test was performed on specimen C1-R on March 7, 2006. In order to perform this test, the bearing area of specimen C1 was repaired using epoxy grout thus creating specimen C1-R. The specimen was then rotated 180 degrees and loaded. By rotating the specimen, the major portion of the load was placed on the portion of the column that was not significantly damaged by test C1. This specimen was then cracked using splitting wedges prior to loading. The crack width was determined by increasing the value used for

specimen C2 (0.048 in.) by 75 percent. The resulting crack width used for specimen C1-R was 0.084 inches. This would correspond to a crack width of 0.3 inches in the prototype. Dial gauges were placed near the top of the model column on all four sides to measure the crack widths that were generated using the splitting wedges. The elongation of the cracks was also measured during loading. The results from the test are given in the following sub-sections.

### 5.5.1 Load Capacity

Before testing began the load capacity of a sound column was predicted in the same manner as the previous tests. The specimen was then loaded until failure occurred. Table 5.5 compares the predicted capacity of a sound column to the actual capacity of the damaged column determined from experimental testing. The results show a 16 percent reduction in load carrying capacity when comparing the actual damaged capacity to the predicted sound capacity calculated based on critical bearing stresses.

**Table 5.5: Specimen C1-R Load Capacity**

	Predicted Biaxial-Flexure Capacity (Sound Column)	Predicted Bearing Capacity (Sound Column)	Test Failure Load (Damaged Column)
Maximum Load (kips)	600	471	395
Compressive Strength (psi)	5900	5900	5900

### 5.5.2 Deflection Measurements and Cracking

Deflection measurements were taken using the same procedure that was used to test specimen S2. The load vs. deflection plots are given in Appendix C.

The maximum tip deflections of specimen C1-R were 0.26 inches in the X-direction and 0.06 inches in the Y-direction.

The elongation of the preformed cracks was measured during the testing of specimen C1-R. The cracks on the east and west face approximately doubled in size while the crack widths on the north and south face remained relatively the constant.

### **5.5.3 Strain Measurements**

Strains were not measured for this test.

### **5.5.4 Failure**

Like the previous four specimens, the failure of specimen C1-R occurred in the local zone directly underneath the most heavily loaded bearing pad. The failure was a brittle type failure. Like the other specimens, the mode of failure was diagnosed as concrete crushing due to excessive bearing stresses. When comparing the test results in Tables 5.5 and 5.4, it can be seen that the 75 percent increase in precracking of specimen C1-R, when compared to specimen C2, reduced the capacity of the column by about 12 percent. If the experimental capacity of specimen C1-R is compared to that of initially undamaged specimen S2, an overall reduction in ultimate load carrying capacity of 17 percent is observed.

### **5.5.5 Damage**

The damage in specimen C1-R was similar to the damage in the previous four specimens. The majority of the damage was directly underneath the most heavily loaded bearing pad. Again, the first sign of damage observed was a longitudinal crack which formed just behind the back side of the bearing pads located on the most heavily loaded side of the column. However, in this case the

crack formed at approximately 82 percent of the ultimate load and only propagated a few inches down the side of the column before the concrete began to spall and crush under the heavily loaded pad. The transverse ties near the bearing area did not fracture in specimen C1-R. Figures 5.13a – 5.13d show the resulting damage in specimen C1-R.

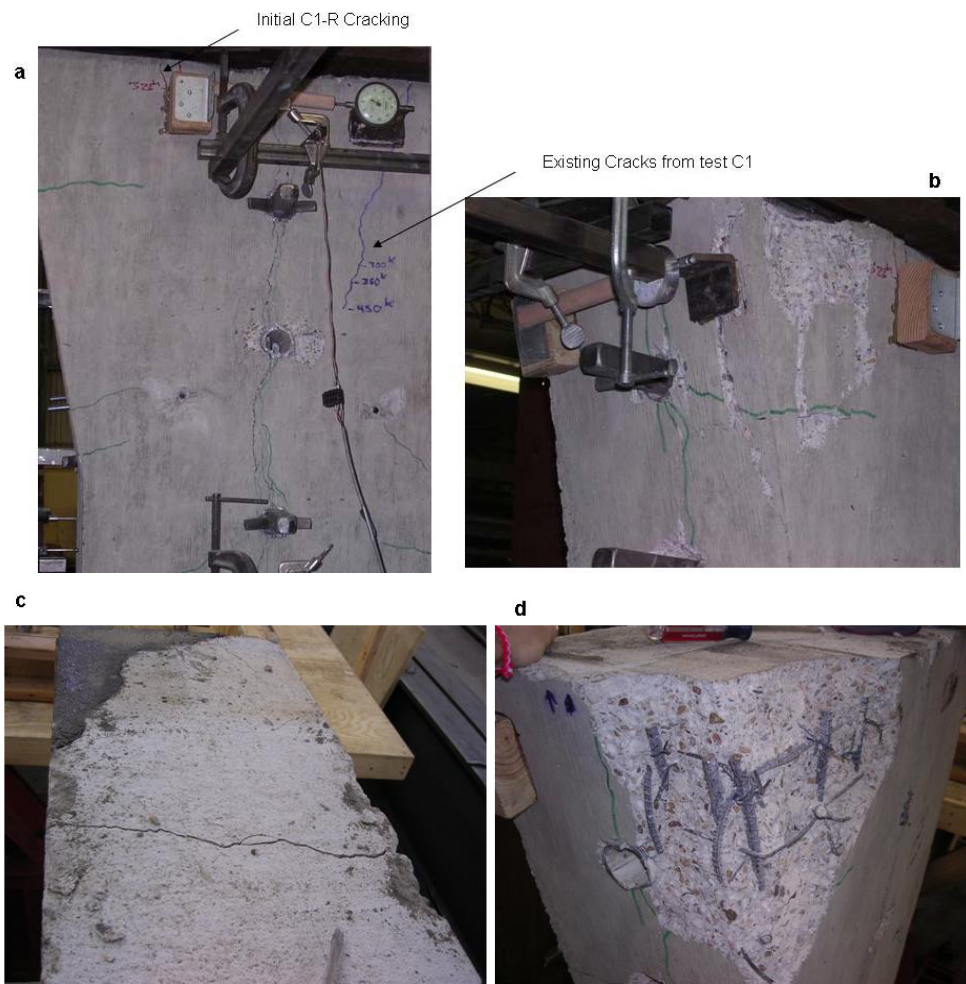


**Figure 5.13 (a-d): Specimen C1-R Damage**

# **CHAPTER 6**

## **Interpretation of Test Results**

### **6.1 INTRODUCTION**

The purpose of this chapter is to outline a structural assessment methodology which can be used to evaluate structural elements in the San Antonio Y. In addition, this chapter shows how this methodology was used to assess the current structural integrity of pier DD7. When conducting the structural assessment, the researchers had all of the current structural engineering knowledge and practices at their disposal. It is worth noting that many of the concepts and practices available to the engineer today, such as strut-and-tie modeling and the AASHTO LRFR Manual, were not available in US bridge design practice 20 years ago when the San Antonio Y was originally designed.

### **6.2 SUGGESTED STRUCTURAL ASSESSMENT METHODOLOGY**

#### **6.2.1 Review Current Literature**

The effects of ASR on the material properties of concrete have been thoroughly studied, and the current literature offers copious quality information regarding this topic. However, very little information is available regarding the effects of DEF on either material or structural properties of concrete. Therefore, it is important to continue to review any new literature that becomes available regarding DEF and its effect on reinforced concrete. In addition, the information on the effects of ASR on various structural properties of reinforced concrete such as bearing capacity and tensile strength is limited. Only several documented full-scale load tests on structural elements severely damaged by ASR have been conducted. As a result, it is important to continue to search out information

regarding the effect of ASR on the structural properties of reinforced concrete. The limited studies of the effect of ASR on structural properties of reinforced concrete were summarized in Chapter 2.

### **6.2.2 Perform In-situ Site Investigations**

It is important to continue to perform in-situ investigations of the San Antonio Y. The focus of the site investigation should be related to identifying new cracks and continuing to monitor existing cracks. Experimental testing revealed that the first sign of important structural damage in the model columns was a fairly wide vertical crack which formed at the back face of the most heavily loaded bearing pad. Particular close attention should be paid to cracks of this nature as they may be the first sign of serious structural distress. In addition to observing cracks, close attention should be paid to any local crushing that may be observed near the bearing pads. This is a sign that the columns are in a state of severe structural distress. Damage of this nature should be addressed immediately.

### **6.2.3 Determination of Material Strengths**

In order to properly perform a structural assessment, the material strengths of the element under consideration must be determined. Concrete cores have been taken from various critical elements (H19-C, DD6, & DD7, etc.) in order to gain a better understanding of the in-place compressive strength and modulus of elasticity of the existing concrete. ASR and/or DEF can significantly affect the material strengths of concrete. The effect can also vary within a single structural element. Therefore, it is important to consider each structural element on an individual basis when evaluating in-place material strengths. In addition, multiple cores should be taken from each element in order to generate believable average strengths.

#### **6.2.4 LRFR Provisions**

The AASHTO Guide Manual for Condition Evaluation and Load Resistance Factor Rating (LRFR) of Highway Bridges provides guidelines for assessing existing bridge structures. This guide can be used as an additional reference for the evaluation of structural elements in the San Antonio Y. However, there is one critical area in which the University of Texas researchers do not agree with the provisions of AASHTO LRFR. Section 6.1.8.2 of AASHTO LRFR specifies that the evaluation of substructure elements should be done using LRFD Load Case I. However, when referring to the Type I columns which were investigated in this study, this load case does not take into account the effect of biaxial bending. In the current case, biaxial bending resulted in bearing becoming the critical mode of failure. This resulted in a significant decrease (20%) in strength when comparing the actual capacity to the predicted biaxial flexure capacity of the column. Wind loading and truck loadings on one outer edge of these spans can produce substantial transverse (YY axis) moments. At the same time, longitudinal braking forces and alternate span loadings can produce longitudinal moments (XX axis). In this case biaxial bending is important. For this reason LRFD Load Case I is not adequately conservative and is not recommended as the only load case to be used for investigative purposes.

#### **6.2.5 Review of Original Design Calculation**

When performing a structural assessment, it is important to review the calculations made in the original design. While investigating the original design of the Type I piers in the San Antonio Y, it was found that a single worst case loading scenario was used for the design of all of the Type I piers. This design approach ensured that substantial conservatism in pier design was present. With the subsequent ASR and/or DEF damage that conservatism was very fortunate.



However, this worst case loading scenario does not apply to all of the Type I piers. Therefore, in order to gain an accurate estimation of the loads on critical elements of the San Antonio Y, it is necessary to determine the loads for these elements on an individual basis.

Testing of Type I model piers revealed that the critical mode of failure for case III, 2 lane loading was bearing failure underneath the most heavily loaded pad. This prompted an investigation into the original design of the bearing pads of a Type I column. The investigation revealed that the biaxial loading case was not taken into account in the original design of the bearing pads. In addition, a bearing stress (1,000 psi at service load) greater than that recommended by the 1983 AASHTO Provisions (800 psi at service load) was used in the original design. These two design assumptions resulted in bearing becoming the critical mode of failure for the chosen load case. Therefore, particular attention should be paid to the design of the bearings when performing evaluations on various other structural elements in the San Antonio Y.

At the time of the original design of the San Antonio Y, the use of strut-and-tie modeling was not a well recognized method of analysis of structures. Now, however, strut-and-tie modeling is a well known method of analysis which is included in the LRFD Design Specifications and is particularly beneficial when analyzing D-regions in structural elements. Therefore, when assessing critical elements in the San Antonio Y, strut-and-tie modeling should be used to evaluate the existing in-place behavior of critical D-regions.

#### **6.2.6 Evaluation of the Structural Integrity of Existing Elements**

In determining the in-place structural integrity of an existing element of the San Antonio Y, all steps mentioned in the sub-sections above should be taken into consideration. The information obtained in the investigation can be used to

generate an accurate assessment of any negative or positive effects on the capacity of the structural element under investigation. From this information, a reasonable worst case capacity of the existing columns can be determined and compared with the applicable loads on the structure. This comparison will reveal the potential reserve capacity, if any, of the existing element under investigation.

### **6.2.7 Remedial Measures**

If the investigation determines that the structural element does not have sufficient reserve for anticipated loadings, repair and strengthening methodologies can be evaluated on a case by case basis.

## **6.3 APPLICATION OF ASSESSMENT METHODOLOGY TO PIER DD7**

### **6.3.1 Negative Factors Affecting Existing Pier Capacity**

#### ***6.3.1.1 Literature Review***

The review of the current literature revealed several negative factors regarding the effects of ASR on the column under investigation. It was found that ASR can have significant negative effects on the material properties of concrete, including reduction in compressive strength, tensile strength, and modulus of elasticity. Very important to this case, it was found that ASR can cause reductions in bearing capacity of up to 25 percent.

#### ***6.3.1.2 Review of Original Design Calculations***

As mentioned in section 6.2.5, review of the original design calculations revealed that the biaxial loading case was not taken into account in the original design of the bearing pads. AASHTO LRFD Load Case I was used for the original design of the bearing pads. The maximum load on the critical pad for this load case was 34 percent of the total load on the column. This compares to 56

percent of the total load for load case III, 2 lane, which includes biaxial effects. The result is effectively a 65 percent increase in load on the critical pad when biaxial effects are taken into account. In addition, a bearing stress of 1,000 psi at service load was used, which is greater than that recommended by the 1983 AASHTO Provisions (800 psi at service load). The end result is a substantial capacity reducing effect because the pier is governed by failure in bearing instead of its higher capacity in biaxial flexure. It should be noted, however, that calculations (given in Appendix D) performed using the AASHTO LRFD 2005 Provisions indicated that the bearing capacity of the concrete is sufficient to resist the design factored load even when biaxial effects are taken into account.

Review of the original design also required investigation of the reinforcement in the critical D-region at the top of the column. A strut-and-tie model was developed for the model column in order to determine the forces in the column. Particular emphasis was put on the top of the column where the difference in loading and geometry cause tension in the horizontal direction. The details of the strut-and-tie modeling are given in Appendix D. Figure 6.1 shows the basic model that was used and clearly illustrates the tensile force mentioned above.

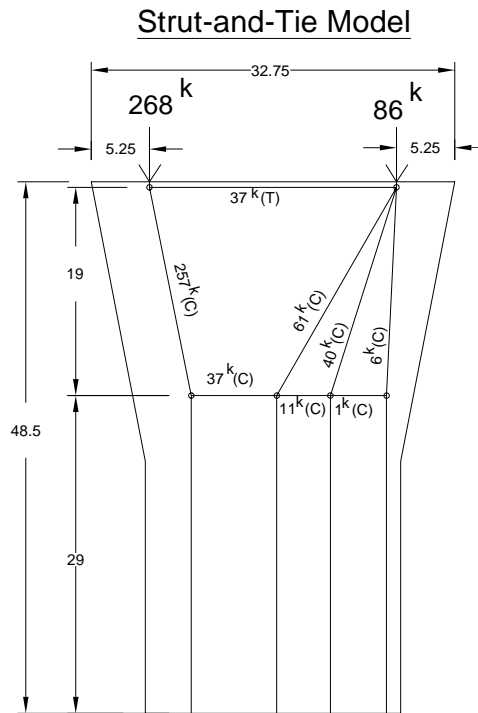


**Figure 6.1: Strut-and-Tie Model for Reduced Scale Model Column**

The purpose of generating the strut-and-tie model was to determine if the transverse reinforcement provided near the top of the column was adequate to resist the tensile force generated. The results from the calculations (given in Appendix D) are listed in Table 6.1.

**Table 6.1: Transverse Reinforcement Capacity**

Load (kips)	STM Tie Force (kips)	Transverse Reinf. Capacity (kips)	Adequacy of Existing Reinforcement
478 (Ult. S1)	37	11	Severely Inadequate
191 (Factored Design, Case III, 2 lane)	15	11	Marginally Inadequate

The results indicate that the transverse reinforcement near the very top which was used in the design of the existing piers is marginally inadequate at the factored load level and very inadequate at the much higher load corresponding to failure of the pier. This helps explain the large splitting cracks and fracturing of the transverse reinforcement which occurred while testing the model piers (see Figures 5.4 & 5.6). This also helps explain the damage observed in column DD6 (Figure 1.2). The large splitting cracks observed at the top of column DD6 are likely due to a combination of DEF and a lack of adequate transverse reinforcement. It is important to consider this critical area when performing an evaluation of DD type columns. Large tensile forces are generated in this D-region as a result of loading and geometry. The current transverse reinforcement in the columns is not adequate to resist such factored loads. If the load factors are removed the current reinforcement is adequate for  $1.0D + 0.5(L + I)$ . In addition, more tensile forces in this region can occur as a direct result of ASR and/or DEF related expansion. These observations indicate that this portion of the column is a critical area in which repairs may need to be considered. External post-tensioning would easily replace this deficiency and would be easy to apply in this region.

It should be noted that the amount of transverse reinforcement chosen to resist the tensile force in the original strut-and-tie model was determined somewhat arbitrarily. As a result, a modified strut-and-tie model was developed to more accurately represent the transverse reinforcement in the pier. This model is given in Appendix D. From the modified model it was determined that the transverse reinforcement resisting the top tensile tie was not adequate. The results from this model were very similar to the original model. Therefore, it was concluded that the original model is an accurate representation of the reinforcement in the top of the pier.

### 6.3.1.3 Effect of Cracking on Deflections and Capacity

The experiments conducted for this study provide information about the effect of various levels of cracking on the capacity and deflections of the piers under investigation. Five specimens were tested in total. Two of the specimens were uncracked, and three were precracked to varying size crack widths. Table 6.2 lists the various levels of cracking for the five specimens. Corresponding crack widths in the prototype pier are shown based on direct modeling theory.

**Table 6.2: Test Specimen Crack Widths**

Specimen	S1	S2	C1	C2	C1-R
Model Crack Width (in.)	0.0	0.0	0.02	0.048	0.084
Prototype Crack Width (in.)	0	0	0.07	0.18	0.31

In order to gain a better understanding of the effect of cracking on deflections, graphs were generated from data collected in the experimental study which display the load versus tip deflection for tests S2, C1, C2, and C1-R. Figures 6.2 and 6.3 show the load versus tip deflection for the four tests in the X and Y directions respectively. It should be noted that due to spalling of the concrete near the deflection measuring devices accurate readings were not able to be obtained after failure occurred. Therefore, the graphs do not reflect measurements taken after the failure load was reached. The point for the full “unfactored” axial load represents the axial load without load factors positioned at the X and Y eccentricities at which the specimens were loaded. It is extremely important to note that the failure loads of all of the initially uncracked and severely cracked specimens were substantially higher than their service and

factored load requirements. There was a substantial margin of reserve in all test specimens.

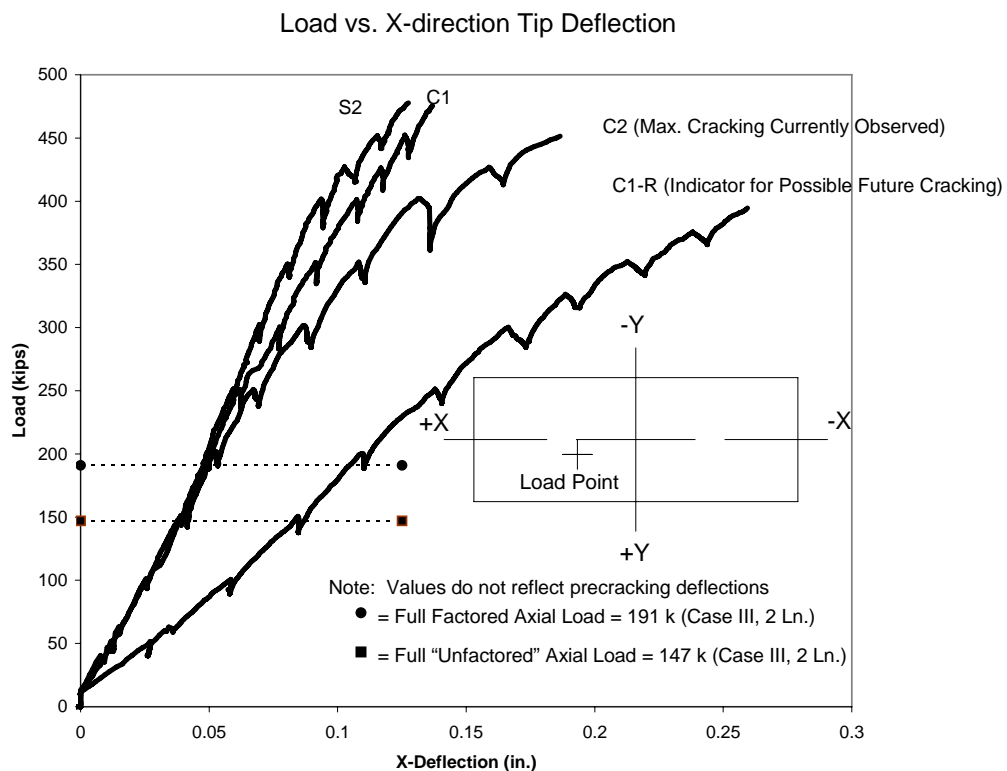


**Figure 6.2: Load vs. X-direction Tip Deflection**

### Load vs. Y-direction Tip Deflection

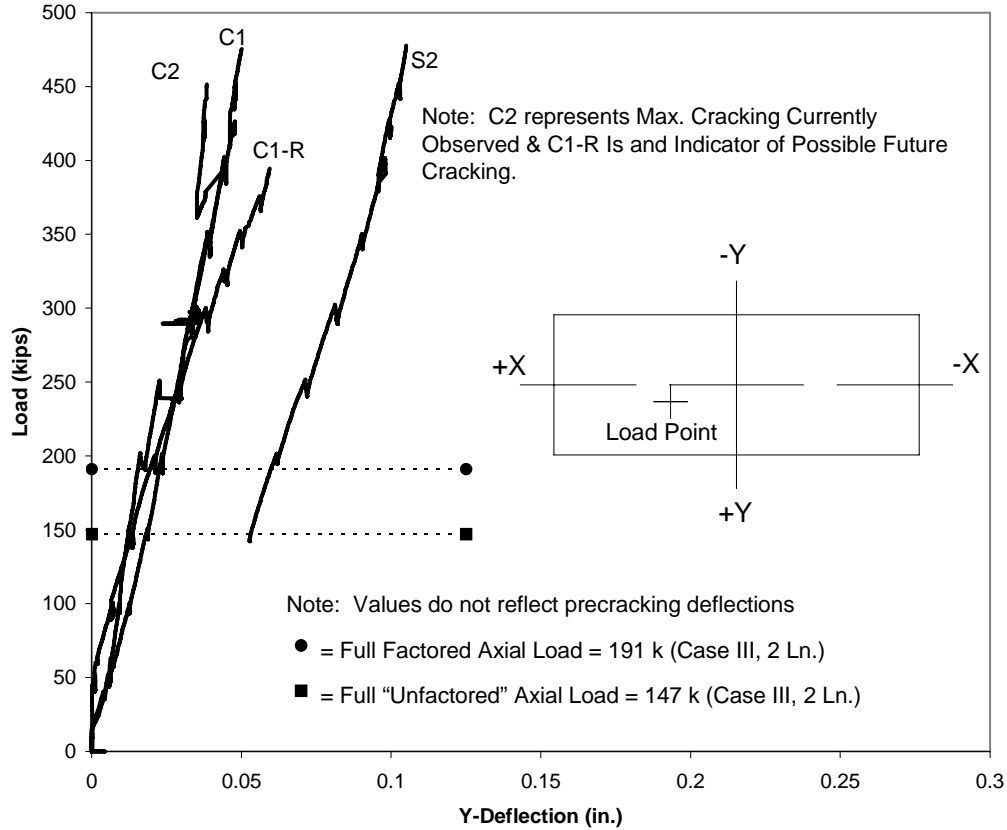


**Figure 6.3: Load vs. Y-direction Tip Deflection**

Figure 6.2 shows a trend between initial damage and deflections. As initial damage in the form of precracking is increased, deflections at ultimate load increase. The graph shows that deflections in the X-direction remained relatively linear up to the point of failure for specimens S2 and C1. However, this was not the case for specimens C2 and C1-R, which had a substantial increase in precracking when compared to S2 and C1. For specimens C2 and C1-R, the large crack widths caused a reduction in the stiffness of the columns in the X-direction.

The effect of precracking on ultimate capacity was also investigated. Table



6.3 compares the crack width to the test failure load for four of the five tests. Test S1 was omitted due to lack of confidence in results.

**Table 6.3: Ultimate Load vs. Crack Width**

<b>Specimen</b>	<b>Crack Width (in.)</b>	<b>Prototype Crack Width (in.)</b>	<b>Test Failure Load (kips)</b>	<b>% of Test Failure Load of Specimen S1</b>
S2	0	0	478	100 %
C1	0.02	0.07	476	100 %
C2	0.048	0.18	451	94 %
C1-R	0.084	0.31	395	83 %

The table shows that precracking does not change the test failure load of the columns at the minimal crack width present in specimen C1. However, as the cracks increase in size to significant levels (specimen C2 has cracking similar to the present maximum cracking in SAY Pier DD6), the test failure load is clearly reduced. For cracking simulating around twice the largest crack level currently experienced in the DD series of piers (C1-R), a reduction in capacity of approximately 20 percent was observed. Figure 6.4 shows the normalized critical bearing stress at the failure load for different levels of precracking. The figure indicates that as the level of precracking is increased, the ultimate bearing capacity decreases. However, the bearing capacity is well above the factored design level as shown in Figure 6.4. In Figure 6.4 and for future discussion the “service” load case indicates the load case in which load factors are removed from dead and live loads but are not removed from wind loads. The load factor is not removed from wind loads because the value of this load factor is 0.39. Removing this would result in a larger wind load corresponding to hurricane conditions and is not representative of the service case.

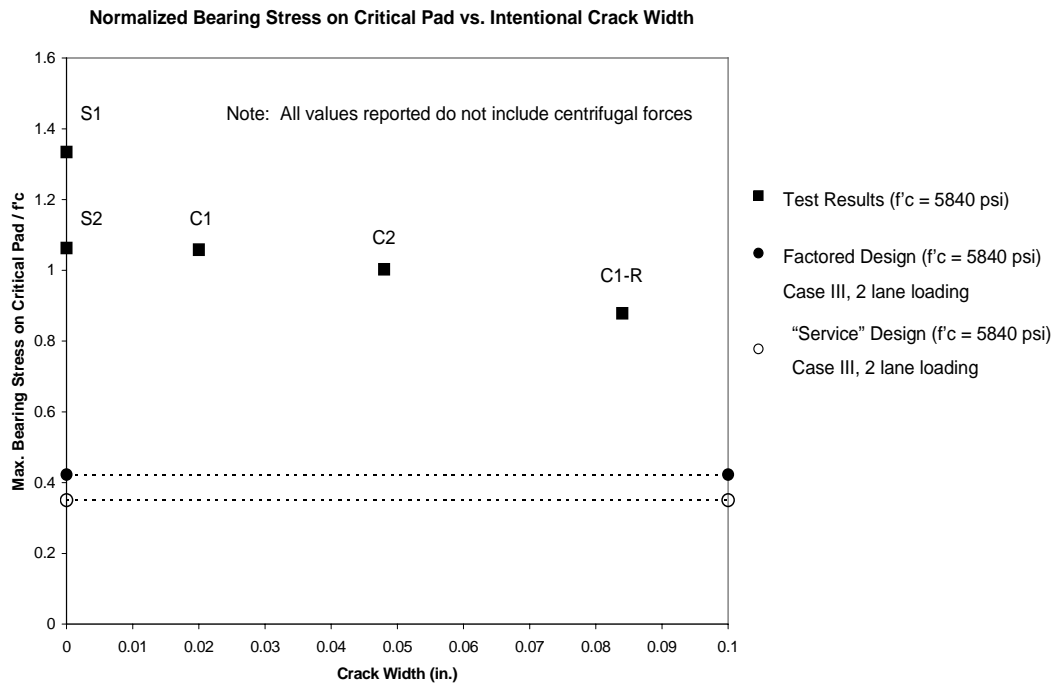


**Figure 6.4: Effect of Cracking on Bearing Capacity**

### 6.3.2 Positive Factors Affecting Existing Pier Capacity

Investigation of pier DD7 in the San Antonio Y revealed several positive factors affecting the in-place capacity of the pier. In-situ testing of concrete cores revealed a significant excess of compressive strength of the concrete in the pier as compared to the design strength. Core testing revealed a compressive strength of approximately 5,780 psi compared to a assumed compressive strength of 3,600 psi used in the original design. This increase in compressive strength has a significant beneficial effect on the ultimate capacity of the column.

In addition to the increased concrete compressive strength, review of the design calculations revealed that substantial centrifugal force moments were included in the design of column DD7. The DD series of columns are positioned in a relatively straight line. Therefore, the moments which result from the

inclusion of centrifugal forces approach zero. Thus the loads that are actually on pier DD7 are significantly less than the loads used to design the pier. The end result is that the original pier was over designed resulting in substantial increase in reserve capacity when compared to the original design.

An additional intended reserve capacity is also provided by the load factor on the dead load used in the original design. For the critical load case (III, 2 lane), the unfactored axial load is composed of 91 percent dead load. The load factor on the dead load is 1.3. As a result of the superstructure being composed mainly of precast elements, it is not likely that the 30 percent increase in dead load provided by the load factor is actually seen on the structure. A more realistic load factor for the dead load would be around 1.1. Applying this load factor to the dead load would result in a 14 percent decrease in the factored axial load for case III, 2 lane loading. This decrease in axial load provides an additional reserve capacity in addition to that provided by the increased concrete strength and the inclusion of centrifugal force moments mentioned above. However, this reserve would not generally be counted.

One final positive observation comes from the literature review of Chapter 2. Several documented full-scale load tests were conducted on structural elements severely damaged by ASR. These load tests revealed that although the observed damaged appeared to be severe, it had only minimal effects on the actual structural capacity of the elements under investigation.

### **6.3.3 Net Affect of Factors on Pier Capacity**

After identifying the positive and negative factors affecting the existing column capacity, a fairly accurate representation of the in-place structural integrity of pier DD7 can be determined. Through experimental testing, the critical mode of failure for the model columns was determined to be bearing

failure under the critical pad. With this in mind, some idea of the current and future reserve capacity of pier DD7 can be obtained by comparing results from the experimental program to some probable loading scenarios. Figure 6.5 compares the normalized bearing stress on the critical pad for the undamaged specimen (S2) and most severely damaged specimen (C1-R) to the normalized critical bearing stress for load case III, 2 lane loading determined from the design calculations. In addition, two other cases are added to the figure. One case applies a 25 percent reduction to the maximum normalized bearing stress determined from test S2. This case represents the 25 percent reduction in bearing capacity which may result from ASR related deterioration. The other case is the “service” load case. Comparison with this case shows the total reserve capacity of the structure. Figure 6.5 assumes a concrete compressive strength of 5,840 psi. This value represents the average compressive strength of all five experimental tests and is close to the compressive strength of DD7 (5,780 psi) determined from concrete cores. Figure 6.6 compares the same values mentioned for Figure 6.5. However, a compressive strength of 3,600 psi is used to normalize the bearing stress calculated for the case III, 2 lane loading scenarios. This compressive strength represents the compressive strength assumed in the original design. It is possible (but not likely) that the piers may have concrete strengths closer to the 3,600 psi assumed in design.

Potential Reserve Capacities of Pier DD7

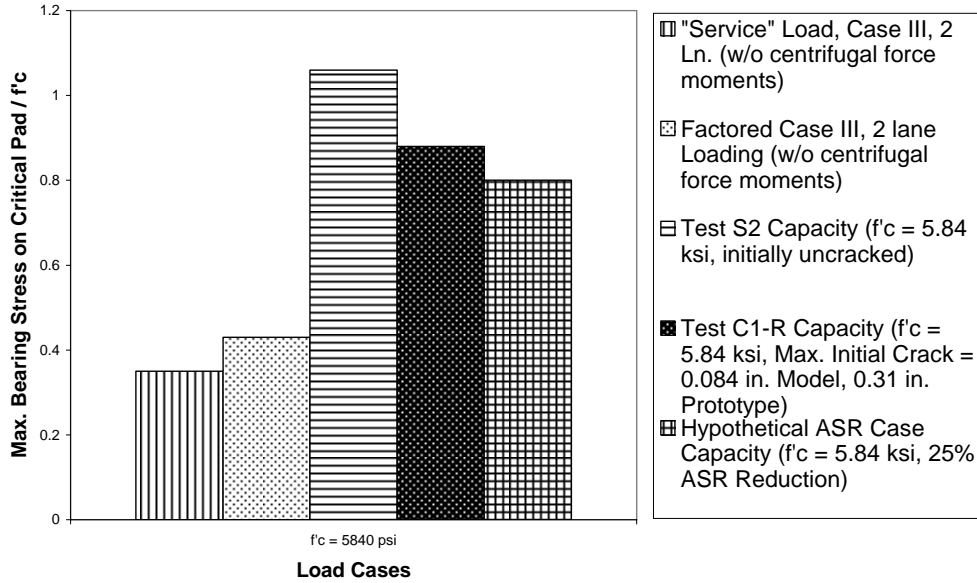


Figure 6.5: Potential Column Reserve Capacities (f'c = 5840 psi)

Potential Reserve Capacities of Pier DD7

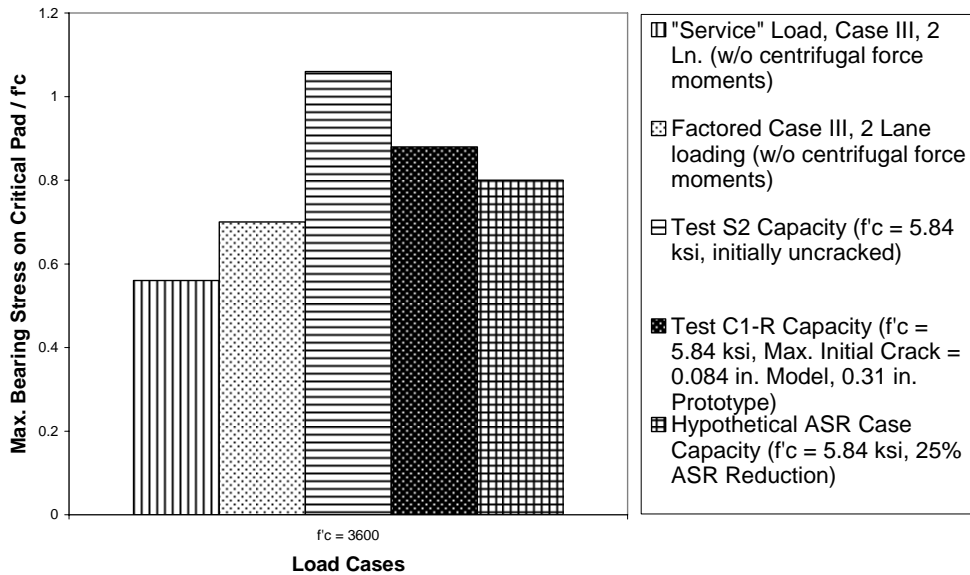


Figure 6.6: Potential Column Reserve Capacities (f'c = 3600 psi)

Figures 6.5 and 6.6 illustrate that pier DD7 has adequate capacity to resist load even in a cracked and ASR damaged state based on knowledge to date. In other words, the positive effects of increased concrete strength and inclusion of centrifugal force moments in design outweigh the negative factors of reduced capacity due to ASR or severe mechanical cracking and underdesign of the bearing pads. This results in a net positive reserve capacity for pier DD7 compared to LRFR requirements. However, these positive effects do not compensate for the shortage of transverse reinforcement in the top of the pier. Figure 6.6 indicates that even at the design compressive strength of 3,600 psi, a reserve exists when comparing the worst case capacity (25% ASR reduction of specimen S1) to the worst case loading scenario (Load case III, 2 lane). A more probable capacity of 251 percent of design requirements is obtained by comparing the capacity determined from test C1-R to the “service” load case shown in Figure 6.5 (Remember the level of damage induced in C1-R corresponds to a crack width 175% wider than the widest crack width observed to date in the DD series on piers).

By following the design methodology, it was determined that even at these very severe levels of damage, the current capacity of column DD7 is sufficient to resist the worst case loads that may be applied to this structural element. In fact, Figure 6.5 shows that a substantial reserve capacity exists at the current level of damage.

#### **6.3.4 Remedial Measures**

Through the experimental evaluation and strut-and-tie modeling, it was determined that the critical section of the piers under investigation is at the top of the column near the bearing area. Remedial measures which involve providing confinement at the top of the column can serve two beneficial purposes.

Confinement can be used to effectively increase the concrete compressive strength resisting bearing pressures at the top of the column. This increased concrete compressive strength results in an increase in bearing capacity. In addition, confining forces will counter act the outward thrusting forces which are present in the top of the pier (transverse tensile tie force shown at the top in Figure 6.1). This will help to supplement the already small amount of reinforcement present in the top of the pier. Figure 6.7 shows confining forces acting around the perimeter of the top of the column.

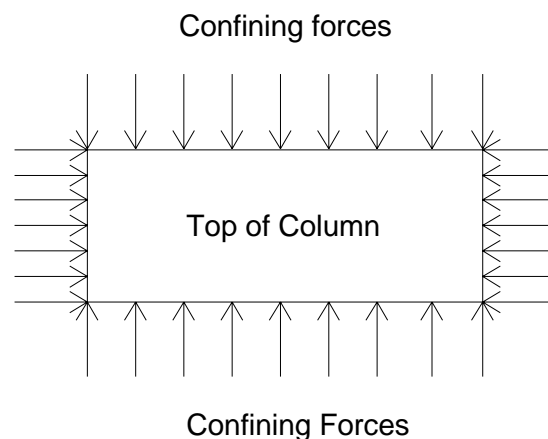


***Figure 6.7: Remedial Confining Forces***

The exact method in which these confining forces would be provided will be further explored in later phases of this project. More research is necessary in order to better understand the forces generated by ASR and/or DEF related expansion. Further tests are planned to produce cracking by such means. Once these forces are determined, they can be combined with the forces which develop from differences in loading and geometry. Then, various remedial measures such as post tensioning with steel plates or carbon fiber wrapping can be properly evaluated.

# **CHAPTER 7**

## **Conclusions and Implementation**

### **7.1 BRIEF SUMMARY**

The focus of this thesis is on the examination and evaluation of the ASR and/or DEF damaged DD series piers in the San Antonio Y. The main objective of this research program was to generate a structural assessment methodology that could be used to evaluate the current and future integrity of damaged structural elements in the San Antonio Y. In order to accomplish this task, a detailed examination of a typical structural element was conducted. The element chosen for investigation was a Type I Pier, specifically DD7. The examination involved performing an in depth literature review, investigating the basis for the existing design, determining the in-place material properties, and performing an experimental investigation. The focus of the literature review was on the effect of ASR and/or DEF on the material and structural properties of reinforced concrete and reinforced concrete structures. Review of the original design calculations was performed in order to determine any positive or negative factors present in the original design that may affect the current in-place structural integrity of the pier under investigation. Determining the in-place material properties was necessary to properly evaluate the structural capacity of the existing pier. The experimental investigation was used to determine the most likely mode of failure as well as the effect of the type of cracking present in the field on the capacity of the chosen pier. After these four portions of the examination were completed, a structural assessment methodology was generated and validated using results from the examination. In this way, the objective of developing a structural assessment



methodology which can be used to evaluate the current and future integrity of structural elements in the San Antonio Y was accomplished.

## **7.2 CONCLUSIONS**

Throughout the course of this research study several conclusions were reached which allowed for the evaluation of the current structural integrity of the in-place Type I Piers in the San Antonio Y. The key conclusions reached are listed as follows:

- Centrifugal force moments, which were taken as substantial and played a fairly major role in the original design of the prototype pier, approach zero for the pier under investigation. It should be noted that the original design was based on a worst case scenario for all piers and centrifugal force moments were appropriate in other locations in the San Antonio Y.
- AASHTO LRFD load case III, 2 lane loading (without centrifugal force moments) was determined to be the most realistic and critical loading scenario for the piers under investigation.
- The exclusion of biaxial effects in the original design of the bearing pads resulted in bearing being the critical mode of failure for the model piers when subjected to load case III, 2 lane loading.
- Testing of concrete cores taken from the prototype pier revealed that the in-place compressive strength of the column under investigation is substantially larger (60%) than the compressive strength assumed in the original design. This increase is reflected in substantially higher capacities for bearing and for combined axial-flexure when LRFD based analysis is used. It should be noted that the increase in compressive strength results in an approximately linear increase in bearing capacity.

However, it does not provide any benefit in regards to the tensile capacity at the top of the column.

- Review of the current literature indicates that ASR can reduce the bearing capacity of reinforced concrete. A worst case estimate for the amount of reduction is thought to be in the neighborhood of 25% for large scale specimens.
- Testing model piers revealed that fairly wide precracking reduced the effective capacity of the piers by reducing the bearing capacity. The trend indicated that increases in precracking resulted in increased reduction in bearing capacity. Precracking the model piers to a scaled crack width 1.75 times the maximum crack width observed in the DD series of columns reduced the effective capacity of the model piers by 17 percent.
- Strut-and-tie modeling indicated that the transverse reinforcement in the top of the piers is marginally inadequate for resisting tensile forces generated from differences in loading and geometry. Also, additional tensile forces in these locations may result from ASR and/or DEF related expansion.
- The positive effects of increased concrete strength and inclusion of centrifugal force moments in design outweigh the negative factors of reduced capacity due to ASR or severe mechanical cracking and underdesign of the bearing pads. This results in a net positive reserve capacity for pier DD7 compared to LRFR requirements. However, these positive effects do not compensate for the shortage of transverse reinforcement in the top of the pier. It may be necessary to add external reinforcement to control cracking due to this shortage of transverse reinforcement.

### **7.3 IMPLEMENTATION**

The conclusions listed in the section above validate that the structural assessment methodology proposed in Chapter 6 can be used to gain an accurate portrayal of the in-place integrity of structural elements in the San Antonio Y. Therefore, it is proposed that this methodology be used by TxDOT to check structural elements in the San Antonio Y which are thought to be under distress. The methodology in conjunction with in-situ monitoring can be used to evaluate the current and future reserve capacities of critical elements. By implementing the methodology proposed, TxDOT engineers can continuously evaluate the current and future integrity of structural elements in the San Antonio Y. This methodology will need to be continuously updated as further information on the effects of ASR and DEF becomes available.

### **7.4 RECOMMENDATIONS FOR FUTURE RESEARCH**

Over the course of the investigation and experimental program, several key areas which may require future research have become apparent. Suggested avenues for further research are listed as follows:

- Test model piers with concrete suffering from ASR and/or DEF related deterioration under the same loading conditions used in this experiment.
- Perform a sub-series of tests on the critical bearing portion of the model piers in order to better determine the effect of ASR and/or DEF on the bearing capacity of this critical region.
- Generate a 3-dimensional strut-and-tie model for the top of the model pier. Use the forces attained from this model in conjunction with estimated tensile forces resulting from ASR and/or DEF to develop a repair strategy for the critical top portion of the column, if necessary.

- Generate a finite element model of the prototype pier that includes cracking effects which can be used to evaluate the strength of existing columns with varying levels of ASR and/or DEF damage.
- Conduct an in-depth investigation into the footing of the prototype pier and determine the role that ASR and/or DEF related damage in the footing plays in relation to the entire structural element.

# Appendix A

## Additional Design Information

### A.1 ORIGINAL DESIGN CALCULATIONS

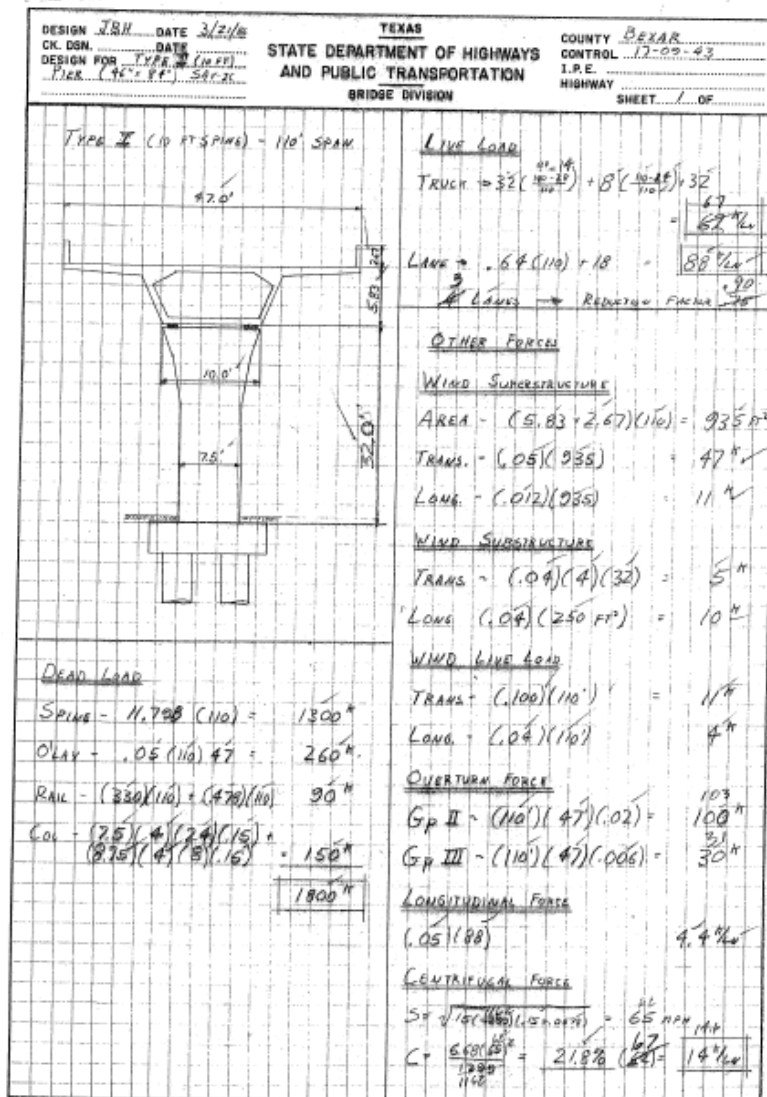


Figure A.1: Original Design Calculations (1 of 27)

DESIGN <u>JBH</u> DATE <u>4/15/66</u>		TEXAS		COUNTY <u>SEAN</u>	
CK. OSM. <u>JBH</u> DATE <u>4/15/66</u>		STATE DEPARTMENT OF HIGHWAYS		CONTROL <u>12-09-73</u>	
DESIGN FOR <u>TYPICAL CROWN</u>		AND PUBLIC TRANSPORTATION		I.P.E. <u>J.R.S.</u>	
<u>Design (10 ft)</u>		BRIDGE DIVISION		HIGHWAY <u>283</u>	
				SHEET <u>2</u> OF <u>4</u>	
<u>MOMENTS</u>			<u>MOMENTS</u>		
<u>TRANSVERSE</u>			<u>LONGITUDINAL</u>		
<u>LIVE LOAD</u>			ASSUME 10 TO DRILL <sup>START</sup> & FIXITY <sup>7</sup> (LOAD HAS BEEN TAKEN AT TOP OF FOOTING) BUT <u>NOT</u> <u>FORWARD</u> DESIGN.		
1 Ln - (88)(18.5) =	1630 <sup>ft</sup>		11 (46.25)	=	510 <sup>ft</sup>
2 Ln - 88(6.5) =	570 <sup>ft</sup>		10 (26)	=	260 <sup>ft</sup>
3 Ln - 88(-5.5) =	-480 <sup>ft</sup>		<u>WIND LINE LOAD</u>		
4 Ln - 88(-17.5) =	-1540 <sup>ft</sup>		4 (53.83)	=	215 <sup>ft</sup>
<u>WIND</u>			<u>LONG. FORCE</u>		
47 (36.25) =	1700 <sup>ft</sup>		2 Ln - 2(4.4)(53.83) =	475 <sup>ft</sup>	
5 (16) =	80 <sup>ft</sup>		3 Ln - 3(4.4)(53.83)(.9) =	640 <sup>ft</sup>	
	1780 <sup>ft</sup>		4 Ln - 4(4.4)(53.83)(.75) =	710 <sup>ft</sup>	
<u>LIVE LOAD WIND</u>			<u>LOADING COMBINATIONS</u>		
11 (43.83) =	480 <sup>ft</sup>		<u>GR I</u>		
<u>OVERTURNING</u>			2 Ln		
Gr II - 100(11.75) =	1175 <sup>ft</sup>		Pu - 1.3(1800) * [2.17(2X80)] =	2720 <sup>ft</sup>	
Gr III 30(11.75) =	350 <sup>ft</sup>		Mut - 2.17(430*520) + 1.3(1230) =	6375 <sup>ft</sup>	
<u>CONTINUOUS FORCE</u>			3 Ln		
2 Ln - 14(43.83)(.9) =	1230 <sup>ft</sup>		Pu - 1.3(1800) * [2.17(2)(88)(.9)] =	2855 <sup>ft</sup>	
3 Ln - 14(3)(43.83)(.9) =	1660 <sup>ft</sup>		Mut - [2.17(430*510+480)(.9)] + 1.3(1660)	=	5517 <sup>ft</sup>
4 Ln - 14(4)(43.83)(.75) =	1840 <sup>ft</sup>		4 LANES NOT USED		

Figure A.2: Original Design Calculations (2 of 27)

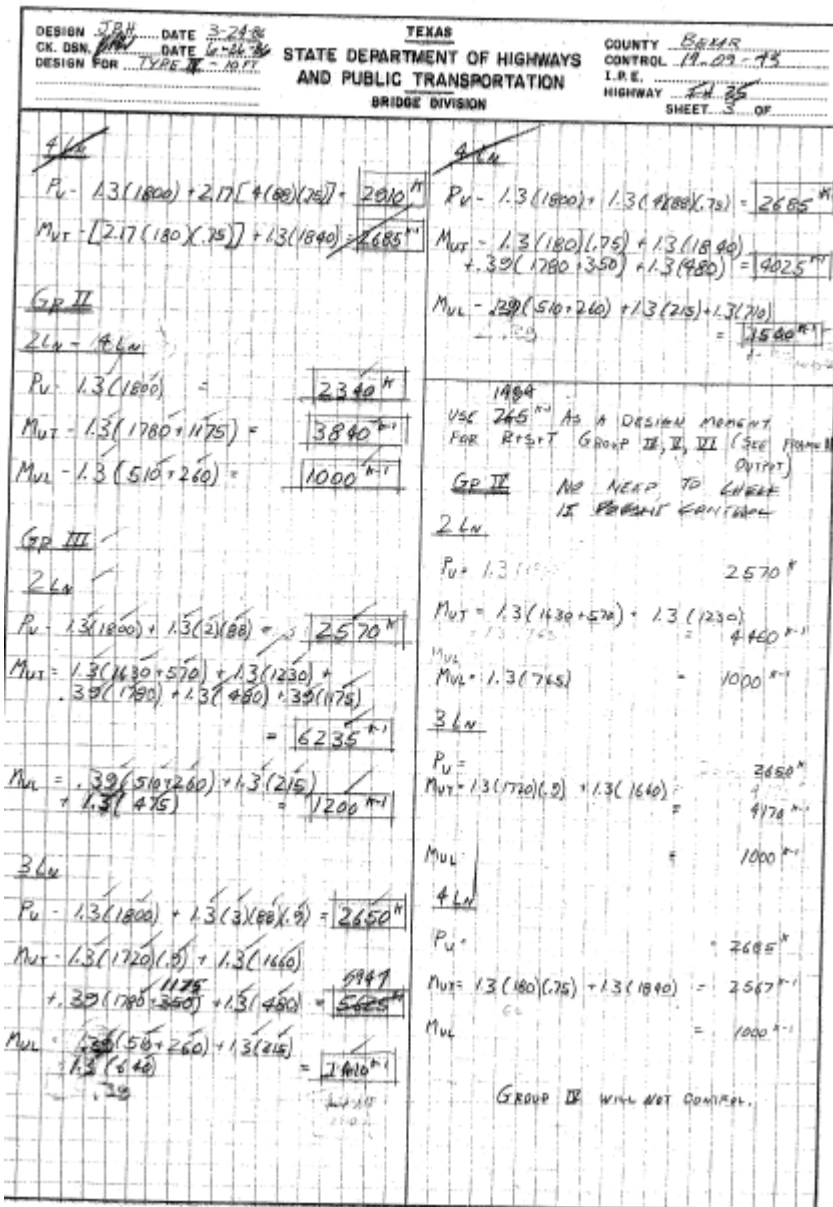


Figure A.3: Original Design Calculations (3 of 27)

DESIGN <u>JPH</u> DATE <u>2/16/80</u> C.K. DSN. <u>88</u> DESIGN FOR <u>TYP. I</u>	TEXAS <b>STATE DEPARTMENT OF HIGHWAYS                  AND PUBLIC TRANSPORTATION</b> BRIDGE DIVISION	COUNTY _____ CONTROL _____ I.P.E. _____ HIGHWAY _____ SHEET _____ OF _____
--	--	--

GP II

2 LN - PLN

$P_u = (1.25)(1800) = 2250^k$

$M_{ut} = 1.25(1780 + 1175) = 3690^k-ft$

$M_{ul} = 1.25(510 + 260) + 1.25(265) = 1820^k-ft$   
1924  
2818

GP III GP II WILL NOT CONTROL ✓

2 LN

$P_u = 1.25(1800) + 1.25(12)(88) = 2470^k$

$M_{ut} = 1.25(2200) + 1.25(1200) + 375(1780 + \frac{260}{175}) + 1.25(980) = 5996^k-ft$

$M_{ul} = 375(\frac{560}{175} + 260) + 1.25(215) + 1.25(765) + 1.25(475) = 2400^k-ft$   
3010

3 LN

$P_u = 1.25(1800) + 1.25(12)(88) = 2470^k$

$M_{ut} = 1.25(1760)(5) + 1.25(1660) + 375(1080 + \frac{175}{175}) + 1.25(980) = 5720^k-ft$   
5575 + 125(1980) + 125(640)

$M_{ul} = 1513 + 1.25(690) = 2400^k-ft$

4 LN

~~$P_u = (1.25)(1800) + 1.25(12)(88) = 2580^k$~~

~~$M_{ut} = 1.25(1800)(7.5) + 1.25(1840) + 375(1780 + 300) + 1.25(980) = 3870^k-ft$~~

~~$M_{ul} = 1513 + 1.25(710) = 2400^k-ft$~~

Figure A.4: Original Design Calculations (4 of 27)



PROB (CONTD) I  
 1 TYPE COLUMN -- 3-6 & 40.0 KSI - 1%  
 46" x 84" (7-7-6-6) 26-#11/3

TABLE 5. LOADING AND MOMENT CONTROL DATA

LOAD TYPE	2
NO. OF LOADS OR GROUPS	1
AXIS OPTION (1=X, 2=Y, 3=BOTH)	3

TABLE 7. AXIAL LOADS

LOAD (KIPS)	INITIAL LOAD (KIPS)		LOAD INCREMENT (KIPS)		FINAL LOAD (KIPS)	RESULTANT MOMENT (K-FT)
	0.	500.	500.	500.	15000.	
	LOAD MOMENTS (K-FT)		BIAXIAL (K-FT)			
	ABOUT X	ABOUT Y	ABOUT X	ABOUT Y		
0.	4741.	2524.	3450.	1948.	4138.	
500.	5827.	3133.	4294.	2297.	4870.	*
1000.	6682.	3603.	4733.	2534.	5369.	*
1500.	7282.	3920.	4981.	2670.	5652.	*
2000.	8107.	4410.	5398.	2903.	6129.	*
2500.	8736.	4757.	5698.	3066.	6471.	*
3000.	9173.	4997.	5882.	3169.	6681.	*
3500.	9414.	5136.	5963.	3215.	6775.	*
4000.	9472.	5183.	5941.	3207.	6751.	*
4500.	9337.	5067.	5822.	3140.	6615.	*
5000.	8877.	4810.	5606.	3029.	6372.	*
5500.	8302.	4498.	5309.	2872.	6036.	*
6000.	7608.	4122.	4937.	2669.	5612.	*
6500.	6775.	3675.	4475.	2421.	5088.	*
7000.	5798.	3147.	3919.	2122.	4457.	*
7500.	4676.	2533.	3268.	1766.	3715.	*
8000.	3483.	1885.	2507.	1356.	2850.	*
8500.	2250.	1216.	1668.	902.	1896.	*
9000.	940.	506.	737.	397.	837.	*
9500.	0.	0.	0.	0.	0.	*
10000.	0.	0.	0.	0.	0.	*
10500.	0.	0.	0.	0.	0.	*
11000.	0.	0.	0.	0.	0.	*
11500.	0.	0.	0.	0.	0.	*
12000.	0.	0.	0.	0.	0.	*
12500.	0.	0.	0.	0.	0.	*
13000.	0.	0.	0.	0.	0.	*
13500.	0.	0.	0.	0.	0.	*
14000.	0.	0.	0.	0.	0.	*
14500.	0.	0.	0.	0.	0.	*
15000.	0.	0.	0.	0.	0.	*

Figure A.5: Original Design Calculations (5 of 27)

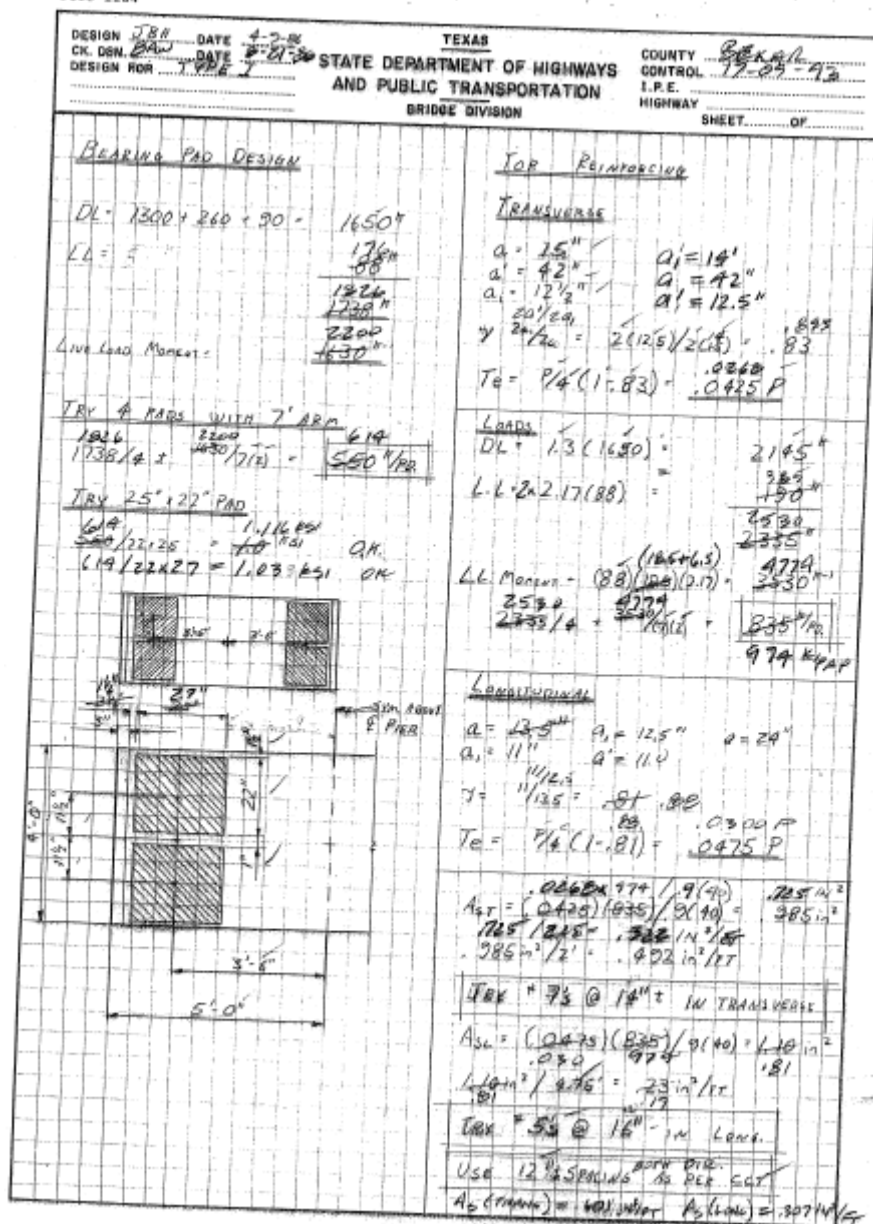


Figure A.6: Original Design Calculations (6 of 27)

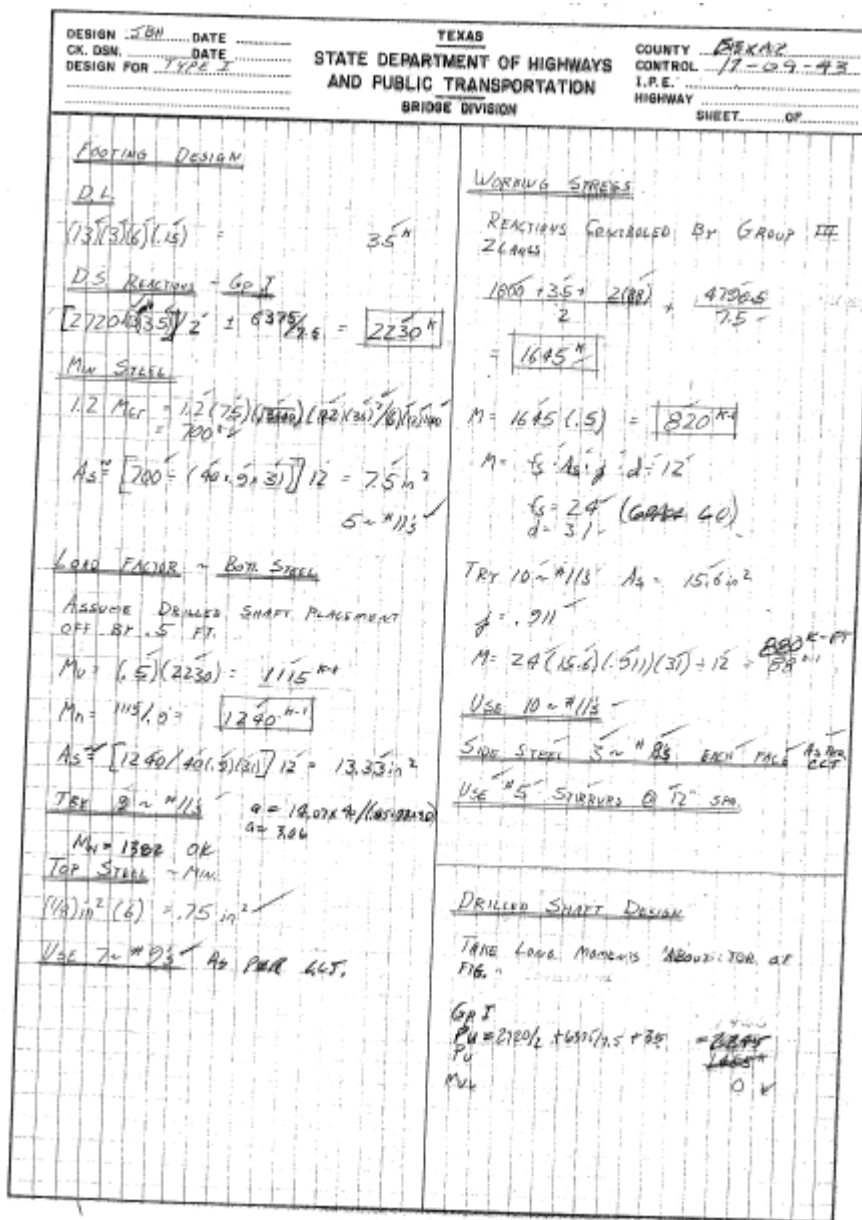


Figure A.7: Original Design Calculations (7 of 27)

DESIGN <u>J.R.H.</u> DATE <u>8/26/86</u>		TEXAS		COUNTY <u>BELLEVILLE</u>
CK. DBN. <u>B.A.W.</u>	DATE <u>8/26/86</u>	STATE DEPARTMENT OF HIGHWAYS AND PUBLIC TRANSPORTATION		CONTROL <u>17-09-43</u>
DESIGN FOR		BRIDGE DIVISION		I.P.E. _____
				HIGHWAY _____
				SHEET _____ OF _____
<u>Grp II</u>				
$P_u$	$= 2770/2 + 300/1.5 + 85$	$= 1717^k$		
$P_o$	$2300/2$	$1170^k$		
$M_u$	$1800/2$	$900^k$		
	$725/2$	$360^k$		
<u>Grp III</u>				
$P_u$		$2153$		
$P_o$		$1540^k$		
$M_u$		$705$		
		$475^k$		
		$70$		
<u>Grp IV</u>				
$P_u$		$1652$		
$P_o$		$1125^k$		
$M_u$		$1409$		
		$825^k$		
<u>Grp V</u>				
$P_u$		$2072$		
$P_o$		$1200^k$		
$M_u$		$1608$		
		$1050^k$		
From Interaction Diagram 18 Steel (18" x 23) 15 C.H.				
<u>LONG TS. MOMENTS WITH 24" COL</u>				
<u>GROUP IV</u>				
$M_{uL}$	$= 1.25(997) + 1.25(991.0 + 200)$			
	$= 1025 \text{ K-FT}$			
$P_u$	$= (2250 + 2)7.5 + (1487 + 1175)1.25 + 7.5 = 1609^k$			
<u>GROUP III</u>				
$M_{uL}$	$= 1.25(1997) + 1.25(1991.0 + 200)$			
	$+ 1.25(191.3 + 1.25(540))$			
	$= 1218 \text{ K-FT}$			
$P_u$	$= (2950 + 2)7.5 + 1.25(1900)7.5 + 1.25(416)7.5 + 1.25(1487 + 1175)7.5 = 1672^k$			
24" x 32" COLUMNS <del>FOR</del> USE 18" SHAFTS				

Figure A.8: Original Design Calculations (8 of 27)

PROB (CONTD)

1

DR. SHAFT -- ROUND -- 3.0 & 40.0 KSI

42" # 14-#93

TABLE 5. LOADING AND MOMENT CONTROL DATA

LOAD TYPE	2
NO. OF LOADS OR GROUPS	1
AXIS OPTION (1=X, 2=Y, 3=BOTH)	3

TABLE 7. AXIAL LOADS

INITIAL LOAD (KIPS)	LOAD INCREMENT (KIPS)		FINAL LOAD (KIPS)		RESULTANT MOMENT (K-FT)
	0.	100.	3500.	3500.	
	LOAD MOMENTS (K-FT)		BIAXIAL (K-FT)		
(KIPS)	ABOUT X	ABOUT Y	ABOUT X	ABOUT Y	
0.	700.	706.	507.	493.	707.
100.	789.	793.	560.	557.	790.
200.	862.	859.	602.	616.	862.
300.	918.	913.	645.	648.	915.
400.	944.	949.	674.	665.	947.
500.	1005.	1010.	713.	712.	1008.
600.	1069.	1065.	754.	750.	1068.
700.	1120.	1115.	791.	789.	1117.
800.	1157.	1157.	818.	817.	1156.
900.	1185.	1186.	836.	842.	1186.
1000.	1207.	1203.	850.	855.	1205.
1100.	1213.	1215.	860.	858.	1215.
1200.	1211.	1216.	857.	857.	1212.
1300.	1200.	1201.	849.	848.	1200.
1400.	1174.	1176.	832.	830.	1175.
1500.	1139.	1139.	808.	804.	1140.
1600.	1098.	1097.	778.	775.	1098.
1700.	1052.	1050.	743.	742.	1050.
1800.	998.	995.	704.	705.	996.
1900.	936.	934.	660.	662.	935.
2000.	866.	866.	611.	615.	867.
2100.	789.	790.	557.	559.	790.
2200.	704.	706.	498.	499.	705.
2300.	610.	613.	433.	432.	611.
2400.	509.	510.	362.	359.	510.
2500.	404.	403.	286.	285.	404.
2600.	295.	293.	207.	208.	294.
2700.	179.	180.	126.	127.	179.
2800.	56.	55.	39.	39.	55.
2900.	0.	0.	0.	0.	0.
3000.	0.	0.	0.	0.	0.
3100.	0.	0.	0.	0.	0.
3200.	0.	0.	0.	0.	0.
3300.	0.	0.	0.	0.	0.

Figure A.9: Original Design Calculations (9 of 27)

Form 1284A			
TEXAS SDHPT BRIDGE DIVISION	County	Highway	Design <u>J.E.H.</u> Date
	C-S-J		Cl. Ord. Date
	Structure		
	Design for		Sheet <u>    </u> of <u>    </u>

FORCES IN COLUMN DUE TO SUPERSTRUCTURE PRELIMINARY

700' SPAN <sup>215</sup> 11 STRANDS ✓

$$P = (11)(.25)^2(.75)(270 \text{ ksi}) = 7010$$

$$\Delta ES = \frac{7010(300)}{(49)(6.76 \text{ in}^2)} = \frac{0.825}{1.0707} \text{ FT}$$

CREEP

$$\Delta C = 1.5(.0825) = \frac{.1060}{1.735 \text{ FT}}$$

TEMP.

$$\Delta T = (.000006)(45)(300) = .081 \text{ FT}$$

$$\Delta = \frac{.1060}{.208} + .081 = \frac{.187}{.2088 \text{ FT}}$$

$$= \frac{2.45 \text{ IN}}{2.25 \text{ IN}}$$

SHEAR FORCE

$$F = (\text{MODULUS})(\text{AREA})(\Delta) / L$$

$$= (180)(480)(2.45) / 4$$

$$= \frac{53760}{4}$$

480

ASSUME Modulus = 180,000  
Area = 20' x 24'  
L = 4'

Figure A.10: Original Design Calculations (10 of 27)

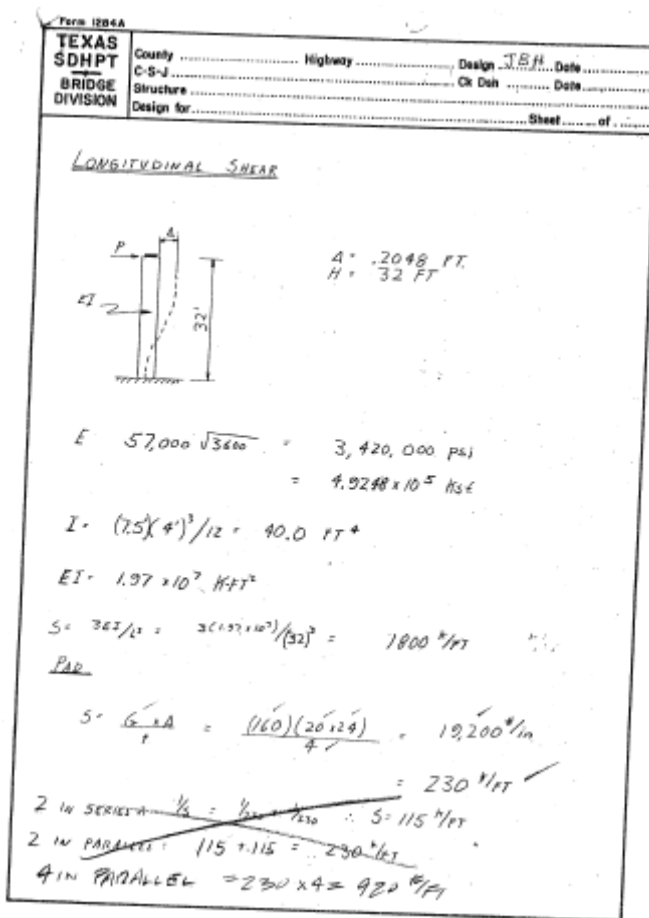


Figure A.11: Original Design Calculations (11 of 27)

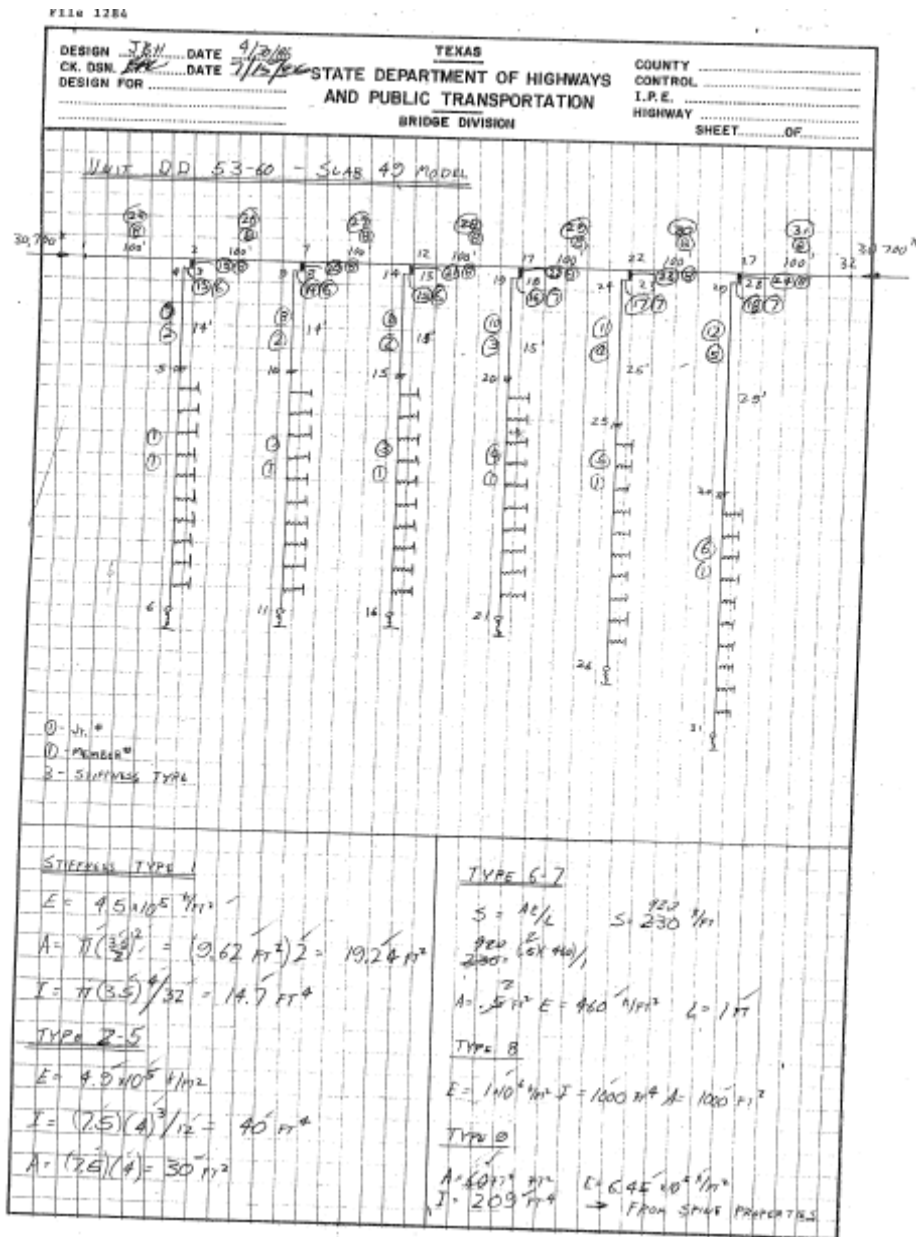


Figure A.12: Original Design Calculations (12 of 27)



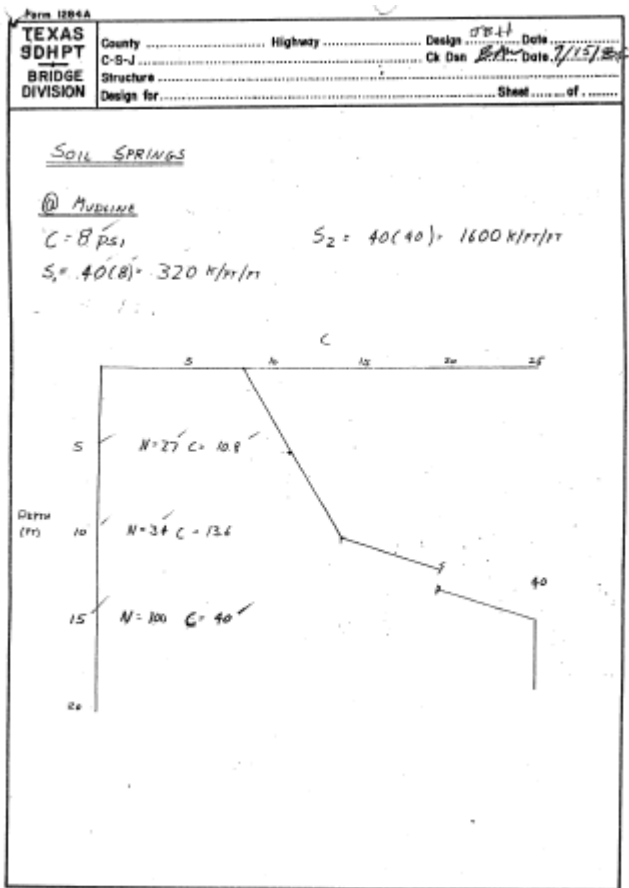


Figure A.13: Original Design Calculations (13 of 27)

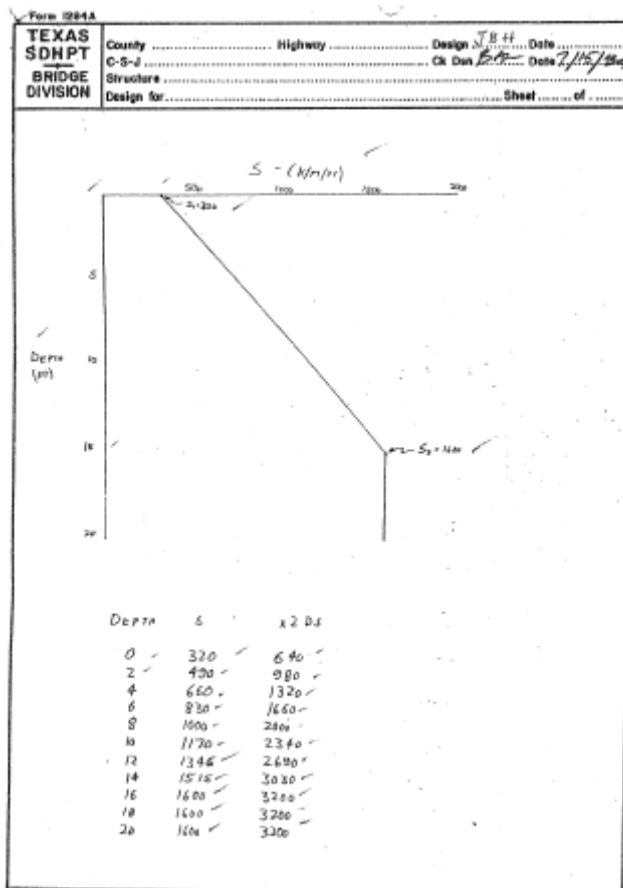


Figure A.14: Original Design Calculations (14 of 27)

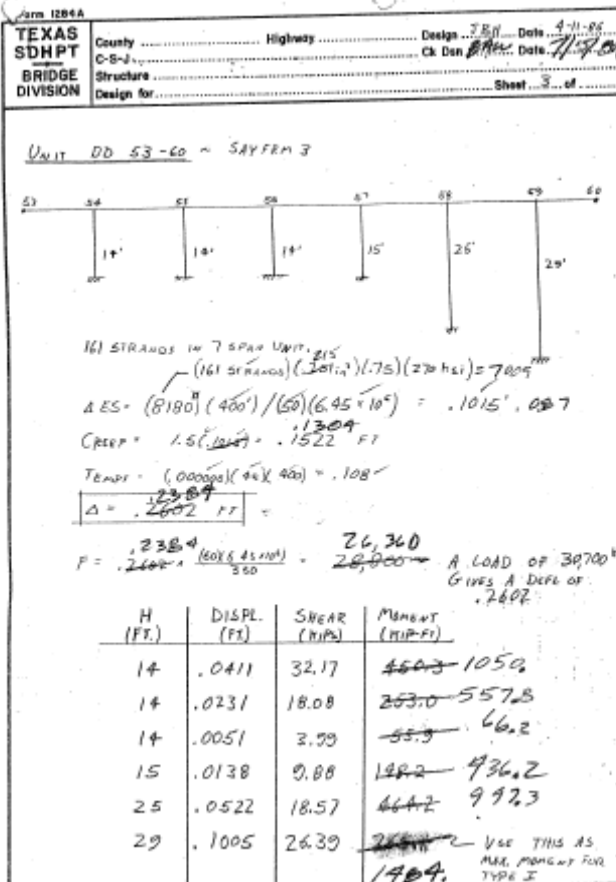


Figure A.15: Original Design Calculations (15 of 27)

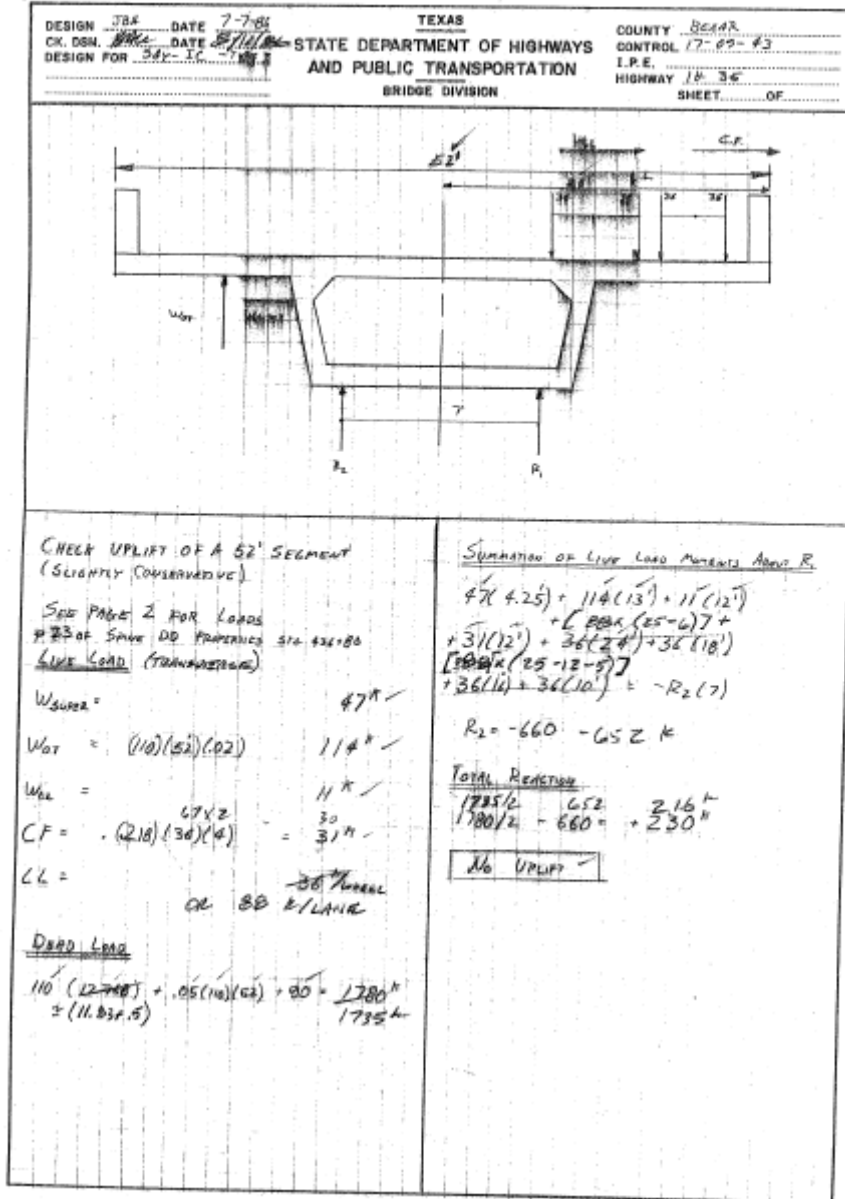


Figure A.16: Original Design Calculations (16 of 27)

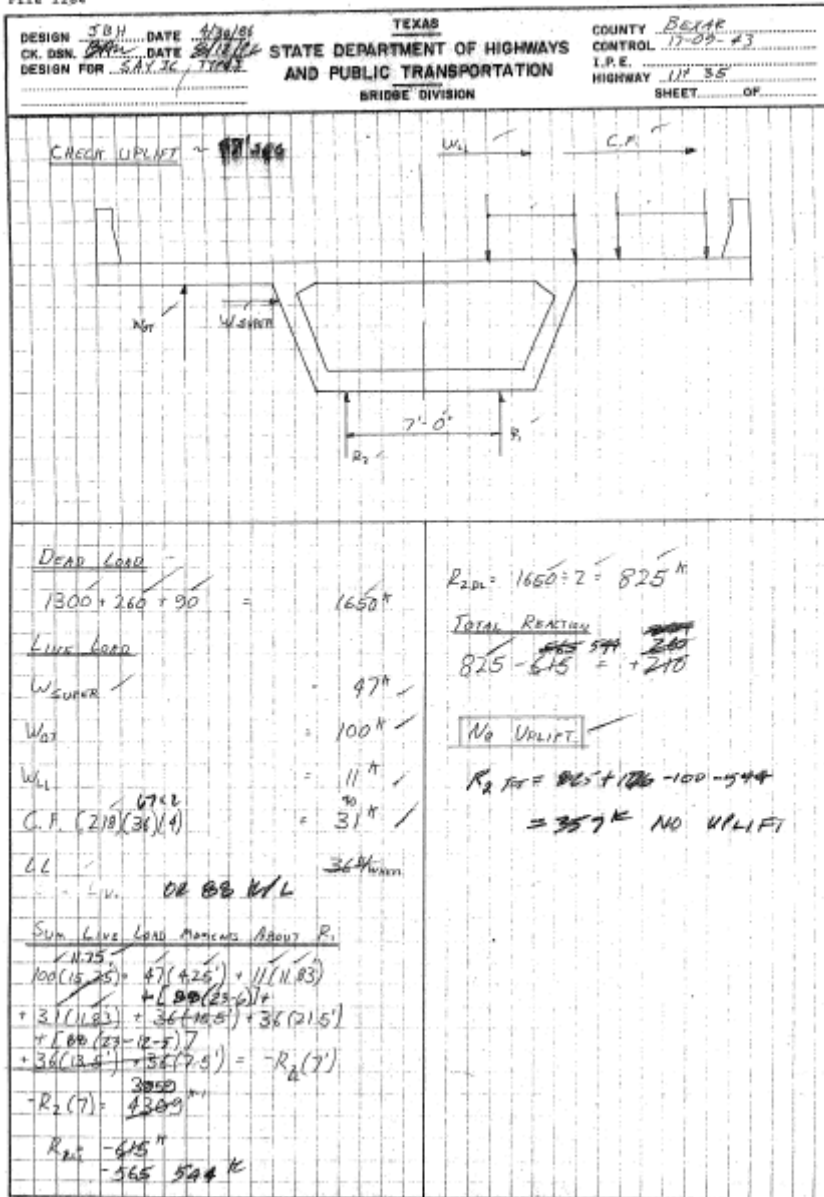


Figure A.17: Original Design Calculations (17 of 27)

Form 1285A

TEXAS SDHPT BRIDGE DIVISION	County	BELLEVUE	Highway	111 35	Design	JSH	Date	4/29/86
	C-S-J	17-09-43			Cl. Dan	Edm	Date	8/18/86
	Structure	509-12						
	Design for	CRANE LOADINGS TYPE J CR.						

CRANE LOADING ~ 42' SEGMENT - SLAB 49

REACTIONS

VOID  
SEE NEW SLAB 49  
BUNIS WITH NEW CRANE  
LOADINGS

LOAD CASE I

-4.6	24.2	P = 252.4 k
<u>79.1</u>	<u>228.2</u>	M = 816 k-ft
74.5	252.4	

$M = [228.2 - 252.4 \frac{1}{2}] 8 = 816$

LOAD CASE II

-12.1	18.9	P = 275.7 k
<u>62.4</u>	<u>266.8</u>	M = 951 k-ft
50.3	275.7	

$M = [266.8 - 275.7 \frac{1}{2}] 8 = 951$

LOAD CASE III

-6.2	130.4	P = 294.7 k
<u>38.6</u>	<u>164.3</u>	M = 135 k-ft
32.4	294.7	

$M = [164.3 - 294.7 \frac{1}{2}] 8 = 135$

Figure A.18: Original Design Calculations (18 of 27)

LINE	PROJ.	CRANE #	END	(42 FT. SEG.)	(POS. 1)	BSLAB49			
000168	1-C								
000169	301								
000170									
000171	1	0	0	2	0	5	0	2	
000172	42	100			1.0			1.0	.15
000173	0	1	0	99	2.710E+04	2.710E+04			
000174	42	1	42	99	2.710E+04	2.710E+04			
000175	1	0	41	100	5.420E+04	5.420E+04			
000176	16	0	26	100	6.780E+06	6.780E+06			
000177	17	0	17	0					1,000E+10
000178	25	0	25	0					1,000E+10
000179	17	100	17	100					1,000E+10
000180	25	100	25	100					1,000E+10
000181	1	1	42	100	4.607E+04				
000182	17	1	26	100	5.759E+06				
000183	10	2	10	2					- 9.0
000184	32	2	32	2					- 14.0
000185	10	22	10	22					-104.0
000186	32	22	32	22					-100.0
000187	33	40	33	40					- 40.0
000188	0								
000189	100								
000190	302								
000191	1	1	1	1	0	500	1	1	-1
000192	0	0	0	0					- 54.0
000193	10	2	10	2					- 89.0
000194	32	2	32	2					- 54.0
000195	10	22	10	22					- 89.0
000196	32	22	32	22					- 40.0
000197	33	40	33	40					
000198	303								
000199	1	1	1	1	0	500	1	1	-1
000200	0	0	0	0					-123.0
000201	10	2	10	2					-111.0
000202	32	2	32	2					- 28.0
000203	10	22	10	22					- 25.0
000204	32	22	32	22					- 40.0
000205	33	40	33	40					
000206	CEASE								

Figure A.19: Original Design Calculations (19 of 27)

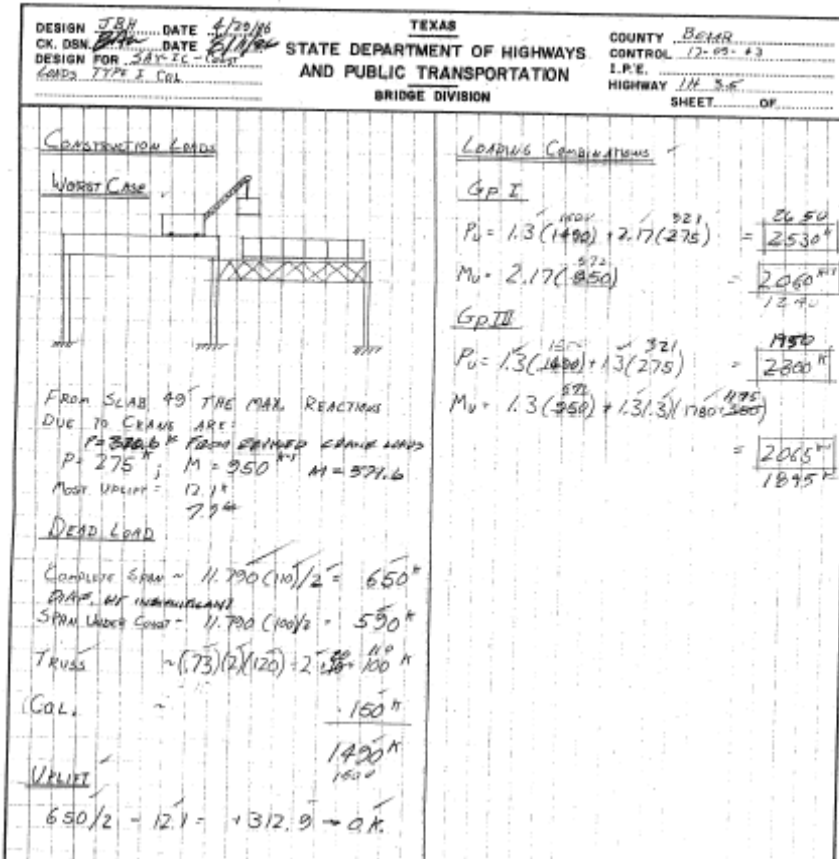


Figure A.20: Original Design Calculations (20 of 27)



FILE 1284

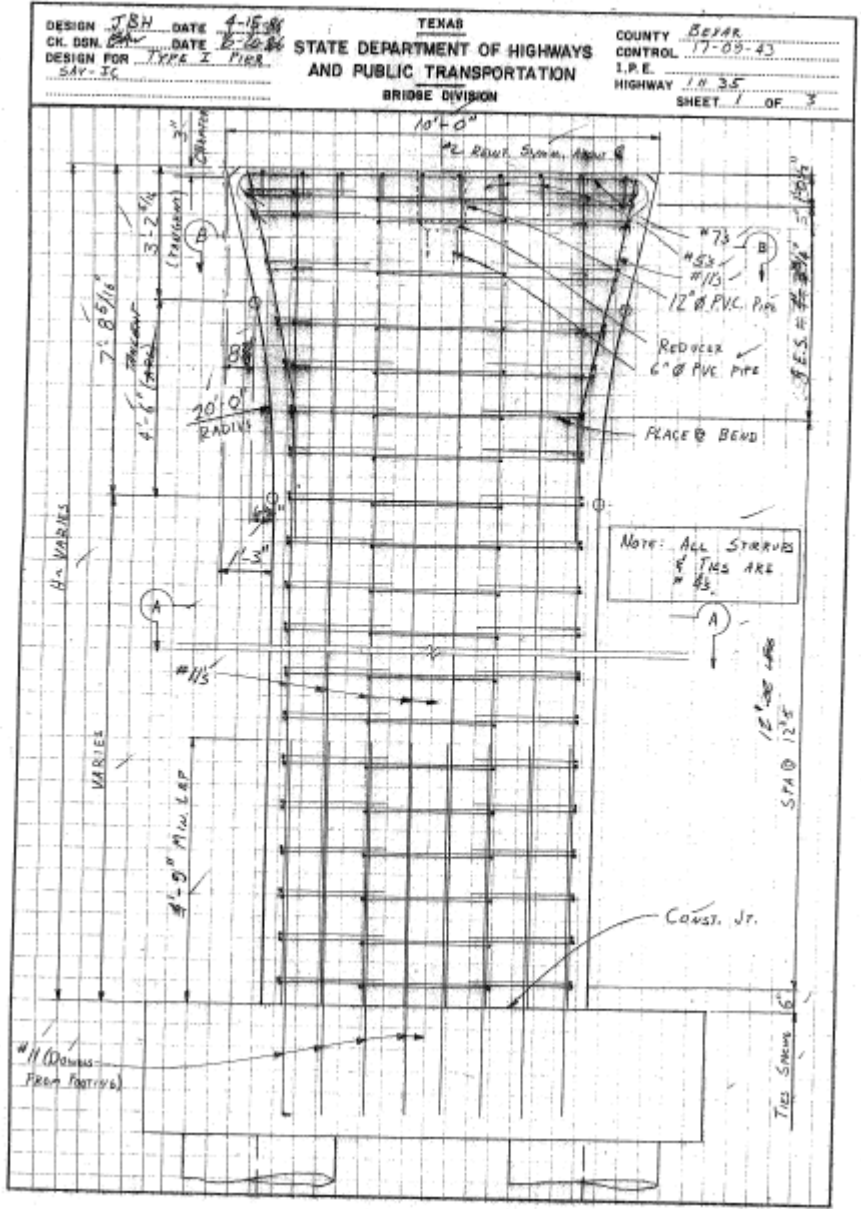


Figure A.21: Original Design Calculations (21 of 27)

File 1284

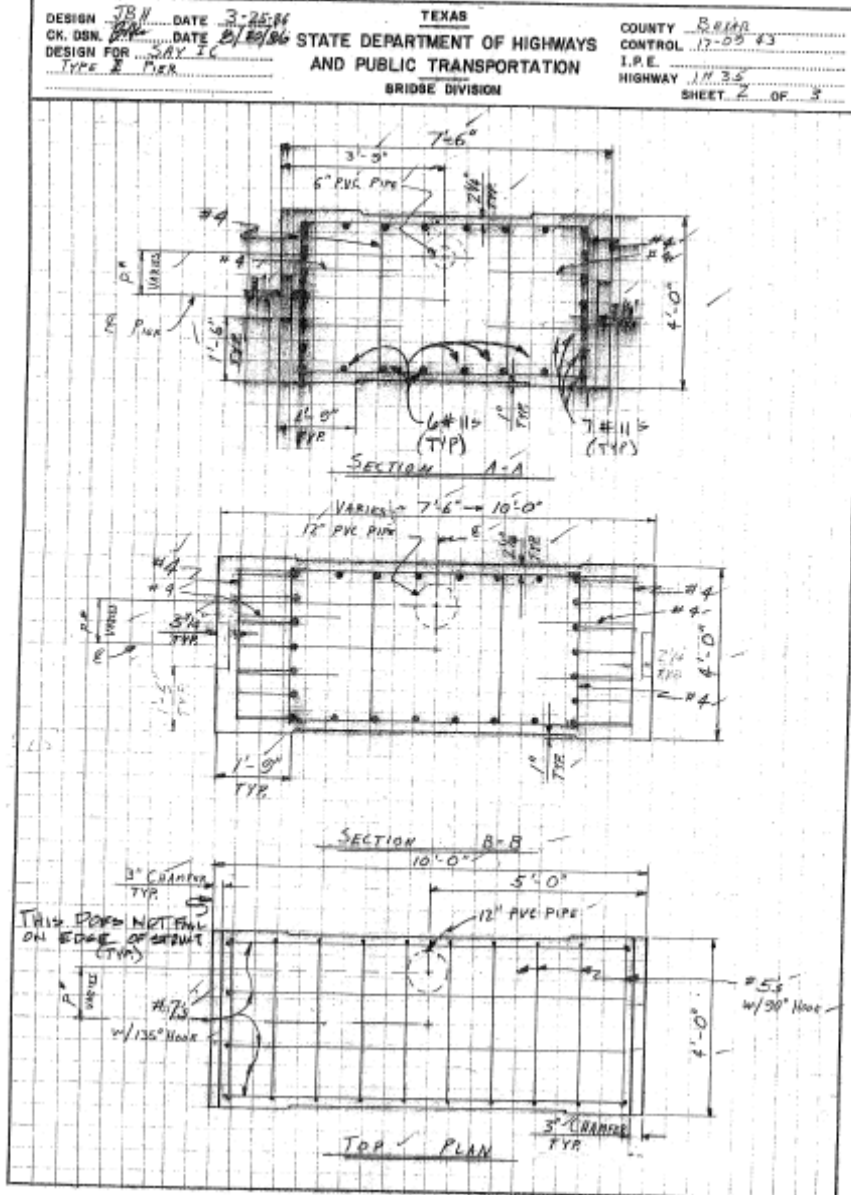


Figure A.22: Original Design Calculations (22 of 27)

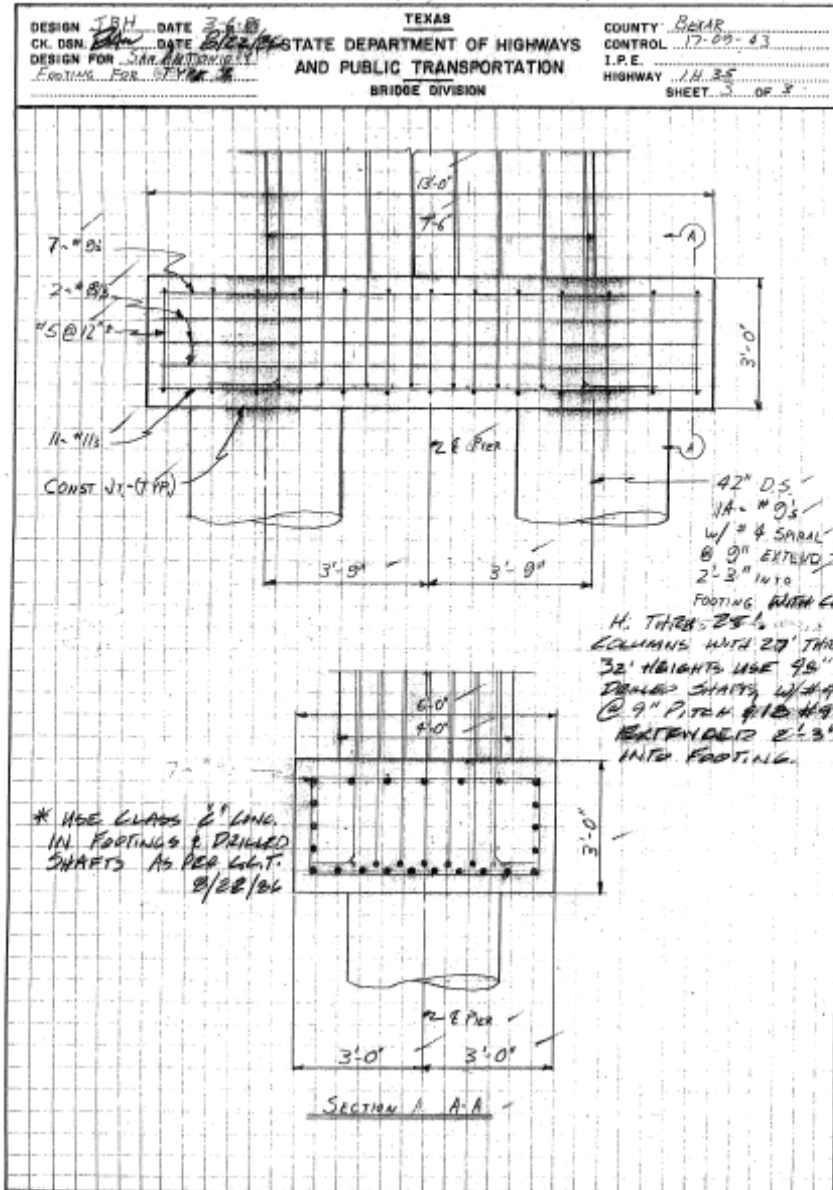


Figure A.23: Original Design Calculations (23 of 27)

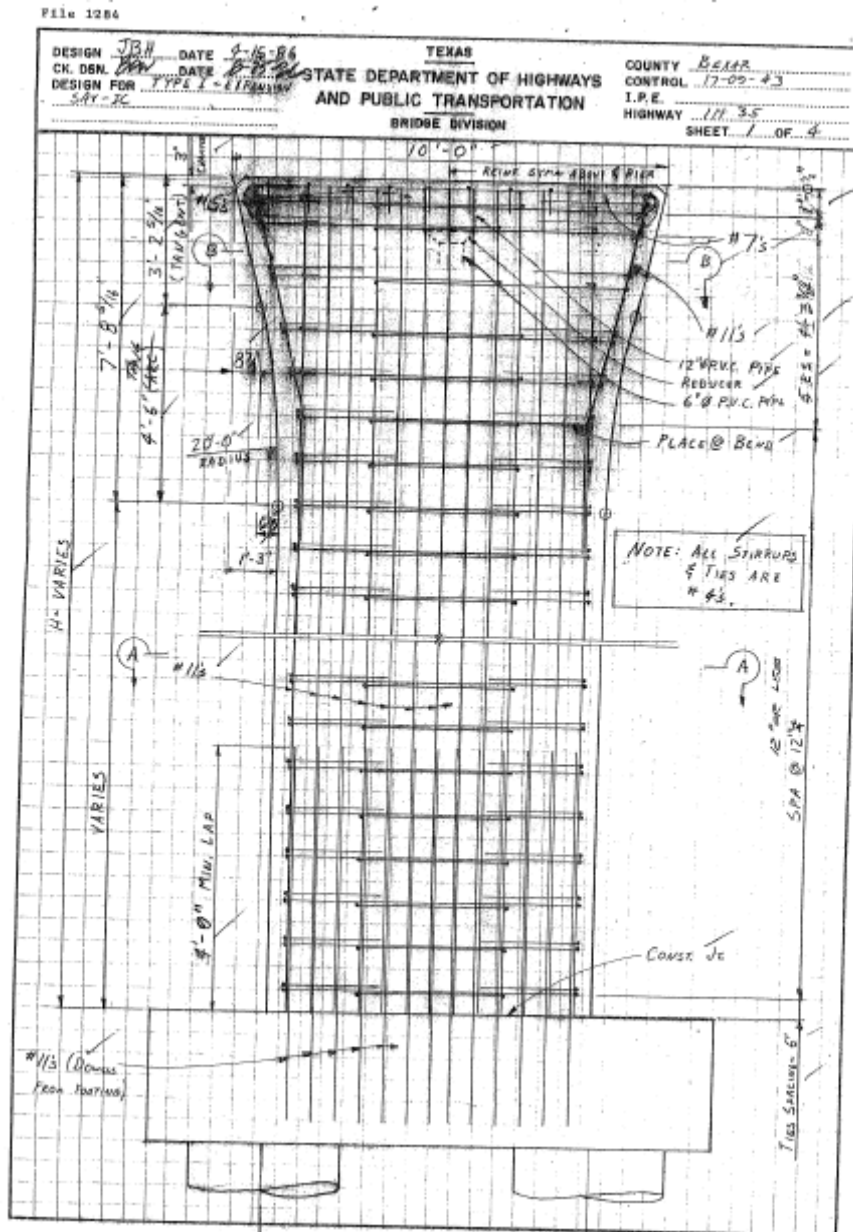


Figure A.24: Original Design Calculations (24 of 27)

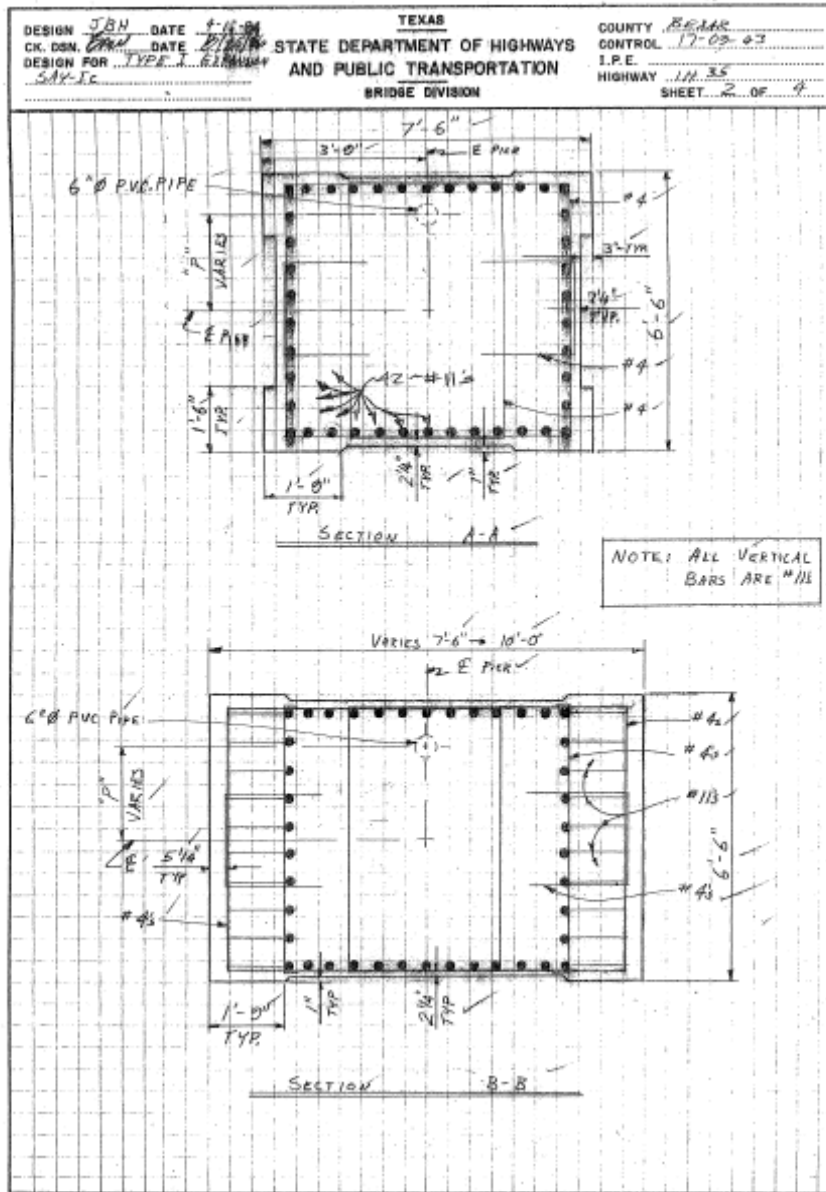


Figure A.25: Original Design Calculations (25 of 27)

File 1284

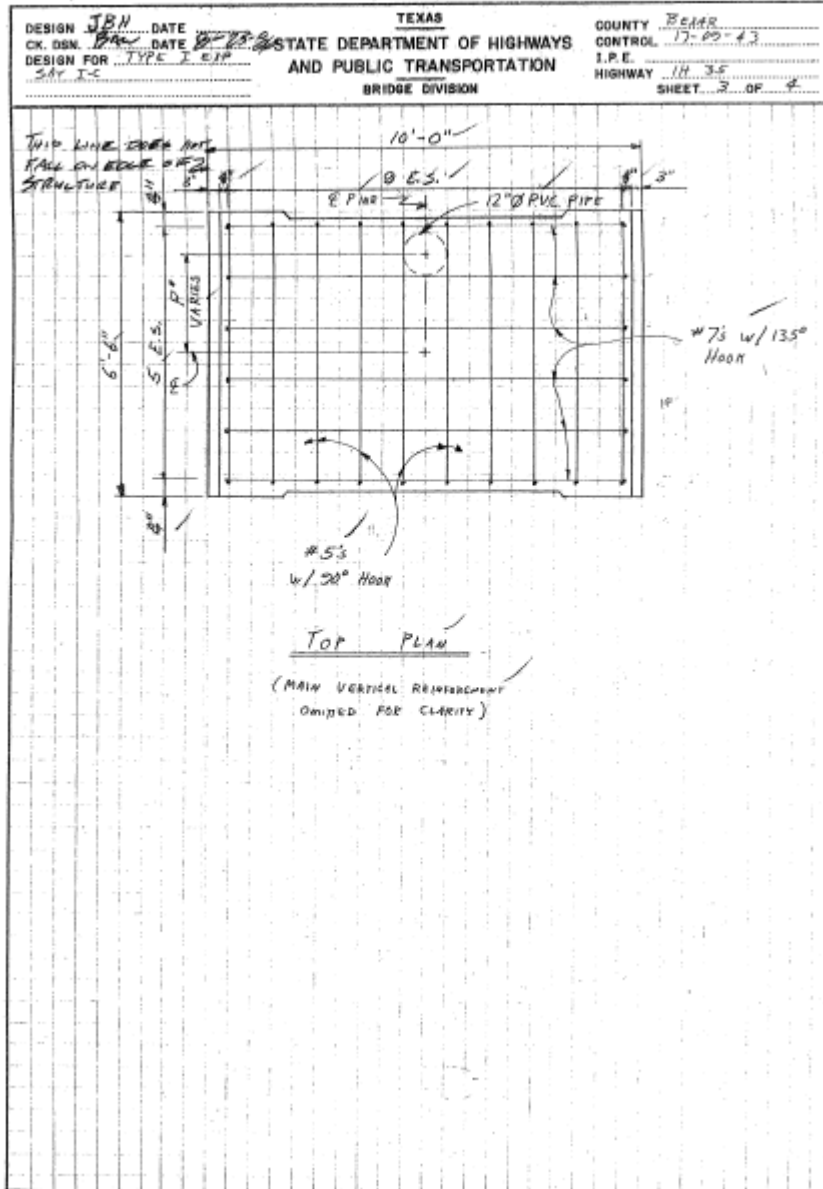


Figure A.26: Original Design Calculations (26 of 27)

File 1284

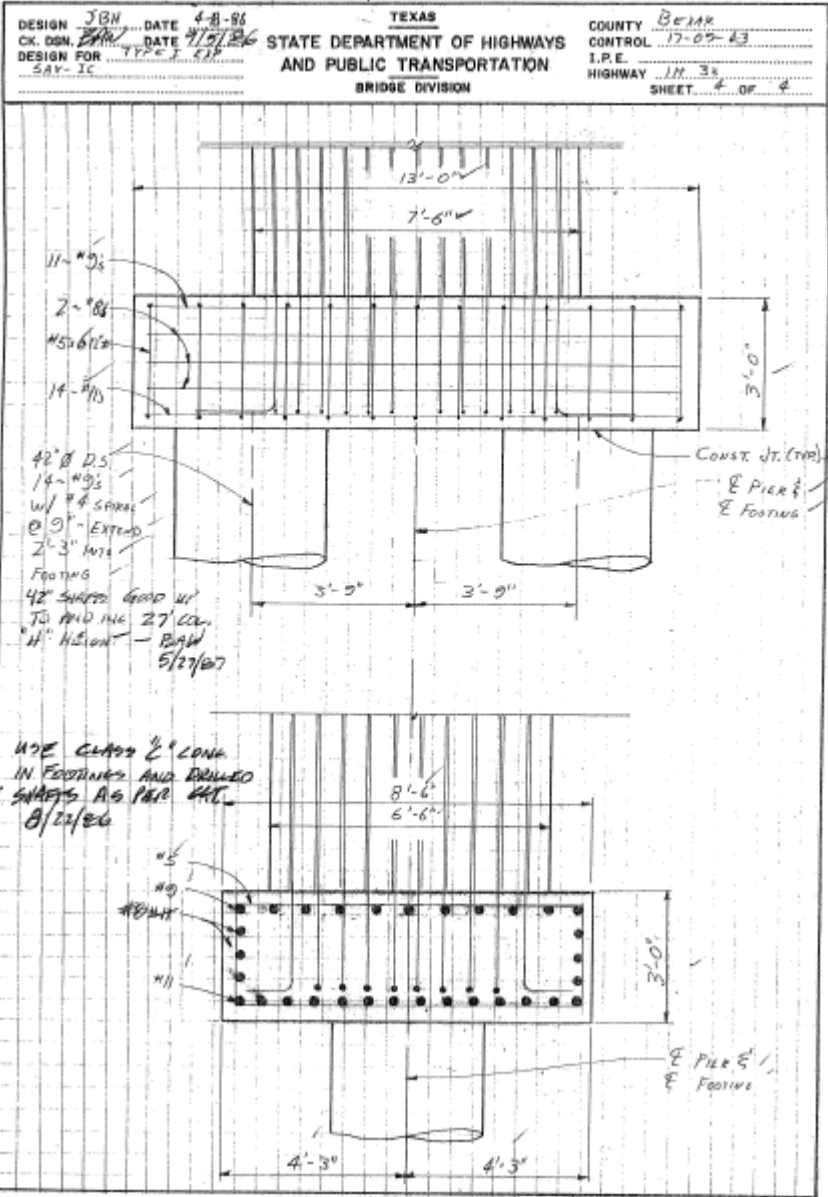


Figure A.27: Original Design Calculations (27 of 27)

## A.2 APPLICATION OF ASSESSMENT METHODOLOGY TO PIER DD7

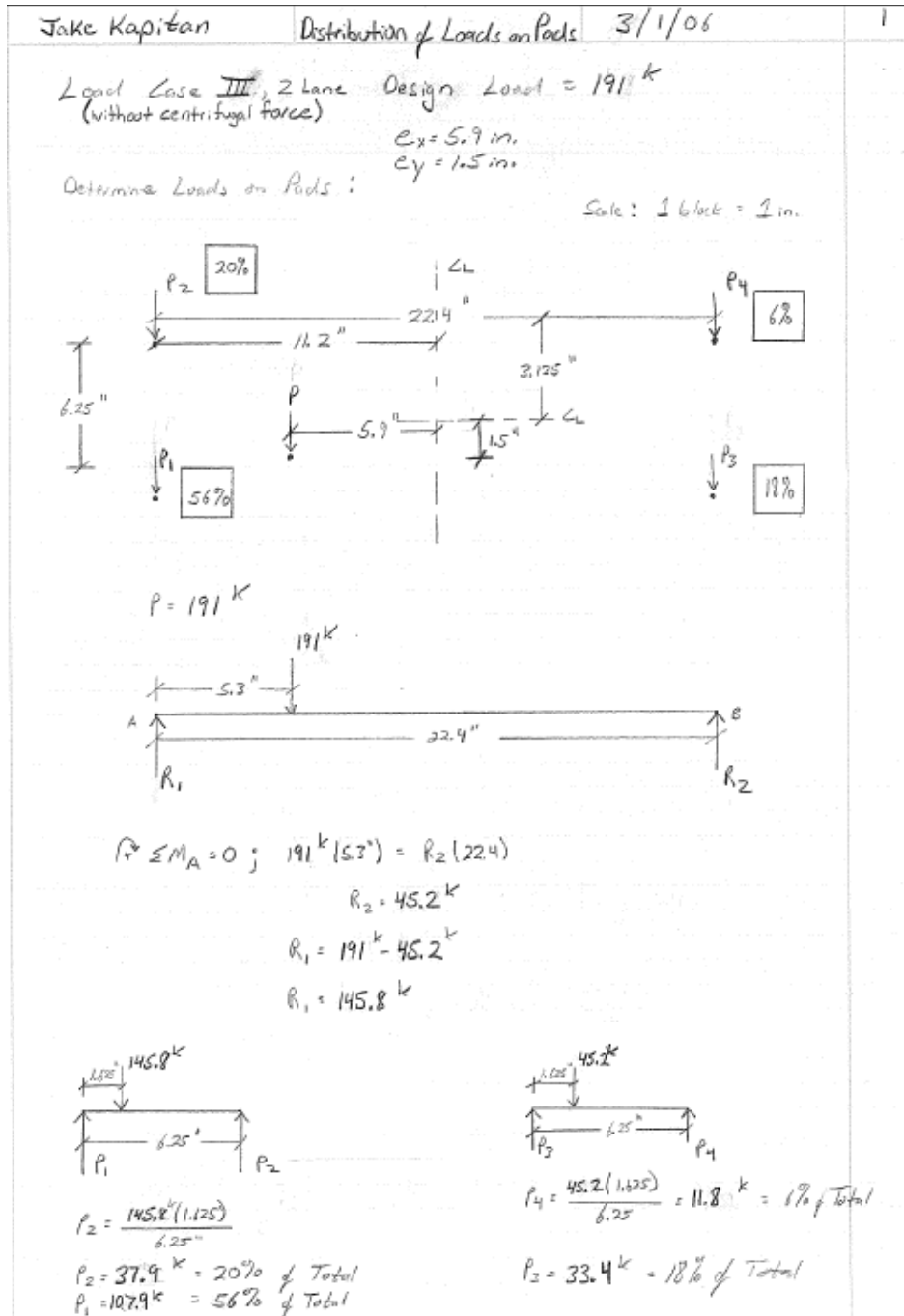


Figure A.28: Biaxial Load Distribution



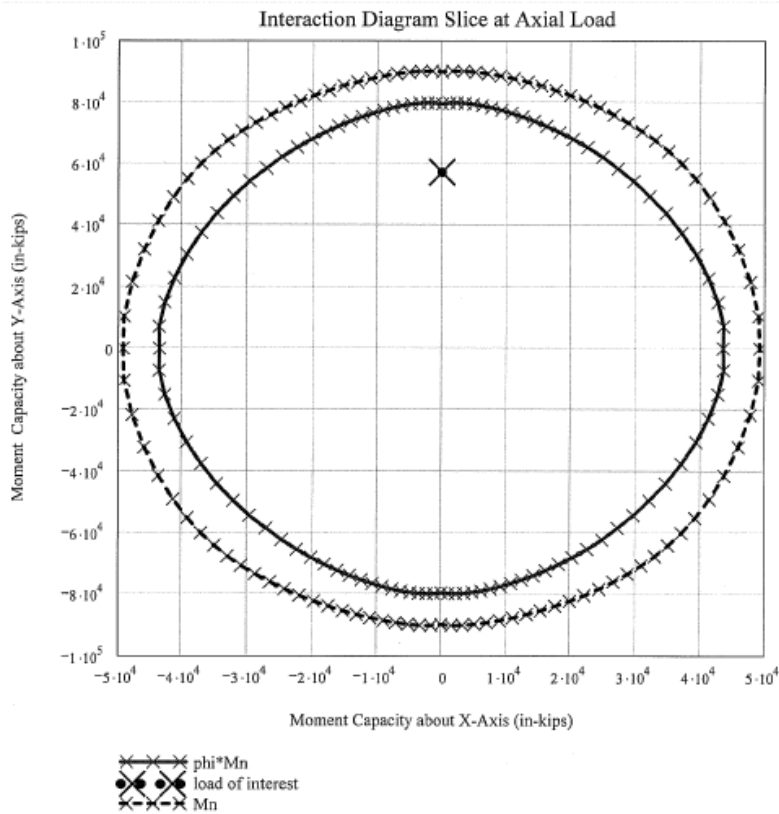
# Appendix B

## Additional Experimental Program Information

### B.1 INTERACTION FAILURE SLICES

*Case I, 2 Lane*

point := 0      user<sub>axial</sub> point = 2720      SpliceStress<sub>point</sub> = 0       $\sqrt{5.828 \times 10^4}$   
(pos. value indicates tension)

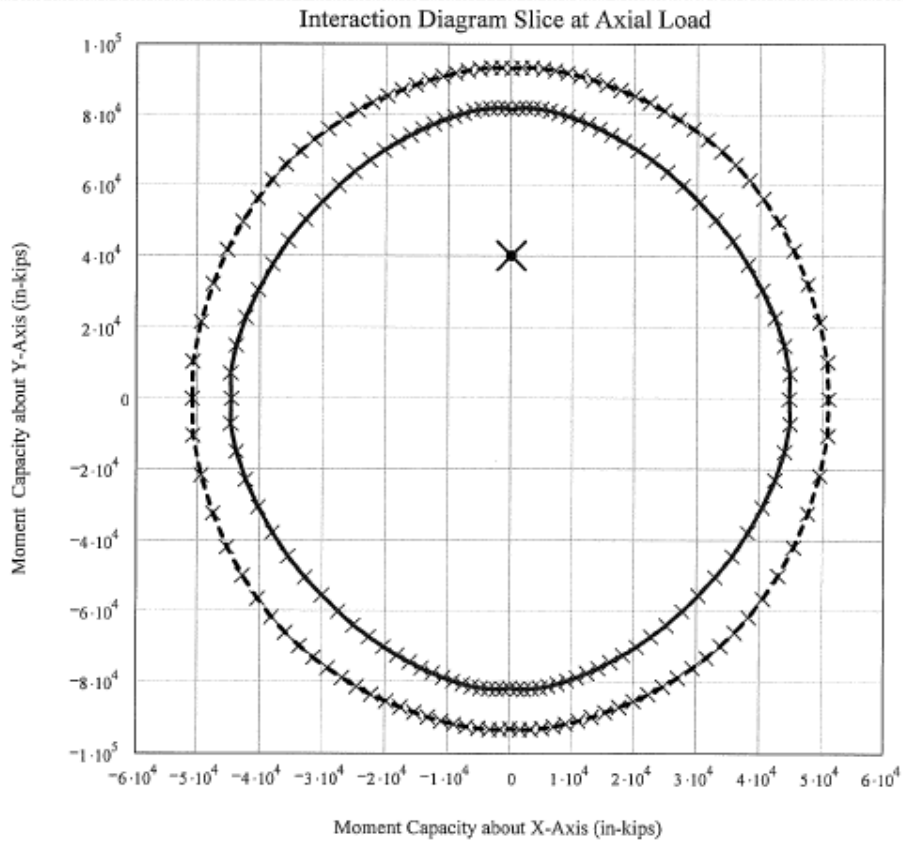


*$P = 2720 \text{ k}$*   
 *$M_y = 57,312 \text{ k}\cdot\text{in.}$*   
 *$M_x = 0 \text{ k}\cdot\text{in.}$*

**Figure B.1: Interaction Slice, Load Case I-2 Lane**

# Case I, 3 Lane

point := 1      user\_axial\_point = 2855      SpliceStress\_point = 0      (3.828 × 10<sup>4</sup>)  
 (pos. value indicates tension)



$\times$   $\phi \cdot M_n$   
 $\circ$  load of interest  
 $\times$   $M_n$

$P = 2855 \text{ k}$   
 $M_y = 40,308 \text{ k}\cdot\text{m}$   
 $M_x = 0 \text{ k}\cdot\text{m}$

Figure B.2: Interaction Slice, Load Case I-3 Lane

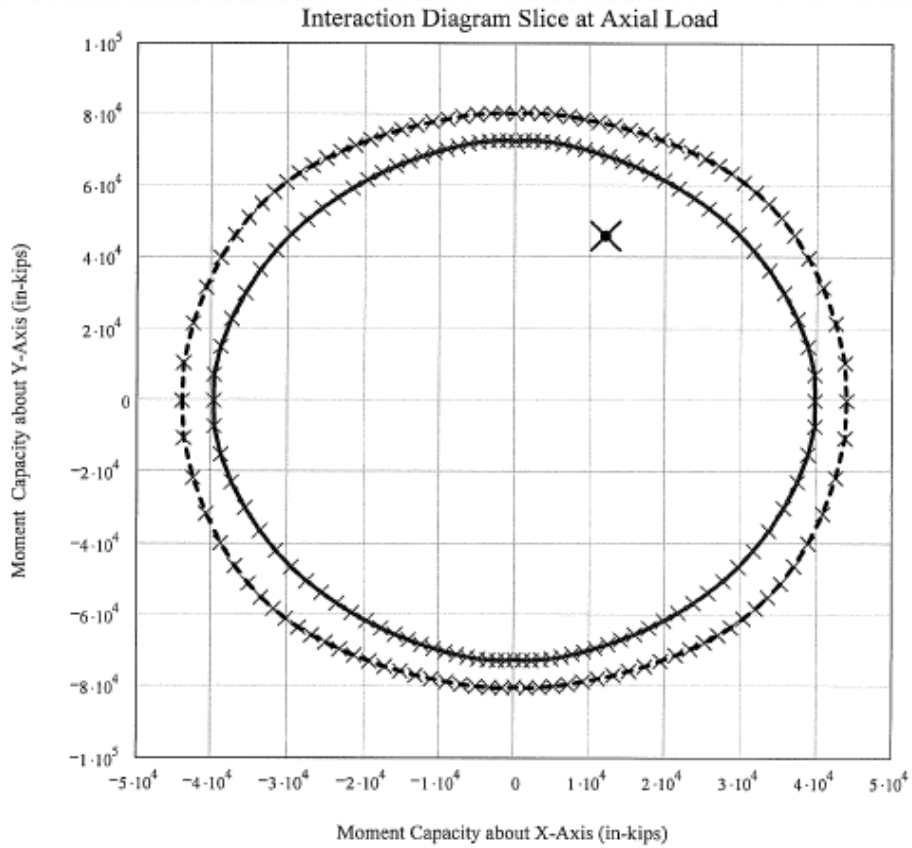
# Case II

point := 2

user<sub>axial</sub> <sub>point</sub> = 2340

SpliceStress <sub>point</sub> = 0

( $3.828 \times 10^4$ )  
(pos. value indicates tension)



$\times$   $\times$   $\times$   $\times$   $\times$  phi\*Mn  
 $\circ$   $\circ$   $\circ$   $\circ$   $\circ$  load of interest  
 $\times$   $\times$   $\times$   $\times$   $\times$  Mn

$$P = 2340 \text{ k}$$

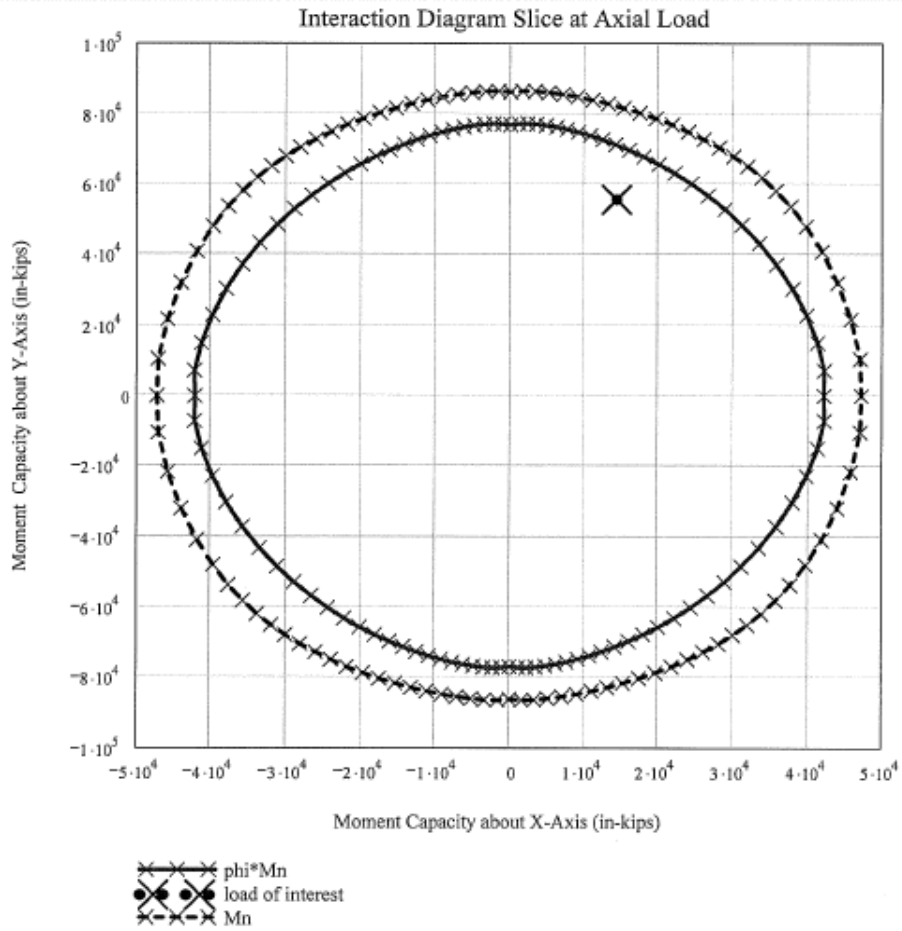
$$M_y = 46,080 \text{ k}\cdot\text{m}$$

$$M_x = 12,000 \text{ k}\cdot\text{m}$$

Figure B.3: Interaction Slice, Load Case II

# Case III, 2 Lane

point := 3      useraxial<sub>point</sub> = 2570      SpliceStress<sub>point</sub> = 0      (pos. value indicates tension) (5.828 × 10<sup>4</sup>)



$$P = 2570 \text{ k}$$

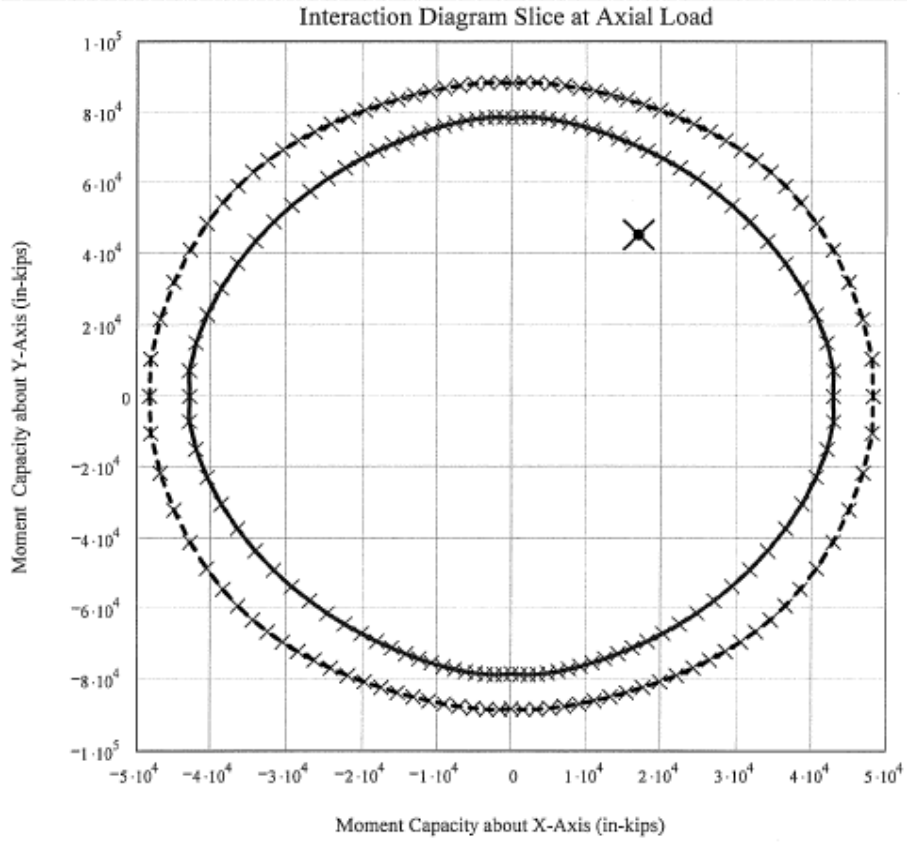
$$M_y = 55,632 \text{ k}\cdot\text{in.}$$

$$M_x = 14,400 \text{ k}\cdot\text{in.}$$

Figure B.4: Interaction Slice, Load Case III-2 Lane

# Case III - 3 Lane

point := 4      user\_axial\_point = 2650      SpliceStress\_point = 0      (3.828 x 10 )  
 (pos. value indicates tension)



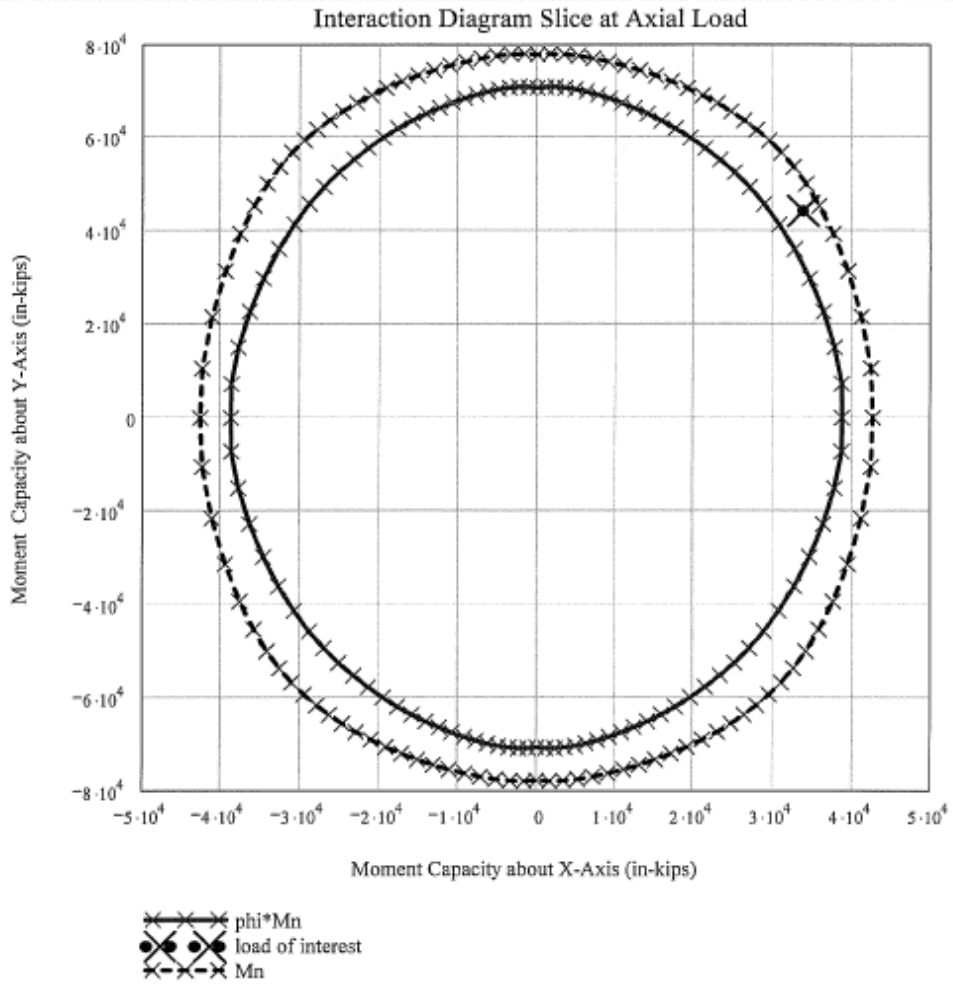
phi\*Mn  
 load of interest  
 Mn

$P = 2650 \text{ k}$   
 $M_y = 45,468 \text{ k}\cdot\text{m}$   
 $M_x = 16,920 \text{ k}\cdot\text{in}$

Figure B.5: Interaction Slice, Load Case III-3 Lane

# Case V

point := 5      useraxial\_point = 2250      SpliceStress\_point = 0      (pos. value indicates tension) \ 3.858 x 11



$$P = 2250 \text{ k}$$

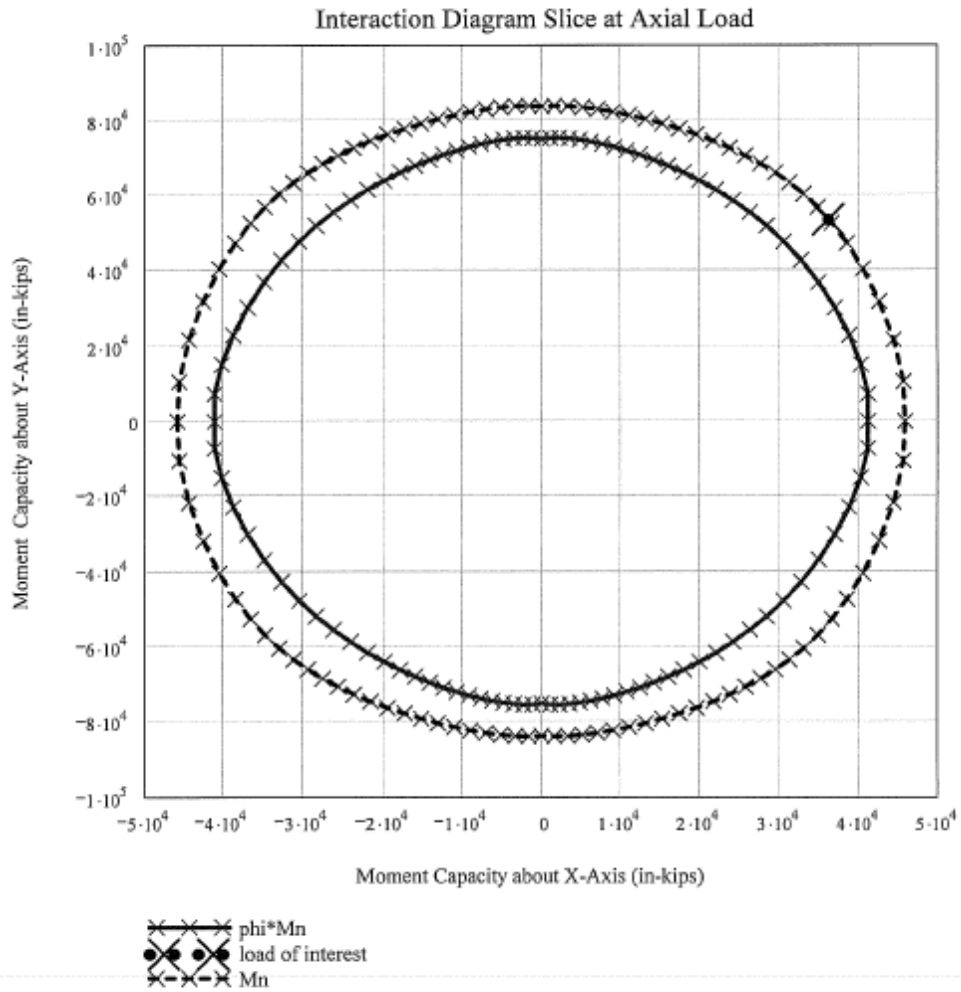
$$M_y = 44,280 \text{ k}\cdot\text{in.}$$

$$M_x = 33,816 \text{ k}\cdot\text{in.}$$

**Figure B.6: Interaction Slice, Load Case V**

# Case VI, 2 Lane

point := 6      user<sub>axial</sub><sub>point</sub> = 2470      SpliceStress<sub>point</sub> = 0       $\sqrt{3.828 \times 11}$   
 (pos. value indicates tension)



$$P = 2470 \text{ k}$$

$$M_y = 53,508 \text{ k}\cdot\text{in.}$$

$$M_x = 36,120 \text{ k}\cdot\text{in.}$$

Figure B.7: Interaction Slice, Load Case VI-2 Lane

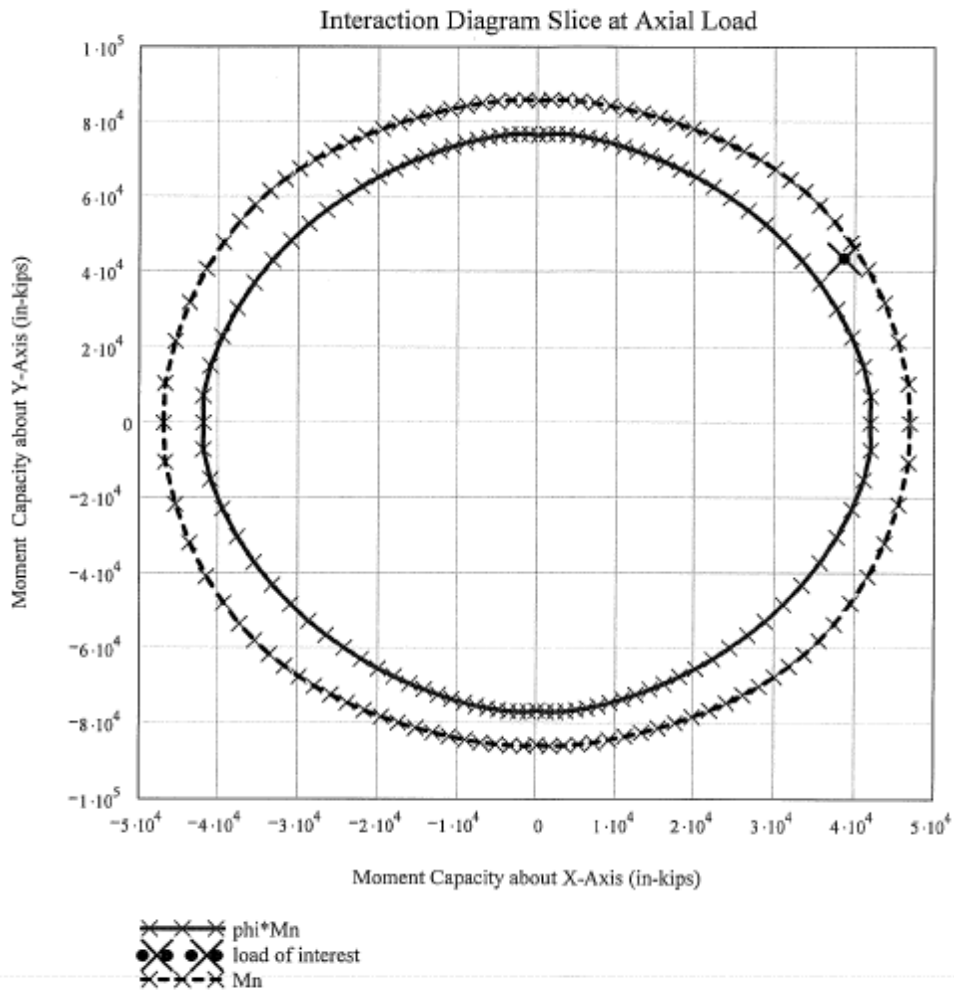
# Case VI, 3 Lane

point:= 7

user\_axial\_point = 2550

SpliceStress\_point = 0

\ 5.828x  
(pos. value indicates tension)



$$P = 2550 \text{ k}$$

$$M_y = 43,740 \text{ k}\cdot\text{in.}$$

$$M_x = 38,580 \text{ k}\cdot\text{in.}$$

12

Figure B.8: Interaction Slice, Load Case VI-3 Lane



## B.2 BIAXIAL COLUMN V2.3 OUTPUT

*Program Output for Case I, 2 Lane*

### Interaction Diagram Concrete Column

© 2000 Florida Department of Transportation

#### Data

##### constants

kip = 1000 · lbf      ksi = 1000 · psi      data := READPRN("values.out")      StressStrain := READPRN("strline.out")  
 $\phi_{axial} := data_5$        $\phi_{flexure} := data_4$        $\phi_{axial} = 0.7$        $\phi_{flexure} = 0.9$

##### materials

$f'_c := data_0 \cdot ksi$        $E_s := data_1 \cdot ksi$        $F_y := data_2 \cdot ksi$        $E_p := data_6 \cdot ksi$        $f_{pe} := data_7 \cdot ksi$   
 $f'_c = 3.6 ksi$        $E_s = 2.9 \times 10^4 ksi$        $F_y = 60 ksi$        $E_p = 0 ksi$        $f_{pe} = 0 ksi$   
 $\Phi Type := data_8$        $Tie Type := data_9$        $\Phi Type = 0$        $Tie Type = 0$   
*0 indicates std AASHTO*      *1 indicates ACI App B*      *0 indicates std*      *1 indicates spiral*

##### analysis locations

$divs := data_3$  (min value is 3)       $divs = 100$        $vdiv := 100$

##### shape contour

$contour := READPRN("contour.out")$

##### rebar locations

$rebar := READPRN("rebar.out")$

$bar_{area} := rebar_{0,2}$        $bar_{area} = 1.56$  (in<sup>2</sup>)

##### loads

$loads := READPRN("loads.out")$

$bar_{type} := rebar_{0,3}$        $bar_{type} = 0$   
*0 mild steel*  
*1 lo lax*  
*2 stress rel*  
*3 A722 bar*  
*4 user def*

$user_{axial} := (loads^{(0)})$        $user_{mom,y} := (loads^{(1)})$        $user_{mom,x} := (loads^{(2)})$

##### file name

$filename := vec2str(READPRN("filename.out"))$        $ext := ".cld"$

$filename := concat(filename, ext)$

Figure B.9: Program Output (1 of 12)

```

(0)
tmparray := for i ∈ 0..vdiv
            for j ∈ 0..4
              tmpi,j ← 0
            tmp
strengthdivs-1 := tmparray

ia := 0..(divs - 1)
thia := ia · (  $\frac{2}{divs} \cdot \pi$  )

strength0 := finteractionnc ( contour, rebar,  $\frac{F_y}{ksi}$ ,  $\frac{f_c}{ksi}$ , thia, vdiv )

```

	0
0	[102, 5]
1	[102, 5]
2	[102, 5]
3	[102, 5]
4	[102, 5]
5	[102, 5]
6	[102, 5]
7	[102, 5]
8	[102, 5]
9	[102, 5]
10	[102, 5]
11	[102, 5]
12	[102, 5]
13	[102, 5]
14	[102, 5]
15	[102, 5]

```

strength =
strength := cnt ← 0
           i ← 0
           while i ≤ last(strength)
             if strengthi ≠ 0
               anscnt ← strengthi
               cnt ← cnt + 1
             i ← i + 1
           ans

intershape := sum ← strength0
            for k ∈ 1..(last(strength))
              sum ← stack(sum, strengthk)
            sum

ig := 0..(rows(strength) - 1)

```

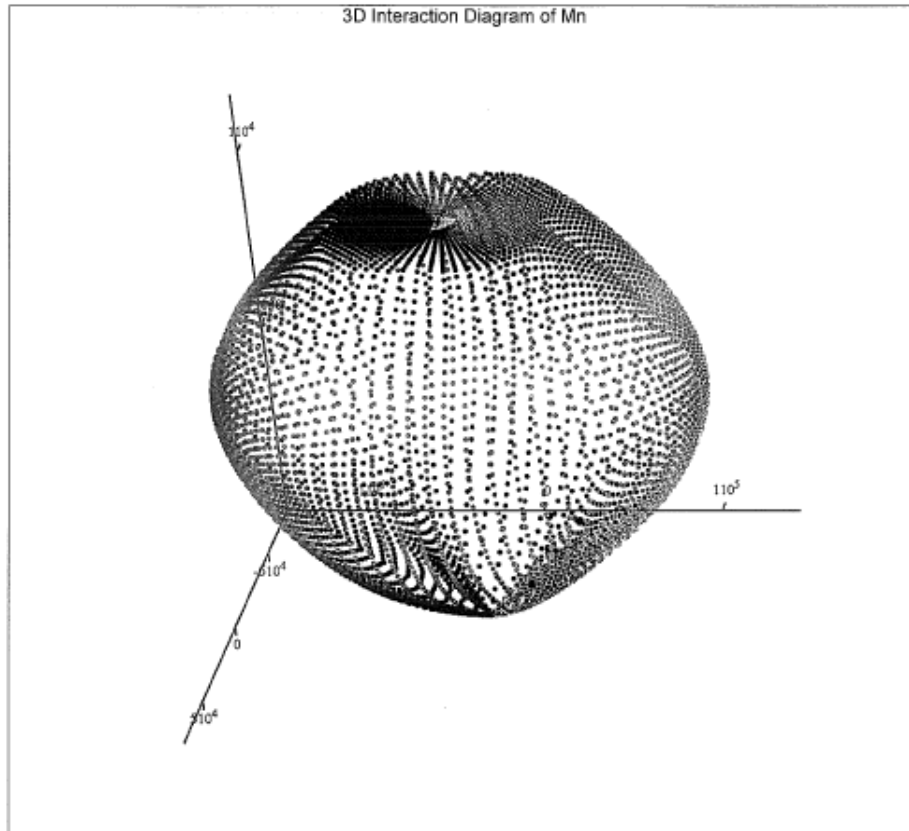
---

```

xi := intershape(0)
yi := intershape(1)
zi := intershape(2)

```

Figure B.10: Program Output (2 of 12)



$(xi, yi, zi), (user_{axial}, user_{mom.x}, user_{mom.y})$

$top := \max(\text{contour}^{(i)}) + 1$      $rside := \max(\text{contour}^{(i)}) + 1$      $boff := \min(\text{contour}^{(i)}) - 1$      $lside := \min(\text{contour}^{(i)}) - 1$

$centroid_{analysis} := \text{fPlasticCentroid}\left(\text{rebar}, \text{fConeCentroid}(\text{contour}, 0), 0, \frac{F_y}{\text{ksi}}, \frac{f_c}{\text{ksi}}, \text{Prop}(\text{fPropCoord}(\text{contour}))_0\right)$

**Figure B.11: Program Output (3 of 12)**

```

centroid_analysis = (42 23)      location of centroid used for analysis
centconc = fConcCentroid(contour, 0)  centconc = (42 23)      gross centroid
area := Prop(fPropCoord(contour))_0  area = 3864      gross area

```

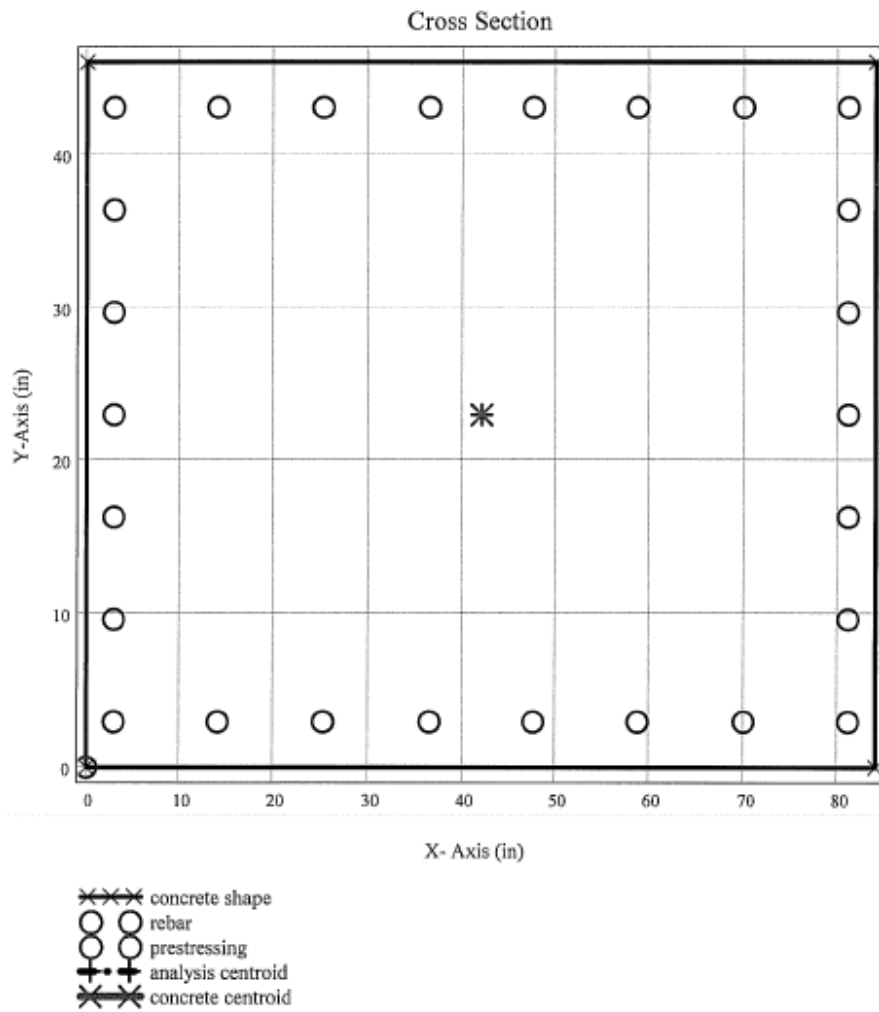


**Figure B.12: Program Output (4 of 12)**

```

fPhiFactor(st, cr, fc) :=
  cprop ← fPropCoord(cr)
  area ← Prop(cprop)0
  cv ← 0.1 · area · fc
  lastr ← rows(st)
  for j ∈ 0..(lastr - 1)
    if stj,0 ≥ cv
      resj,0 ← stj,0 · φaxial
      resj,1 ← stj,1 · φaxial
      resj,2 ← stj,2 · φaxial
    if stj,0 ≤ 0
      resj,0 ← stj,0 · φflexure
      resj,1 ← stj,1 · φflexure
      resj,2 ← stj,2 · φflexure
    if (stj,0 < cv) · (stj,0 > 0)
      phi ←  $\frac{cv - st_{j,0}}{cv} \cdot (\phi_{flexure} - \phi_{axial}) + \phi_{axial}$ 
      resj,0 ← stj,0 · phi
      resj,1 ← stj,1 · phi
      resj,2 ← stj,2 · phi
  resj,3 ← stj,3
res

```

*Figure B.13: Program Output (5 of 12)*

```

fPhiFactorACIB(st) := | lastr ← rows(st)
                       | for j ∈ 0 .. (lastr - 1)
                       |   if stj,4 < 0.002
                       |     resj,0 ← stj,0 · φaxial
                       |     resj,1 ← stj,1 · φaxial
                       |     resj,2 ← stj,2 · φaxial
                       |   if (stj,4 ≥ 0.002) · (stj,4 ≤ 0.005)
                       |     phi ←  $\frac{st_{j,4} - 0.002}{0.003} \cdot (\phi_{flexure} - \phi_{axial}) + \phi_{axial}$ 
                       |     resj,0 ← stj,0 · phi
                       |     resj,1 ← stj,1 · phi
                       |     resj,2 ← stj,2 · phi
                       |   if stj,4 > 0.005
                       |     resj,0 ← stj,0 · φflexure
                       |     resj,1 ← stj,1 · φflexure
                       |     resj,2 ← stj,2 · φflexure
                       |   resj,3 ← stj,3
capacityia := | ans ← fPhiFactor( strengthia, contour,  $\frac{r_c}{ksi}$  ) if PhiType = 0
               | ans ← fPhiFactorACIB( strengthia ) otherwise
               | ans

```

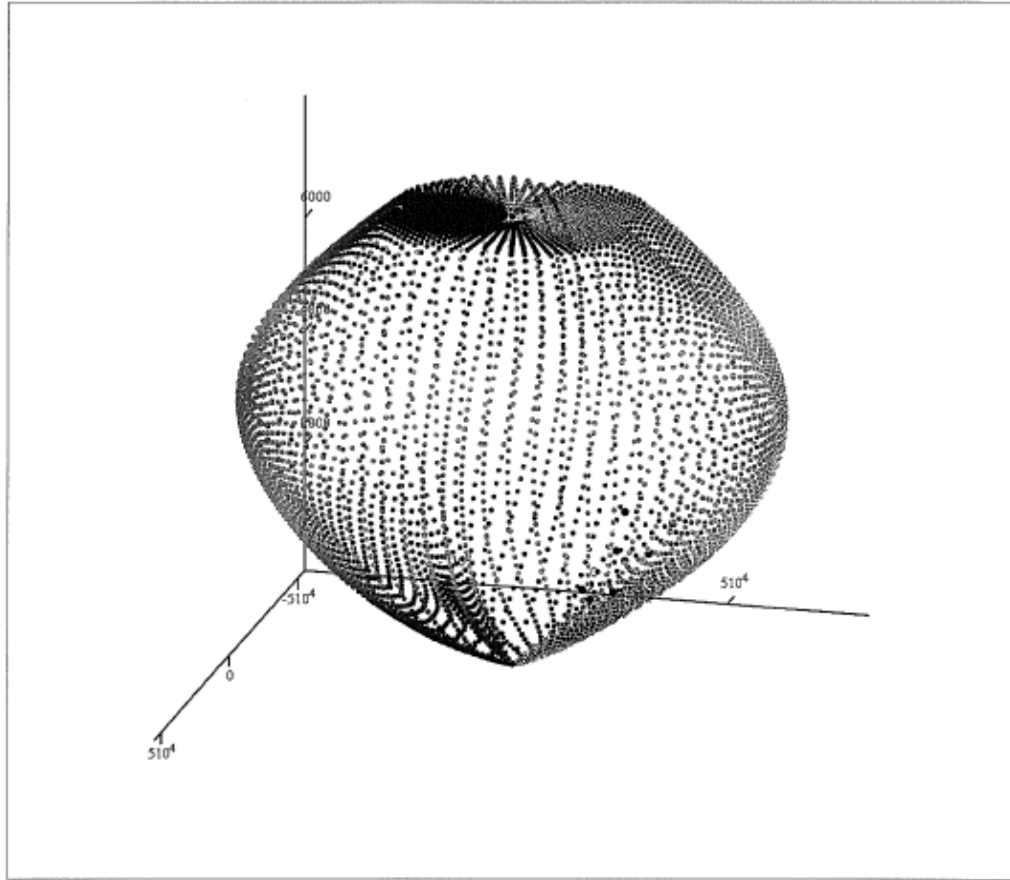
```

FactoredCapacity := | sum ← capacity0
                    | for k ∈ 1 .. (rows(strength) - 1)
                    |   sum ← stack( sum, capacityk )
                    | sum

```

*Figure B.14: Program Output (6 of 12)*

$cap_x := \text{FactoredCapacity}^{(1)}$     $cap_y := \text{FactoredCapacity}^{(1)}$     $cap_z := \text{FactoredCapacity}^{(2)}$



$(cap_x, cap_y, cap_z), (user_{axial}, user_{mom.x}, user_{mom.y})$

*Figure B.15: Program Output (7 of 12)*

```

fPlane(ux, s) := for j ∈ 0..(rows(ux) - 1)
                for k ∈ 0..(rows(s) - 1)
                    tmp ← sk
                    if uxj > tmp0,0
                        resk,0 ← 0
                        resk,1 ← 0
                        resk,2 ← 0
                        continue
                    for z ∈ 1..(rows(tmp) - 1)
                        if (tmpz,0 ≤ uxj) · (tmpz-1,0 > uxj)
                            resk,0 ←  $\frac{ux_j - tmp_{z-1,0}}{tmp_{z,0} - tmp_{z-1,0}} \cdot (tmp_{z,1} - tmp_{z-1,1}) + tmp_{z-1,1}$ 
                            resk,1 ←  $\frac{ux_j - tmp_{z-1,0}}{tmp_{z,0} - tmp_{z-1,0}} \cdot (tmp_{z,2} - tmp_{z-1,2}) + tmp_{z-1,2}$ 
                            resk,2 ←  $\frac{ux_j - tmp_{z-1,0}}{tmp_{z,0} - tmp_{z-1,0}} \cdot (tmp_{z,3} - tmp_{z-1,3}) + tmp_{z-1,3}$ 
                            break
                    resk+1,0 ← res0,0
                    resk+1,1 ← res0,1
                    resk+1,2 ← res0,2
                    ansj ← res
                ans

```

```

Momentfailure := fPlane(useraxial, strength)
Momentenvl := fPlane(useraxial, capacity)
Momentenvl =  $\begin{pmatrix} \{101,3\} \\ \{101,3\} \\ \{101,3\} \\ \{101,3\} \\ \{101,3\} \\ \{101,3\} \\ \{101,3\} \end{pmatrix}$ 

```

Figure B.16: Program Output (8 of 12)



```

fClosePoint(c, fy, x1, y1, z1) :=
  lastr ← rows(c) - 1
  x1 ← x1 · 1000
  for j ∈ 0 .. lastr
    x0 ← cj,0 · 1000
    if j = 0
      res ← cj,3
      distmin ←  $\left[ \frac{(c_{j,1} \cdot z1 - c_{j,2} \cdot y1)^2 + (c_{j,2} \cdot x1 - x0 \cdot z1)^2 + (x0 \cdot y1 - c_{j,1} \cdot x1)^2}{x1^2 + y1^2 + z1^2} \right]^{0.5}$ 
      continue
    continue if x0 < x1
    if x1 ≤ 0
      res ← fy
      break
    dist ←  $\left[ \frac{(c_{j,1} \cdot z1 - c_{j,2} \cdot y1)^2 + (c_{j,2} \cdot x1 - x0 \cdot z1)^2 + (x0 \cdot y1 - c_{j,1} \cdot x1)^2}{x1^2 + y1^2 + z1^2} \right]^{0.5}$ 
    if dist < distmin
      distmin ← dist
      res ← cj,3
  res

inv := 0 .. rows(user_axial) - 1
SpliceStressinv := fClosePoint( intershape,  $\frac{F_y}{lcsi}$ , user_axialinv, user_mom.yinv, user_mom.xinv)

```

SpliceStress =	$\begin{pmatrix} 0 \\ 0 \\ 0 \\ 0 \\ 0 \\ 0 \\ 0 \\ 0 \end{pmatrix}$	.....	user_axial =	$\begin{pmatrix} 2720 \\ 2855 \\ 2340 \\ 2570 \\ 2650 \\ 2250 \\ 2470 \\ 2550 \end{pmatrix}$	.....	user_mom.y =	$\begin{pmatrix} 57312 \\ 40308 \\ 46080 \\ 55632 \\ 45468 \\ 44280 \\ 53508 \\ 43740 \end{pmatrix}$	.....	user_mom.x =	$\begin{pmatrix} 0 \\ 0 \\ 1.2 \times 10^4 \\ 1.44 \times 10^4 \\ 1.692 \times 10^4 \\ 3.382 \times 10^4 \\ 3.612 \times 10^4 \\ 3.858 \times 10^4 \end{pmatrix}$
----------------	--	-------	--------------	--	-------	--------------	--	-------	--------------	---

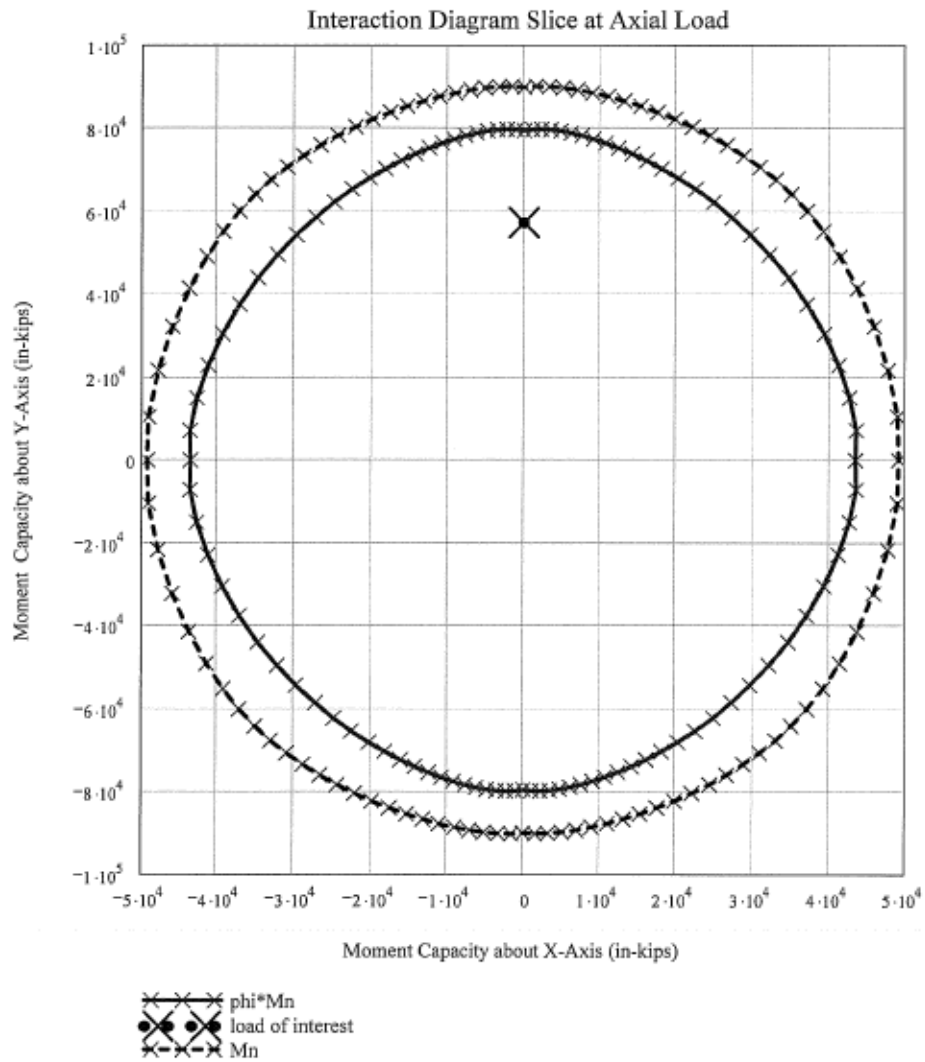
*Figure B.17: Program Output (9 of 12)*

point := 0

user\_axial\_point = 2720

SpliceStress\_point = 0

(pos. value indicates tension)



*Note:  $\phi * Mn$  is incorrect for Moment envelope slices not centered around 0.0*

**Figure B.18: Program Output (10 of 12)**

mid := 0

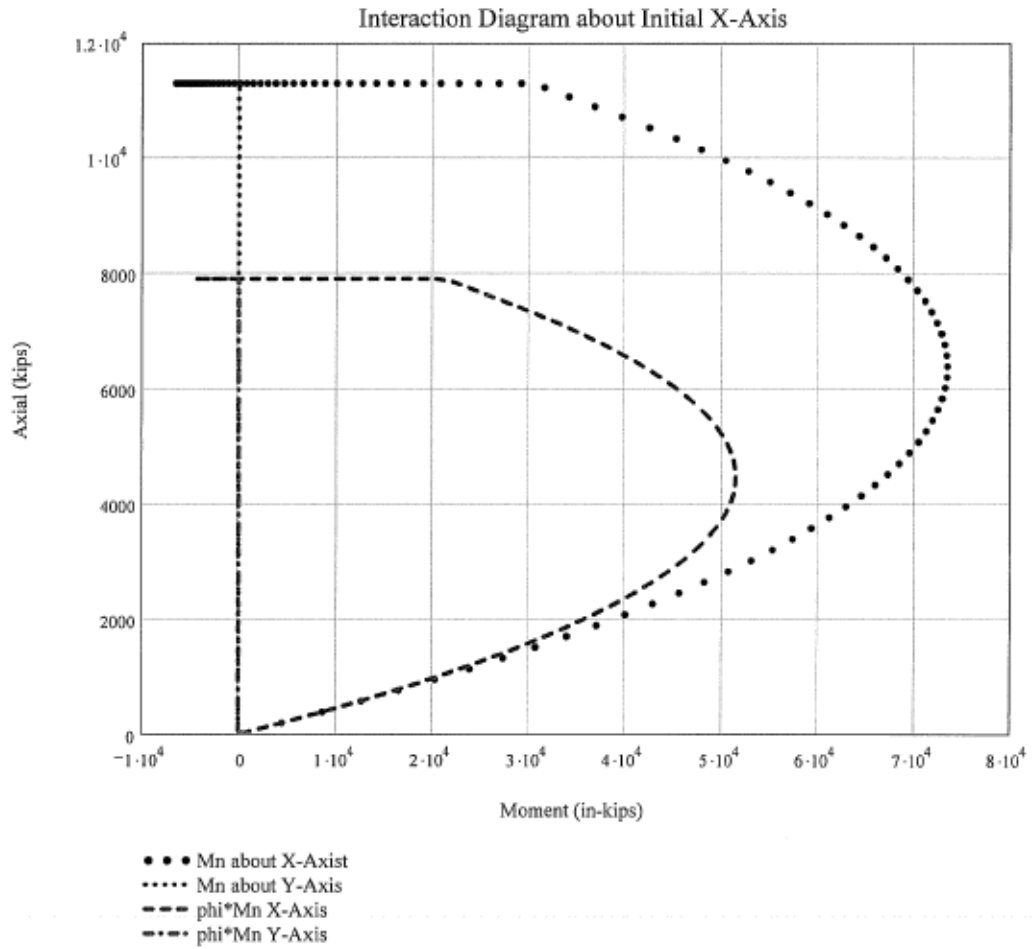


**Figure B.19: Program Output (11 of 12)**

```

data0 :=  $\frac{E_s}{\text{ksi}}$       data1 :=  $\frac{F_y}{\text{ksi}}$       data2 :=  $\frac{f_c}{\text{ksi}}$       data3 := contour      data4 := rebar
data5 := strength      data6 := centconc      data7 := area      data8 := centroidanalysis      data9 := divs
data10 :=  $\phi_{\text{axial}}$       data11 :=  $\phi_{\text{flexure}}$       data12 :=  $\frac{E_p}{\text{ksi}}$       data13 :=  $f_{pe}$ 
data14 := TieType      data15 := PhiType

WRITEPRN(filename) := data

```

Figure B.20: Program Output (12 of 12)

### B.3 P vs. M INTERACTION CURVES

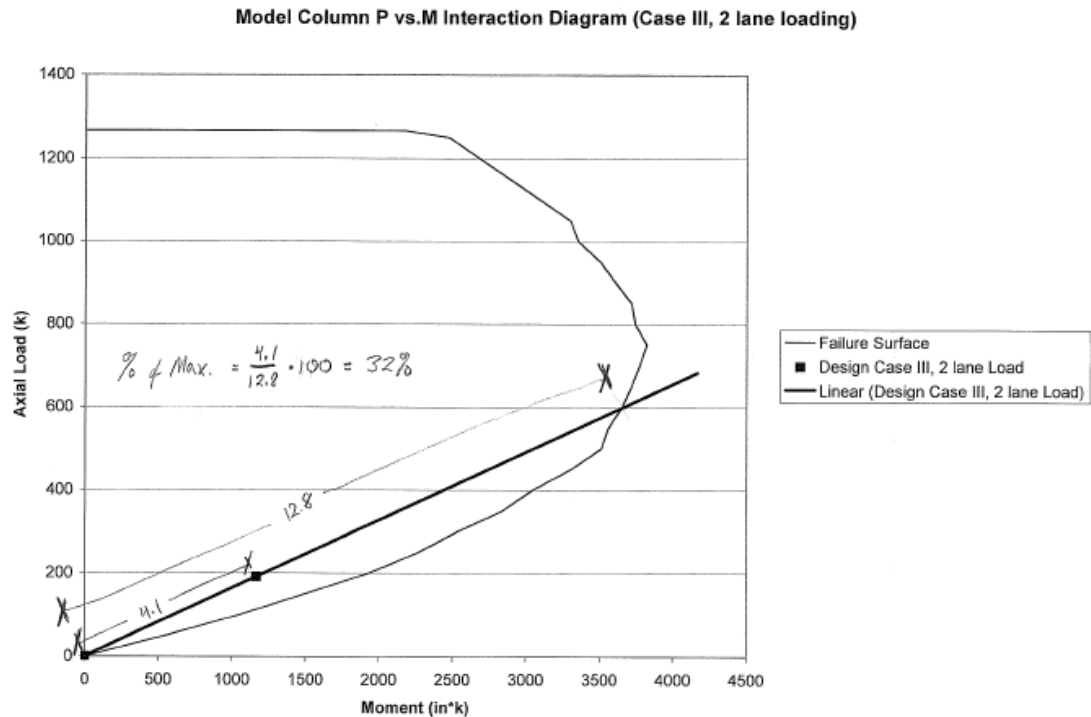
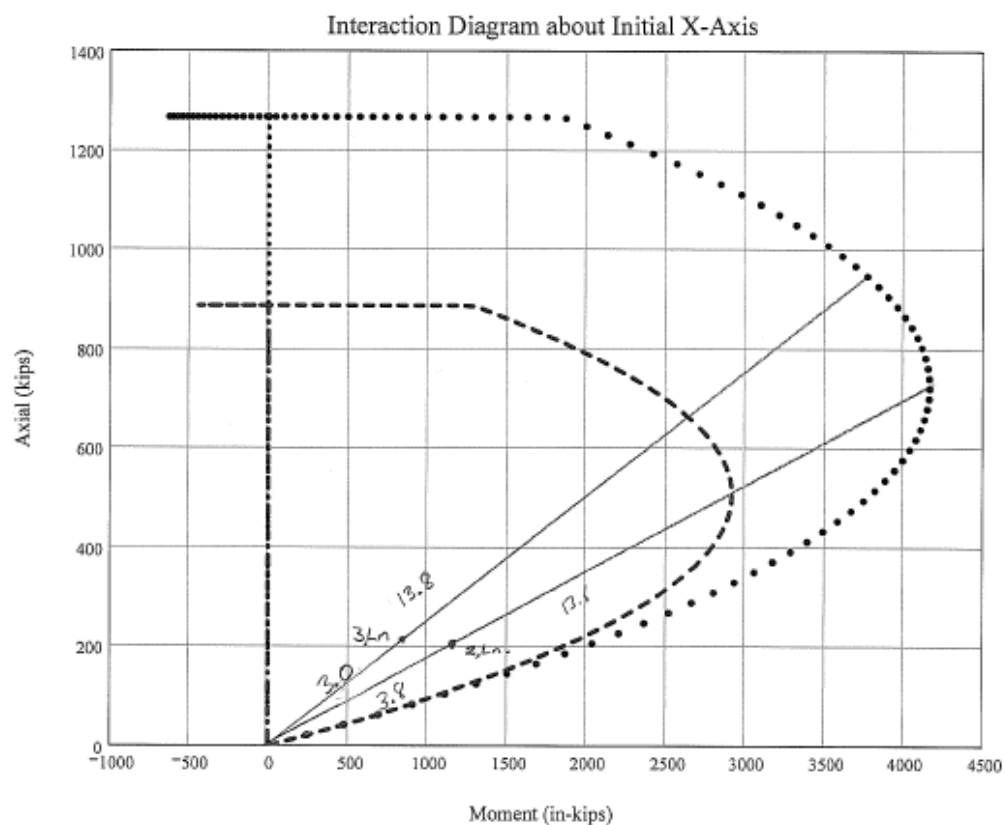


Figure B.21: Interaction Curve, Case III-2 Lane Loading

mid = 0  
 Case I, 2 Lane  
 +  
 Case I, 3 Lane



- Mn about X-Axis
- ..... Mn about Y-Axis
- phi\*Mn X-Axis
- .- phi\*Mn Y-Axis

$$\% \text{ of Max. (2 Lane)} = \frac{3.8}{13.6} \cdot 100 = 28\%$$

$$\% \text{ of Max. (3 Lane)} = \frac{3}{13.8} \cdot 100 = 22\%$$

**Figure B.22: Interaction Curve, Cases I, 2 and 3 Lane Loading**

# B.4 REINFORCEMENT DETAILS

## B.4.1 Prototype Pier Reinforcement

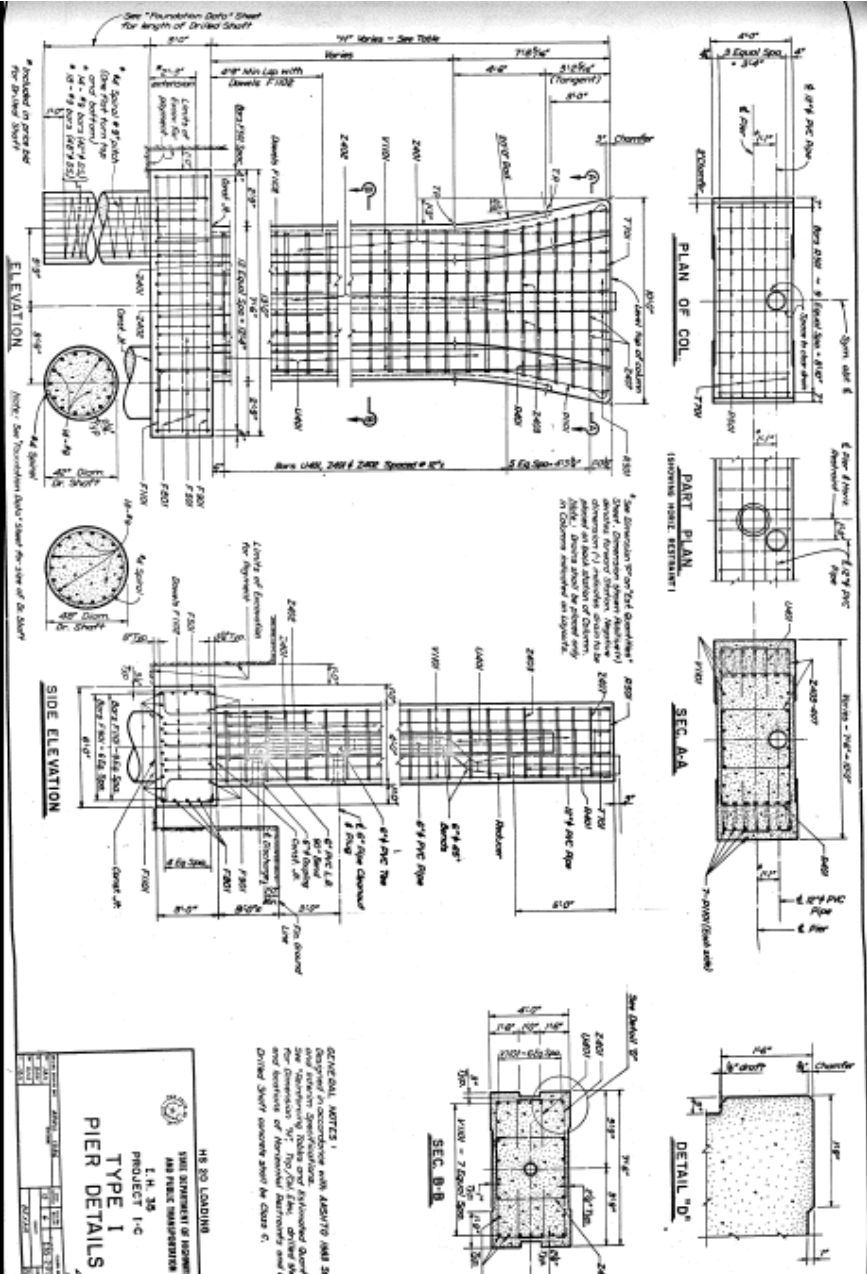


Figure B.23: Prototype Column Reinforcement (1 of 2)

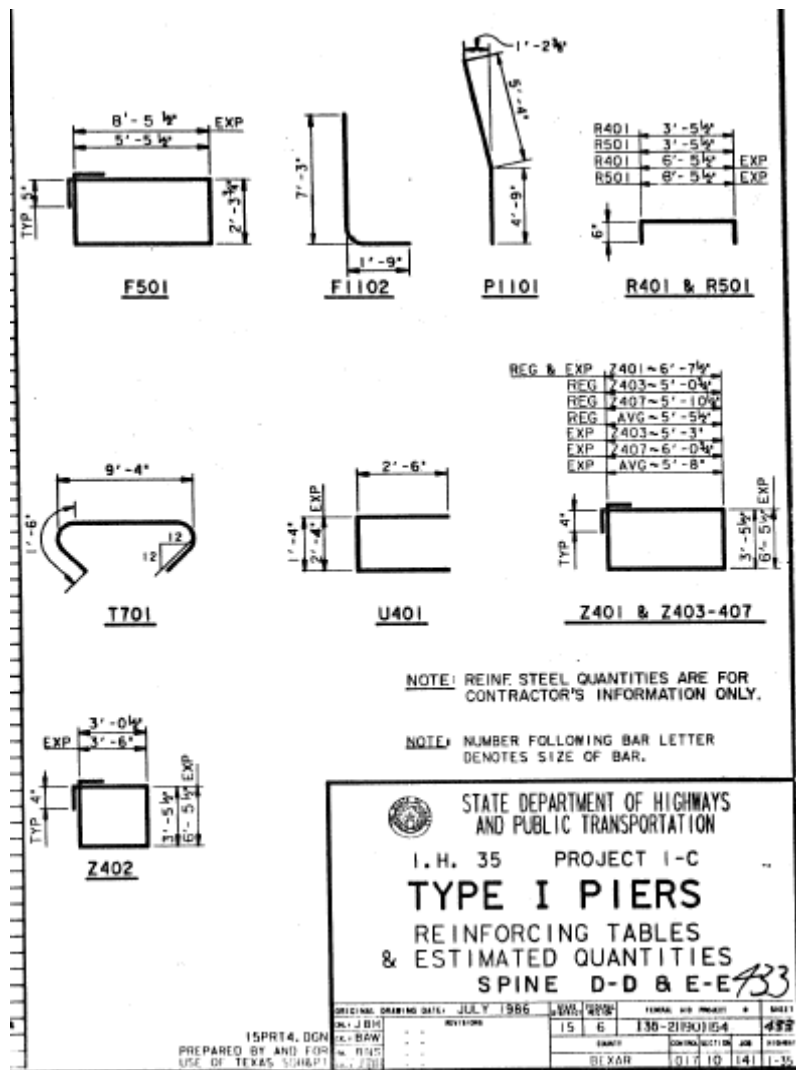
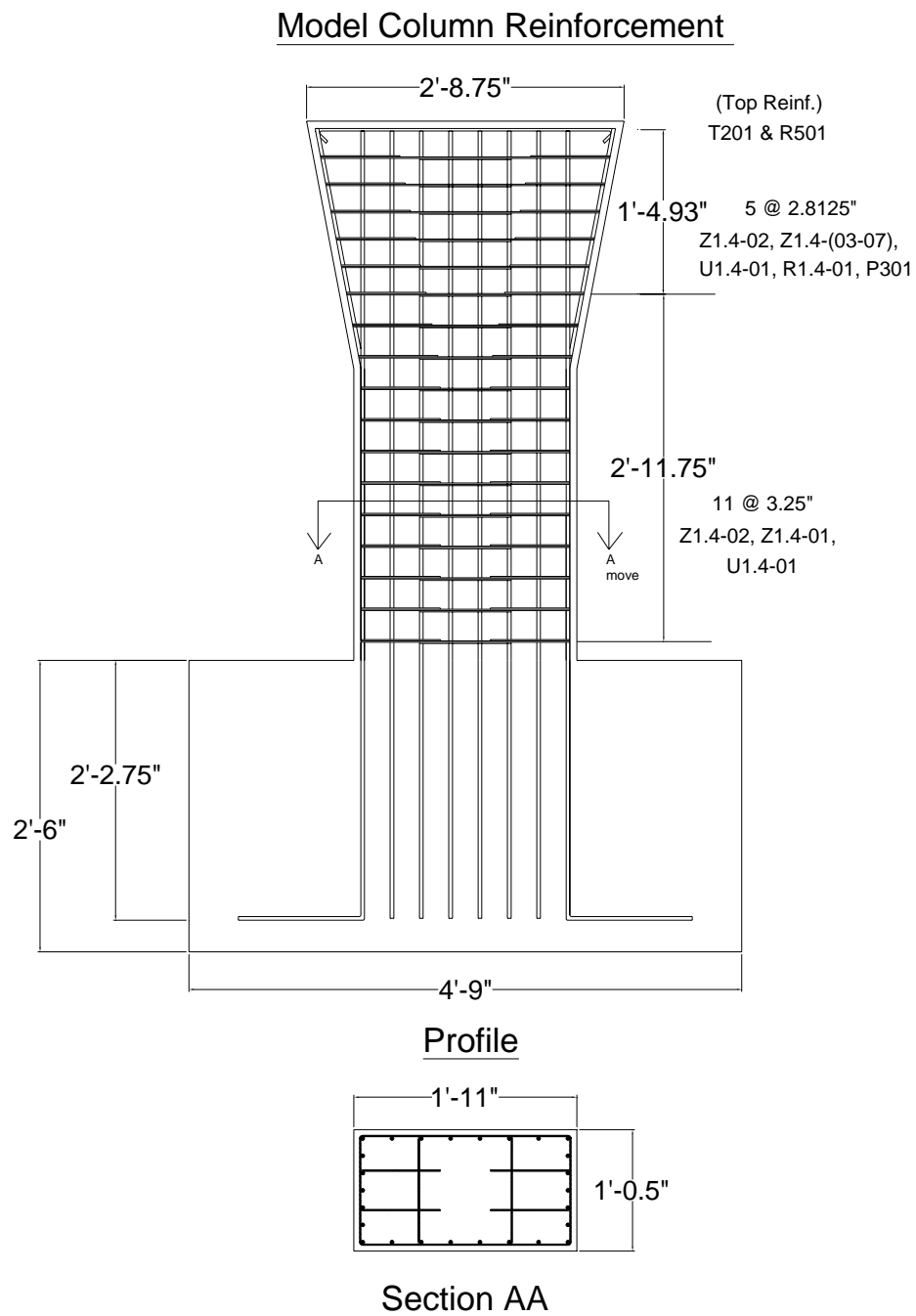


Figure B.24: Prototype Pier Reinforcement (2 of 2)

## B.4.2 Model Pier Reinforcement



*Figure B.25: Model Pier Reinforcement (1 of 4)*



Proj. # 5218

Model Column Reinf. Steel

8/11/05



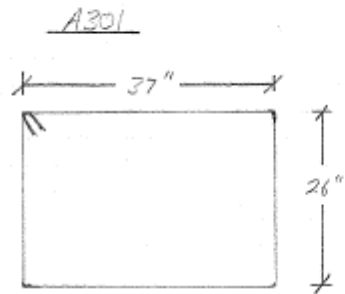
Quantity = 104  
Bar Size = #3

Scale: 1 in = 20 in.

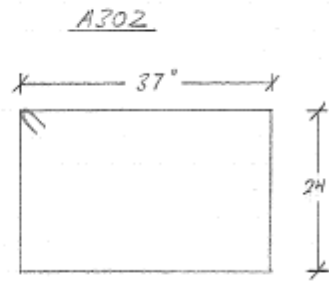
Note: All Reinforcing Steel is Grade 60  
All Quantities are for making 4 specimens



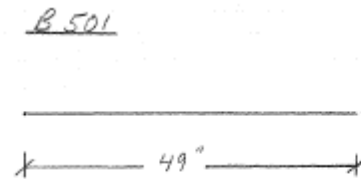
Quantity = 56  
Bar Size = #3



Quantity = 32  
Bar Size = #3



Quantity = 32  
Bar Size = #3



Quantity = 144  
Bar Size = #5

35510 - 100 sheets  
35520 - 200 sheets

Figure B.26: Model Pier Reinforcement (2 of 4)

Proj. # 5218

Model Column Reinf. Steel

8/11/05

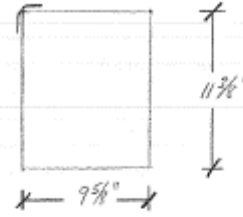
Scale: 1 in = 10 in.

Z1.4-01



Quantity = 52  
Bar Size = D1.4 wire

Z1.4-02



Quantity = 52  
Bar Size = D1.4 wire

Z1.4-03



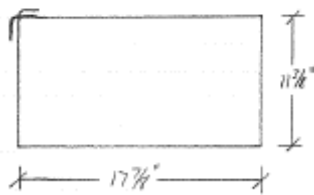
Quantity = 8  
Bar Size = D1.4 wire

Z1.4-04



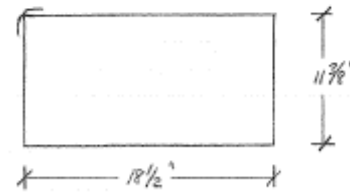
Quantity = 8  
Bar Size = D1.4 wire

Z1.4-05



Quantity = 8  
Bar Size = D1.4 wire

Z1.4-06



Quantity = 8  
Bar Size = D1.4 wire

Note: All reinforcing steel is Grade 60  
All quantities are for making 4 specimens

Figure B.27: Model Pier Reinforcement (3 of 4)

Sheet 35510 - 100 sheets  
Sheet 35520 - 200 sheets

Proj. # 5218

Model Column Reinf. Steel

8/11/05

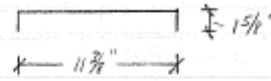
R1.4-07



Quantity = 8  
Bar Size = D1.4 Wire

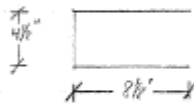
Scale: 2 in = 10 in.

R1.4-01



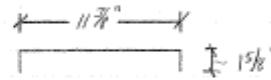
Quantity = 40  
Bar Size = D1.4 wire

U1.4-01



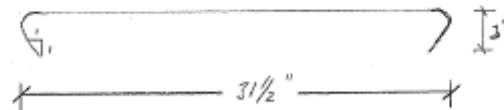
Quantity = 144  
Bar Size = D1.4 Wire

R1.7-01



Quantity = 40  
Bar Size = #17 in. diameter deformed wire

T201



Quantity = 16  
Bar Size = #2

Note: All reinforcing steel is Grade 60  
All quantities are for making 4 specimens

35530 - 100 sheets  
35520 - 200 sheets

Figure B.28: Model Pier Reinforcement (4 of 4)

### B.4.3 Footing Reinforcement for Model Pier

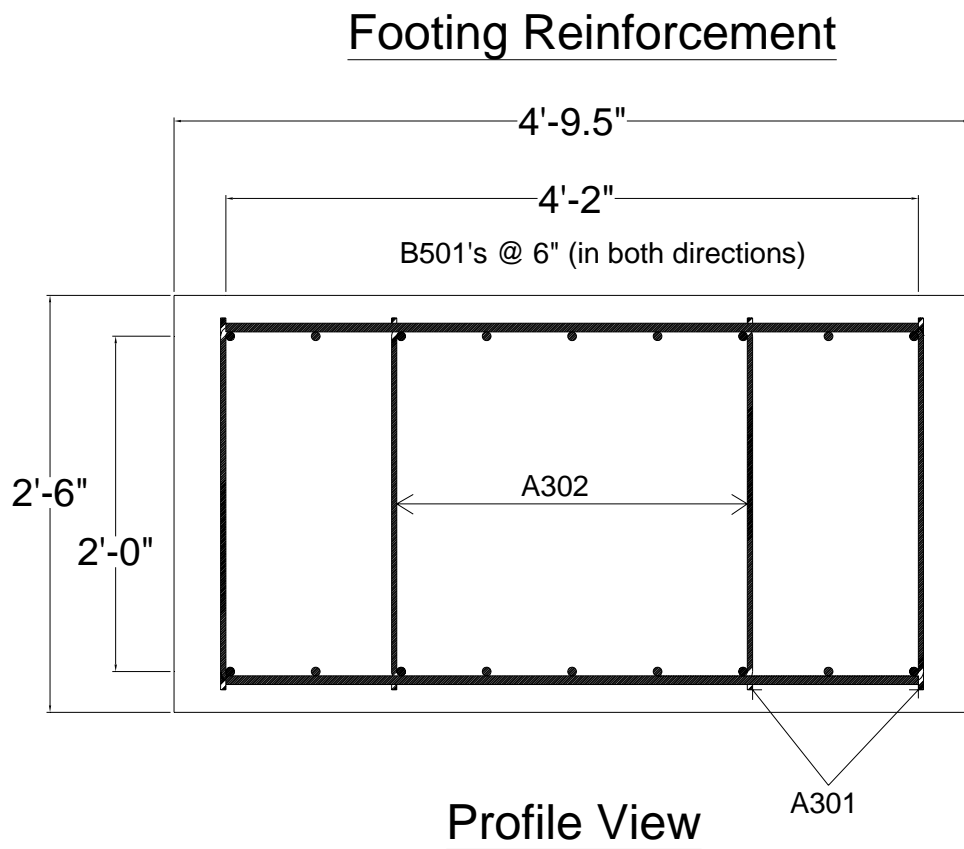


*Figure B.29: Footing Reinforcement for Model Pier (1 of 2)*

35510 - 100 sheets  
35520 - 200 sheets

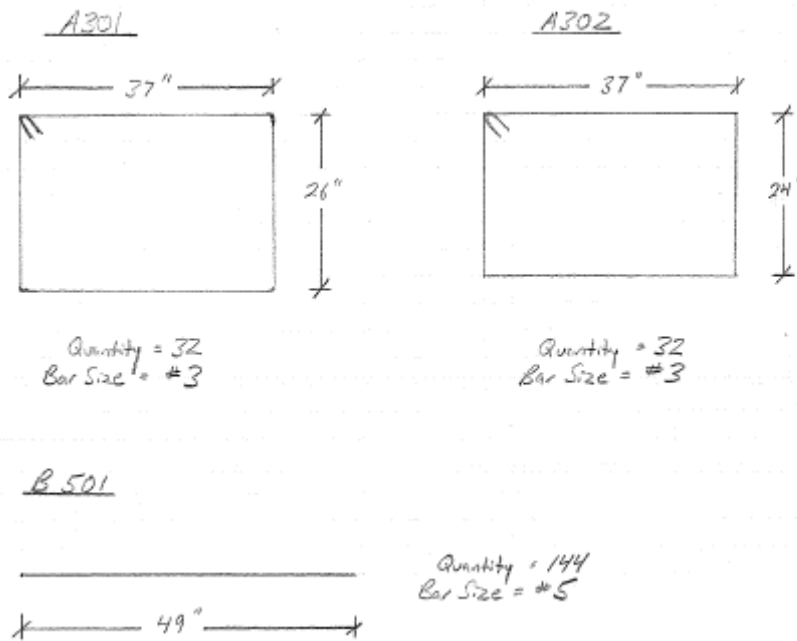


**Figure B.30: Footing Reinforcement for Model Pier (2 of 2)**

## B.5 FORMWORK

### B.5.1 Cracking Experiment

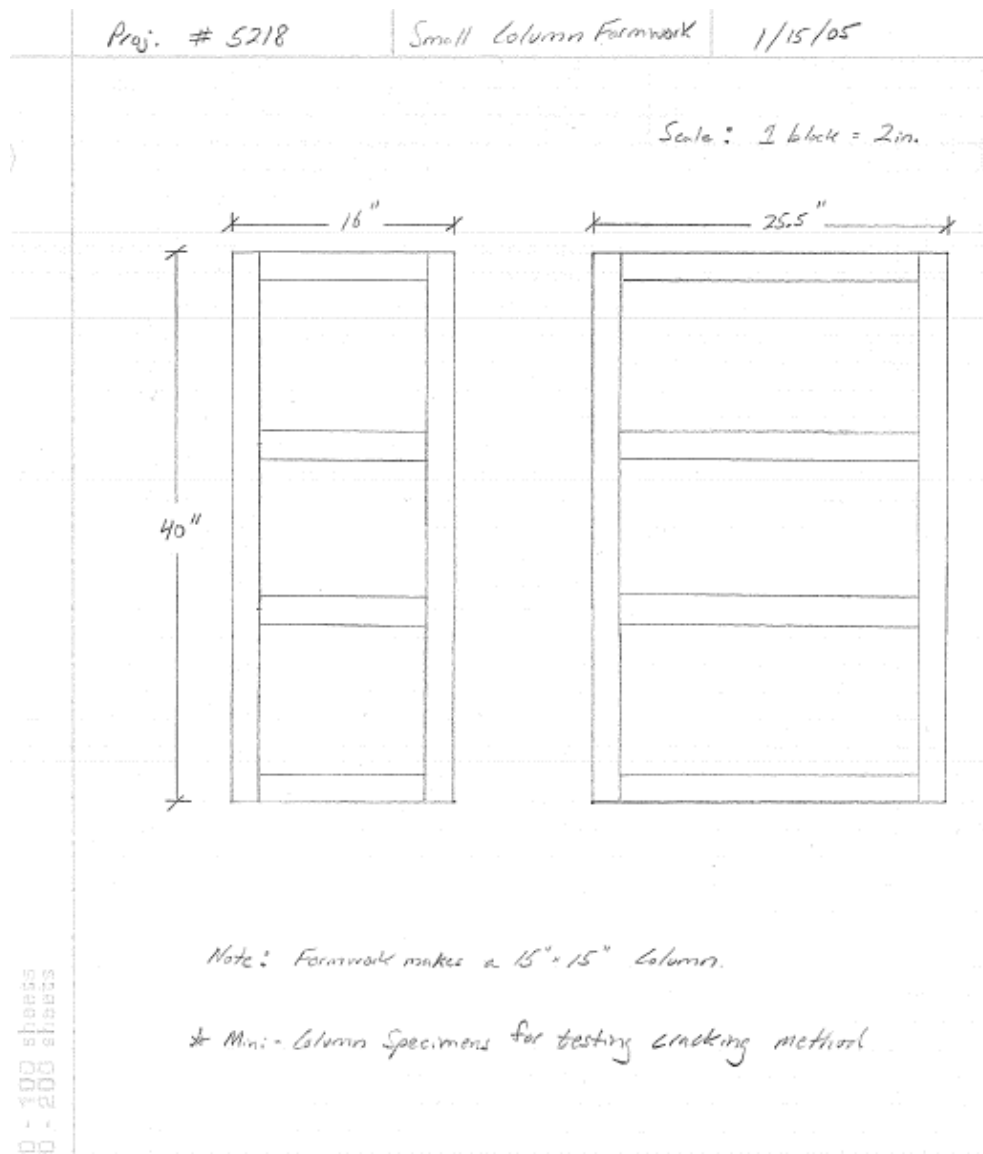


**Figure B.31: Cracking Experiment Formwork**

## B.5.2 Model Pier

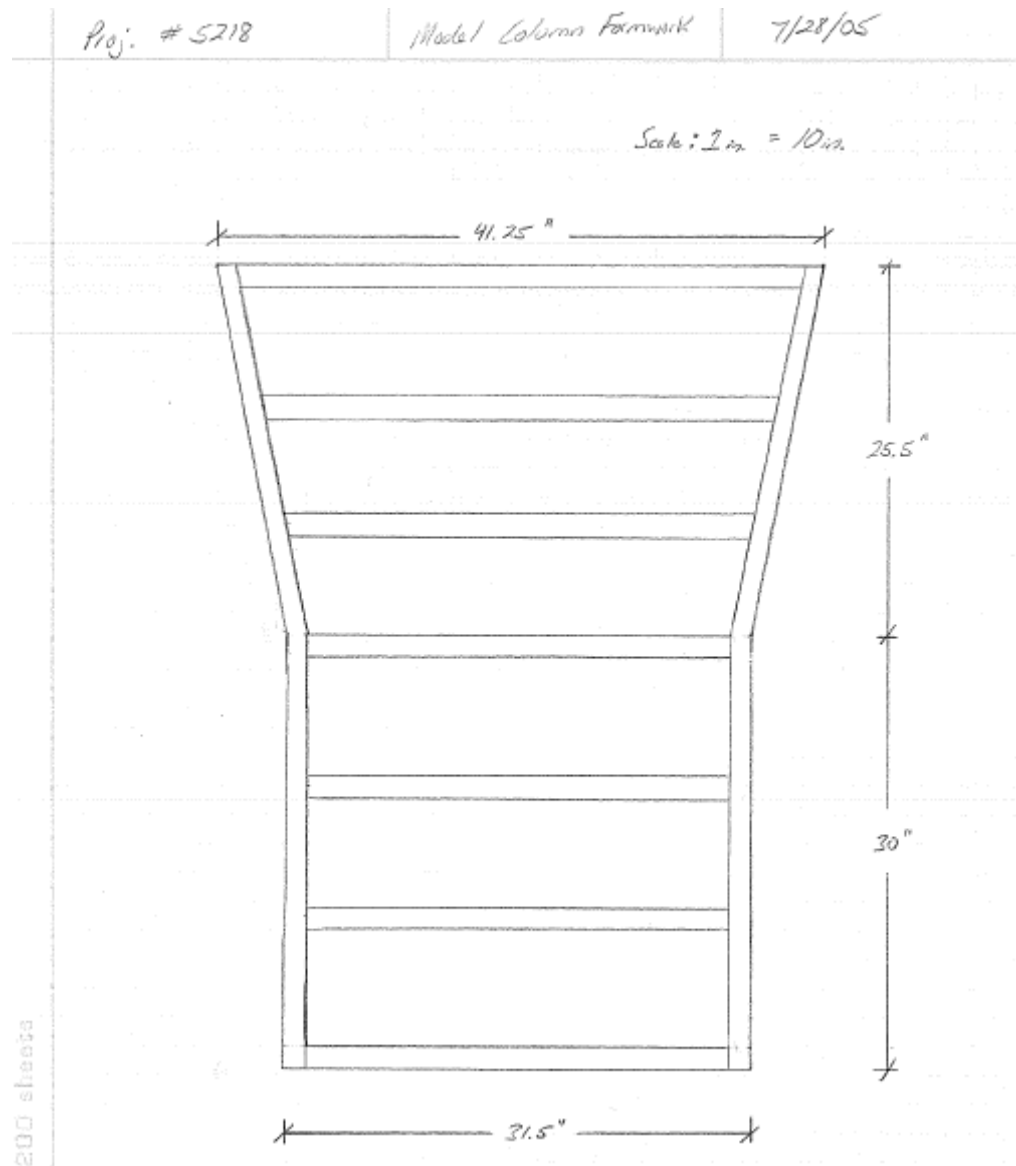


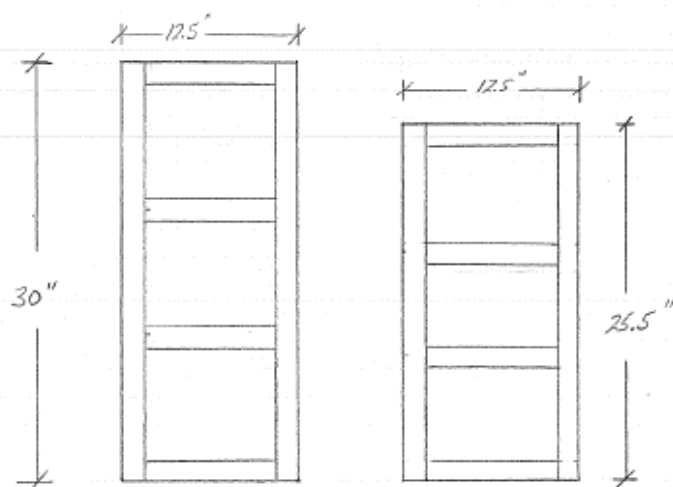
**Figure B.32: Model Pier Formwork (1 of 2)**

Proj. # 5218

Model Column Formwork

7/29/05

Scale: 2 in. = 10 in.



35510 - 100 sheets  
35520 - 200 sheets

**Figure B.33: Model Pier Formwork (2 of 2)**



### B.5.3 Footing for Model Pier

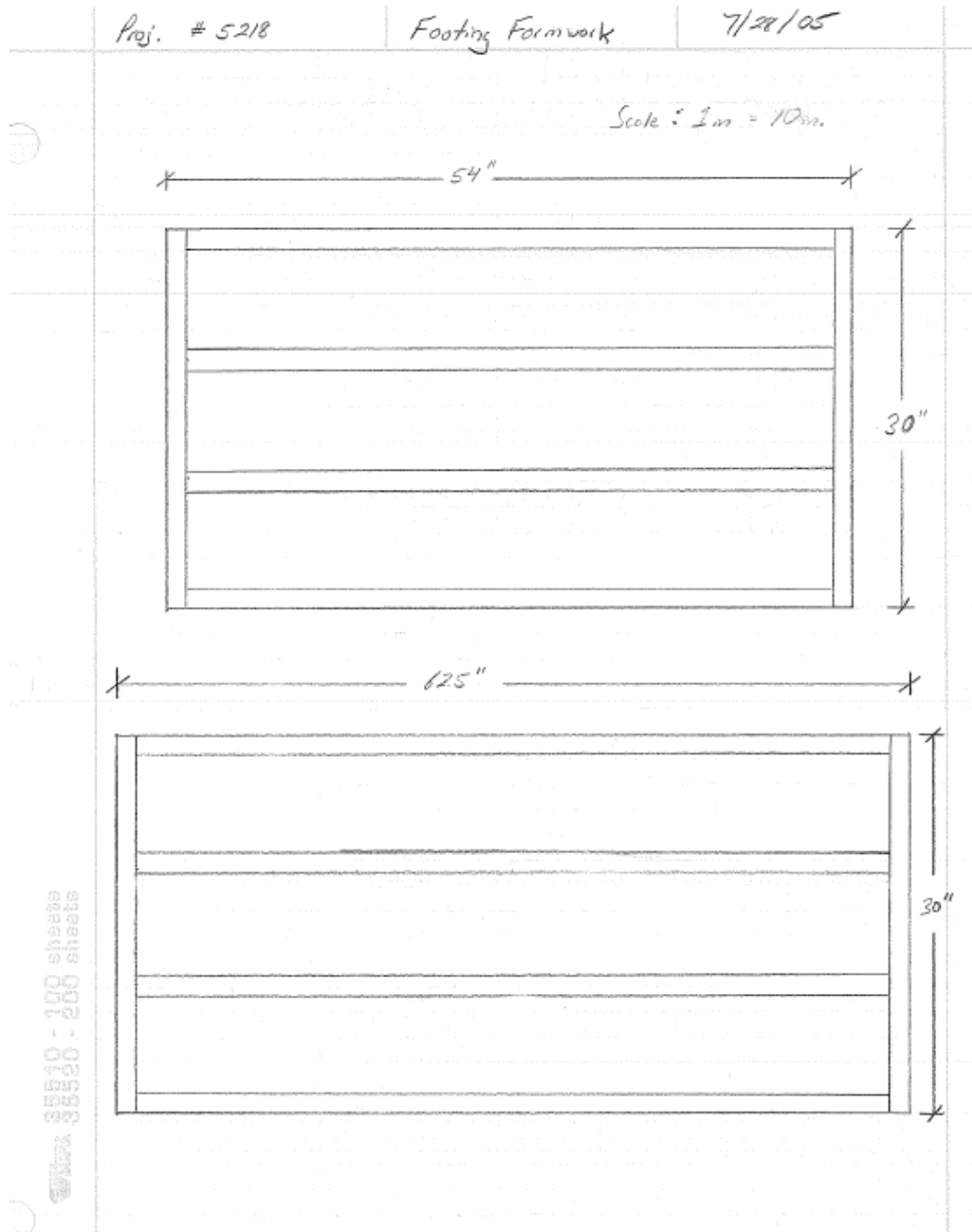


**Figure B.34: Footing Formwork**

## B.6 POSITION OF EXTERNAL GAUGES

### B.6.1 Specimen S2

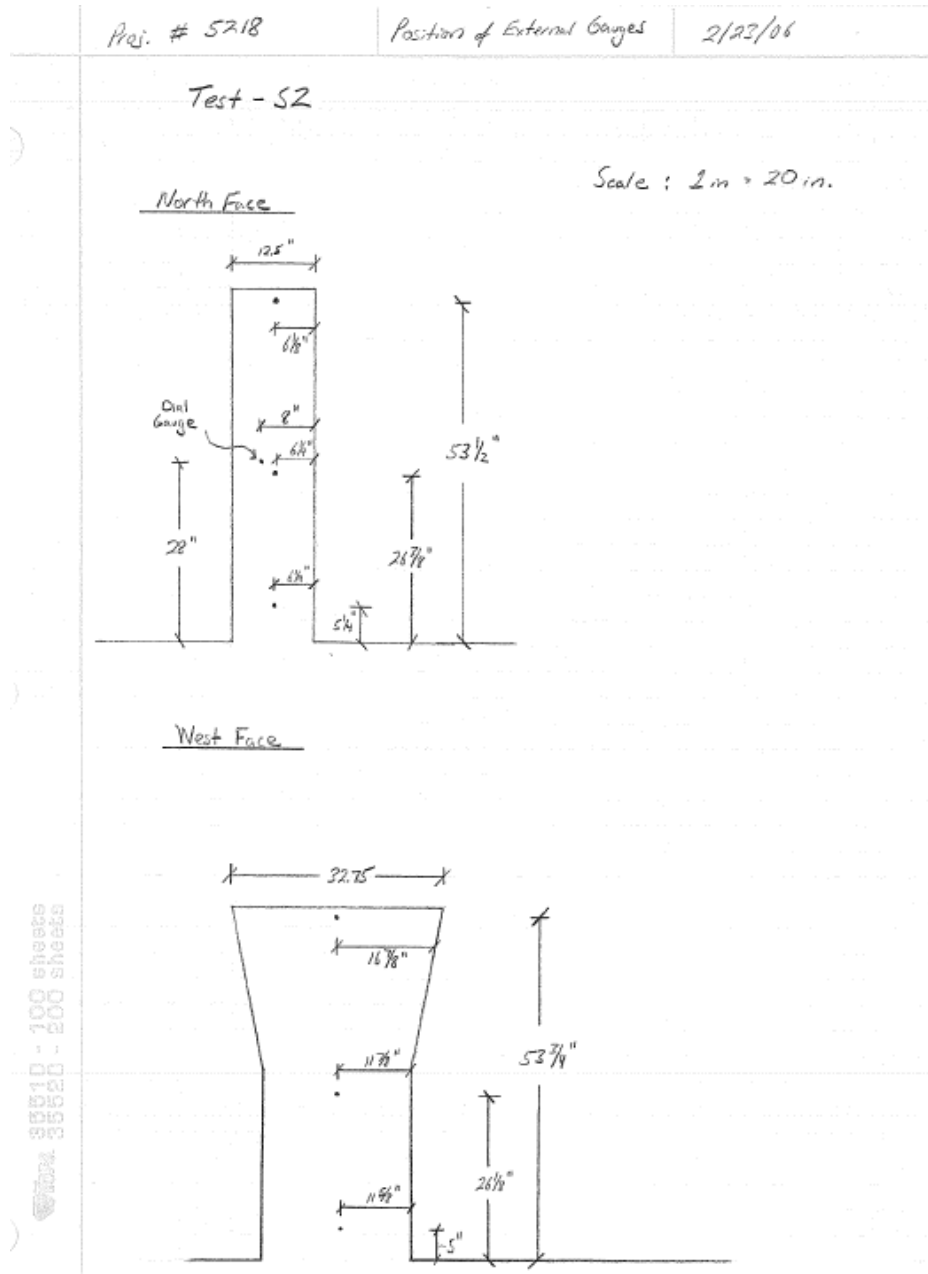


**Figure B.35: S2 – Position of External Gauges**

## B.6.2 Specimen C1

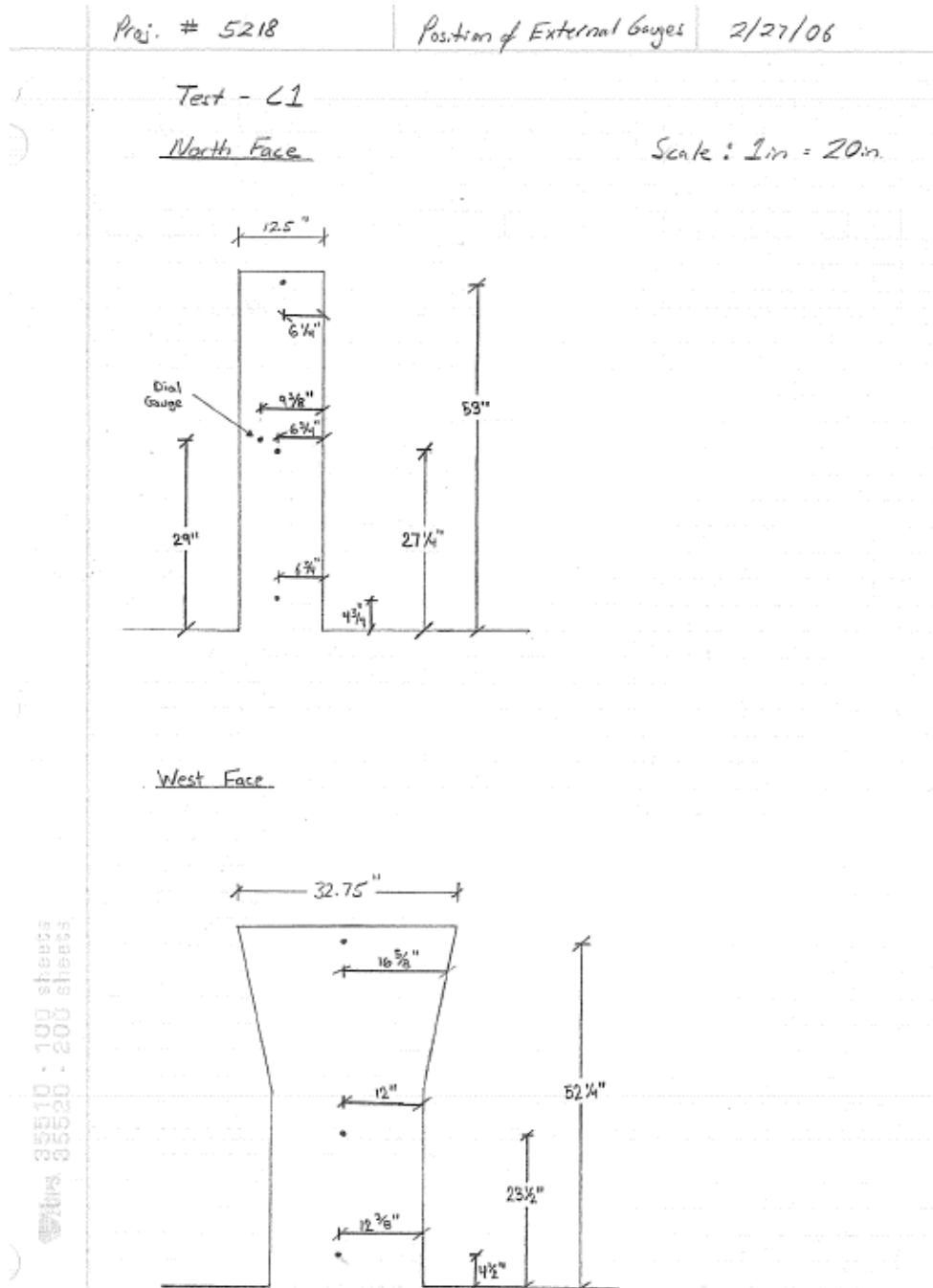
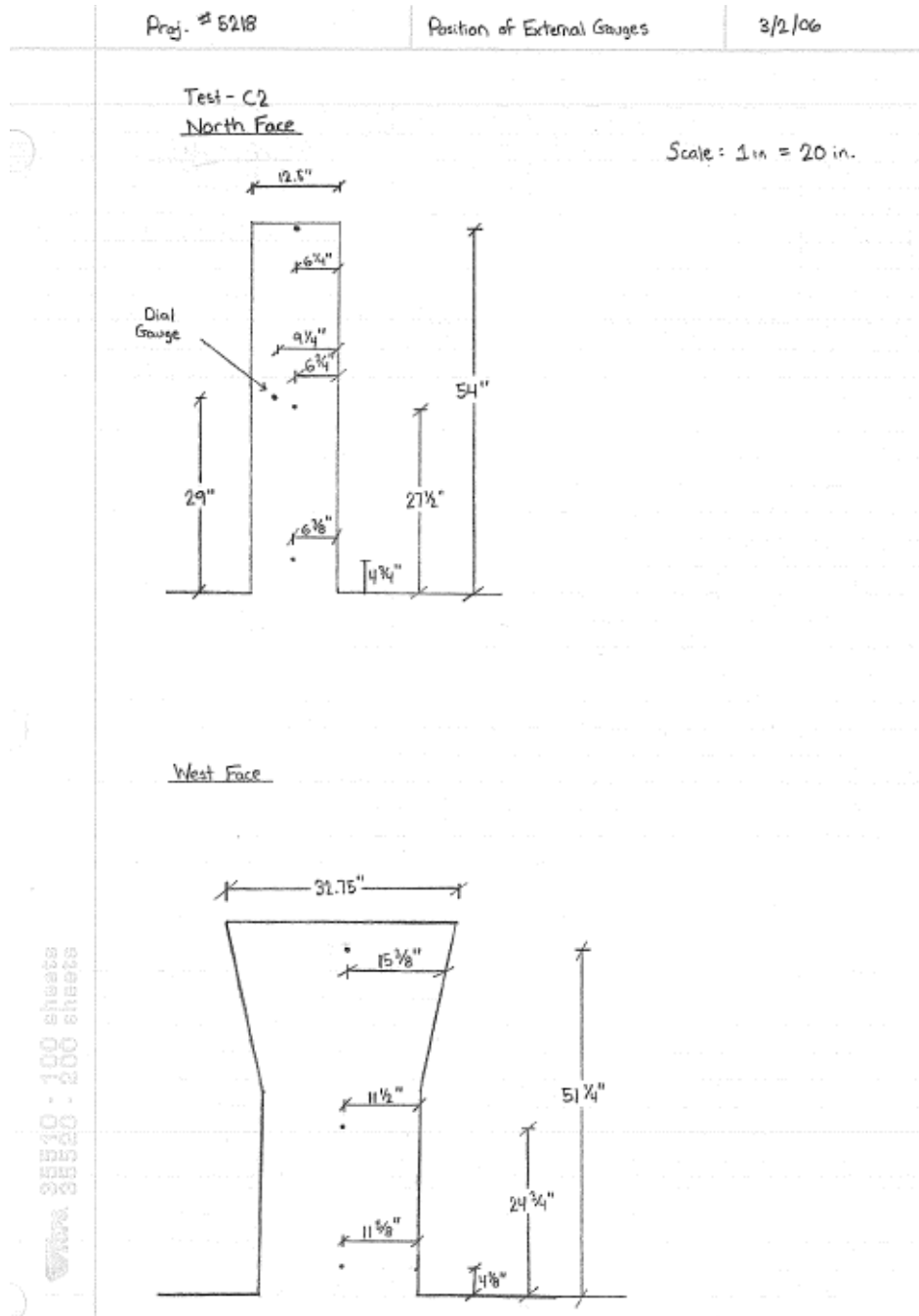


Figure B.36: C1 - Position of External Gauges

### B.6.3 Specimen C2



**Figure B.37: C2 – Position of External Gauges**

### B.6.4 Specimen C1-R

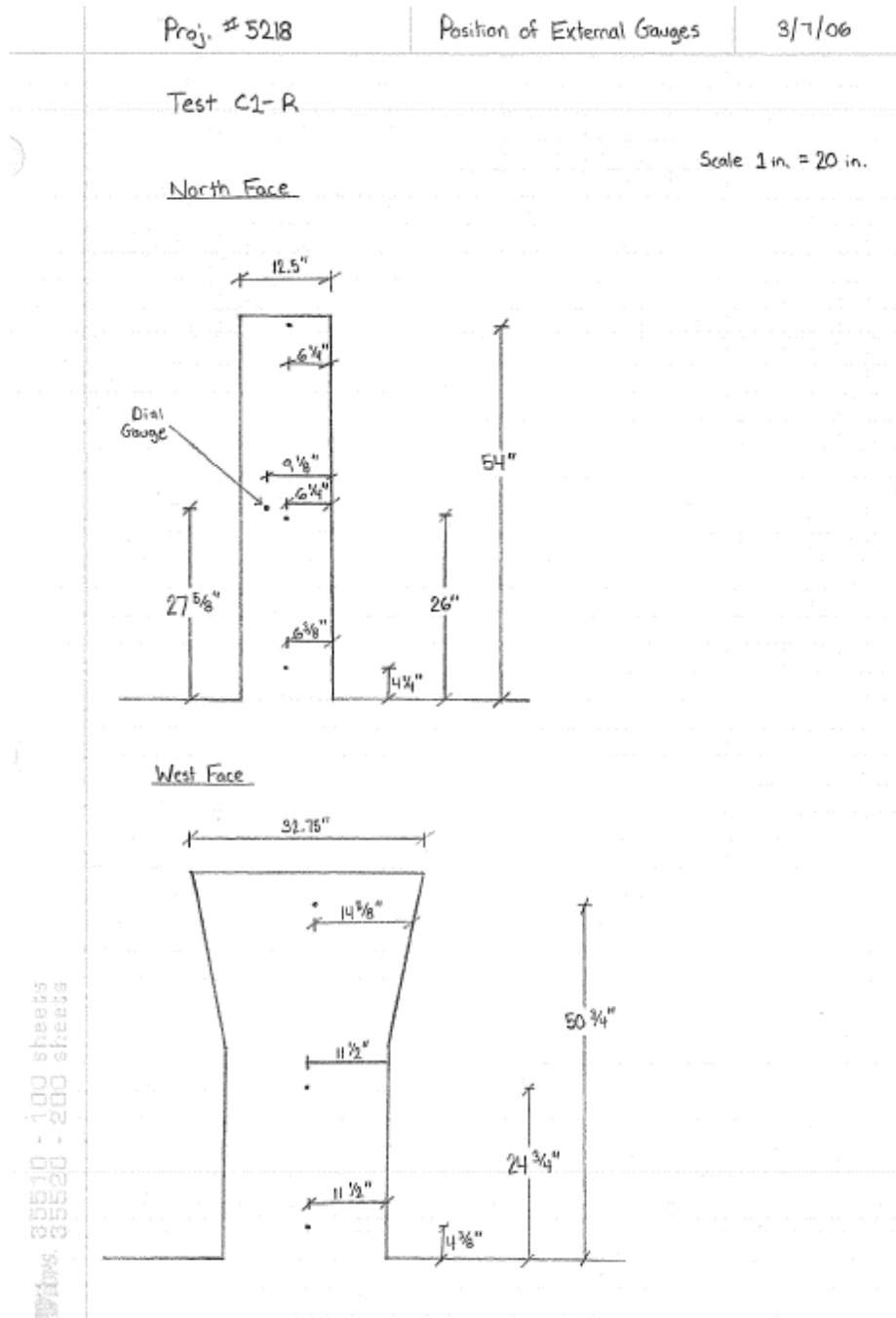


**Figure B.38: C1-R – Position of External Gauges**

## B.7 POSITION OF DIAL GAUGES ON PRECRACKED SPECIMENS

### B.7.1 Specimen C1

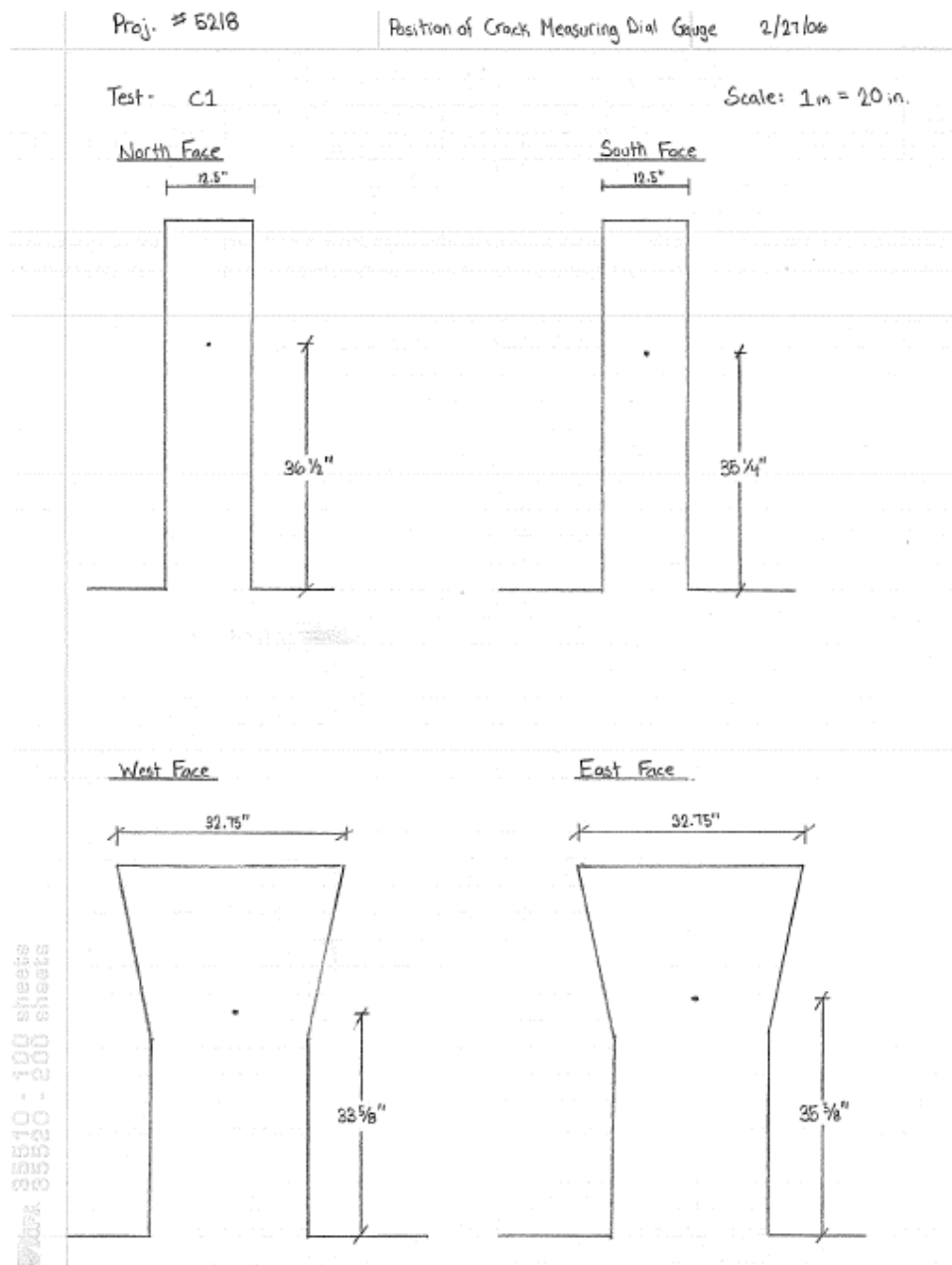
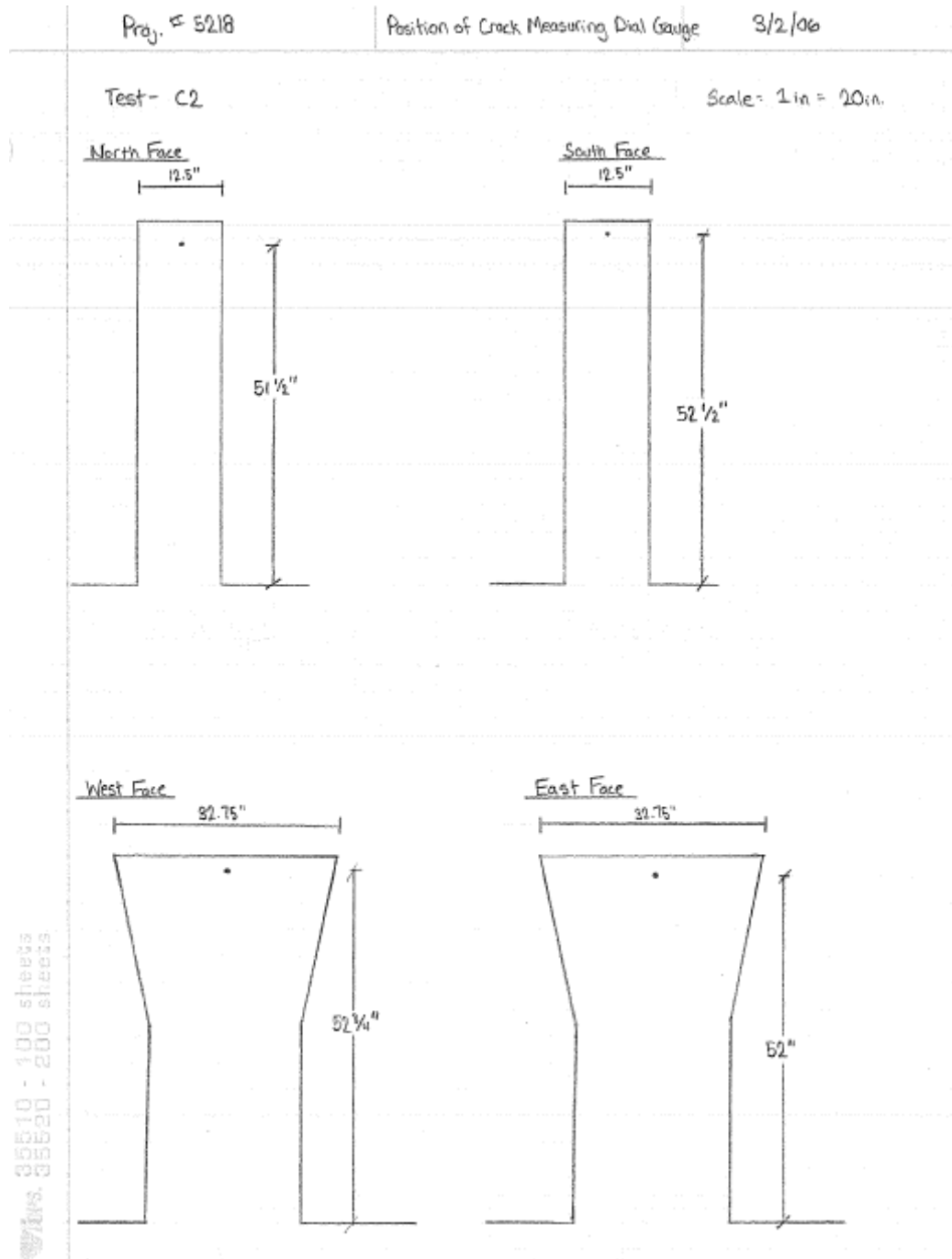


Figure B.39: C1 - Position of Dial Gauges

## B.7.2 Specimen C2



**Figure B.40: C2 – Position of Dial Gauges**

### B.7.3 Specimen C1-R

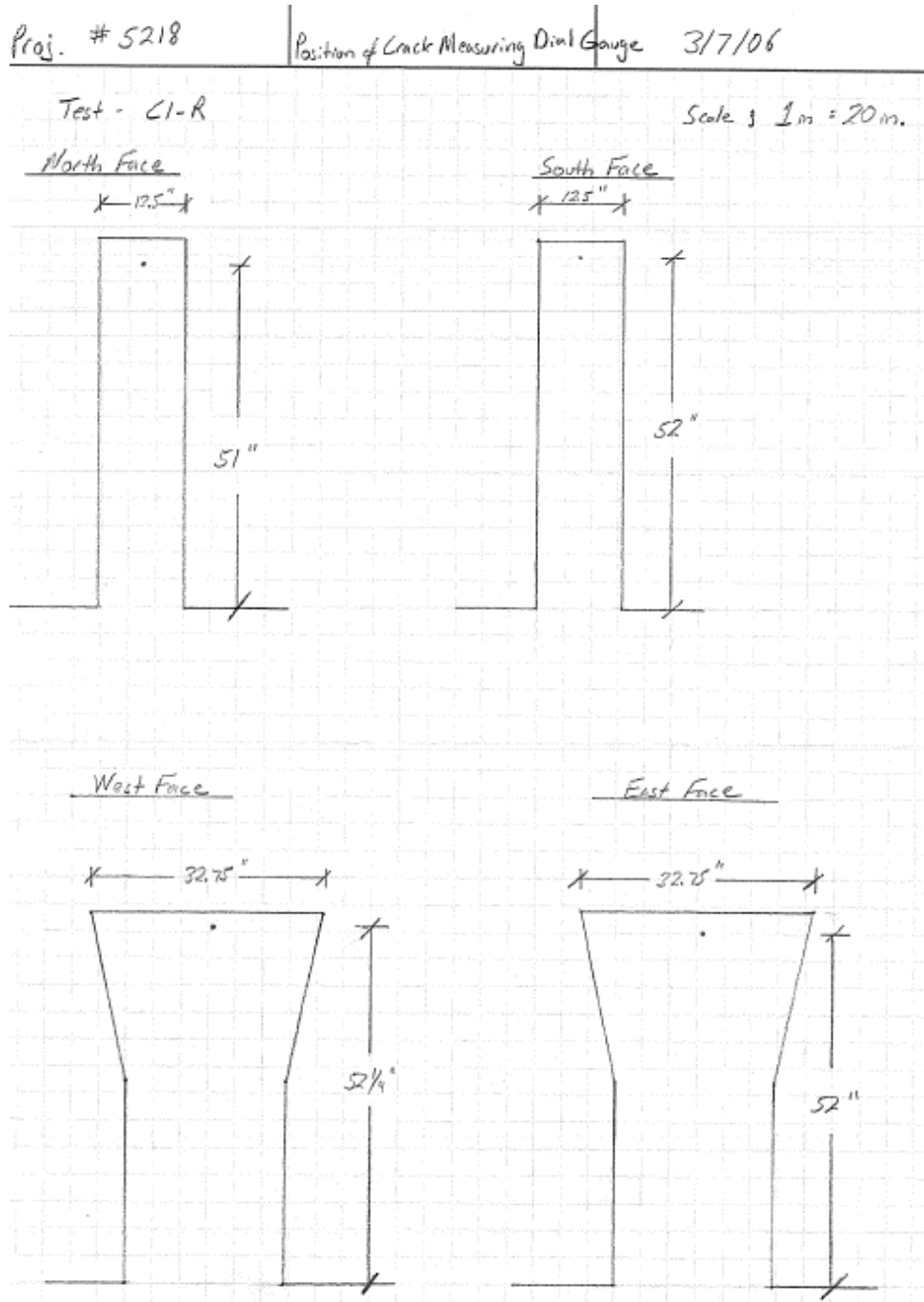


Figure B.41: C1-R – Position of Dial Gauges



# Appendix C

## Additional Experimental Results

### C.1 SPECIMEN S2

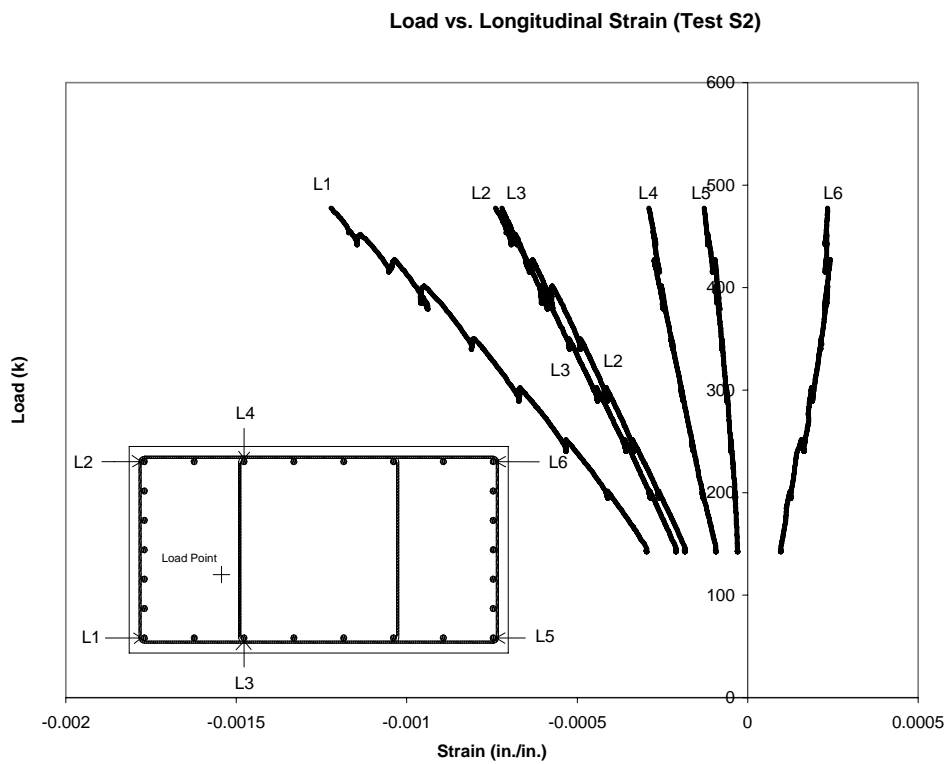


*Figure C.1: S2 – Load vs. Longitudinal Reinforcement Strain*

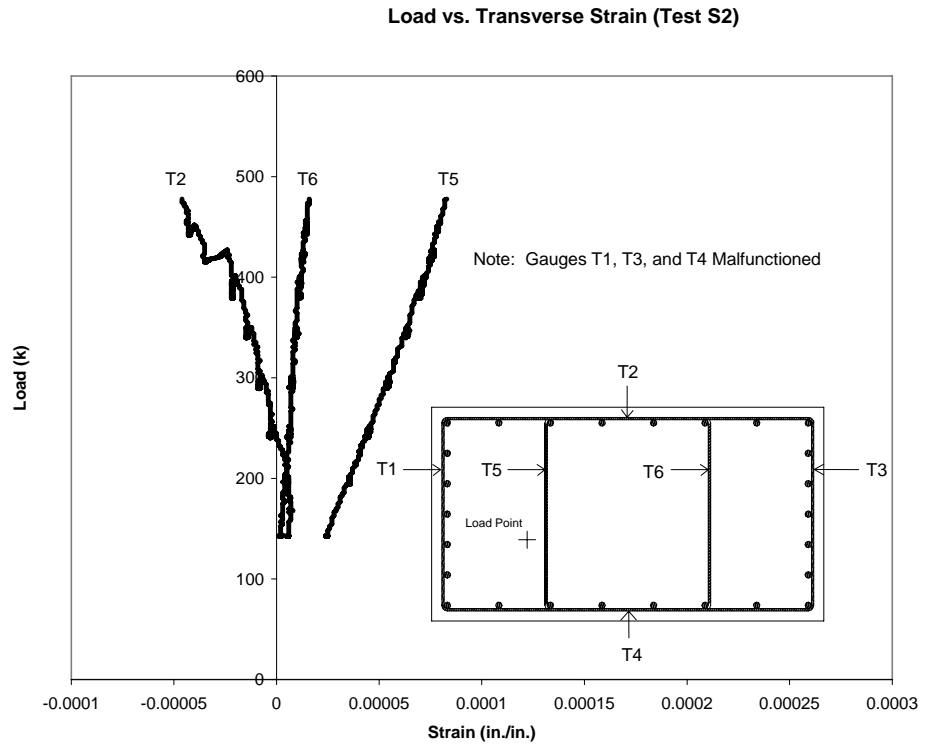


**Figure C.2: S2 – Load vs. Transverse Reinforcement Strain**

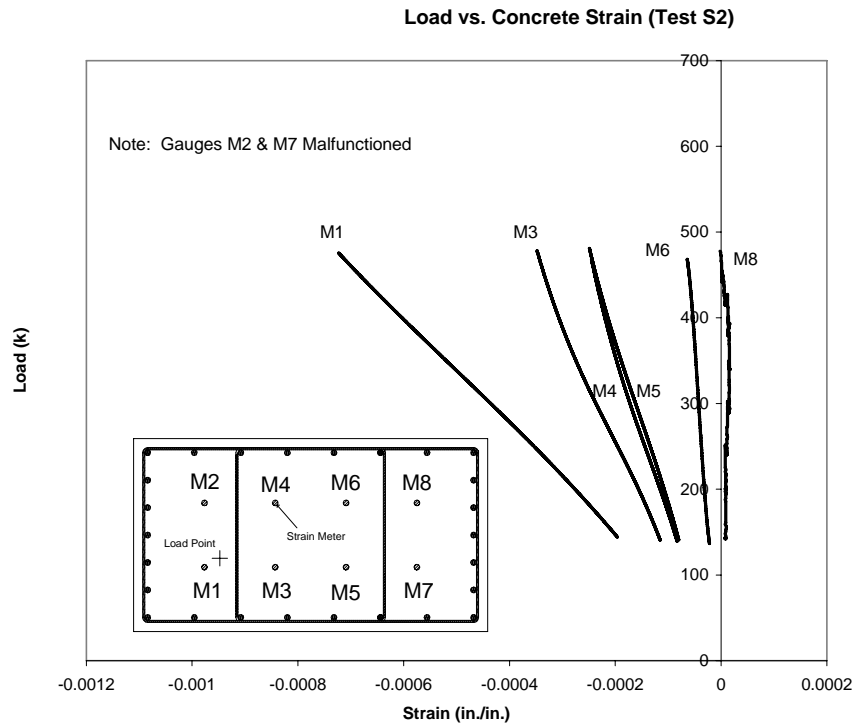


**Figure C.3: S2 – Load vs. Concrete Strain**

**C.2 SPECIMEN C1**

**C.2.1 Load vs. Deflection**

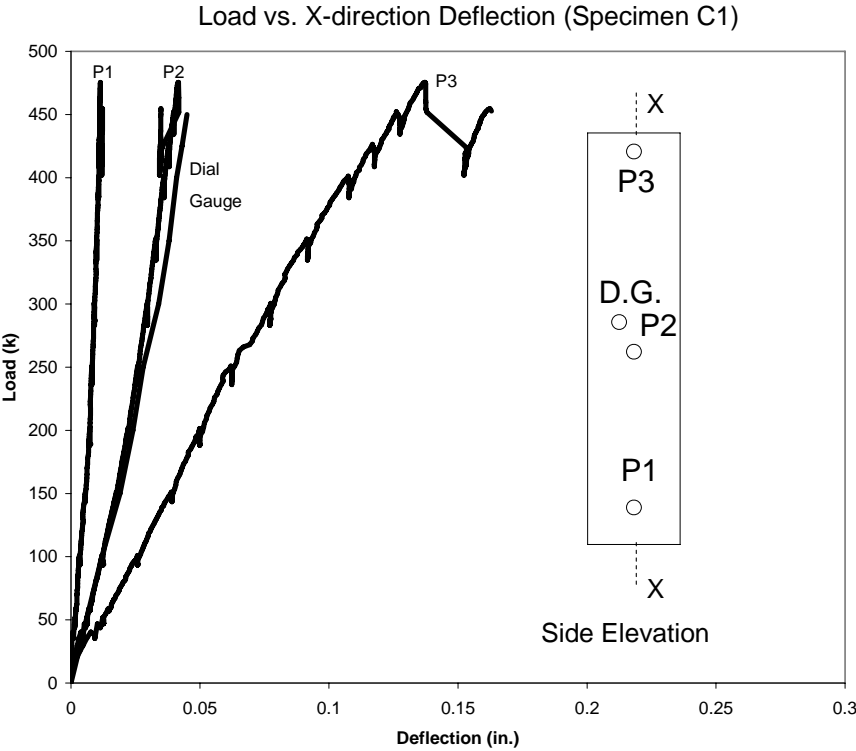


*Figure C.4: C1 – Load vs. X-direction Deflection*

Load vs. Y-direction Deflection (Specimen C1)

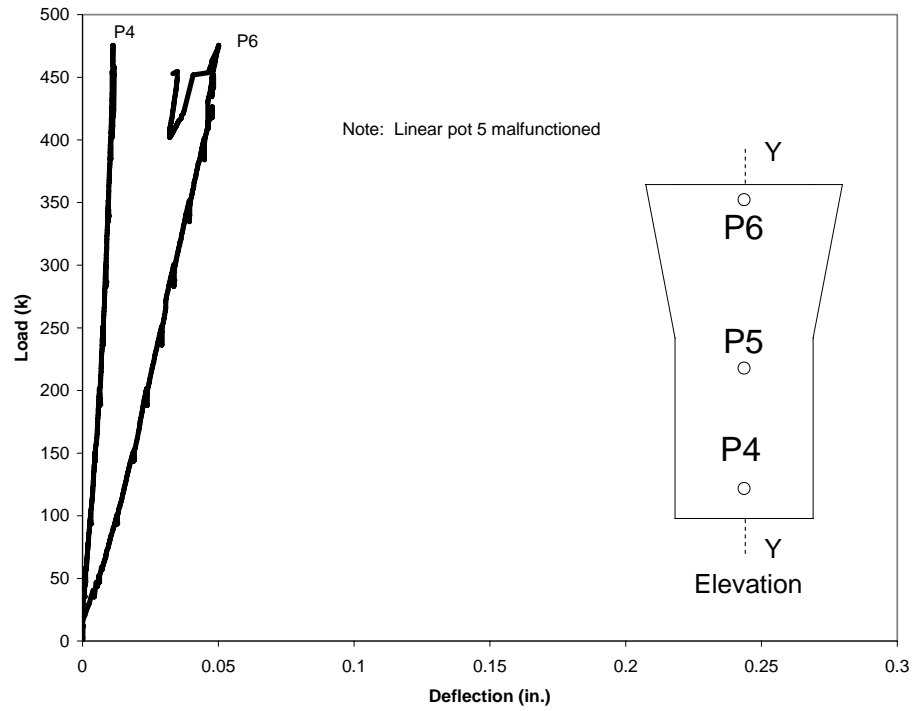


Figure C.5: C1 – Load vs. Y-direction Deflection

C.2.2 Load vs. Strain

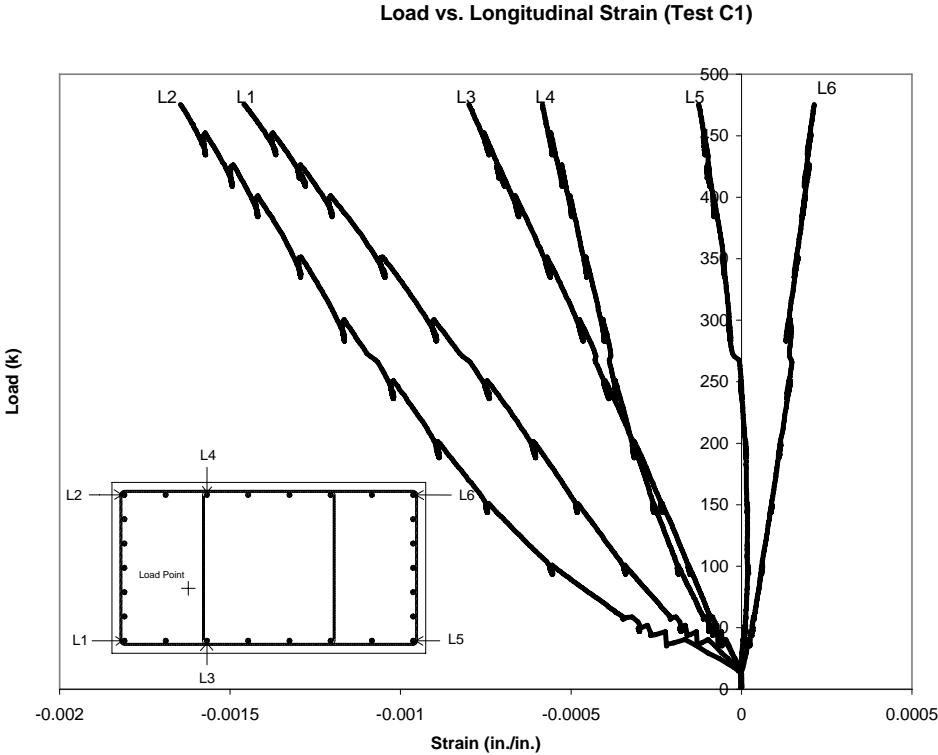


Figure C.6: C1 – Load vs. Longitudinal Reinforcement Strain

Load vs. Transverse Strain (Test C1)

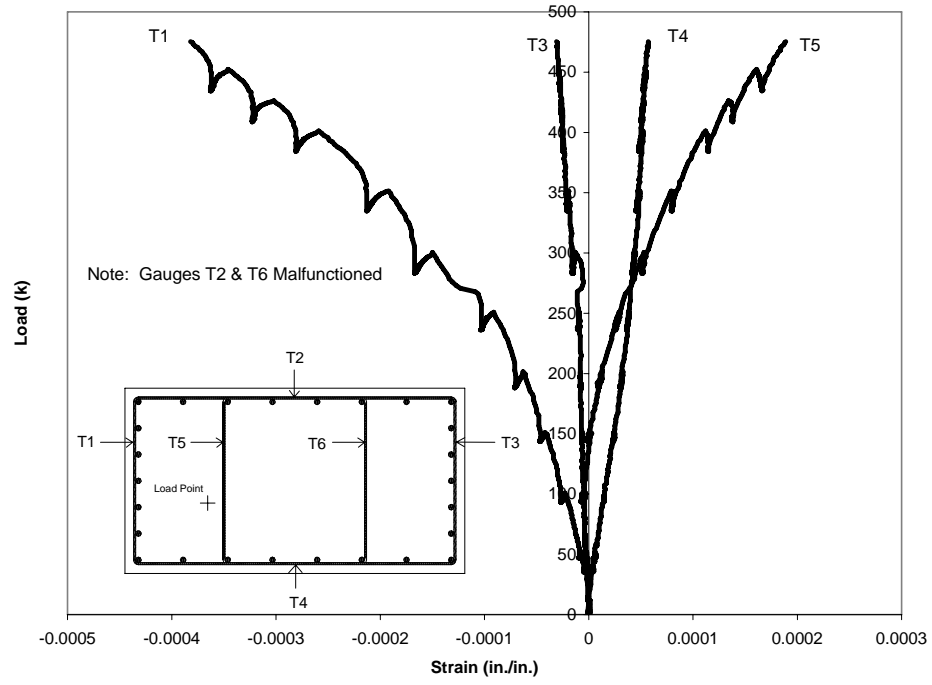


Figure C.7: C1 – Load vs. Transverse Reinforcement Strain

Load vs. Concrete Strain (Test C1)

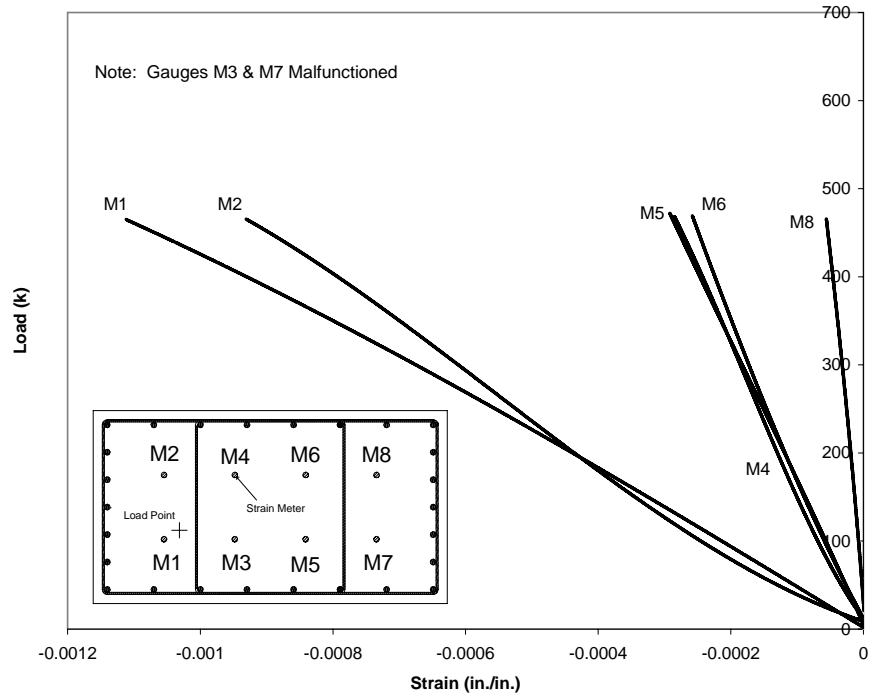
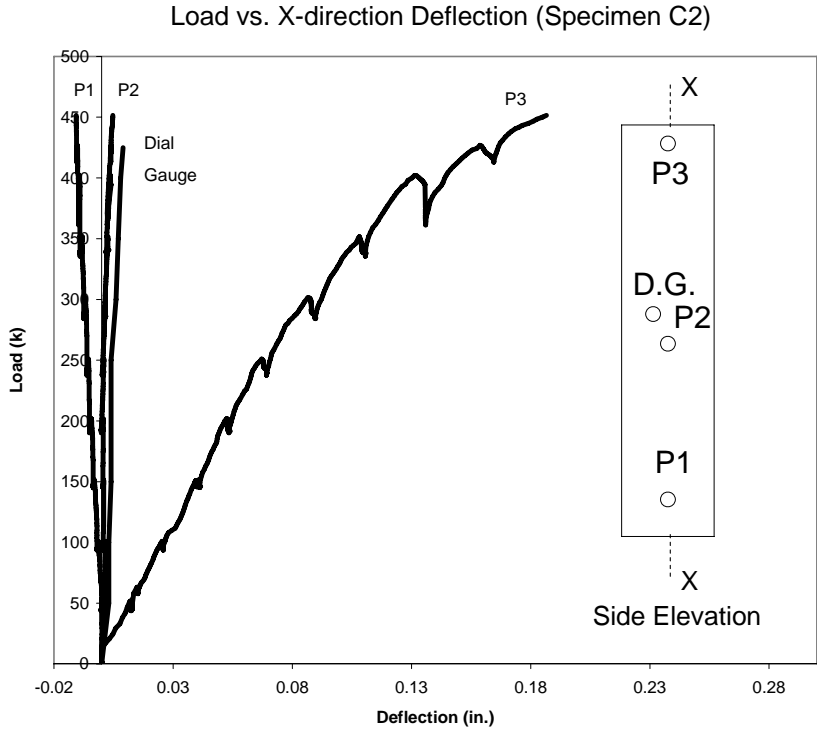


Figure C.8: C1 – Load vs. Concrete Strain



**C.3 SPECIMEN C2**

**C.3.1 Load vs. Deflection**



*Figure C.9: C2 – Load vs. X-direction Deflection*

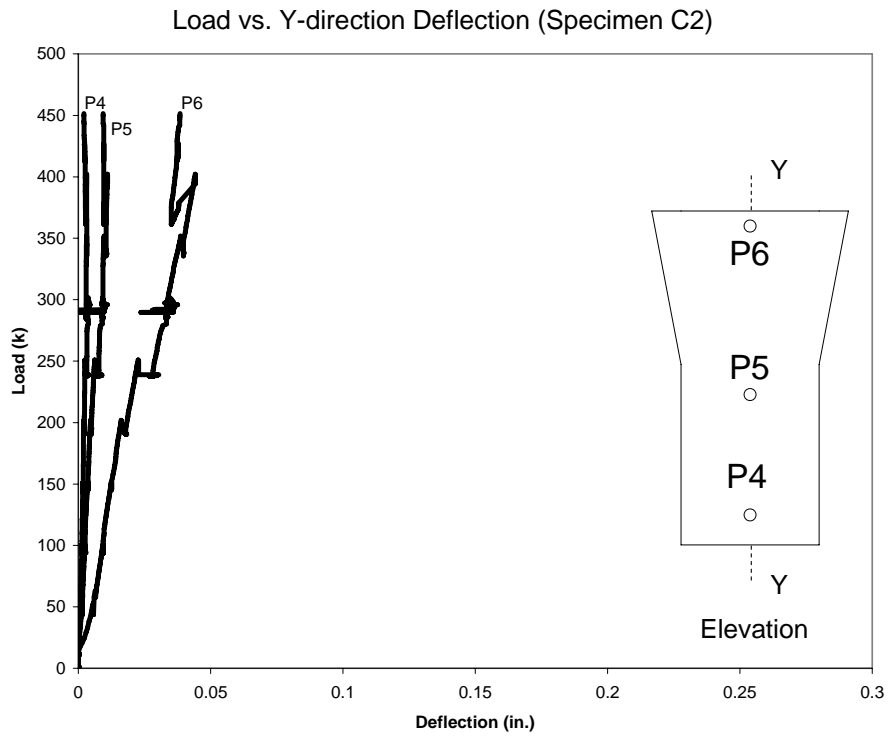


**Figure C.10: C2 – Load vs. Y-direction Deflection**

C.3.2 Load vs. Strain

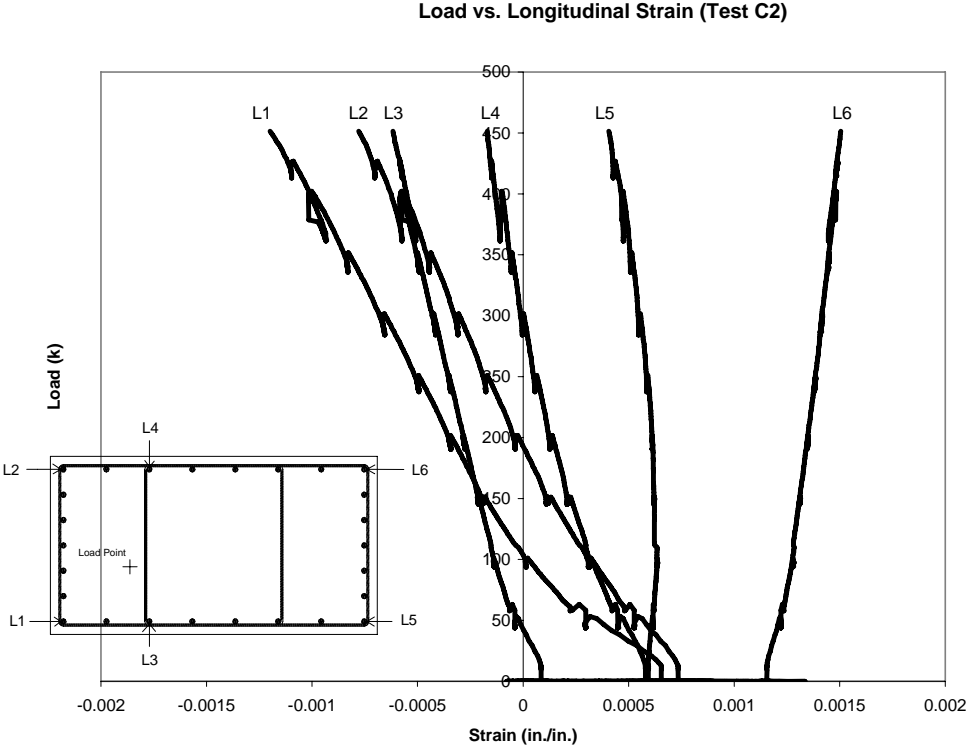


Figure C.11: C2 – Load vs. Longitudinal Reinforcement Strain

Load vs. Transverse Strain (Test C2)

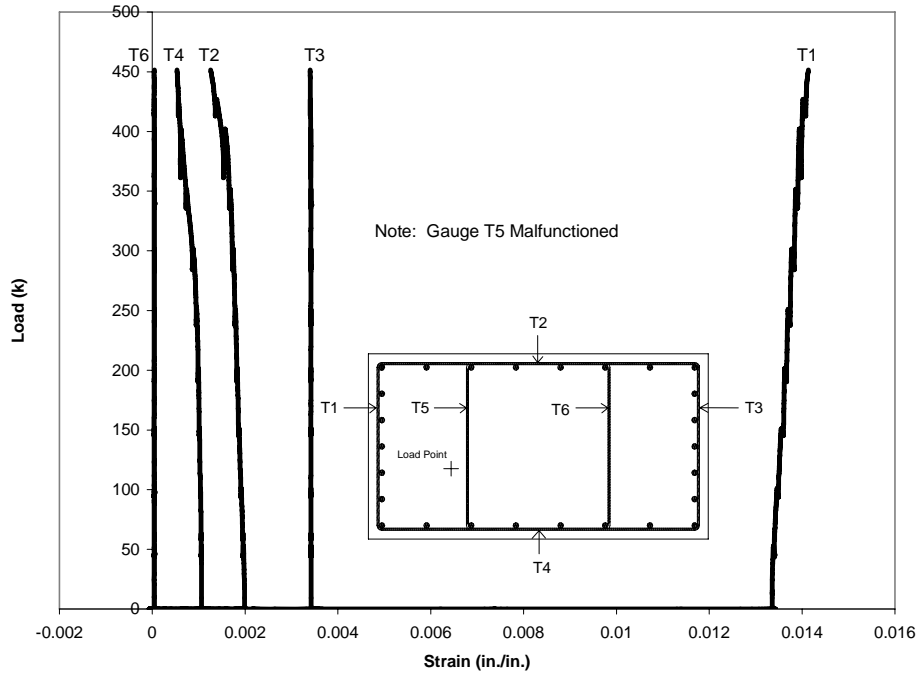


Figure C.12: C2 - Load vs. Transverse Reinforcement Strain

Load vs. Concrete Strain (Test C2)

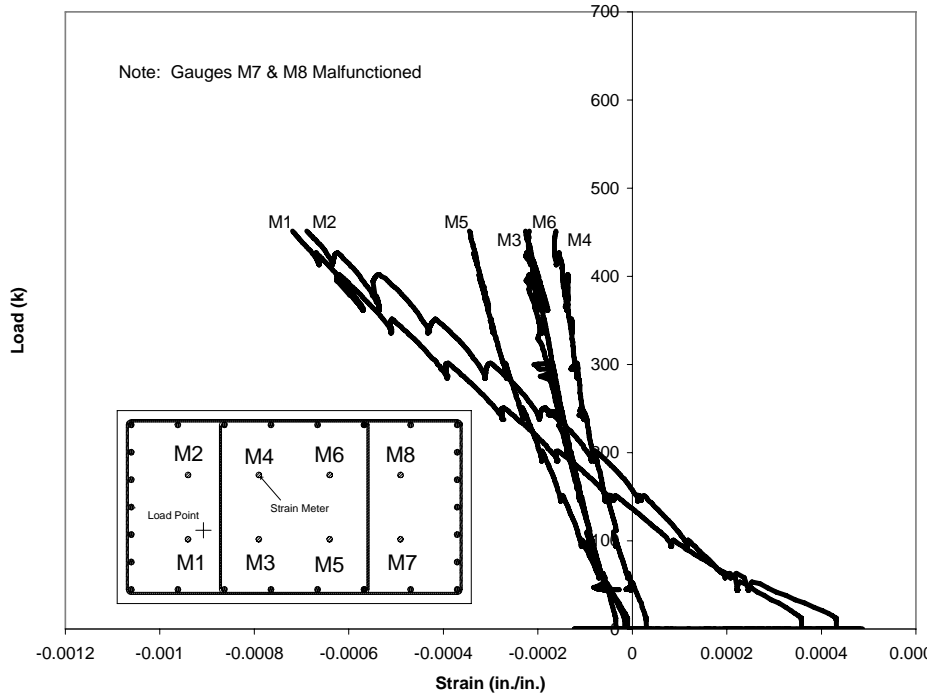
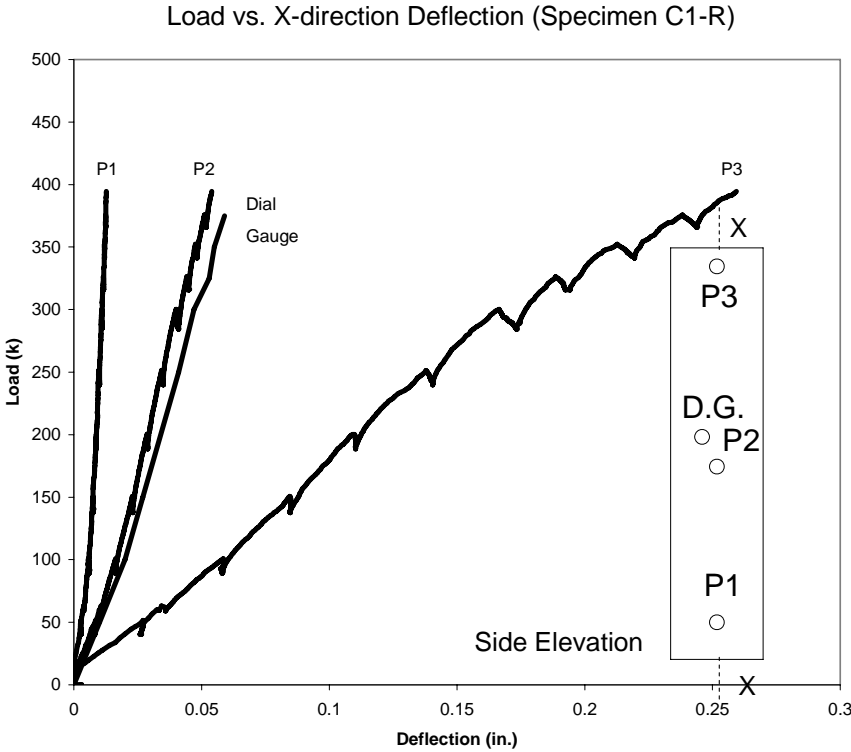


Figure C.13: C2 - Load vs. Concrete Strain

**C.4 SPECIMEN C1-R**

**C.4.1 Load vs. Deflection**



*Figure C.14: C1-R – Load vs. X-direction Deflection*

Load vs. Y-direction Deflection (Specimen C1-R)

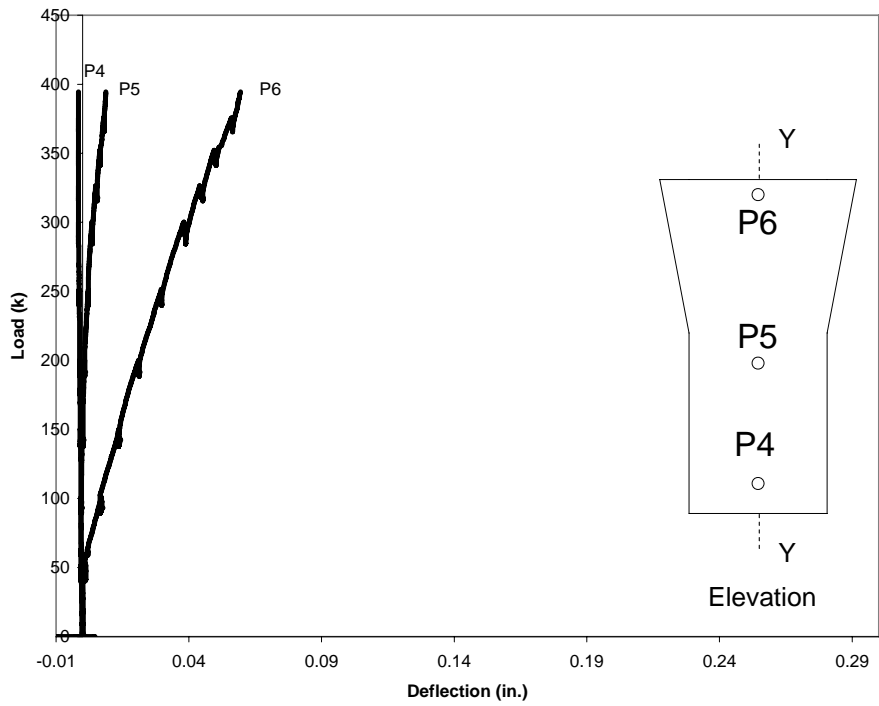
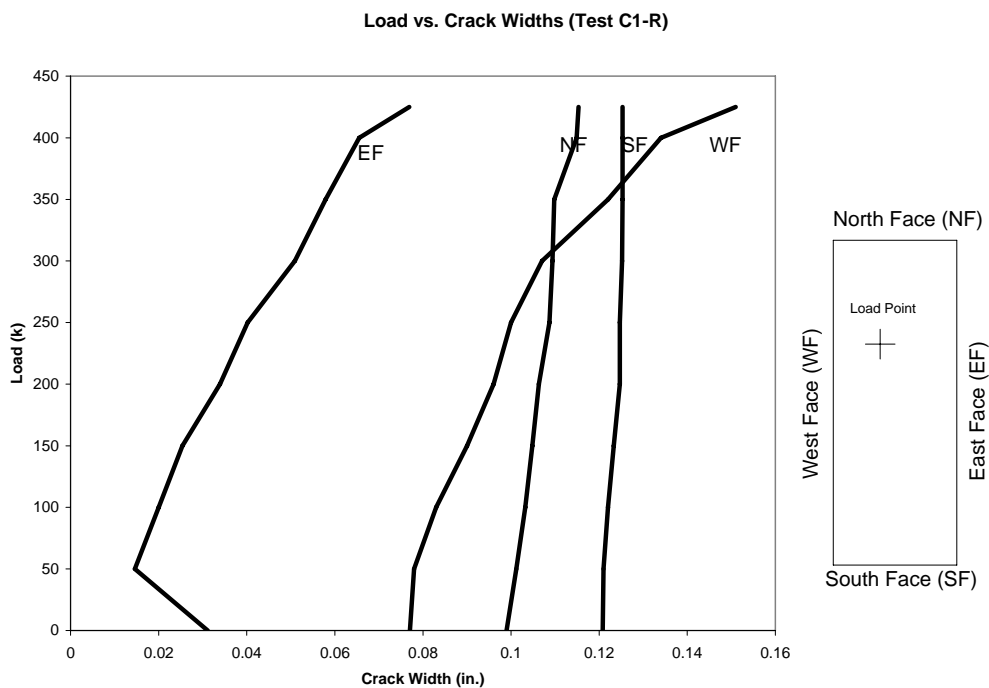


Figure C.15: C1-R – Load vs. Y-direction Deflection

## C.4.2 Crack Elongation



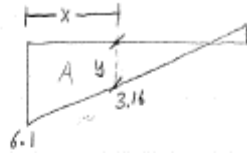
Note: The initial crack width on the east face was significantly lower than the target value. This was due to the position of the wedges. It was observed that the crack width along most of the east face was near the target value. The small crack width was only present near the top of the specimen where the dial gauge was located.

**Figure C.16: C1-R – Crack Elongation**





Find Area of the trapezoid that gives  $268^k$ :  $A_1$



$$m = \frac{7.3}{23}$$

$$y = 6.1 - \frac{7.3}{23}(x)$$

$$y(9.26) = 3.16$$

$$A = \frac{6.1 + y}{2} \cdot x$$

$$A = \frac{6.1 + (6.1 - \frac{7.3}{23}x)}{2} \cdot x$$

$$A = 6.1x - \frac{7.3}{46}x^2$$

$$F = 6.25A$$

$$268^k = 6.25 [6.1x - \frac{7.3}{46}x^2]$$

$$x = 9.26 \text{ in.}$$

Find Centroid of  $A$ :



$$A_1 = 9.26(3.16)$$

$$A_1 = 29.26 \text{ m}^2$$

$$A_2 = \frac{1}{2}(9.26)(3.94)$$

$$A_2 = 13.6 \text{ m}^2$$

$$Q_1 = \bar{y}_1 A_1$$

$$Q_1 = 4.62(29.26)$$

$$Q_1 = 135.5$$

$$Q_2 = \bar{y}_2 A_2$$

$$Q_2 = 3.09(13.6)$$

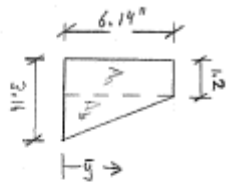
$$Q_2 = 42$$

$$\bar{y} = \frac{\sum Q}{\sum A} = \frac{177.5}{42.86} = 4.14 \text{ in.}$$

35510 - 100 sheets  
 35520 - 200 sheets

Figure D.2: S-T-M Model (2 of 6)

Find Area Centroid of  $A_2$ :



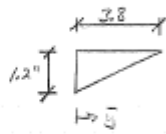
$$A_a = 7.37 \text{ in}^2 \quad A_b = 6.02 \text{ in}^2$$

$$\bar{y}_a = 3.07 \text{ in} \quad \bar{y}_b = 2.05 \text{ in}$$

$$Q_a = 22.6 \text{ in}^3 \quad Q_b = 12.0 \text{ in}^3$$

$$\bar{y} = \frac{22.6 + 12}{7.37 + 6.02} = 2.58 \text{ in}$$

Find Centroid of  $A_3$ :



$$\bar{y} = \frac{1}{3}(2.8)$$

$$\bar{y} = 1.27 \text{ in}$$

Location of Critical Points for STM:

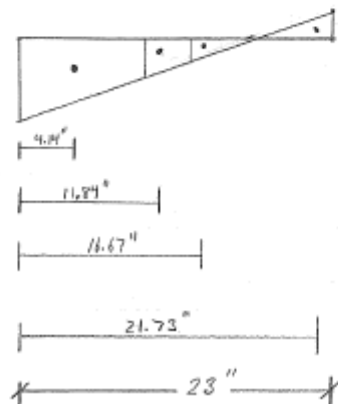
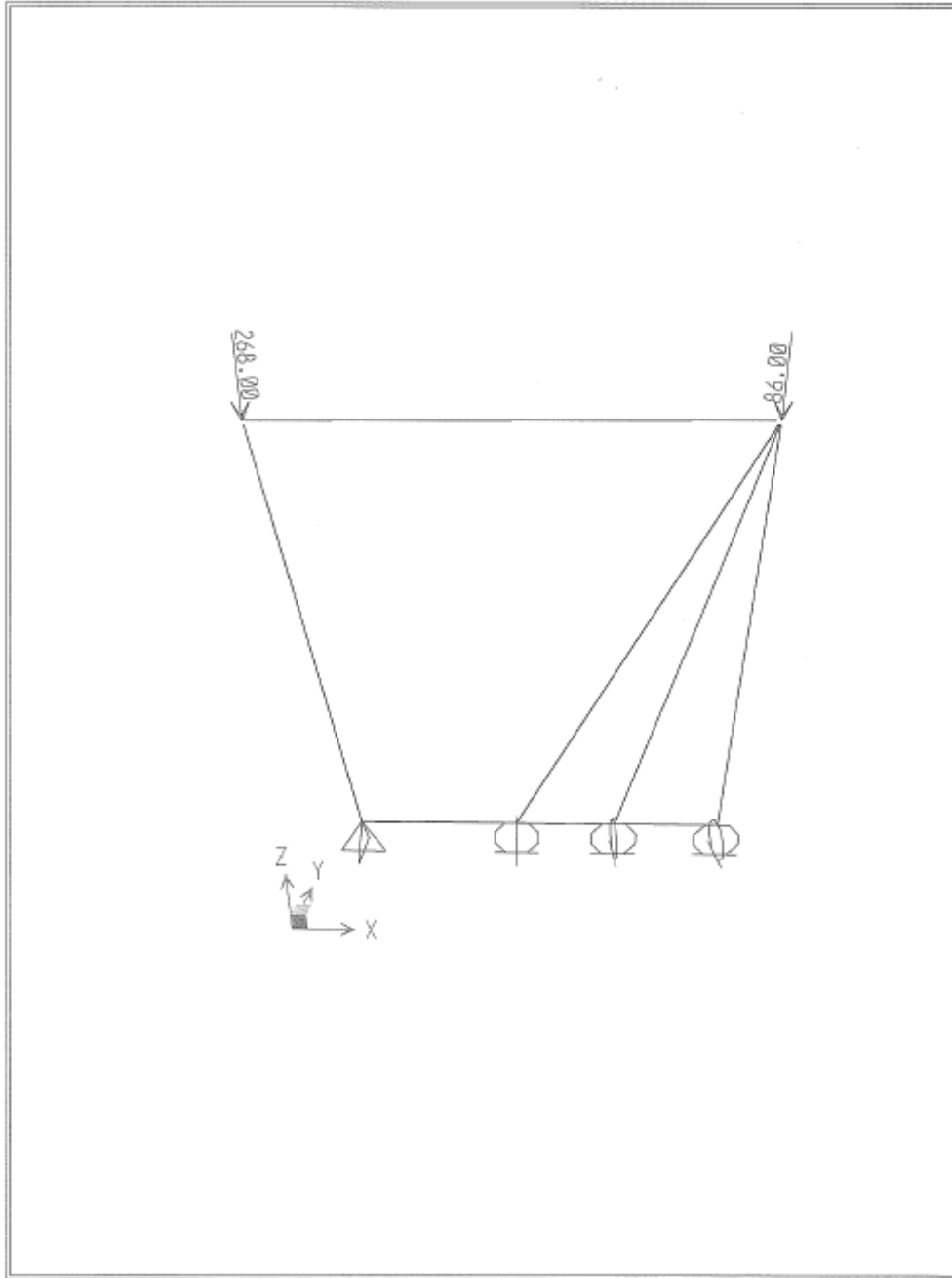
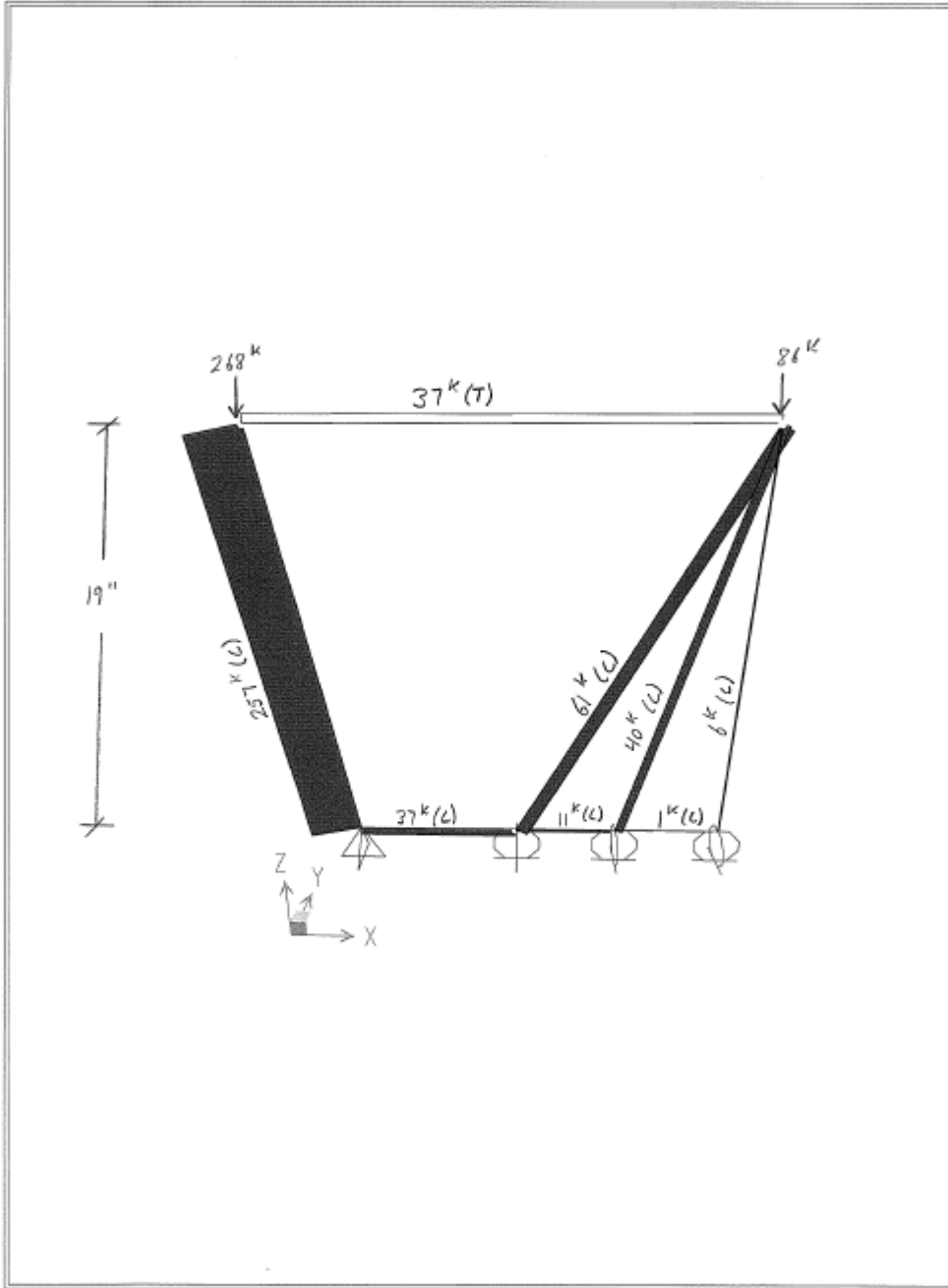


Figure D.3: S-T-M Model (3 of 6)



SAP2000 v8.2.7 - File:STM (axial and Moment) - Joint Loads (DEAD) (As Defined) - Kip, in, F Units

**Figure D.4: S-T-M Model (4 of 6)**



SAP2000 v8.2.7 - File:STM (axial and Moment) - Axial Force Diagram (DEAD) - Kip, in, F Units

**Figure D.5: S-T-M Model (5 of 6)**

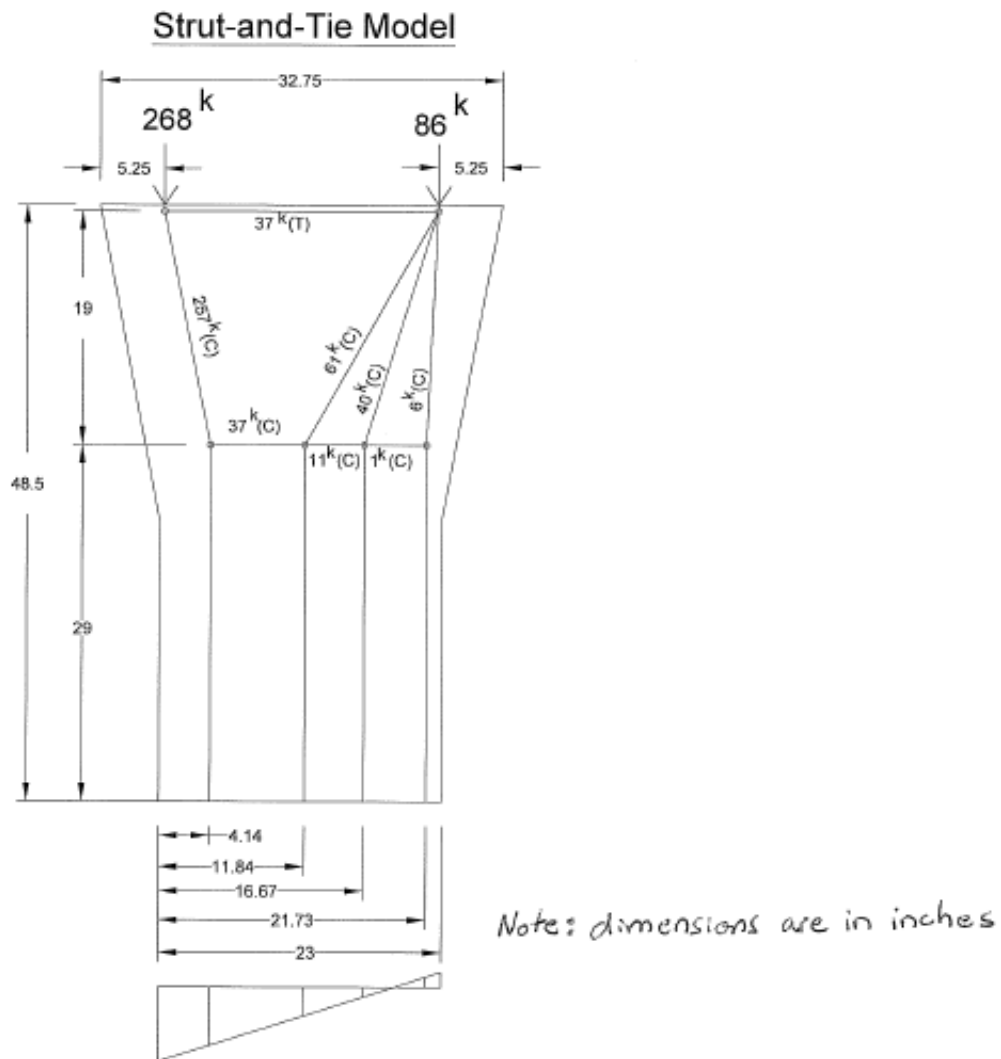


**Figure D.6: S-T-M Model (6 of 6)**

## D.1.2 Transverse Reinforcement in Model Pier

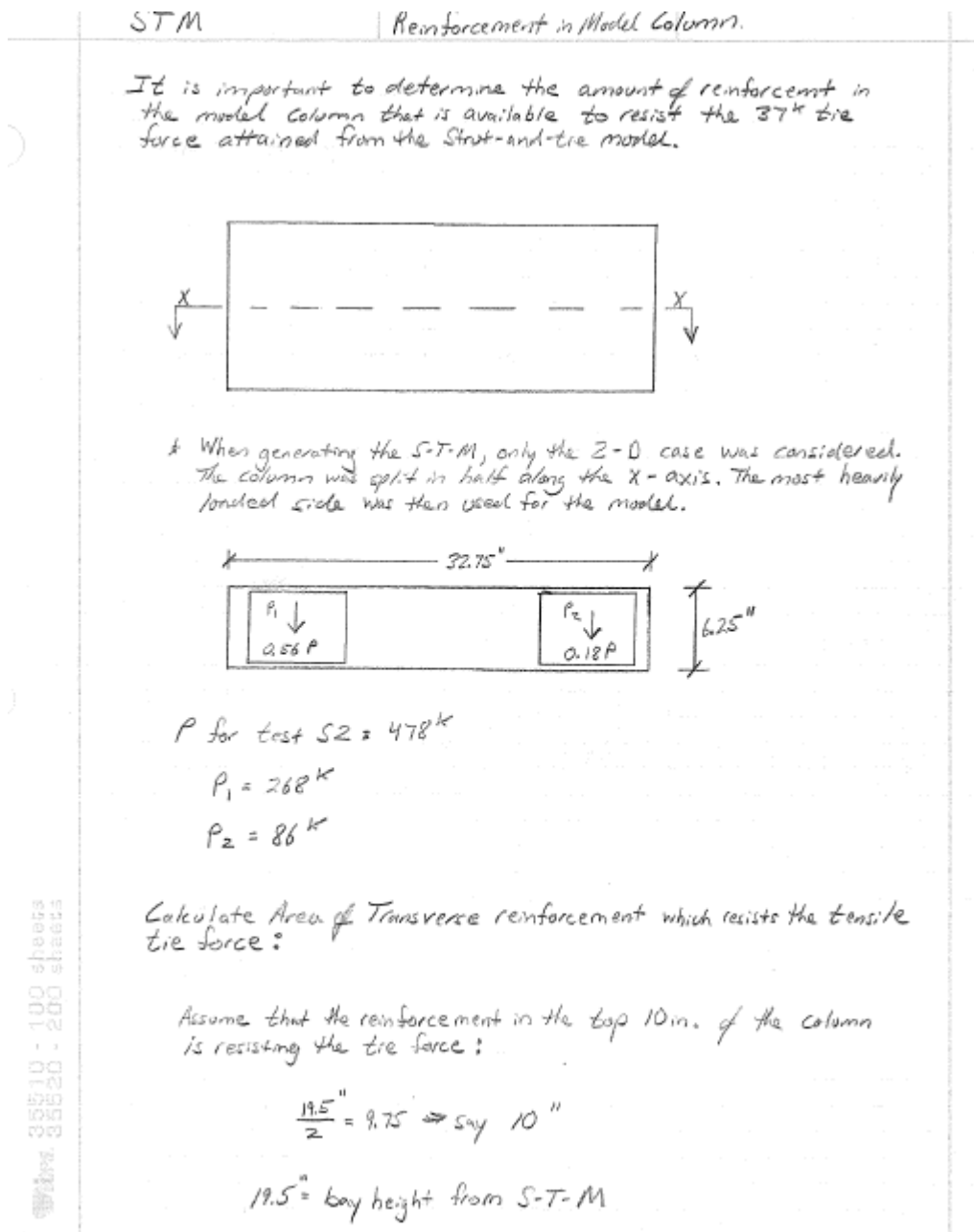


**Figure D.7: Model Pier Reinforcement (1 of 2)**

1 Layer #2 bars ; Quantity = 2

$$A = \frac{\pi(0.225)^2}{4} = 0.049 \text{ in}^2$$

$$A_1 = 2(0.049) = 0.098 \text{ in}^2$$

3 Layers D14 Wire ; Quantity = 2

$$A = \frac{\pi(0.125)^2}{4} = 0.014 \text{ in}^2$$

$$A_2 = 2(2)(0.014)$$

$$A_2 = 0.084 \text{ in}^2$$

$$A_{tot} = A_1 + A_2$$

$$A_{tot} = 0.098 + 0.084$$

$$A_{tot} = 0.182 \text{ in}^2$$

$$f_y = 60 \text{ ksi}$$

$$F = A_{tot} f_y = (0.182 \text{ in}^2)(60 \text{ ksi})$$

$$F = 10.92 \text{ k say } 11 \text{ k}$$

$11 \text{ k} < 37 \text{ k} \rightarrow$  Not the transverse reinf. avail. is not sufficient to resist the tensile tie force at Ultimate Load

Check Tie Force at Design Load

$$S_1 (UH) = 478 \text{ k}$$

$$\text{Design Load} = 191 \text{ k}$$

$$\% \text{ Load } \frac{191}{478} = 0.40$$

$$\text{Tie Force at Design Load} \approx 0.40 (37 \text{ k}) \approx 14.8 \text{ k}$$

$14.8 \text{ k} > 11 \text{ k}$  Note: At design Load the transverse reinf. is not adequate

**Figure D.8: Model Pier Reinforcement (2 of 2)**



The total amount of service dead and live load that can be resisted by the current reinforcement configuration was calculated using strut-and-tie modeling. The end results indicated that the current reinforcement pattern can resist 1.0 (D) + 0.5 (L+I).

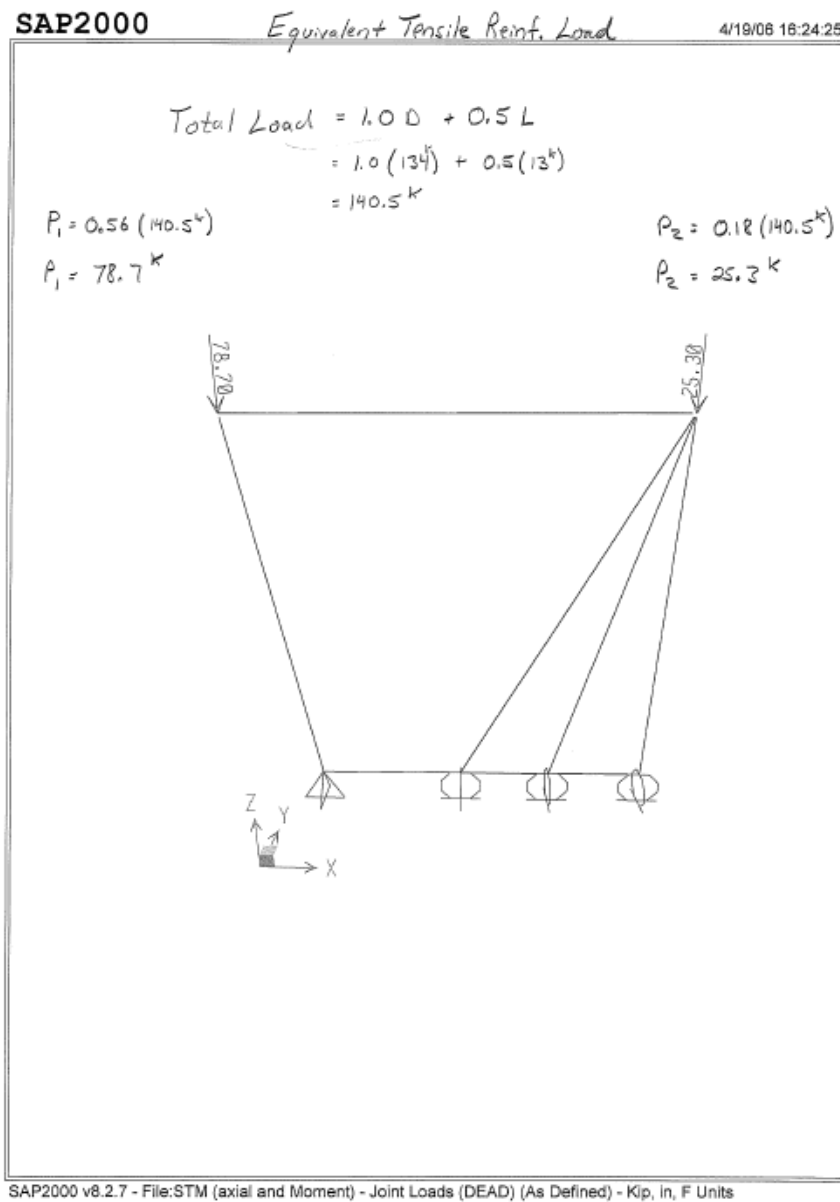
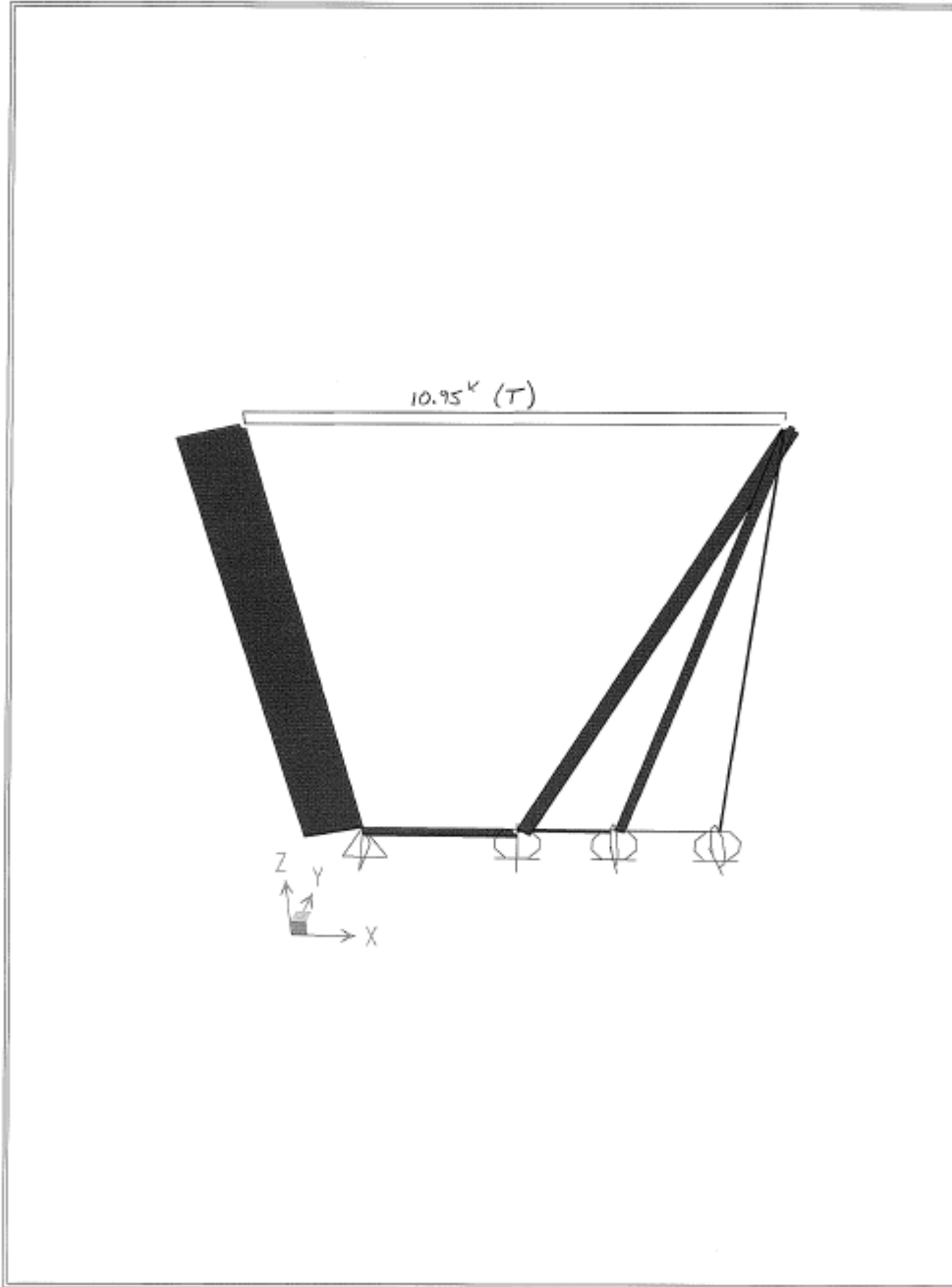


**Figure D.9: Equivalent Tensile Reinf. Loading (1 of 2)**



SAP2000 v8.2.7 - File:STM (axial and Moment) - Axial Force Diagram (DEAD) - Kip, in, F Units

**Figure D.10: Equivalent Tensile Reinf. Loading (2 of 2)**

### D.1.3 Modified Strut-and-Tie Model

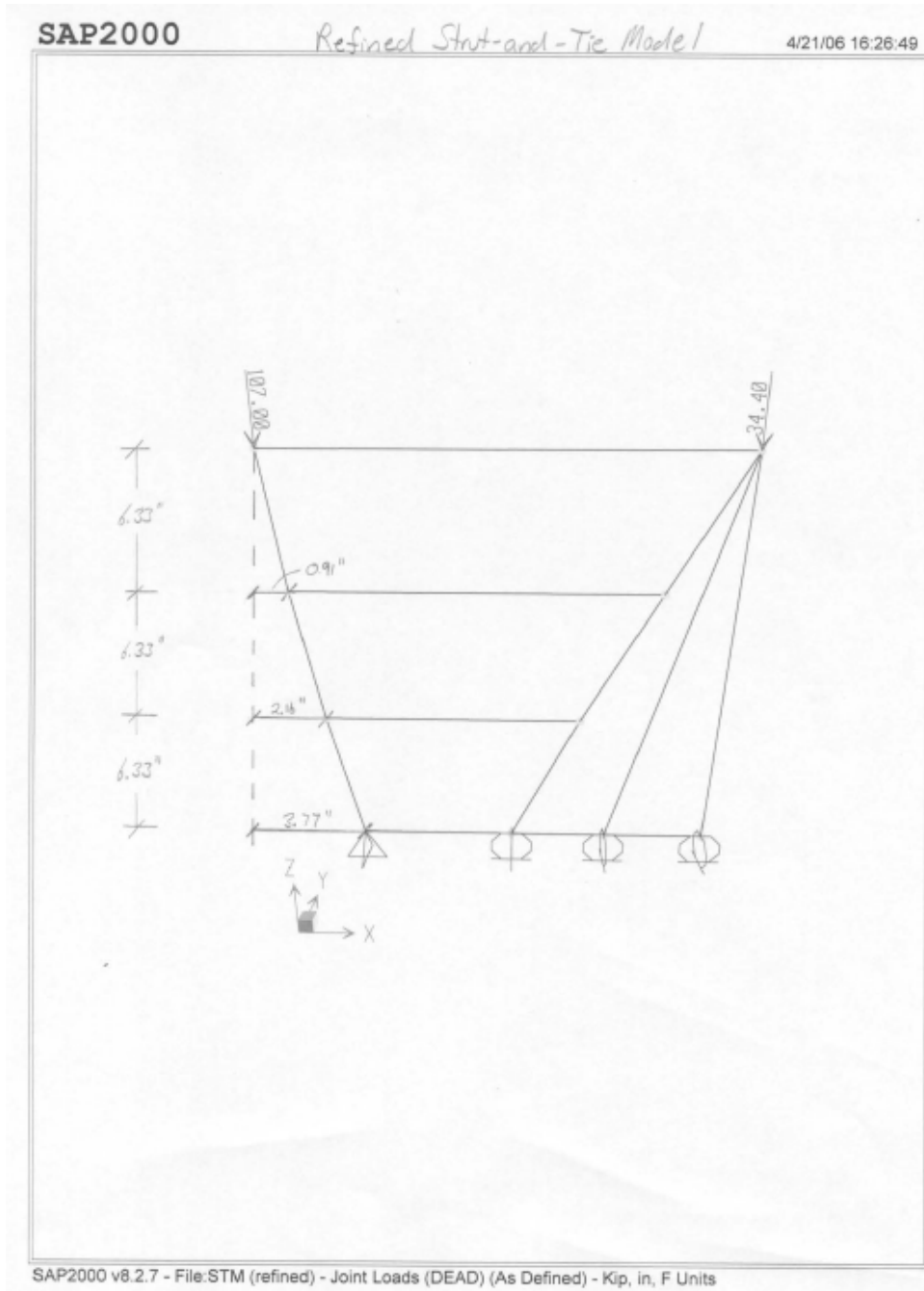
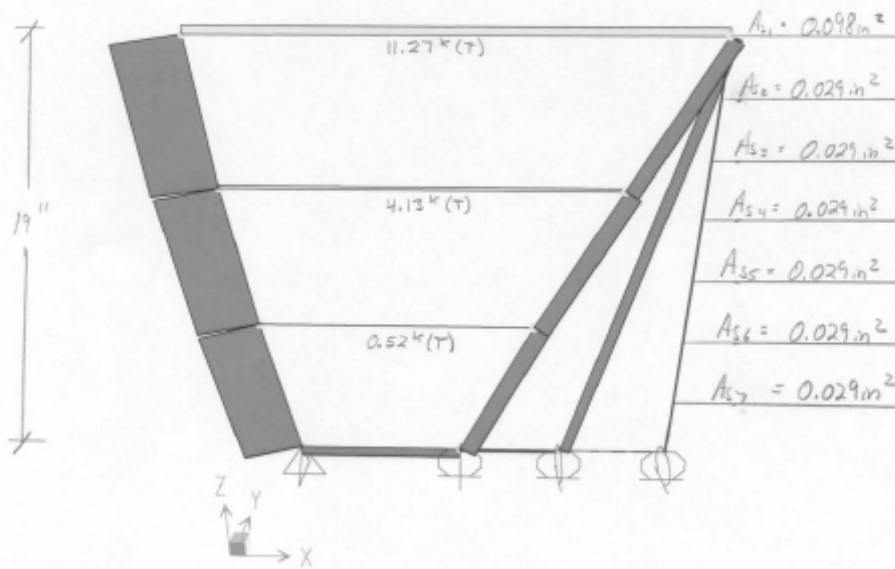


Figure D.11: Modified S-T-M (1 of 2)

$$\begin{aligned}
 \text{Transverse Reinf. Capacity at Top} &= (A_{s1} + A_{s2} + A_{s3}) f_y \\
 &= (0.098 + 0.029 + 0.029)(60) \\
 &= 9.36^k < 11.27^k \rightarrow \text{Moderately Insufficient}
 \end{aligned}$$



SAP2000 v8.2.7 - File:STM (refined) - Axial Force Diagram (DEAD) - Kip, in, F Units

Figure D.12: Modified S-T-M (2 of 2)



Highest Load =  $P_{max} = 108 \text{ k}$  or 56% of Total Load  
on pad

$$\sigma = \frac{P}{A}$$

$$A_{pad} = 5.75 \cdot 7.5 \text{ in}^2$$

$$\sigma_{max} = \frac{P_{max}}{A_{pad}}$$

$$A_{pad} = 43.125 \text{ in}^2$$

$$\sigma_{max} = \frac{108 \text{ k}}{43.125 \text{ in}^2}$$

$$\sigma_{max} = 2,504 \text{ ksi}$$

$$\sigma_{max} = 2,504 \text{ psi}, \text{ Factored Load}$$

#### AASHTO 1983 Recommendations

- The average unit pressure on elastomeric bearings shall not exceed 500 psi under a combination of dead plus live load, not including impact, for Service Load Levels.
- The Average unit pressure due to dead load only shall not exceed 500 psi.

(Section 14.2.5)

#### AASHTO LRFD 2005 Provisions

##### 14.7.6.3.2 Compressive Stress Method A

Note: Service Limit State

Steel-reinf. Elastomeric bearings

$$\sigma_s \leq 1.0 \text{ ksi} \text{ and } \sigma_s \leq 1.0 G S \quad (14.7.6.3.2-4)$$

where  $G$  = shear modulus of elastomer (ksi)

$S$  = shape factor of the thickest layer of the bearing

For 60 durometer pad use  $G = 0.130 \text{ ksi}$

For 0.2 in. thickness use  $S = 6$

$$\sigma_s \leq 1.0(0.13)(6)$$

$$\sigma_s \leq 0.78 \text{ ksi}$$

**Figure D.14: Bearing Calculations (2 of 9)**

3

14.7.5.3.2 Compressive Stress Method B

Note: Service Limit State

- For bearings subject to shear deformation:
 
$$\sigma_s \leq 1.66 GS \leq 1.6 \text{ ksi} \quad (14.7.5.3.2-1)$$
- For bearings fixed against shear deformation:
 
$$\sigma_s \leq 2.00 GS \leq 1.75 \text{ ksi} \quad (14.7.5.3.2-3)$$

$\sigma_s$  = service average compressive stress due to the total load (ksi)  
 $G$  = Shear modulus of elastomer (ksi)  
 $S$  = Shear factor of the thickest layer of the bearing

$$\sigma_s \leq 1.11 GS \leq 1.61(0.13)(6.1)$$

$$\sigma_s \leq 1.29 \text{ ksi}$$

Method A :  $\sigma_{max} = 0.78 \text{ ksi}$  } At Service Load  
 Method B :  $\sigma_{max} = 1.29 \text{ ksi}$  }

Case III, 2b, Factored Load:  $\sigma_{max} = 2.504 \text{ ksi}$

Note: "Service" conditions are evaluated in subsequent calculations.

35510 - 100 sheets  
35520 - 200 sheets

**Figure D.15: Bearing Calculations (3 of 9)**

### Bearing Stress on Concrete

#### 5.7.5 Bearing

- In the absence of confinement reinforcement in the supporting concrete

$$P_r = \phi P_n \quad (5.7.5-1)$$

$$P_n = 0.85 f'_c A_1 m \quad (5.7.5-2)$$

where:  $P_n$  = nominal bearing resistance (kip)

$A_1$  = area under bearing device (in<sup>2</sup>)

$m$  = modification factor

$A_2$  = actual area (in<sup>2</sup>)

$\phi = 0.70$  for bearing on concrete

$$m = \sqrt{\frac{A_2}{A_1}} \leq 2.0$$

Scale: 1 block = 1 in.

#### Profile

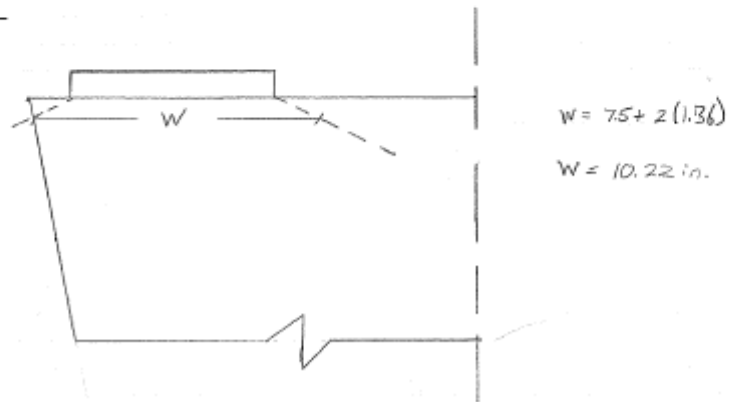
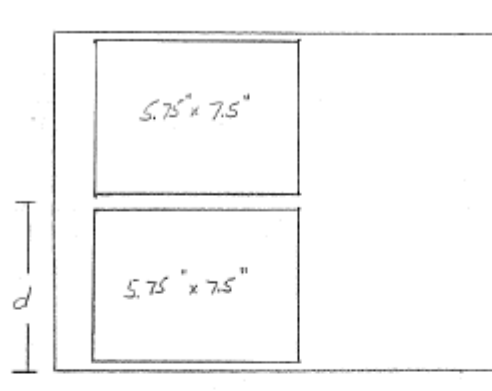


**Figure D.16: Bearing Calculations (4 of 9)**



Plan

Scale: 1 block = 1 m.



$$d = 5.75 + 0.25 + 0.25$$

$$d = 6.25''$$

$$A_2 = W \cdot d$$

$$A_2 = 10.22'' \cdot 6.25''$$

$$A_2 = 63.875 \text{ in}^2$$

$$A_1 = 5.75'' \cdot 7.5''$$

$$A_1 = 43.125 \text{ in}^2$$

$$m = \sqrt{\frac{A_2}{A_1}} \leq 2.0$$

$$m = \sqrt{\frac{63.875 \text{ in}^2}{43.125 \text{ in}^2}}$$

$$m = 1.22$$

$$P_n = 0.85 f_c' A_c m$$

$$P_n = 0.85 (5.8) (43.125) (1.22)$$

$$P_n = 259 \text{ k}$$

$$P_r = \phi P_n \quad P_r = 0.7 (259 \text{ k}) = 181 \text{ k} > 108 \text{ k} \quad \text{OK}$$

Figure D.17: Bearing Calculations (5 of 9)

Bearing Stresses on concrete at Failure

$P_u$  = Maximum Load from experimental testing

$$P_u \approx 475 \text{ k}$$

$P_{u1}$  = portion of max. Load on most critical pad

$$P_{u1} = 475 \text{ k} (0.56)$$

$$P_{u1} = 266 \text{ k}$$

$$\bar{\sigma}_u = \frac{266 \text{ k}}{43.125 \text{ in}^2} = 6.168 \text{ ksi} = 6,168 \text{ psi}$$

$$\sigma_n = 0.85 f'_c m$$

$$\sigma_n = 0.85 (5.8)(1.22)$$

$$\sigma_n = 6.015 \text{ ksi} = 6,015 \text{ psi}$$

Note: The results indicate very close correlation between the calculated bearing capacity of a sound column and the bearing stress on the column.

**Figure D.18: Bearing Calculations (6 of 9)**

7

"Service" Load Case III, 2 Lane  
(w/o centrifugal force)

Determination of "Service" Load from Original Design:

$$P = 1800^k + 2(88^k)$$

$$P = 1976^k$$

$$P_{mod.} = \frac{1976^k}{3.667^2}$$

$$P_{mod.} = 147^k$$

$$M_T = 1.0(1630+570) + 0.39(1780) + 1.0(480) + 0.39(1175)$$

$$M_T = 3833 \text{ k}\cdot\text{ft}$$

$$M_{y_{mod.}} = \frac{3833}{(3.667)^2} \cdot 12 = 933 \text{ k}\cdot\text{in.}$$

$$e_y = \frac{933}{147} = 6.3 \text{ in.}$$

$$M_L = 0.39(510+260) + 215 + 475 = 990 \text{ k}\cdot\text{ft}$$

$$M_{x_{mod.}} = \frac{990 \text{ k}\cdot\text{ft}}{(3.667)^2} \cdot 12 = 241 \text{ k}\cdot\text{in.}$$

$$e_y = \frac{241 \text{ k}\cdot\text{in.}}{147} = 1.6 \text{ in.}$$

"Service" Load

$$P = 147^k$$

$$e_x = 6.3 \text{ in.}$$

$$e_y = 1.6 \text{ in.}$$

35510 - 100 sheets  
35520 - 200 sheets

Figure D.19: Bearing Calculations (7 of 9)

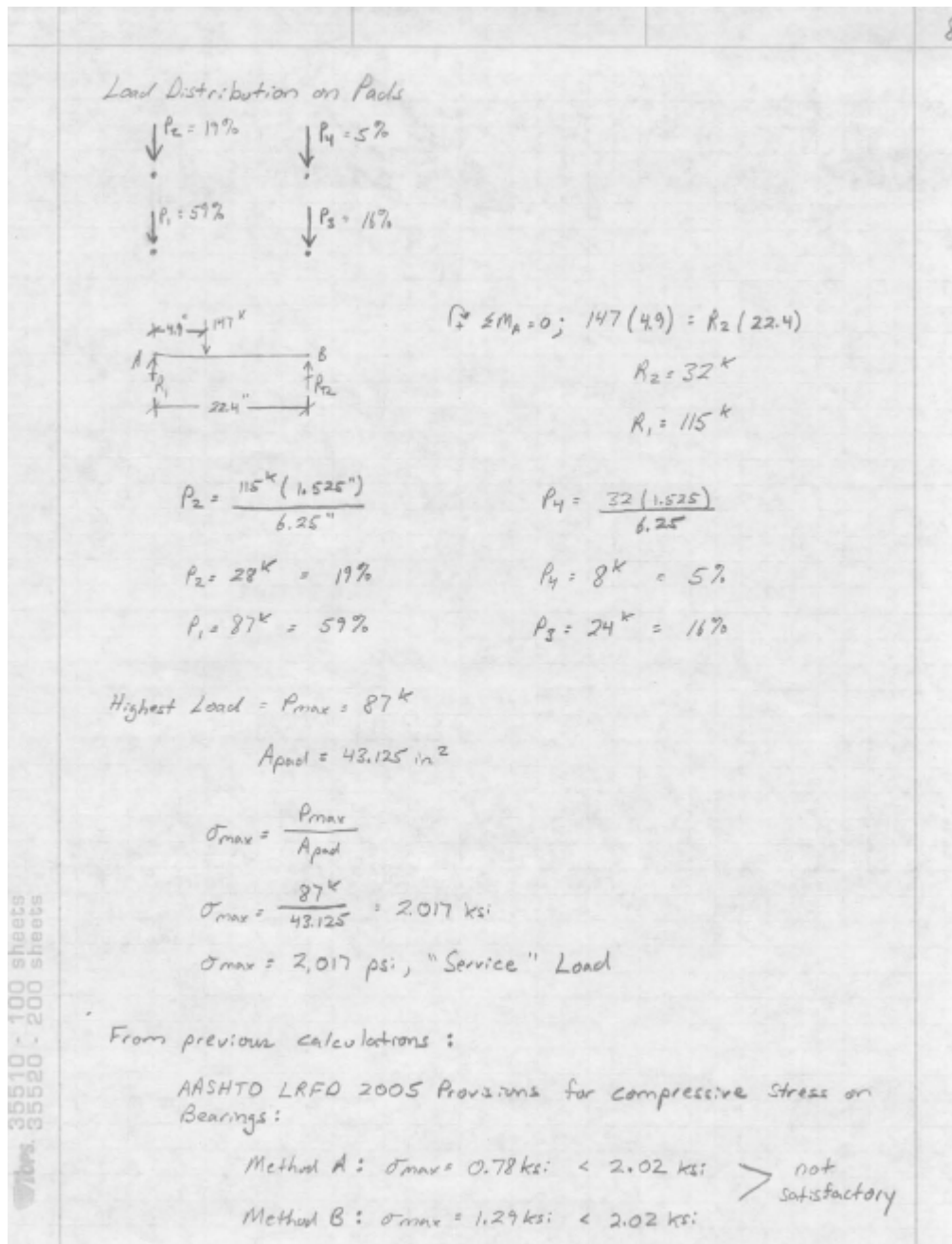


**Figure D.20: Bearing Calculations (8 of 9)**

Bearing Stress on Concrete:

$$P_n = 0.85 f'_c A_1 m$$

$$A_1 = 43.125 \text{ in}^2$$

$$f'_c = 5.8 \text{ ksi}$$

$$m = 1.22$$

$$P_n = 0.85 (5.8) (43.125) (1.22)$$

$$P_n = 259 \text{ k}$$

$$P \text{ (for most heavily loaded pad at "Service" Load)} = 87 \text{ k}$$

$$P_n = 259 \text{ k} > 87 \text{ k} \text{ bearing on Concrete O.K.}$$

35510 - 100 sheets  
35520 - 200 sheets

Figure D.21: Bearing Calculations (9 of 9)

## References

- AASHTO LRFD**, “*AASHTO LRFD Bridge Design Specifications, 2005 Interim Revisions*,” 3<sup>rd</sup> Edition, American Association of State Highway and Transportation Officials, 2005.
- AASHTO**, “*Standard Specifications for Highway Bridges*,” 13<sup>th</sup> Edition, American Association of State Highway and Transportation Officials, Washington, D.C., 1983.
- AASHTO LRFR**, “*Guide Manual for Condition Evaluation and Load and Resistance Factor Rating (LRFR) of Highway Bridges, 2005 Interim Revisions*,” 1<sup>st</sup> Edition (2003), American Association of State Highway and Transportation Officials, 2005.
- ACI**, “*Building Code Requirements for Structural Concrete (ACI 318-05) and Commentary (ACI 318R-05)*,” ACI 318-05 R 5.6.5.4, American Concrete Institute, Farmington Hills, MI, 2005.
- ACI**, “*Models for Concrete Structures*,” SP-24, American Concrete Institute, Detroit, MI, 1970.
- Ahmed, T., Burley, E. and Rigden, S.**, “*Effect of Alkali-Silica Reaction on Tensile Bond Strength of Reinforcement in Concrete Tested under Static and Fatigue Loading*,” ACI Materials Journal, V. 96, No. 4, Farmington Hills, MI, 1999.
- Ahmed, T., Burley, E. and Rigden, S.**, “*Effect of Alkali-Silica Reaction on Bearing Capacity of Plain and Reinforced Concrete*,” ACI Structural Journal, V. 96, No. 4, Farmington Hills, MI, 1999.

- Aldridge, W.W. and Breen, J.E.**, “*Useful Techniques in Direct Modeling of Reinforced Concrete Structures*,” Modeling for Concrete Structures, SP 24-5, American Concrete Institute, Detroit, MI, 1970.
- Bergmeister, K., Breen, J.E., Jirsa, J.O. and Kreger, M.E.**, “*Detailing for Structural Concrete*,” Research Report 1127-3F, Center for Transportation Research, Austin, TX, 1993.
- Baillemont, G. and Brouxel, M.**, “*Diagnosis, Treatment and Monitoring of a Bridge Damaged by AAR*,” Proceedings of the 11<sup>th</sup> International Conference on Alkali-Aggregate Reaction, Quebec (Canada), pp. 1099-1108, 2000.
- Blight, G.E.**, “*Engineering Properties of Reinforced Concrete Damaged by AAR*,” Proceedings of the 10<sup>th</sup> International Conference on Alkali-Aggregate Reaction, London (England), pp. 987-994, 1996.
- Blight, G.E. and Ballim, Y.**, “*Properties of AAR-Affected Concrete Studied Over 20 Years*,” Proceedings of the 11<sup>th</sup> International Conference on Alkali-Aggregate Reaction, Quebec (Canada), pp. 1109-1118, 2000.
- Blight, G.E., Alexander, M.G., Ralph, T.K. and Lewis, B.A.**, “*Effect of Alkali Aggregate Reaction on the Performance of a Reinforced Concrete Structure over a six-year Period*,” Magazine of Concrete Research, V. 41, No. 47, pp. 67-77, 1989.
- Clayton, N.**, “*Structural Performance of ASR Affected Concrete*,” Proceedings of the 8<sup>th</sup> International Conference on Alkali-Aggregate Reaction, Kyoto (Japan), pp. 671-676, 1989.
- Colleparidi, M.**, “*A State-of-the-Art Review on Delayed Ettringite Attack on Concrete*,” Cement and Concrete Composites, V. 25, No. 4-5, pp. 401-407, 2003.

- CSA International**, “*Guide to the Evaluation and Management of Concrete Structures Affected by Alkali-Aggregate Reaction*,” CSA International A864-00, Toronto, Ontario, 2000.
- Folliard, K.J.**, “*Extending Service Life of Large or Unusual Structures Affected by Premature Concrete Deterioration*,” TxDOT Project No. 0-5218 Proposal, Austin, TX, 2004.
- Folliard, K.J., Barborak, R., Drimalas, T., Garber, S., Ideker, J., Ley, T., Williams, S., Juenger, M., Fournier, B. and Thomas, M.D.A.**, “*Preventing ASR/DEF in New Concrete: Final Report*,” TxDOT Project No. 4085-3 Report, Austin, TX, 2005.
- Fournier, B., Berube, M.A., Thomas, M.D.A., Smaoui, N. and Folliard, K.J.**, “*Evaluation and Management of Concrete Structures Affected by Alkali-Silica Reaction- A Review*,” 7<sup>th</sup> CANMET/ACI International Conference on Recent Advances in Concrete Technology, Las Vegas, NV, 2004.
- Gere, J.M., Timoshenko, S.P.**, “*Mechanics of Materials*,” International Thomson Publishing Inc., 4<sup>th</sup> ed., 1987.
- Imai, H., Yamasaki, T., Maehara, H. and Miyagawa, T.**, “*The Deterioration by Alkali-Silica Reaction of Hanshin Expressway Concrete Structures- Investigation and Repair*,” Proceedings of the 7<sup>th</sup> International Conference on Alkali-Aggregate Reaction, Ottawa (Canada), pp. 131-135, 1987.
- IStructE**, “*Structural Effects of Alkali-Silica Reaction, Technical Guidance on the Appraisal of Existing Structures*,” The Institution of Structural Engineers, London, England, 1992.
- Monette, L., Gardner, J. and Gratten-Bellew, P.**, “*Structural Effects of the Alkali-Silica Reaction on Non-loaded and Loaded Reinforced Concrete Beams*,” Proceedings of the 11<sup>th</sup> International Conference on Alkali-Aggregate Reaction, Quebec (Canada), pp. 999-1007, 2000.



- Okada, K., Utoh, S., Imai, H. and Ono K.,** “*Concrete Structures Damaged by Alkali-Silica Reaction,*” Proceedings of the 8<sup>th</sup> International Conference on Alkali-Aggregate Reaction, Kyoto (Japan), pp. 791-796, 1989.
- Ono, K., Taguchi, M.,** “*Long-Term Behavior of AAR Bridge Pier and the Internal Deterioration,*” Proceedings of the 11<sup>th</sup> International Conference on Alkali-Aggregate Reaction, Quebec (Canada), pp. 1167-1174, 2000.
- Siemes, T. and Gulikers, J.,** “*Monitoring of Reinforced Concrete Structures Affected by Alkali-Silica Reaction,*” Proceedings of the 11<sup>th</sup> International Conference on Alkali-Aggregate Reaction, Quebec (Canada), pp. 1205-1214, 2000.
- Takemura, K., Ichitsubo, M., Tazawa, E. and Yonekura, A.,** “*Mechanical Performance of ASR Affected Nearly Full-Scale Reinforced Concrete Columns,*” Proceedings of the 8<sup>th</sup> International Conference on Alkali-Aggregate Reaction, Kyoto (Japan), pp. 665-670, 1989.
- Wood, J.G.M. and Wickens, P.J.,** “*Structural Effects of AAR on Reinforced Concrete and Consideration of Remedial Action,*” Proceedings of the 6<sup>th</sup> International Conference on Alkalis in Concrete, Copenhagen (Denmark), pp. 487-494, 1983.
- Zia, P., White, R.N. and Vanhorn, D.A.,** “*Principals of Model Analysis,*” Modeling for Concrete Structures, SP 24-2, American Concrete Institute, Detroit, MI, 1970.

## VITA

Jacob G. Kapitan was born on June 15, 1982 to Michael and Terilyn Kapitan in Hammond, Indiana. He is the third of four children – sisters Jenica and Jillian and brother Josef. After completing his work at Lake Central High School in St. John, Indiana, in 2000, Jacob went on to study civil engineering at Tri-State University. He graduated in May of 2004 with a Bachelor of Science in Civil Engineering. At which time, he left Indiana to pursue a Master of Science in Structural Engineering at The University of Texas at Austin. While at Texas, he worked with Dr. John E. Breen. Jacob graduated in May 2006 and accepted a position with Walter P. Moore in Houston, Texas.

Permanent Address: 6607 Brodie Ln. Apt. #1432  
Austin, TX 78745

This thesis was typed by the author.